Applied Physics Letters

REVIEW ARTICLE | JUNE 28 2024

Roadmap on photonic metasurfaces

Sebastian A. Schulz ; Rupert. F. Oulton ; Mitchell Kenney ; Andrea Alù ; Isabelle Staude ; Ayesheh Bashiri ; Zlata Fedorova ; Radoslaw Kolkowski ; A. Femius Koenderink ; Xiaofei Xiao ; John Yang ; William J. Peveler ; Alasdair W. Clark ; George Perrakis ; Anna C. Tasolamprou ; Maria Kafesaki ; Anastasiia Zaleska ; Wayne Dickson ; David Richards ; Anatoly Zayats ; Haoran Ren ; Yuri Kivshar; Stefan Maier ; Xianzhong Chen ; Muhammad Afnan Ansari ; Yuhui Gan ; Arseny Alexeev ; Thomas F. Krauss ; Andrea Di Falco ; Sylvain D. Gennaro ; Tomás Santiago-Cruz ; Igal Brener ; Maria V. Chekhova ; Ren-Min Ma ; Viola V. Vogler-Neuling ; Helena C. Weigand ; Ülle-Linda Talts ; Irene Occhiodori; Rachel Grange ; Mohsen Rahmani ; Lei Xu ; S. M. Kamali; E. Arababi; Andrei Faraon ; Anthony C. Harwood ; Stefano Vezzoli; Riccardo Sapienza ; Philippe Lalanne ; Alexandre Dmitriev ; Carsten Rockstuhl ; Alexander Sprafke ; Kevin Vynck ; Jeremy Upham ; M. Zahirul Alam; Israel De Leon ; Robert W. Boyd ; Willie J. Padilla ; Jordan M. Malof; Aloke Jana ; Zijin Yang ; Rémi Colom; Qinghua Song ; Patrice Genevet ; Karim Achouri ; Andrey B. Evlyukhin ; Ulrich Lemmer ; Ivan Fernandez-Corbaton

Check for updates

Appl. Phys. Lett. 124, 260701 (2024)
https://doi.org/10.1063/5.0204694

View Online
Export Citation

16 July 2024 09:29:41

Journal of Applied Physics
Special Topic:
Phonon-Magnon Interactions:
From Fundamentals to Device Physics
Guest Editors: Vasily V. Temnov, Alexey V. Scherbakov, Yoshi Chika Otani, Paolo Vavassori
Submit Today!
AIP Publishing

AIP Publishing

Roadmap on photonic metasurfaces

Cite as: Appl. Phys. Lett. **124**, 260701 (2024); doi: 10.1063/5.0204694
Submitted: 22 February 2024 · Accepted: 18 May 2024 ·
Published Online: 28 June 2024

View Online Export Citation CrossMark

Sebastian A. Schulz,[1,a] Rupert. F. Oulton,[2,a] Mitchell Kenney,[3,a] Andrea Alù,[4,5] Isabelle Staude,[6] Ayesheh Bashiri,[6] Zlata Fedorova,[6] Radoslaw Kolkowski,[7] A. Femius Koenderink,[8] Xiaofei Xiao,[2] John Yang,[2] William J. Peveler,[9] Alasdair W. Clark,[10] George Perrakis,[11] Anna C. Tasolamprou,[12] Maria Kafesaki,[11,13] Anastasiia Zaleska,[14] Wayne Dickson,[14] David Richards,[14] Anatoly Zayats,[14] Haoran Ren,[15] Yuri Kivshar,[16] Stefan Maier,[15,17] Xianzhong Chen,[18] Muhammad Afnan Ansari,[18] Yuhui Gan,[19] Arseny Alexeev,[20] Thomas F. Krauss,[21] Andrea Di Falco,[19] Sylvain D. Gennaro,[22] Tomás Santiago-Cruz,[23] Igal Brener,[23] Maria V. Chekhova,[24] Ren-Min Ma,[25] Viola V. Vogler-Neuling,[26] Helena C. Weigand,[27] Ülle-Linda Talts,[27] Irene Occhiodori,[27] Rachel Grange,[27] Mohsen Rahmani,[28] Lei Xu,[28] S. M. Kamali,[29] E. Arababi,[30] Andrei Faraon,[31] Anthony C. Harwood,[2] Stefano Vezzoli,[2] Riccardo Sapienza,[2] Philippe Lalanne,[32] Alexandre Dmitriev,[33] Carsten Rockstuhl,[34,35] Alexander Sprafke,[36] Kevin Vynck,[37] Jeremy Upham,[38,39] M. Zahirul Alam,[38,39] Israel De Leon,[40,41] Robert W. Boyd,[38,39] Willie J. Padilla,[42] Jordan M. Malof,[43] Aloke Jana,[44] Zijin Yang,[45] Rémi Colom,[46] Qinghua Song,[45] Patrice Genevet,[44] Karim Achouri,[47] Andrey B. Evlyukhin,[48,49] Ulrich Lemmer,[50,51] and Ivan Fernandez-Corbaton[35]

For affiliations, please see the end of the Reference section.

[a]Authors to whom correspondence should be addressed: sas35@st-andrews.ac.uk; r.oulton@imperial.ac.uk; and Mitchell.Kenney@nottingham.ac.uk

16 July 2024 09:29:41

ABSTRACT

Here we present a roadmap on Photonic metasurfaces. This document consists of a number of perspective articles on different applications, challenge areas or technologies underlying photonic metasurfaces. Each perspective will introduce the topic, present a state of the art as well as give an insight into the future direction of the subfield.

© 2024 Author(s). All article content, except where otherwise noted, is licensed under a Creative Commons Attribution (CC BY) license (https://creativecommons.org/licenses/by/4.0/). https://doi.org/10.1063/5.0204694

TABLE OF CONTENTS

EDITORIAL 3
I. PERSPECTIVE ON PHOTONIC METASURFACES 4
A. Introduction 4
B. State of the art 4
C. Future directions and outlook 5
II. METASURFACES FOR CONTROLLING LIGHT EMISSION 7
A. Introduction 7
B. State of the art 8
1. Emission enhancement 8
2. Shaping the emitted light 9
3. Dynamic tuning of emission 10
4. Chiral light control 10
5. Methods: Design and fabrication 10
C. Future directions and outlook 10
1. Materials and their integration 10
2. Fabrication challenges 11
3. Emission stability 11
4. Magnetic dipole transitions 11
5. 2D materials and valleytronics 11
6. Emerging trends in metasurface design 11
7. High-power applications 12
8. Tunable light sources 12
9. Topological, non-Hermitian, and temporal effects 12
D. Concluding remarks 12
III. NONLINEAR OPTICAL METASURFACES 12
A. Introduction 12
B. State of the art 14
1. Local resonance—surface plasmons 14

© Author(s) 2024

2. Local resonance—Mie and multipolar modes . 14
3. Local resonance—Fano interference 14
4. Collective resonance—bound states in the continuum 15
5. Collective resonance—surface lattice resonance 15
6. Material resonance—epsilon near zero materials 15
7. Integrating metasurfaces with nonlinear materials 15
8. Nonlinear metasurface selection rules 15
C. Nonlinear generation rate and efficiency. 15
D. Future directions of nonlinear optical metasurfaces 17
1. Metasurfaces for nonlinear wave-front control 17
2. Metasurfaces for modulation and switching. . . 17
3. Reduced power non-perturbative nonlinear optics. 17
IV. METASURFACES FOR BIOSENSING. 17
A. Introduction 17
B. Biosensors: Plasmonic vs dielectric. 18
C. Biosensing. 18
D. Refractometric sensors 18
E. Plasmonic refractometric sensors 18
F. Dielectric refractometric sensors 19
G. Chiral sensors 19
H. Enhanced vibrational spectroscopy 19
I. Nanoholes 20
J. Future directions and outlook—cross-reactive metasurface biosensors. 20
V. METASURFACES FOR PASSIVE RADIATIVE COOLING. 22
A. Introduction 22
B. State of the art 23
C. Future directions and outlook. 25
VI. METASURFACES FOR PHOTOCATALYSIS. 26
A. Introduction 26
B. State of the art 27
C. Future directions and outlook. 29
D. Concluding remarks 30
VII. ORBITAL ANGULAR MOMENTUM AND WAVEFRONT CONTROL 30
A. Introduction 30
B. State-of-the-art 30
C. Future directions and outlook. 32
VIII. METASURFACES FOR HOLOGRAPHY AND STRUCTURAL COLOR. 33
A. Introduction 33
B. Optical field manipulation in polarization-based holography 33
C. Toward 3D polarization structures: challenges and future directions. 35
IX. META-OPTICS FOR AUGMENTED REALITY APPLICATIONS. 37
A. Introduction 37
B. State of the art 38
1. Parameters 38
2. System architectures and technological platforms 38
C. Future perspectives 39
X. METASURFACES FOR QUANTUM STATES GENERATION. 40
A. Introduction 40
B. Single-photon generation 41
C. Biphoton generation 43
D. Future directions. 45
XI. METASURFACE LASERS. 46
A. Introduction 46
B. Key performance parameters. 46
C. Eigenmode engineering in a single microscale laser cavity 47
1. Enhance laser performance 47
2. Enhancing local field 47
3. Controlling radiation field. 47
D. Eigenmode engineering in arrayed lasers 47
1. Large area single mode 47
2. High dimensional radiation. 49
3. Reconfigurable phased array nanolasers 49
E. Future directions 49
F. Summary. 50
XII. SOLUTION-DERIVED NANOFABRICATION FOR NONLINEAR METASTRUCTURES. 50
A. Introduction 50
B. Nanoimprint and solution derived principles and advantages. 50
C. The challenges of solution-based processing of metasurfaces. 51
D. Roadmap towards high-performing solution-based metasurfaces 52
E. Future directions 53
1. Exploration of other materials and processes. . 53
2. Nonlinear applications with high scalability, transparency ranges, robustness, and dimensionality 53
3. Unexplored properties and more fundamental aspects. 54
XIII. SEMICONDUCTOR METASURFACES: MATERIALS AND NANOFABRICATION APPROACHES. 54
A. Introduction 54
B. Semiconductor metasurfaces and fabrication challenges 54
C. Group IV semiconductor metasurfaces 55
D. Group III–V semiconductor metasurfaces 55
E. Multi-layered semiconductor metasurfaces 56
F. Metasurfaces made of hybrid and emerging materials 58
G. Conclusions and future perspectives 58
XIV. CONFORMAL AND FLEXIBLE METASURFACES: A BRIEF PERSPECTIVE 58
A. Introduction and brief history 58
B. Design, fabrication, and applications 61
1. Optical design 61
2. Fabrication techniques 61
3. Applications 62

16 July 2024 09:29:41

© Author(s) 2024

C. Challenges, opportunities, and future perspectives 63
XV. TIME MODULATED METASURFACES 64
A. Introduction 64
B. Time-varying metasurfaces 64
C. Time-modulation in spatial metasurfaces 65
D. Space-time metasurfaces 66
E. Conclusion 67
XVI. DISORDERED OPTICAL METASURFACES: PHYSICS, THEORY AND DESIGN 67
A. Introduction 67
B. State-of-the-art 67
1. Diffuse (incoherent) vs. specular (coherent) light 68
2. Full-wave analysis 68
3. Approximate models 69
4. Fabrication 69
C. Future directions and outlook 70
1. Prospective applications 71
2. Metasurfaces on curved substrates 71
3. Striving for ultra-low costs with augmented resilience to fabrication imperfections 72
XVII. FROM PRINCIPLES TO PERFORMANCE: EPSILON-NEAR-ZERO METASURFACES FOR NONLINEAR OPTICAL DEVICES 72
A. Introduction: The physics of ENZ 72
1. Materials with ENZ properties 73
2. ENZ induced behavior in TCOs 73
3. Incorporating metasurfaces with ENZ materials 75
4. Metasurfaces exploiting the nonlinear ENZ response 75
5. Future of applications 77
a. Speed of modulation 77
b. Absorptive losses 77
c. Saturation and damage threshold 77
d. Alternative modulation mechanisms 77
e. Pushing back technical limits 77
B. Perspective on future work 77
C. Conclusion 78
XVIII. DEEP LEARNING FOR PHOTONIC METASURFACES 78
A. Introduction 78
1. State of the art 80
2. Future directions and outlook 81
XIX. COMPLEX-VALUED SINGULARITIES FOR METASURFACE DESIGNS 83
A. Introduction 83
B. Designing metasurfaces according to the position of complex-plane zero singularities 84
C. Asymmetric full 2π phase engineering based on exceptional points in metasurfaces 87
D. Concluding remarks and future perspective 88
XX. MULTIPOLAR DESIGN METHODS FOR METASURFACES 89
A. Introduction 89
B. State of the art 89
1. Theoretical framework of a multipolar description 89
2. Numerical implementation 91
3. Analytical investigations 92
C. Future directions and outlook 93
1. A description using polarizabilities 93
2. Multipolar interface conditions 94
3. Further developments 94
D. Conclusions 95

EDITORIAL

Sebastian A. Schulz,* Rupert F. Oulton,** and Mitchell Kenney***

*sas35@st-andrews.ac.uk
**r.oulton@imperial.ac.uk
***Mitchell.Kenney@nottingham.ac.uk

Over the last decade, the topic of metasurfaces has flourished like no other field in optics. This is primarily due to the appeal of compact flat optical components with wide design flexibility inherent to these artificial two-dimensional materials. As can be seen in this roadmap, metasurfaces can be made from a wide range of materials, from metals and other plasmonic materials to dielectrics and even flexible and conformable platforms. In all cases, a metasurface's overall properties follow not only from the those of the constituent materials but also from the shape and arrangement of meta-atoms, engineered on nanoscopic dimensions. The broad range of metasurface applications available stem from the rich physics that emerges from the arrangement and geometry of the meta-atoms; by arranging these into periodic or disordered distributions, that display local or non-local responses, as well as exhibiting conventional or topological characteristics, these "design parameters" allow us to influence light's amplitude, phase, polarization, and nonlinearity.

This document offers a comprehensive overview of the physics and applications of photonic metasurfaces which sets the context for discussion of future research directions. As commissioning editors, we have invited 20 perspectives from the community, where each has given equal importance to reviewing the historic development of the field, presenting highlights of current research and then pointing to future challenges and outlook. Andrea Alu sets the scene with a general introduction (I). The roadmap is then organized into three sections of perspectives: ten perspectives on the applications of photonic metasurfaces; three perspectives on the fabrication and material platforms; and finally, six perspectives on the emerging topics and the theory of metasurfaces. The roadmap explore several key application areas for metasurfaces, including metasurfaces for: the control of light emission (II); nonlinear optics (III); biosensing (IV); passive radiative cooling (V); photocatalysis (VI); orbital angular momentum and wavefront control (VII); holography and structural color (VIII); augmented reality (IX); quantum state generation (X); and finally metasurface based lasers (XI). The section on fabrication and material platforms includes solution derived metasurface fabrication (XII); semiconductor based metasurfaces (XIII); and flexible metasurfaces (XIV). The final six perspectives explore metasurfaces for or with time modulation (XV); disorder (XVI); epsilon-near-zero characteristics (XVII); deep learning (XVIII); complex-valued singularities (XIX); and, last but not least, multipolar characteristics (XX).

In contrast to previous reviews (e.g., Refs. 1–3) and roadmaps,[4] which focus exclusively on either past or future development of the

16 July 2024 09:29:41

© Author(s) 2024

field, we have aimed instead to provide a comprehensive overview that gives equal weight to past, present and future of the selected topics. This gives the necessary context for the discussion of future research directions and outlook whilst also providing a valuable up to date resource by indexing the rapidly amassed literature in this field.

This roadmap is truly the culmination of a world-wide effort of leading contributors from across the metasurface community. We are grateful for their time, effort, and dedication to this compilation of perspectives. We hope that this Roadmap on Photonic Metasurfaces will provide you—the reader—with an up to date reference of the current status, understanding, and direction of photonic metasurface research; whether you are already an experienced researcher looking for a contemporary summary of the research and direction of the field or whether you are looking for a comprehensive introduction to this fascinating area.

I. PERSPECTIVE ON PHOTONIC METASURFACES

Andrea Alù

aalu@gc.cuny.edu

A. Introduction

The field of photonics relies on gaining control over light flows to advance a wide and rapidly growing range of technologies, including energy, sensing, imaging, and computing. Photonics research has been recently unveiling exciting opportunities both in the context of basic science and of its engineering and technological impact. A major role in this recent progress has been played by ultrathin surfaces engineered at the nanoscale, known as metasurfaces,[5] which have been enhancing the way we tailor optical wavefronts over an ultrathin platform, opening a paradigm of compactification of photonic devices for extreme light control. In turn, metasurfaces have also been unveiling unique forms of light–matter interactions emerging from their subwavelength light confinement and extreme light control at the nanoscale. The recent surge of interest for metasurfaces in the photonics community has been driven by the introduction of the "generalized Snell's laws of refraction,"[5,6] according to which a transverse gradient of phase discontinuities imparted by a tailored array of nanostructures can offer enhanced control over wave transmission through a planar interface. These concepts have been building on well-established technologies in the realm of microwave components[7,8] and "flat" diffractive optical elements,[9,10] established fields of research for several decades. Over the years, more sophisticated metasurface designs have been demonstrating further mastery over all properties of light, enhancing efficiency, bandwidth, polarization, and wavefront control through metasurfaces,[11–16] which, in turn, have been translated into ultrathin devices for lensing, holograms and lasing, among many other applications.

While the early demonstrations of metasurfaces were mostly based on plasmonic nanostructures, which enable field enhancement and light focusing at deeply subwavelength scales, the associated material loss have driven the field toward alternative materials, including high-index dielectrics and doped semiconductors. Today, the possibilities offered by metasurfaces to efficiently control light with nanoscale resolution over an ultrathin platform have translated into myriads of opportunities, not only limited to high-profile academic research, but also to commercial companies.[17,18] The progress in this area has been truly impressive, leveraging the combination of theoretical advances in our understanding of the interactions of light with nanostructures, and progress in nanofabrication of a wide range of materials, also over large area. In turn, the discoveries driven by photonic metasurface research have also translated back to lower frequencies, where the fields of reflect- and transmit-arrays, as well as frequency-selective surfaces, originally demonstrated wavefront and spectrum control for radiowaves, driving the interest in a new wave of hardware platforms known as reconfigurable intelligent surfaces for wireless communications.[19]

B. State of the art

The first demonstrations of optical metasurfaces, e.g., Fig. 1(a), were limited in terms of efficiency and of functionalities, due to a variety of challenges. For the most part, they relied on metallic resonant elements, associated with significant absorption, and on polarization conversion mechanisms, which tend to be inefficient and limited by symmetries, to control the amplitude and phase of the scattered fields. The overall efficiency and the type of transformations that could be implemented on the incoming wavefront were significantly limited in these first demonstrations.[14] By contrast, over the years new generations of photonic metasurfaces have flourished into a plethora of exciting functionalities for holography,[20] multi-functional and multi-wavelength operation,[21] lensing and imaging,[22] and several other impressive demonstrations of complex wavefront shaping using ultrathin optical devices, becoming competitive with bulky optical technologies in terms of several performance metrics. Figure 1 shows a few demonstrations of the state of the art of this technology, in which tailored nanostructured apertures are able to imprint the desired wavefront to the electromagnetic fields at the wavelength of interest. Figure 1(b), for instance, shows high-efficiency holograms created by tailored nanostructured surfaces, and Fig. 1(c) an ultrathin metalens that can focus light at multiple frequencies.

Several design principles have been explored to tailor the optical wavefront, spanning from coupled resonances locally tuned to control the amplitude and phase[23] to polarization conversion[5] and geometric phase concepts,[24] each coming with their own advantages and trade-offs. For instance, coupled resonances tend to introduce unwanted frequency dispersion, modulating the scattering amplitude as we tailor the local phase of each metasurface elements. Polarization conversion can powerfully tailor the phase of the scattered fields, but its efficiency is typically limited. Geometric phase concepts can partially address these challenges, but they are conventionally limited to circularly polarized responses.

While all these design principles offer a powerful playground for wavefront control, metasurfaces often face fundamental constraints in terms of efficiency and bandwidth of wavefront manipulation, which stem from their ultrathin footprint and inherent symmetry constraints. Over the years, several of these bounds have been unveiled,[11,14,25,26] indicating that extreme compactification of optical devices comes at a price, which needs to be taken into account when compared to other more bulky solutions. For instance, it is hard to imagine that a fully metasurface-based approach may be able to compete with a sophisticated EOS camera lens, but metasurfaces may be able to replace specific components. Hybrid approaches leveraging metasurfaces appear to be certainly competitive, and metasurfaces may be excellent at specific tasks, or for targeted wavelengths of operation.

16 July 2024 09:29:41

© Author(s) 2024

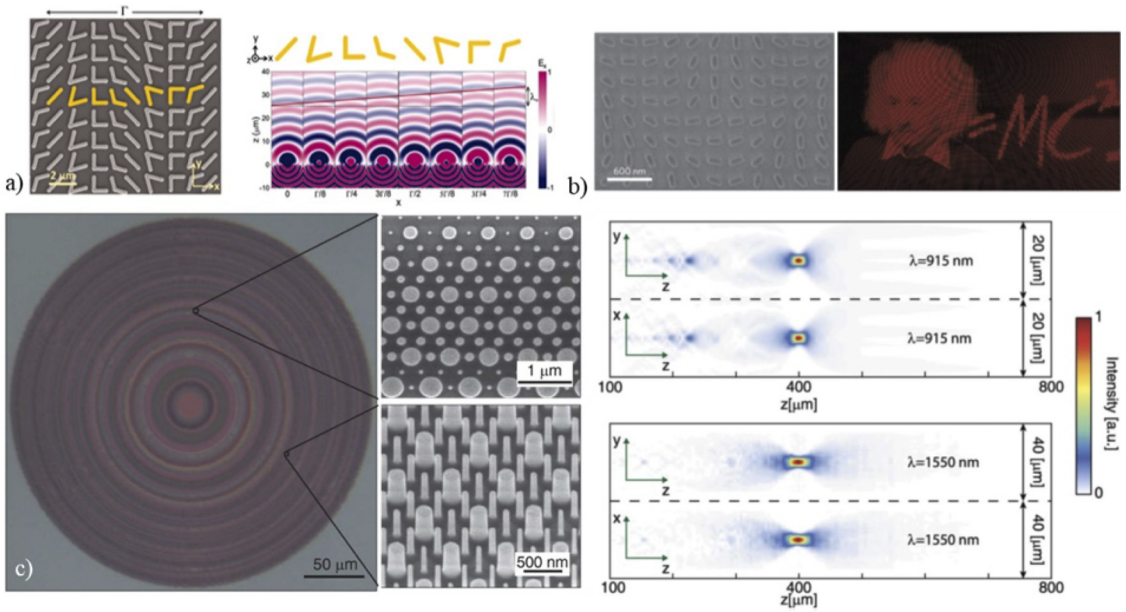

FIG. 1. Metasurfaces for wavefront control. (a) Generalized laws of refraction for beam steering through phase gradients (reproduced with permission from Yu *et al.*, Science **334**, 333 (2011). Copyright 2011 AAAS;[5] (b) metasurface holograms with high efficiency (from Ref. 20); (c) multi-wavelength, polarization-insensitive metalenses (from Ref. 21). All images are reprinted (adapted) with permission from the respective Journal and copyright remains with the original publisher.

While the conventional approach to metasurface design has been the one of locally patterning the aperture with nanoscale resonators that control point by point the response, a few more recent approaches have been opening new design degrees of freedom. For instance, metagratings[27,28] have been demonstrating that extreme control over the optical wavefront can be achieved with high efficiency, for instance yielding near-grazing beam steering. Metagratings are based on grating resonances that stem from an overarching long-range periodicity of the structure, while the individual metasurface elements are designed to control the way the incident wavefront locally couples to the available diffraction orders. These principles have been further empowered by nonlocal metasurfaces, in which the coupling among distant elements across the metasurface aperture is not fought against, but rather leveraged through more sophisticated design principles that exploit lattice resonances locally perturbed by symmetry-breaking defects.[29] Nonlocal metasurfaces provide a more sophisticated control over the spectral response, and open new opportunities for wavefront manipulation, including wavefront selectivity,[30] and multifunctionality.[31]

The recent progress in metasurface design principles, fabrication and also tunability of their response has led to a surge of exciting applications. Figure 2 summarizes a few relevant highlights of metasurfaces that realize complex structured wavefronts, relevant for e.g., optical communications and holography,[32] for eye tracking applications,[33] for quantum technologies,[36] for catalysis and chemical reactions,[34] and for augmented reality (AR).[35] These breadth of applications holds the promise of a vibrant future for metasurfaces, opening exciting prospects for the near future.

C. Future directions and outlook

The opportunities for photonic metasurfaces have been growing by the day, fostered by continuous progress on multiple fronts, which drives the future of this research area. From the modeling perspective, enhancing the ultimate performance of metasurfaces requires sophisticated modeling tools that can capture and optimize their design. Given that most metasurfaces are non-periodic, rational design tools, fast simulation and optimization techniques have been emerging as exciting prospects, for instance in the context of adjoint methods, topology optimization and machine learning. Physics-driven design and optimization approaches, such as the use of singularities in the complex frequency plane, topological concepts, bound states in the continuum (BIC) and exceptional points are emerging directions that unveil new optical phenomena and add new designer tools for photonic metasurfaces.[37–40]

Emerging applications of nonlocal metasurfaces include the possibility of filtering and processing images in momentum space, realizing Fourier and even nonlinear operations over an ultrathin, efficient platform. The idea is to leverage the engineered nonlocality in metasurfaces to perform mathematical operations on the incoming images,[41–43] and even realize optical analog computers that can solve complex mathematical problems[44–46] [Figs. 3(a) and 3(b)]. Tailored nonlocalities in metasurfaces can also add spatial and temporal coherence, ideally suited to pattern and control thermal emission and photoluminescence. These ideas are paving the way to the realization of ultrathin surfaces that emit tailored wavefronts with desired amplitude, phase, and polarization without the need for an external coherent source driving them.[47,48] Figure 3(c) shows a thermal metasurface, based on an underlying periodic lattice that can control the degree of temporal and spatial coherence endowed to thermal emission, and

16 July 2024 09:29:41

© Author(s) 2024

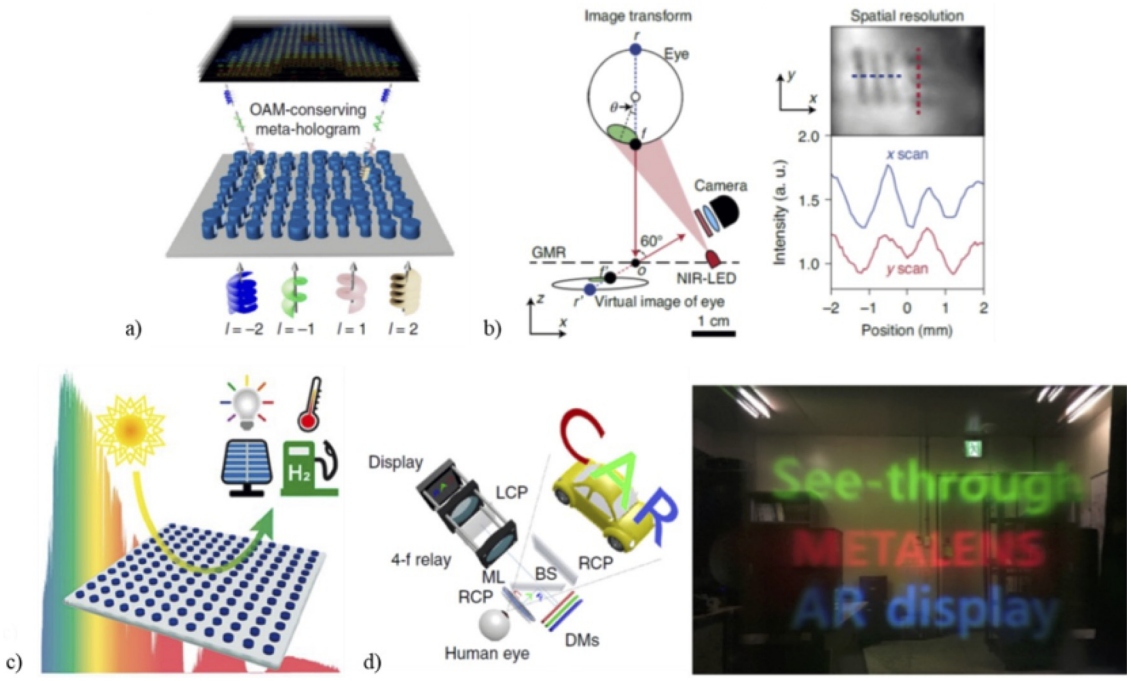

FIG. 2. (a) Metasurface for complex wavefront shaping to impart orbital angular momenta to the impinging light (reproduced with permission from Ren *et al.*, Nat. Commun. **10**, 2986 (2019). Copyright 2019 Springer Nature Publishing Group;[32] (b) nonlocal metasurface for eyetracking applications (from Ref. 33); (c) concept of metasurfaces to facilitate chemical processes (from Ref. 34); (d) metasurface for augmented reality applications (from Ref. 35). All images are reprinted (adapted) with permission from the respective Journal and copyright remains with the original publisher.

whose local perturbations control the polarization and wavefront shape of thermal emission. Future efforts may be able to demonstrate ultrathin patterned surfaces that embed their own optical sources and pattern them with extreme flexibility.

On the material front, the use of two-dimensional (2D) materials integrated with metasurfaces, such as graphene[51] and transition metal dichalcogenides[49] [Fig. 3(d)], and even direct patterning of bulk 2D materials, holds the promise for exciting opportunities both in the

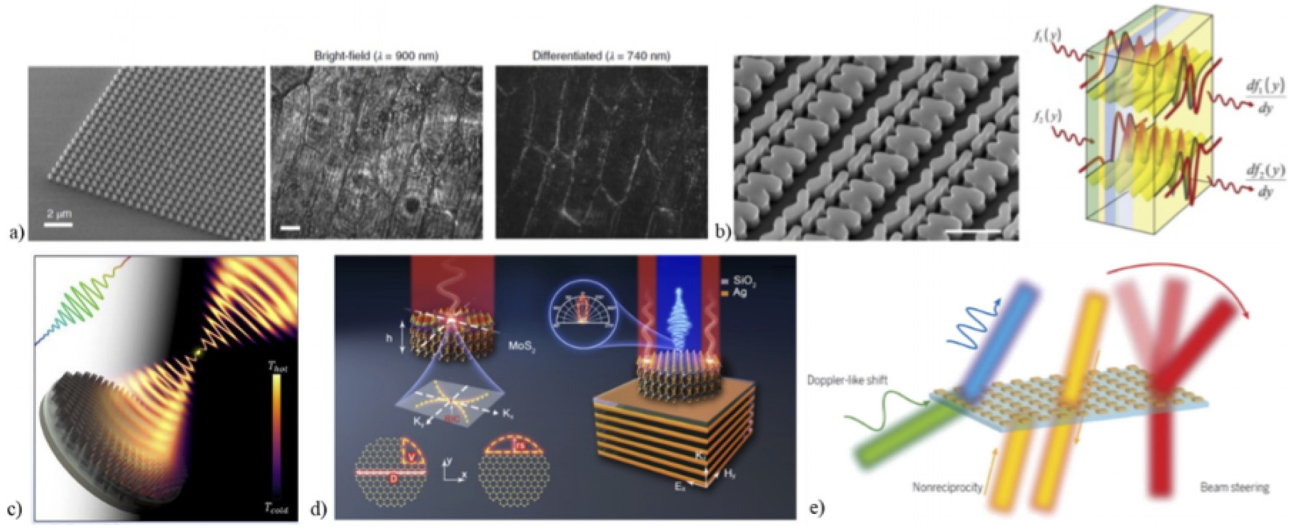

FIG. 3. (a) Edge detection metasurfaces for image processing and biomedical applications (from Ref. 42); (b) analog optical computing based on nonlocal metasurfaces (from Refs. 44 and 46); (c) nonlocal metasurface to manipulate thermal emission (from Ref. 47); (d) metasurfaces integrating 2D materials (from Ref. 49); (e) spatiotemporally modulated metasurface to extend the degree of control over wavefront manipulation to space-time diffraction (from Ref. 50). All images are reprinted (adapted) with permission from the respective Journal and copyright remains with the original publisher.

16 July 2024 09:29:41

© Author(s) 2024

context of basic science and applications. These materials offer interesting forms of light–matter interactions in the form of plasmon, exciton, phonon polaritons, in which light and matter are so intertwined to form quasi-particles. Combined with metasurface concepts, these phenomena can further boost light control, and impart exotic photonic features to polaritonic responses. Polaritonic materials can be also ideally suited to boost optical nonlinearities, opening exciting opportunities to extend metasurface operations and wavefront control to nonlinear optical processes, such as wave mixing, frequency generation, limiting, up- and downconversion.[52,53] These materials can also be exciting prospects to efficiently integrate and pattern optical gain in metasurfaces, paving the way to a plethora of interesting non-Hermitian wave phenomena.[38,39,54]

Nonlinearities can also offer powerful tools to reconfigure and modulate in time the metasurface response, which becomes crucial to make an impact in many technologies. Beyond the importance of manipulating in real-time the spatial degrees of freedom of the incoming wavefront, creating enhanced forms of spatial light modulators,[55] but also their temporal and frequency content. Suitable temporal modulation schemes can break reciprocity and efficiently mix frequencies,[56] as well as induce nontrivial parametric phenomena, including Doppler shifts, and active beam steering,[50] largely expanding the reach and opportunities offered by optical metasurfaces, as schematically shown in Fig. 3(e). For various applications, real-time dynamic programmability may become necessary moving forward the field of metasurfaces, for instance in the context of image processing, dynamic scene creation, and holograms. The integration of 2D and polaritonic materials may enable faster and more efficient forms of modulation.

Finally, photonic metasurfaces may truly flourish once its realization becomes fully compatible with large-area and inexpensive fabrication techniques, pushing metasurfaces from proof of concept implementations to foundry-level production. Roll-to-roll, nanoimprinting, and self-assembly techniques appear promising in this context, and efforts to develop design principles compatible with the constraints of these techniques in terms of materials and disorder tolerance are becoming necessary. Overall, photonic metasurfaces have a bright future ahead, continuously evolving along the years with new concepts, new material playgrounds and a highly interdisciplinary broad research community. As the field continues to mature, the exotic wave phenomena at the basis of photonic metasurfaces are empowering photonic technologies and exciting several industries.

ACKNOWLEDGMENTS

Our work on these topics has been supported by the Simons Foundation and the Air Force Office of Scientific Research.

II. METASURFACES FOR CONTROLLING LIGHT EMISSION

Ayesheh Bashiri, Zlata Fedorova, Radoslaw Kolkowski, A. Femius Koenderink, and Isabelle Staude*

*isabelle.staude@uni-jena.de

A. Introduction

Optical metasurfaces are two-dimensional (2D) arrangements of subwavelength scale building blocks known as meta-atoms with engineered scattering properties. In contrast to the passive metasurfaces discussed in most other sections of this Roadmap, which manipulate the light propagating from a distant light source, light-emitting metasurfaces incorporate nanoscale light sources in their architecture, allowing the coupling of the emission from the sources to the far-field.[57] Light-emitting metasurfaces offer various functionalities including photoluminescence enhancement,[58] tailored emission directionality,[48,59,60] improved quantum efficiency,[61] color conversion,[62] and controlled degree of coherence,[63] thus offering important opportunities for compact and efficient light sources such as lasers (see also Sec. XI), LEDs,[64] and single-photon sources[65] for quantum technologies (see also Sec. X). Other applications range from displays and optical communication to biomedical applications, and energy harvesting. Note that, in this section, the term "light emission" specifically refers to the fluorescent and photoluminescent sources, while thermal emission is addressed in Secs. I and V.

Light-emitting metasurfaces can be categorized into two main platforms: plasmonic and high-refractive-index all-dielectric. Plasmonic metasurfaces are composed of metallic meta-atoms, where the large confinement of electromagnetic fields in their surroundings can result in a strong reduction of the radiative lifetime of the emitters coupled to the metasurface.[66] However, the applicability of these metasurfaces is limited due to their intrinsic Ohmic losses. All-dielectric metasurfaces, on the other hand, can exhibit low absorption losses and support both electric and magnetic multipolar Mie-type modes without demanding complex geometries.[67] Multipolar superposition then allows for tailoring directional properties, e.g., through the Kerker effect, which facilitates applications in beam steering, lensing, and beam shaping.

Various types of emitters have been considered as active components of light-emitting metasurfaces, such as quantum dots (QDs), dyes, and semiconductors. Recently, many studies concentrated on the coupling of optical metasurfaces with 2D materials. In the family of 2D materials, layered systems of transition metal dichalcogenides (TMDs)[68] have attracted special attention due to their unique optoelectronic properties, including strong photoluminescence, excitonic response at room temperature, and circular dichroism caused by their valley-selective optical transitions.[69]

The key mechanism for controlling light emission by metasurfaces is the engineering of the local density of photonic states (LDOS) through either the localized resonances provided by individual meta-atoms or the collective resonances originating from their overall arrangement or both. In periodic metasurfaces, collective resonances can be regarded as photonic Bloch bands (as in photonic crystals) transformed by the resonant meta-atoms into surface lattice resonances (SLRs).[70] They also include dark modes and quasi bound states in the continuum (quasi-BICs), in which radiative loss is suppressed by destructive interference.[71] Collective resonances can provide high LDOS at the band edges, together with control of spatial coherence and directivity of emission.[59,72] Engineering the individual meta-atoms allows to further tailor the light emission properties, employing both local and nonlocal effects. For example, asymmetric meta-atoms may allow a controlled fraction of the light to be radiated away by turning the perfectly nonradiating BICs into quasi-BICs.[73] Moreover, spatial variation of the meta-atom design can allow for the emission of light fields with shaped wavefronts through metasurface defined spatially varying phase or amplitude profiles.[48,60,74]

16 July 2024 09:29:41

© Author(s) 2024

Although most of the light-emitting metasurfaces demonstrated so far facilitate tailoring of spontaneous emission in the weak coupling regime, their potential for strong coupling and lasing has also been demonstrated.[75,76] The latter is discussed in detail in Sec. XI. Semiclassical strong coupling (ensemble of many emitters) is achieved when the coupling rate of emitters to the photonic resonances exceeds the photonic loss rate, and the rate of spontaneous decay is gauged by the emission spectral bandwidth. This can be achieved by aligning the active material's emission bandwidth with metasurface resonances featuring sharp line widths while aiming to maximize the oscillator strength of the dipole transition. Low-threshold lasers, on the other hand, require high-quality (high-Q) optical cavities and precise spatial and spectral overlap of their modes with the gain material. This can be achieved by engineering the parameters of the metasurface integrated with the gain medium.

The relevant performance factors for light-emitting metasurfaces depend on the specific target application. For instance, to impact high-power LED lighting one must contend with 0.5–1 A/mm^2 current density (blue emitting LEDs), or equivalently for phosphor converting layer of order 1 W/mm^2 emitted power, and 1 W/mm^2 thermal load due to the Stokes shift. This places huge challenges on photostability and absorption coefficients. Another application is light sources for projection or image-projecting metasurfaces. In contrast to general lighting, such applications require a small etendue. Metasurface-based displays must emit a set of selected wavelengths, which can be achieved, e.g., by energy transfer between different types of emitters. For applications like, e.g., AR glasses, it is not overall emission power output that matters, but the combination of emissive behavior with transparency for most of the ambient light. Some factors are relevant for multiple applications, e.g., brightness, photostability, power efficiency, fabrication reliability, scalability, and cost. In addition, a frequently desired property is post-fabrication tunability. Modulating the emission and/or achieving multiple and adjustable functionalities in one design are the key features of light-emitting metasurfaces that can bring them closer to real-world applications.[77]

Figure 4 summarizes many of the aspects of light-emitting metasurfaces discussed in this section.

B. State of the art

1. Emission enhancement

The emission from nanoscale light sources incorporated into metasurfaces can be tailored through a modification of excitation rate (for optical pumping), of radiative decay rate, and of directionality of the emission.[78] Metasurfaces can strongly confine the excitation field in the emissive layer, resulting in an efficient incoupling and further enhancement of the emission. Radiative decay rate enhancement is associated with the Purcell effect and achieved through modifications of the LDOS by resonant metasurfaces. For classical cavities, it is well known that the Purcell factor scales approximately with the ratio of the quality factor Q and the mode volume V. Simple Mie-resonant all-

16 July 2024 09:29:41

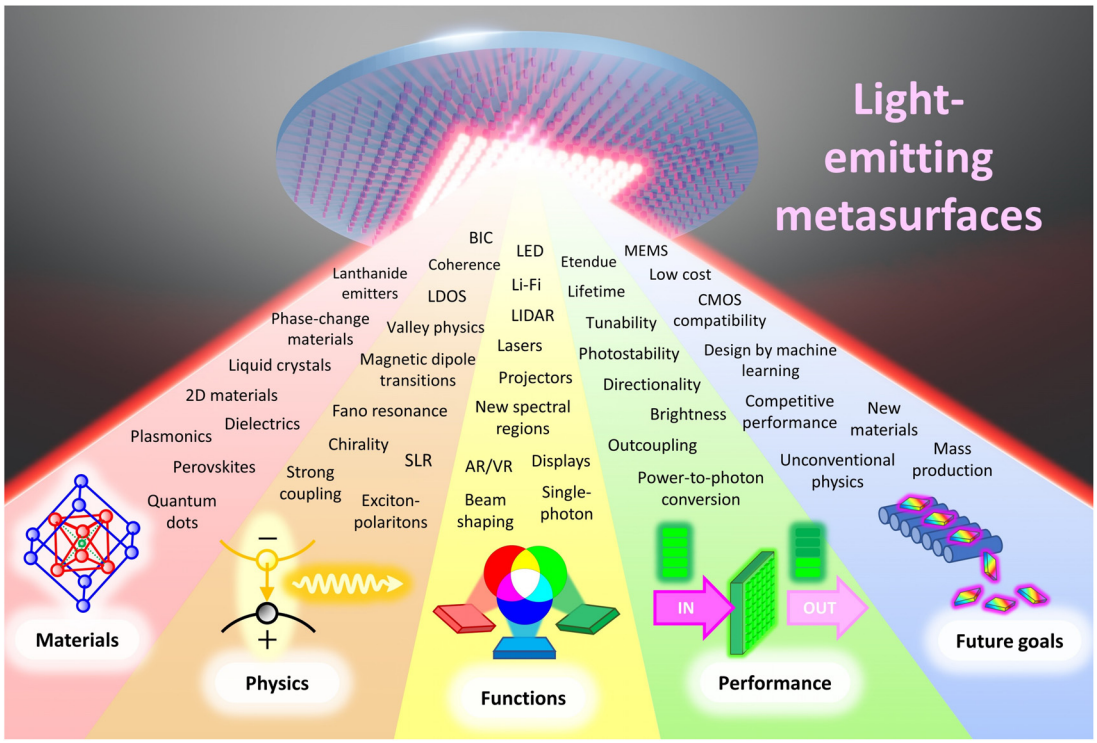

FIG. 4. Summary of the key aspects of light-emitting metasurfaces discussed in this chapter including material platforms, physical mechanisms, desired functionality, performance requirements, as well as future goals.

© Author(s) 2024

dielectric metasurfaces exhibit *Q*-factors on the order of 10–100 and moderate Purcell factors.[79] However, they contribute effectively to the radiative decay rate enhancement due to their negligible absorption losses. This is especially beneficial for emitters with intrinsically high quantum yields. In contrast, plasmonic metasurfaces can offer much smaller mode volumes, resulting in larger Purcell factors,[80] at the cost of enhancing both the radiative and nonradiative decay rate, thus reducing the quantum yield for highly efficient emitters. Hence, they can only be usefully employed for boosting the quantum yield of rather inefficient emitters[78] or should be operated in the regime of high-*Q* SLRs, where the hybridization between plasmon and diffraction resonances is tuned to trade in plasmonic confinement for the quality factor. Indeed, collective metasurface resonances such as SLRs or quasi-BICs generally support significantly high *Q*-factors (in particular for low-loss dielectric implementations) at the cost of relatively high mode volumes. The high *Q*-factors make them suitable for lasing, entangled-photon generation, and luminescence enhancement.[71] For example, a 40-fold enhancement by quasi-BIC for color centers in silicon metasurfaces has been reported[81] [see Figs. 5(a)–5(d)]. For germanium QDs, over three orders of magnitude luminescence enhancement was obtained in dielectric Fano-resonant metasurfaces.[58] Efficient lasing and strong coupling enabled by collective metasurface resonances have been demonstrated, e.g., in a plasmon-exciton-polariton laser, exhibiting a reduced threshold in the strong coupling regime.[82]

2. Shaping the emitted light

Other crucial enabling features of metasurfaces are their areal nature and the diversity of far-field spatial character that their modes can be engineered to support, in particular for spatially varying architectures. As such, the radiative decay rate enhancement can also serve to tailor the emission directionality by channeling the emitted light into carefully tailored spatial modes. This is usually achieved by adjusting the meta-atom geometry or their arrangement,[83] which can span from a basic periodic lattice to a complex, spatially inhomogeneous distribution, as well as the substrate/superstrate material. Tailoring directionality is key for realizing light-emitting devices with efficient outcoupling,[84] emission into a reduced solid angle for augmented/virtual reality (AR/VR) applications[35] and generating arbitrary emission patterns,[48,60,85] e.g., for projectors or light-field displays. The combination of the high *Q*-factors and topological properties of quasi-BICs can also be harnessed for beam shaping, e.g., for generation of vortex laser beams.[86]

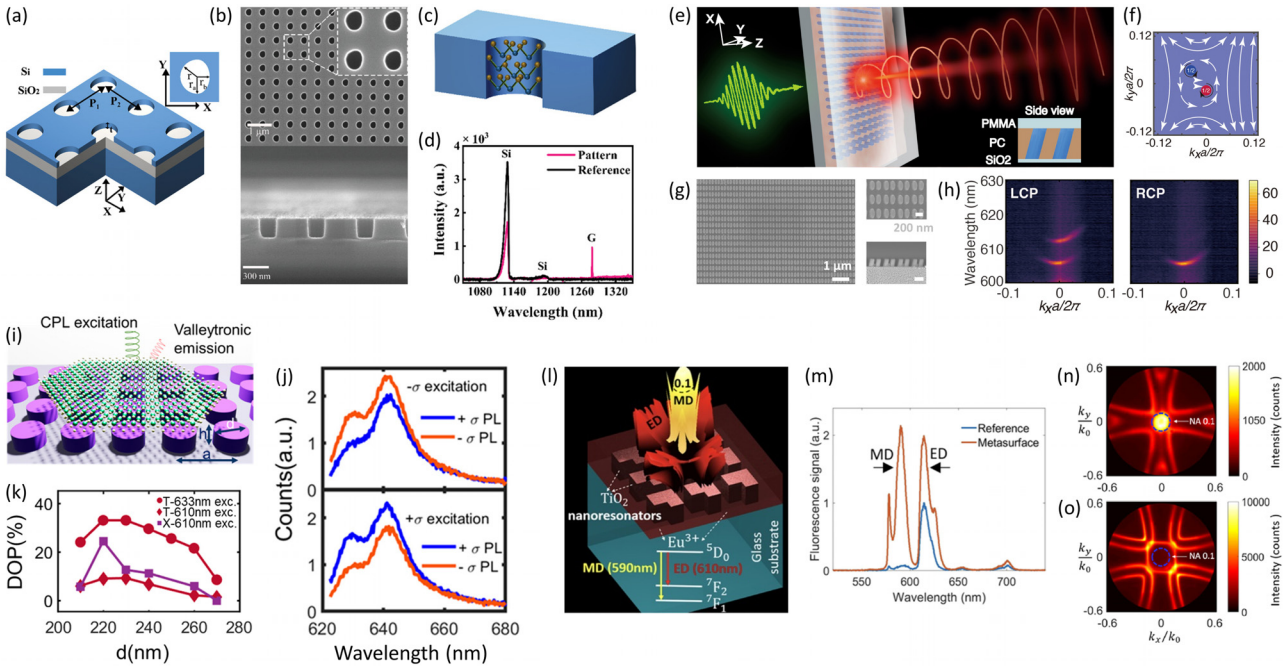

FIG. 5. (a) Schematic illustration of a silicon metasurface supporting high-*Q* quasi-BIC resonances; (b) SEM images of the fabricated metasurface; (c) illustration of the carbon G-centers on the side walls of the etch holes; (d) emission from the carbon G-centers resonantly enhanced by the quasi-BIC [(a)–(d) from Ref. 81]; (e) illustration of chiral emission due to circularly polarized states (CPS) originating from BIC in a metasurface with broken symmetry; (f) distribution of polarization vectors in the momentum space, with a pair of CPS shown as red and blue dots (topological charges ±1/2); (g) SEM images of the fabricated metasurface; (h) enhanced circularly polarized emission from polycarbonate (PC) film doped with 2-methyl-6–(4-dimethylaminostyryl)-4H-pyran (DCM) deposited on the metasurface [(e)–(h) from Ref. 87]; (i) schematic of a single layer TMD integrated with an achiral dielectric metasurfaces for controlling valleytronic emission; (j) detected valley resolved photoluminescence of excitons and trions upon left-handed and right-handed circularly polarized laser excitation for structure shown in (i); (k) measured trion and exciton degree of polarization, for structure shown in (i) [(i)–(k) from Ref. 69)]; (l) schematic of a polymer layer containing Eu^{3+} compound integrated with a broken symmetry TiO_2 metasurface for tailoring directionality and fluorescence enhancement of MD transitions; (m) measured fluorescence spectra for the metasurface scheme shown in (l) (red curve) normalized to the spectra of the substrate (blue curve); (n) measured back focal plane images of (n) MD and (o) ED transitions coupled to the metasurface shown in (l) [(l)–(o) from Ref. 72]. All images are reprinted (adapted) with permission from the respective Journal and copyright remains with the original publisher.

16 July 2024 09:29:41

© Author(s) 2024

3. Dynamic tuning of emission

Many envisioned applications of light-emitting metasurfaces require dynamic, controllable, and reversible modulation of light emission. Such post-fabrication tunability can be achieved using active materials, which change their optical properties under electrical, optical, or thermal stimuli. Recently, sub-picosecond modulation of photoluminescence has been achieved in semiconductor metasurfaces through optically induced free-carrier effects,[88] which constitutes the current state of the art in modulation speed. On the other hand, large modulation depths can be provided by liquid crystals (LCs) or changing the metasurface geometry, e.g., by stretchable deformation or using micro-electro-mechanical systems (MEMS). The use of both approaches for actively tuning spontaneous emission has already been demonstrated,[89,90] making them promising future platforms for dynamic light-emitting metasurface devices.

4. Chiral light control

Moreover, an important area of application for light-emitting metasurfaces is the creation and manipulation of circularly polarized light—a property that is often desired in classical and quantum optical information processing, communication, sensing, and displays. Several strategies have emerged in this field. In one scenario, circular polarization of the emission is enforced by the metasurface design, while the emitter can be arbitrary. This can be achieved, e.g., by using chiral meta-atoms, photonic spin-valley locking[91] or optical Rashba effect, where lack of inversion symmetry causes splitting of optical spin-polarized states in momentum space. Alternatively, the utilization of chiral quasi-BICs was introduced as a compelling method for narrowband directional chiral light emission[87] [see Figs. 5(e)–5(h)]. In the second scenario, chiral metasurfaces are combined with emitters of circularly polarized light. Prominent examples include the usage of chiral metasurfaces for circular dichroism enhancement or selective coupling with valley-polarized excitons in 2D TMDs. The latter is often motivated by the demands of valleytronics. As to the valleytronic applications of chiral metasurfaces, they, however, face notable limitations as they often promote only one specific valley and would require nanoantenna geometry changes for switching. This leads us to the third scenario, where achiral metasurfaces enable control over the circularly polarized emission. Specifically, achiral metasurfaces were proven to allow for control of the lifetime, the degree of valley polarization, and the spectral shape of chiral 2D TMD emission.[69,92] An example of chiral 2D TMDs coupled to the achiral metasurfaces is shown in Figs. 5(i)–5(k). However, a comprehensive understanding of the coupling mechanisms in such complex hybrid systems, which would be essential for testing their applicability for valleytronics, is still missing. Notably, coherent coupling between excitons and meta-atom resonances offers new avenues for the tunability of chiral properties, including via the magneto-optical effect.[93]

5. Methods: Design and fabrication

Various numerical methods, including rigorous coupled-wave analysis (RCWA), finite element method (FEM), and finite-difference time-domain (FDTD), are used to simulate light-emitting metasurfaces.[94,95] RCWA is well-suited for periodic metasurfaces with low refractive index contrast excited by plane waves, and directly computes reflected and transmitted diffraction orders, but requires extra steps for near-field reconstruction. FEM and FDTD can simulate both periodic structures with plane wave excitation and finite structures with open boundary conditions. Importantly, for light-emitting metasurfaces, point dipole excitation mimicking a nanoscale emitter is possible for these techniques.[96] Emission calculations for infinite periodic systems are not as straightforward, since periodic boundary conditions replicate a single emitter in the unit cell to an infinite coherent periodic set. For such systems a Floquet transformation is required, also known in the RF antenna community as the so-called "array scanning method."[97] Alternatively, reciprocity-based methods that relate fluorescence to absorption can be used, which are particularly powerful to simulate extended ensembles of incoherent emitters.[98]

Among the nanofabrication techniques, electron beam lithography (EBL) and focused ion beam milling (FIB) provide state-of-the-art nanoscale precision while preserving high flexibility, and were generally empowering research on metasurfaces over the last decade.[99] The key challenge for the fabrication of light-emitting metasurfaces is the integration of nanoscale emitters into the metasurface architecture. Typically, this is achieved either by fabricating the metasurfaces directly from light-emitting materials or by hybridizing passive metasurfaces with active materials post-fabrication. A typical materials choice for the first approach are direct bandgap semiconductors, including epitaxially grown structures incorporating quantum wells or quantum dots.[100] The latter approach can be achieved, e.g., by spin-coating the metasurfaces with nanoemitter or dye-containing polymers[100,101] or by depositing or chemically binding emitters such as QDs on the surface. 2D or layered active semiconductors are obtained from bulk crystals via exfoliation or grown directly by chemical vapor deposition (CVD). Among the integration techniques, one distinguishes dry and wet transfer as well as various strategies of direct integration.[68]

C. Future directions and outlook

While the field of light-emitting metasurfaces has witnessed significant progress to date, several challenges remain to be overcome to further develop the metasurface platforms for future practical applications. Here, we provide some suggestions for progress in this regard.

1. Materials and their integration

As light-emitting metasurfaces consist of two primary components, namely the metasurface itself and the nanoscale emitter, robust material platforms for both, as well as effective integration techniques are required. Importantly, high radiation efficiencies can only be obtained by using dielectric materials with minimal losses. With much of the recent research on passive metasurfaces resorting to a convenient implementation in silicon, metasurfaces made from wide-bandgap materials such as titanium dioxide (TiO_2), gallium phosphide (GaP), zirconium dioxide (ZrO_2), or lithium niobate ($LiNbO_3$) can be game-changers for the visible spectral range, which is of particular interest for applications of light-emitting metasurfaces.

Regarding the emitters, high quantum efficiency along with strong optical and thermal stability is desired. Importantly, for both metasurface and emitters, fitting the industrial needs and compatibility with electrical devices must be considered. Here, electrical driving schemes are of particular interest, considering that most research works on light-emitting metasurfaces still rely on optical pumping.

16 July 2024 09:29:41

© Author(s) 2024

As such, many hybrid material platforms and integration schemes remain to be explored. For example, fluorescent ions such as trivalent lanthanides could be doped into the constituent materials of the metasurface during the fabrication process or implanted afterwards using ion implantation.

2. Fabrication challenges

Apart from materials and integration, important challenges remain in terms of nanofabrication. First, *Q*-factors in low-loss quasi-BIC metasurfaces are currently limited by fabrication imperfections such as roughness.[102] Thus, it is highly desirable to further improve the structure quality to unlock a range of effects dependent on high *Q*-factors. Second, another grand challenge in terms of fabrication, especially regarding application perspectives, is scalability. While this holds for most metasurface applications, the challenge is even greater for light-emitting metasurfaces due to the need to integrate the active material. For example, although deep-UV photolithography has been proposed as a viable solution for complementary metal–oxide–semiconductor (CMOS)-compatible wafer-scale metasurface production,[103] light-emitting materials are usually not CMOS-compatible, requiring new approaches to be developed. For example, a combination of nanoimprint lithography and selective area sublimation has been proposed for large-scale production of GaN light-emitting metasurfaces.[104] Other alternatives may include, e.g., laser-induced transfer, suitable for creating large-scale periodic arrays of light-emitting nanoparticles.[105] Third, the precise and deterministic placement of the active material only at desired locations within the metasurface geometry still presents a challenge. This can be, e.g., the gap between two meta-atoms where the fields are significantly enhanced, asymmetric locations within the unit cell for beam-steering effects, or positions featuring specific local field characteristics such as chiral density. Suitable placement strategies may be adopted from the field of nanoantennas, with approaches relying on two-step electron-beam lithography showing particular potential for metasurfaces. The large areas that the metasurface spans also suggest that nanoimprint methods may be used to print emissive materials in a registry with meta-atoms if sufficiently precise spatial registration can be achieved.

3. Emission stability

A critical issue concerning a wide range of emitters, spanning from fluorescent dyes to QDs and perovskites is photobleaching, where the excess energy delivered during the excitation process results in the reduction of the emitted light intensity from the emitters over time. Photobleaching is attributed to both pumping conditions and intrinsic properties of the emitters. Therefore, an adequate emitter choice is crucial for minimizing sample photodamage. In this regard, interesting opportunities may be offered by highly stable emitters like nitrogen vacancies and nanodiamonds.[106]

4. Magnetic dipole transitions

The light–matter interaction in the optical frequency range mainly refers to the interaction of the electric field with electric dipolar (ED) electronic transitions. However, certain solid-state emitters, such as trivalent lanthanides and transition-metal-doped crystals, exhibit robust magnetic dipolar (MD)-dominated electronic transitions as a consequence of a selection rule forbidden ED transition.[107] Due to a strong optical magnetic response, all-dielectric metasurfaces were suggested as exquisite candidates for tailoring the fluorescence properties of MD transitions, opening an exciting pathway toward exploring magnetic light–matter interactions at the nanoscale[57,72] [see Figs. 5(l)–5(o)]. A particular challenge associated with commonly studied MD transitions is their slower radiative decay rate and consequently lower emission intensity compared to their ED counterparts. However, in a recent study, a significantly bright and fast optical-frequency MD radiation is identified in 2D hybrid organic-inorganic perovskites (HOIPs) such as butylammonium lead iodide (BA_2PbI_4).[108] It is shown that the MD radiative rate in such systems is up to 3 orders of magnitude faster than previously established MD transitions. Additionally, similar to trivalent lanthanides, 2D HOIPs exhibit spectrally separated ED and MD radiations. MD radiation properties, e.g., emission directionality of such emitters, can be engineered by integrating them with suitable nanophotonic platforms. Particularly, metasurfaces supporting high-*Q* resonances are elegant tools for enabling directional color and/or polarization routing of the emission from MD and ED transition channels. This opens new perspectives on realizing spectrometer-free, low-loss, and CMOS-compatible nanophotonic devices for imaging, sensing, and probing.

5. 2D materials and valleytronics

When dealing with 2D materials as active components, their ultrathin nature presents both advantages and drawbacks. Notably, it entails limited overlap with the excitation field, resulting in a low signal in absolute units. To address this, employing high-*Q* metasurfaces is needed to boost local pump field enhancements, while also being key for superior Purcell enhancements. A significant limitation of all valleytronic devices is the cryogenic temperature requirement due to the presence of phonon-assisted intervalley scattering that prohibits valley polarization under normal conditions. A promising avenue toward realizing non-zero valley polarization at room temperature involves the utilization of TMD-containing van-der-Waals heterostructures. These artificial materials can support a flurry of interesting effects and applications, one of them being that valley polarization can be augmented through mechanisms such as charge or spin transfer and other proximity effects. Adding to the general fabrication challenge, for realistic device applications methods for scalable and high-quality fabrication of 2D materials and heterostructures have to be developed. Here, the CVD-based phase engineering techniques can pave the way for novel heterostructures and junctions with unique electronic phases and customized properties.

6. Emerging trends in metasurface design

Regarding the design of light-emitting metasurfaces, a grand challenge is posed by the high computational demand of suitable approaches like those based on the reciprocity principle. These demands are typically higher than for other metasurface applications: the emission process needs multi-wavelength (optically pumped) and multi-physics analysis (including, e.g., electrical and thermal effects), coherent or incoherent summing over many source positions, and when translated by reciprocity into a scattering problem it involves a continuum of wave vectors. Finally, emissive devices such as LEDs often rely on metasurfaces in complex vertically stratified stacks.

16 July 2024 09:29:41

© Author(s) 2024

Generally in metasurface research, there is a growing preference for optimization algorithms over human-driven approaches due to their capability of efficient systematic investigation of parameters, as detailed in Secs. XVIII and XX. New, highly performing algorithms may thus prove especially useful for active architectures and help to come up with spatially variant architectures of unprecedented complexity or help to tackle specific design issues associated with the integration of emitters. For example, quasi-BICs can be engineered to suppress absorption losses, enabling, e.g., plasmonic-dielectric metasurfaces with theoretically arbitrary high Q-factors,[109] which can potentially lead to high-performance metasurface designs incorporating light-emitting and thus inevitably also absorbing materials.

7. High-power applications

To be competitive as commercial light sources, metasurfaces must reach specific performance values. A challenge for high power applications, such as LEDs is the required combination of high emitter density, high emitter efficiency, and resistance to photobleaching and thermal load. Inherent to the process of emission is that the Stokes shift energy is dissipated as heat, often meaning 0.5–1 eV of dissipated energy for every emitted photon. For example, a metasurface-based LED should withstand of order 1 A/mm^2 input current while maintaining power-to-photon conversion and power handling capacity sufficient for providing 1 W/mm^2 emission intensity. These goals require proper material engineering to obtain sufficiently bright and photostable emitters—the associated dissipated power, or in the case of a color converting layer, the Stokes-energy loss in such systems is also of order 1 W/mm^2. For metasurface lasers, it is important to realize that a very high benchmark is set by III–V surface-emitting lasers that provide continuous-wave output power on the level of 100 W and brightness $>$1 GW/cm^2/sr at power-to-photon conversion $>$0.5 W/A, while maintaining decent beam quality (M^2). This typically requires large-area single-mode operation, which is particularly challenging for metasurfaces. However, the above figures have recently been approached by photonic crystal surface-emitting lasers.[110]

8. Tunable light sources

In addition to simple light sources, many of the emerging applications of light-emitting metasurfaces, such as LiFi, LIDAR, AR/VR, require a reliable way of tuning the emission. In that regard, LCs and MEMS are the most mature technologies, which are also CMOS-compatible and therefore suitable for large-scale and low-cost production.[89,90] Both approaches can offer a large modulation depth while providing a modulation speed that is sufficient for most commercial uses. However, direct integration of MEMS and LCs for specific applications of light-emitting metasurfaces remains to be developed.

9. Topological, non-Hermitian, and temporal effects

In addition to the real-world applications, the research on light-emitting metasurfaces continues to explore unconventional directions such as nontrivial topology,[111] non-Hermitian physics/parity-time (PT) symmetry,[112] and temporal photonics.[50] Topological robustness enables various systems (including, e.g., photonic topological insulators, BICs) to exhibit fragile properties regardless of imperfections, which has been studied especially in the context of large-area single-mode lasing.[113] Photonic systems with gain and loss can support non-Hermitian features known as exceptional points (EPs), which can be used to control the directionality and polarization of emitted light.[54] In temporal photonics, sufficiently fast time modulation can give rise to exotic physical phenomena related to light emission and lasing, such as new mechanisms of light amplification.[114] Currently, the concepts of topological, non-Hermitian, and temporal photonics remain mainly at the level of fundamental research. However, in the future, some of these concepts may revolutionize the field of light-emitting metasurfaces, enabling unprecedented performance and novel functionalities.

D. Concluding remarks

Light-emitting metasurfaces represent a cutting-edge area of research in nanophotonics, offering dynamic control over the properties of emitted light from the incorporated nanoscale light sources. Furthermore, thanks to recent developments in the field of nanofabrication and material processing, light-emitting metasurfaces hold great promise for a wide range of practical applications from advanced displays and communication systems to imaging devices, sensors, and beyond. Although challenges such as energy efficiency and integration with existing technologies need to be addressed to reach their full potential, the ongoing research and development in this area lead us to expect a bright future for advanced light-emitting metasurface devices with novel functionalities as well as their integration into real-world applications. Finally, metasurfaces also offer a unique platform for future scientific applications investigating fundamentally new directions in the area of light emission.

ACKNOWLEDGMENTS

I.S., A.B., and Z.F. acknowledge financial support from the Deutsche Forschungsgemeinschaft (DFG, German Research Foundation) through the International Research Training Group (IRTG) 2675 "Meta-ACTIVE," Project No. 437527638, and through the Emmy Noether Program, Project No. STA 1426/2-1. The work of A.F.K. is part of the Dutch Research Council (NWO) and was performed at the research institute AMOLF. R.K. acknowledges the support of the Research Council of Finland (Grant Nos. 347449 and 353758).

III. NONLINEAR OPTICAL METASURFACES

Xiaofei Xiao, John Yang, and Rupert. F. Oulton*

*r.oulton@imperial.ac.uk

A. Introduction

The field of nonlinear optics, emerging in the 1960s alongside lasers, explores light–matter interactions under extreme light intensities.[115] Effects, such as harmonic generation, three- or four-wave mixing and parametric amplification, have expanded the operational bandwidth of coherent light sources from the extreme ultraviolet to terahertz and produced methods to measure and control light on ultrafast time scales. Applications extend to quantum optics, where parametric downconversion and spontaneous four-wave mixing produce correlated and entangled photon pairs for quantum enhanced sensing, imaging and computing.[116–121]

16 July 2024 09:29:41

© Author(s) 2024

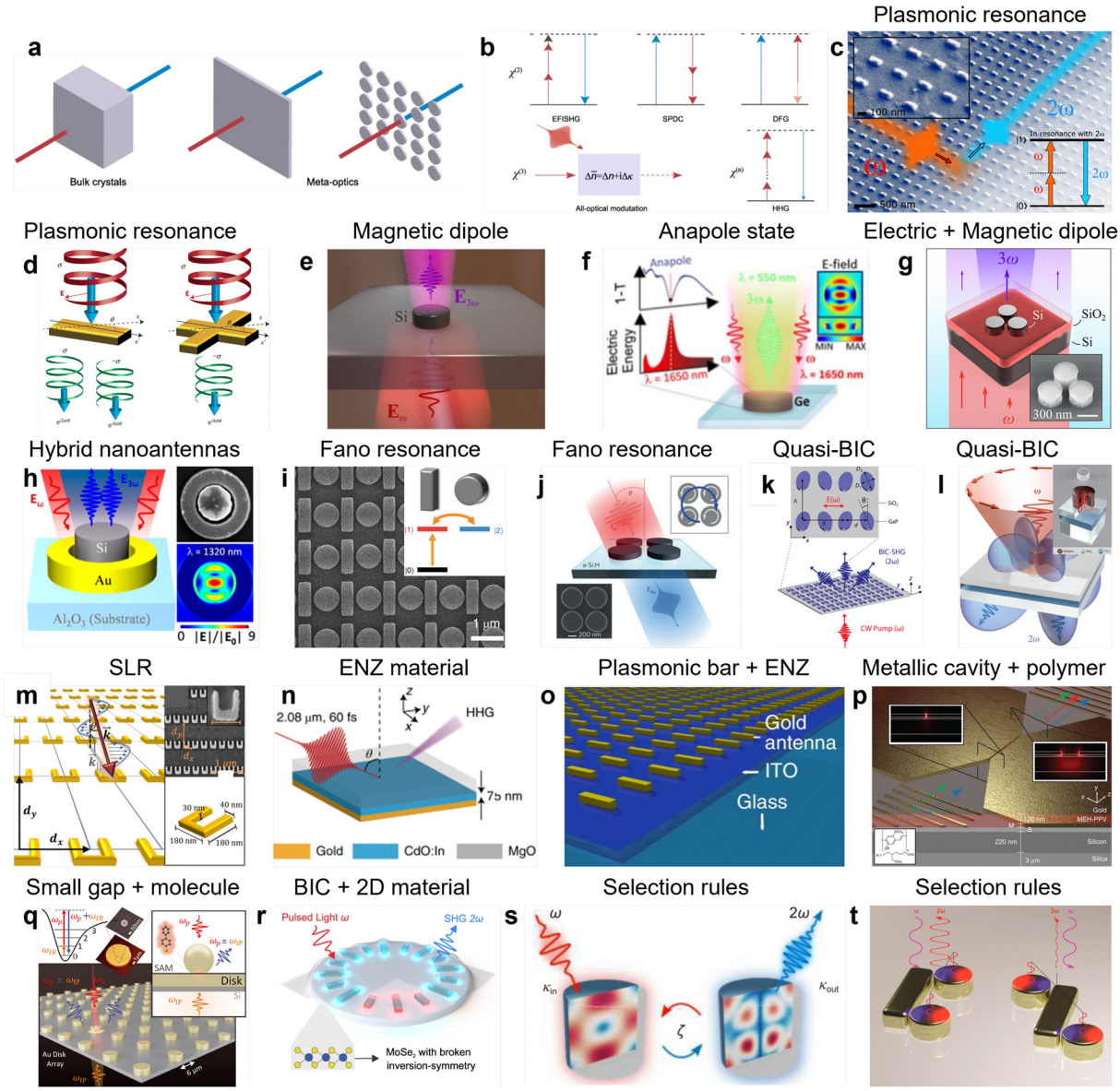

FIG. 6. The variety of mechanisms used in nonlinear optical metasurfaces. (a) Comparison of nonlinear optical medium based on conventional bulk crystals and meta-optics.[142] (b) Representative nonlinear optical processes where meta-optics may have unique advantages.[142] (c) Illumination of strong enhancement of SHG based on plasmonic resonances in an aluminum nanoantenna array.[143] (d) Illustration of the continuous geometry-phase-controlled nonlinear harmonic responses of individual metal nanostructures in plasmonic metamaterials.[144] (e) Schematic of enhanced THG in Silicon nanoparticles driven by magnetic response.[145] (f) Enhanced THG in individual Ge nanodisks excited at an anapole state.[146] (g) Illustration of THG in Si nanodisk trimers and its SEM image.[147] (h) Schematic of efficient THG enhanced by metal-dielectric hybrid nanoantennas.[148] (i) Enhanced high-harmonic generation from an all-dielectric metasurface made of dipolar bar antennas and disk resonators on a sapphire substrate. Inset: level scheme for the mode coupling in a schematic three-level Fano-resonant system.[149] (j) Illustration of the Fano-assistant THG from silicon quadrumers of four a-Si:H nanodisks with SEM image of the sample in the bottom left corner.[150] (k) Illustration of continuous wave SHG enabled by quasi-BIC on gallium phosphide metasurfaces.[151] (l) Illustration of the BIC-assisted SHG in a single nanoresonator under azimuthally polarized vector beam excitation. Inset: SEM and schematic of an individual dielectric nanoresonator.[152] (m) Illustration of enhanced SHG based on SLR in plasmonic nanoparticle arrays. Inset: SEM image and dimensions of each structure.[138] (n) Schematic of high-harmonic generation from an ENZ-assisted sample composed of a MgO substrate, CdO thin film and gold capping layer.[153] (o) Large optical nonlinearity in ENZ material (A 23-nm-thick indium tin oxide (ITO) layer) enhanced by coupling with plasmonic (gold) nanoantennas.[154] (p) Schematic of efficient four-wave mixing based on nanofocusing in a silicon hybrid gap plasmon waveguide. Inset: electromagnetic mode distributions and the chemical formula for MEH-PPV.[124] (q) Illustration of dual-wavelength antenna and frequency upconversion using BPT molecules in a 1.3 nm nano-gap between Au nanoparticle and disk. Inset: schematic of upconversion process, AFM (disk) and SEM (nanoparticle) images.[155] (r) Schematic of radial BIC-enhanced SHG in a $MoSe_2$ monolayer covering the ring structures.[156] (s) Illumination of SHG in a leaky cavity by considering the input (output) coupling coefficient and the spatial overlap between the dominant modes.[157] (t) The interplay of symmetry and scattering phase in SHG from gold nanoantennas.[158] All images are reprinted (adapted) with permission from the respective Journal and copyright remains with the original publisher.

16 July 2024 09:29:41

© Author(s) 2024

Nonlinear processes such as harmonic generation and four-wave mixing can be remarkably efficient when beams being mixed propagate in phase over many millimeters of interaction in a nonlinear crystal. Phase-matching brings material and technical restrictions as it comes at the cost of reduced tuning range and material flexibility. For example, phase-matching may only be achieved at specific wavelengths and temperatures and the large interaction lengths require low absorption. For some photonic applications, new nonlinear materials that can be integrated with the most relevant photonic platforms are important, such as polymers[122–124] and 2D materials.[125–128] Nonlinear optical metasurfaces also hold promise for addressing these challenges [Figs. 6(a) and 6(b)]. First, optical nanostructures can be designed at the nanoscale to enhance local fields and meet symmetry requirements to produce strong nonlinear effects, as we discuss in detail below. Second, nonlinear metasurfaces do not use phase-matching but instead rely on their high intrinsic nonlinearity to produce a useful nonlinear effect. This alleviates tuning, bandwidth and material absorption restrictions. Third, nanostructured metasurfaces can be integrated with a wide variety of nonlinear materials to further strengthen their intrinsic nonlinearity. Finally, their engineered nature allows for nonlinear wavefront control. These design features have led to a burgeoning field of nonlinear metasurfaces.

In this perspective, we present the state-of-the-art in nonlinear photonic metasurfaces, by reviewing the rich variety of mechanisms to engineer a nonlinear response at the nanoscale. Before considering future directions for this field, we present a short study of how the metasurface interaction area affects nonlinear mixing efficiency as a function of incident beam powers and areas. To conclude, we identify the most useful metrics for assessing nonlinear metasurface performance and future direction this field might take.

B. State of the art

Resonances play a crucial role in nonlinear optical metasurfaces, since the linear optical response often dictates the nonlinear one.[129] The relationship between linear and nonlinear susceptibilities is well known,[115] but are not often utilized in phase-matched processes due to the constraints of absorption on interaction length. However, thin metasurfaces can utilize resonance to produce strong nonlinearities. Through structural resonances, metasurface can also enhance the electric and magnetic fields of incident light. These are usually categorized into local and collective resonances.[130] Local resonances, such as surface plasmons,[131] Mie modes of metallic and dielectric nanoparticles,[132,133] and Fano resonances,[134,135] utilize nanostructures that operate independently across the metasurface, while collective resonances, such as guided-mode resonances,[136,137] surface lattice resonance,[70,138,139] and bound states in the continuum[140,141] (BIC), access mutual coherences between nanostructures.

1. Local resonance—surface plasmons

Localized surface plasmon resonances (LSPR) are collective oscillation of free electrons in metal nanoparticles (typically gold or silver) excited by incident light, where resonance is controlled via size, shape, and particle composition. When integrated into metasurfaces, these resonances enhance second harmonic generation (SHG)[143] [as shown in Fig. 6(c)] as well as a range of mixing effects[53,158–160] including third harmonic generation (THG), four-wave mixing, and sum frequency generation, due to their ability to provide strong local light field enhancement. Wavefront control has also been shown [Fig. 6(d)] using the globally varied local nonlinear harmonic response of gold nanoantennas of C3 and C4 rotational symmetries, respectively.[144] Although metal provide excellent confinement, the high nonlinearity of the metal is difficult to use, since metals do not easily admit electric fields—this means interaction volumes are relatively small. Simple plasmonic resonances also provide relatively weak local field enhancement and structures with sharp features and gap that do enhance fields have low damage threshold.[132,161] For example, typical quantum efficiencies of SHG are $\sim 10^{-9}$.

2. Local resonance—Mie and multipolar modes

Metasurfaces made of high refractive index dielectrics, such as silicon, germanium, and gallium phosphide, have emerged recently as a competitive alternative to plasmonic metasurfaces, due to low material loss, larger interaction volumes and the capability to engineer their magnetic response. Their efficiencies compared to plasmonic metasurfaces show improvement by several order of magnitude, mainly due to the higher damage threshold (see Sec. III C).[151,162] These metasurfaces use Mie resonances to control the nonlinear interaction. Although they exhibit some ability to enhance optical fields, the larger interaction volume provides the largest benefit.

Individual Mie resonance modes,[132,135,145] such as electric, magnetic dipoles, and higher-order Mie resonances, have been explored individually to enhance nonlinear conversion efficiency beyond plasmonic metasurfaces.[132,133,163,164] For example, Fig. 6(e) shows that THG conversion efficiency in silicon nanodisks is enhanced by magnetic dipole resonances by two orders of magnitude compared to bulk silicon.[145]

To increase the performance further, resonant coupling is often used. Interference of multiple Mie resonances may result in far-field destructive interference, consequently enhancing the nonlinear effect. For example, the anapole state, associated with the destructive interference of dipole and toroidal moments, suppresses scattering to produce near-field enhancements.[165] Both fundamental and a higher-order anapole states in individual all-dielectric nanodisks have been implemented.[146,166,167] Figure 6(f) shows a fundamental anapole state in a single Ge nanodisk for THG.[146] Here, a minimum in extinction cross section corresponds to a maximum electric energy within the material, producing THG quantum efficiencies as large as 10^{-6}. Coupled resonators also provide stronger nonlinear responses through their mutual coupling.[168–171] For example, Fig. 6(g) shows a nanotrimer of three silicon nanocylinders that improves THG via the interference of electric and magnetic dipoles.[147]

The nonlinearity of nanostructures can be further improved by combining the confinement capabilities of metallic resonances and the interaction volume and radiative control of dielectric resonances.[172,173] For example, the plasmonic resonance of a Au nanoring around a Si nanodisk supporting an anapole state[148] [Fig. 6(h)] shows THG quantum efficiency as high as 10^{-4}.

3. Local resonance—Fano interference

Fano resonance arises from the interference between a broad continuum of states and a narrow discrete resonance.[134] In metasurfaces, this can be realized through the coupling of plasmonic elements with a

16 July 2024 09:29:41

© Author(s) 2024

continuum of modes, leading to asymmetric line shapes and sharp spectral features. The intense and localized electromagnetic fields associated with Fano resonances can greatly boost nonlinear frequency mixing processes.[149] Figure 6(i) shows enhanced high-harmonic generation from an all-dielectric metasurface,[149] where non-perturbative high-harmonic generation is enhanced in a Fano-resonant Si metasurface. Figure 6(j) shows magnetic-Fano-resonance enhanced THG signal via interplay between collective and individual optically induced magnetic responses in quadrumers made of identical dielectric nanoparticles.[150] Plasmonic nanostructures show similar nonlinear enhancements.[169,174] We note nonlinear generation enhanced by Fano resonances are usually anisotropic with respect to the excitation polarization and have narrow operation bands due to their resonant nature.

4. Collective resonance—bound states in the continuum

Collective high-Q resonances in all-dielectric metasurfaces, such as bound states in the continuum (BICs) can offer large improvements in nonlinear metasurface response. BICs are eigenstates of a system that exist within the continuum but do not radiate energy into the surrounding space. They were initially introduced in quantum mechanics and later extended to photonics.[71,140,141,175,176] Mathematical BICs may have vanishing resonant linewidths. In practice, due to finite sample size, material absorption, small amount of radiation leakage, and structural imperfections, BICs manifest with reasonably large Q factors, known as quasi-BICs. The long lifetimes of quasi-BICs are highly desirable for concentrating light in time and thus the nonlinear optical process.[177,178] Figure 6(k) shows SHG in a dielectric (gallium phosphide) metasurface enhanced by two asymmetric cylinders with quasi-BIC resonances.[152]

Quasi-BICs can also be engineered as individual local resonators by exploiting the interference of several Mie modes, similar to the anapole state discussed earlier.[146,166,167] For instance, AlGaAs cylinders placed on an engineered three-layer substrate (SiO_2/ITO/SiO_2) show suppressed radiative losses, as shown in Fig. 6(l), boosting SHG efficiency.[151]

5. Collective resonance—surface lattice resonance

Surface lattice resonances (SLR) also achieve high Q-factors. When a grating Rayleigh anomaly condition crosses a LSPR, a sharp spectral feature occurs, due to the hybridization of the surface and localized resonances.[70] The SLR feature is controlled via nanostructure shape and lattice parameters. The effect of SLRs at the fundamental[139] and the generated nonlinear modes[138] has been studied for boosting the nonlinear optical response.[179] Figure 6(m) shows SLRs used to enhance SHG from a plasmonic nanoparticle array made of split-ring resonators[138] where the SHG intensity improved more than a thirty-fold. Nonlinear metasurfaces based on both localized and collective plasmonic resonances have also enabled the generation of controllable terahertz waves,[180,181] using mechanisms like ponderomotive acceleration of photo-ejected elections[182] and optical rectification.[183]

6. Material resonance—epsilon near zero materials

At the boundary between metals and dielectrics, the nonlinearity of materials with epsilon-near-zero (ENZ) points have also been studied[184–188] (see Sec. XVII). Where ENZ occurs, the surface normal electric field of incident light diverges when the imaginary part of the permittivity approaches zero. This produces field enhancements inversely proportional to ENZ film thickness[189] that boost nonlinear effects.[184–188] Their unique nonlinear optical response and the required deep sub-wavelength thickness of the ENZ film also makes them appealing for high-harmonic generation.[153] Indium-doped cadmium oxide thin films (75 nm) show harmonic generation up to the ninth order,[153] as shown in Fig. 6(n). More on these materials is presented in Sec. XVII of this roadmap. Figure 6(o) shows a metasurface combining plasmonic antennas with an ENZ material.[154] Here, the narrow spectral range and ENZ position of the underlying ENZ material could be engineered to significantly boost the nonlinear optical response.

7. Integrating metasurfaces with nonlinear materials

In attempts to maximize the nonlinearity of metasurfaces, researchers have integrated nonlinear materials with metasurfaces to exploit both material and structural resonances. For example, a 100-path spontaneous parametric downconversion photon-pair source was created by integrating a metalens array (10×10 array of GaN nanopillars) with a β-barium borate (BBO) nonlinear crystal.[190] Another example uses low-loss nonlinear polymer within nanoplasmonic systems.[124,191–193] Figure 6(p) shows efficient four-wave mixing over micrometer-scale interaction lengths at telecommunications wavelengths on silicon can be achieved by combining an integrated plasmonic gap waveguide with a nonlinear organic polymer. Similar ideas have been used to focus light into a nanoscale cavity to enable frequency upconversion from Mid infrared to visible,[155,194] via molecular vibrations [Fig. 6(q)]. Highly resonant BIC metasurfaces may also be integrated with highly nonlinear materials. Figure 6(r) shows a radial BIC was used to boost SHG from monolayers of transition metal dichalcogenide.[156] This brings two advantages: the two-dimensional materials are straightforward to integrate within metasurfaces and their atomic thickness minimizes the deformation of the resonance.

8. Nonlinear metasurface selection rules

Finally, we briefly consider the tensorial nature of non-linear interactions and their corresponding selection rules. Local field enhancement and resonances are not alone sufficient for strong nonlinear effects to be achieved. The non-linear polarization created by pump light in a metasurface must also be able to radiate to the far field to complete the nonlinear process. This requires that the nonlinear tensor components of the metasurface be matched to the desired input and output beams. Moreover, the interaction of the input and output beams with the metasurface should be optimized by both impedance matching, and spatial mode overlap at the various interacting frequencies.[151,195,196] Ideally, the suppression of all radiation channels apart from those for power injection and extraction has been proposed to increased coupling to and from the metasurface,[157] as schematically shown in Fig. 6(s). Indeed, this has been experimental investigated both in plasmonic[158] [as shown in Fig. 6(t)] and all-dielectric[145,197,198] metasurfaces.

C. Nonlinear generation rate and efficiency

Conventional nonlinear materials produce large conversion efficiencies by mediating nonlinear processes over a large interaction

16 July 2024 09:29:41

© Author(s) 2024

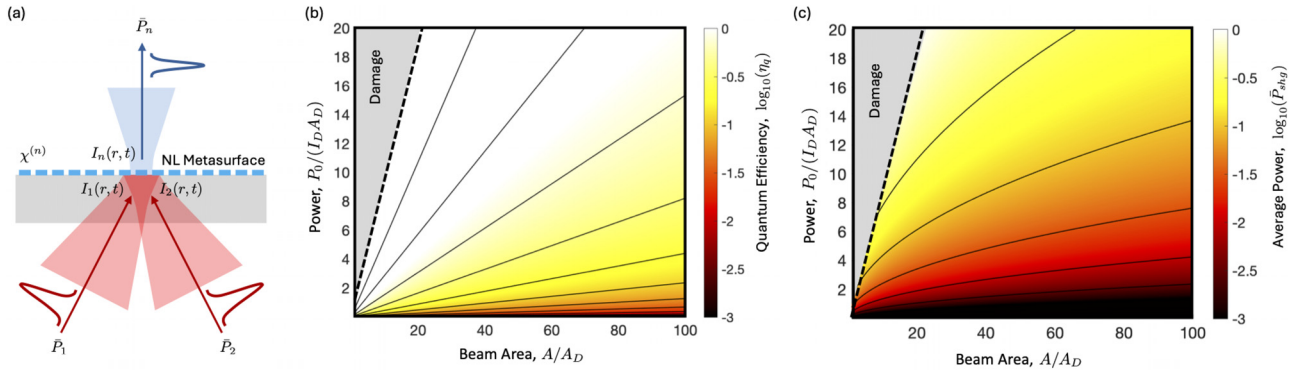

FIG. 7. Nonlinear generation rate and efficiency. (a) Schematic of a nonlinear process at a metasurface involving multiple incident beams and a generated output beam. The conversion process is determined by incident beam powers and the peak intensities that can be achieved at the metasurface. (b) Map of SHG quantum efficiency in log scale as a function of normalised pump power and mode area. Linear contours passing through origin have gradient of intensity. The broken line represents the damage threshold intensity. (c) Map of SHG average power as a function normalised power and mode area. SHG power is maximised at the highest powers along the damage threshold intensity line. The SHG efficiency and average power are normalised to the maximum value.

volume.[115] Thus, large area metasurfaces should produce the highest nonlinear generation rates. To elaborate on this, consider the following analysis of nonlinear frequency mixing at a metasurface.

An nth order nonlinear process is affected by up to n input beams. The ith Gaussian optical pulse intensity in time (t) and space (r) at a metasurface ($z=0$), $I_i(r,t) = P_i/A_i e^{-\pi r^2/A_i - t^2/\tau_i^2}$, where P_i is the peak power, $A_i = \pi w_i^2/2$, is the beam area (w_i is beam waist) and τ_i is the pulse duration. This arrangement is shown in Fig. 7(a). The process generates a nonlinear polarization, $\underline{\mathscr{P}}_n = \underline{\chi}^{(n)} \prod_{i=1}^{n} \underline{E}_i(r,t)$, where $\underline{\chi}^{(n)}$ is the nth order nonlinear susceptibility tensor and $\underline{E}_i(r,t)$ are the mixed electric fields.[115] In most optical metasurfaces, the interaction length is $\ll \lambda$, so that the generated beam intensity is $I_n = \alpha_n \prod_{i=1}^{n} I_i(r,t)$, where α_n is introduced to represent the *intrinsic nonlinearity* of the metasurface. Here, we assume only simple in-plane tensor connections between the input and output beams. (Out-of-plane components generate non-Gaussian beams.) Substituting for the intensities of the mixing and output beams, we find,

$$\frac{P_n}{A_n} e^{-\pi r^2/A_n - t^2/\tau_n^2} = \alpha_n \prod_{i=1}^{n} \frac{P_i}{A_i} e^{-\pi r^2/A_i - t^2/\tau_i^2}. \tag{1}$$

To simplify further, we assume the incident beams have comparable mode area, A_0, and pulse duration, τ_0, so that $\sqrt{n}\tau_n = \tau_0$ and $nA_n = A_0$ at the metasurface. Since we assess nonlinear generation with time averaging detectors, we use the average beam power as a measure of nonlinear conversion, $\bar{P}_n = P_n \Omega \tau_n$, where Ω is the laser repetition rate. Thus, we find the average emission power in terms of the average incident beam powers, $\bar{P}_i$,

$$\bar{P}_n = \frac{\alpha_n}{n\sqrt{n}[A_0 \Omega \tau_0]^{n-1}} \prod_{i=1}^{n} \bar{P}_i. \tag{2}$$

This expression is valid for nth-harmonic generation (nHG), where $\prod_{i=1}^{n} \bar{P}_i = \bar{P}_0^n$. In the case of four wave mixing, for example,

$$\bar{P}_{fwm} = \frac{\alpha_3}{3\sqrt{3}[A_0 \Omega \tau_0]^2} \bar{P}_p^2 \bar{P}_s, \tag{3}$$

where $\bar{P}_p$ and $\bar{P}_s$ are average powers in the pump and signal beams, respectively. Average photon generation is improved for pulsed pumping over CW by a factor $[\sqrt{n}\Omega\tau_0]^{1-n}$, but the advantage does not apply to peak powers. In this analysis, we assume that $\Omega\tau_0$ is fixed, and we instead concentrate on the influence of beam power and area. We also focus on SHG for simplicity. SHG efficiency is assessed against two common metrics in the literature. The first efficiency, $\eta_p = \bar{P}_{shg}/\bar{P}_0^2$, is chosen since it is independent of pump power by definition, where $\eta_p = \alpha_n/[2\sqrt{2}A_0\Omega\tau_0]$. The second efficiency, $\eta_q = \bar{P}_{shg}/\bar{P}_0 = \eta_p \bar{P}_0$, is a power dependent quantum efficiency.

These SHG efficiencies are both influenced by mode area, A_0, and pulse duration, τ_0. Clearly, the best conversion rates occur when the incident average pump power is high and the mode area and pulse duration are small. Inevitably, SHG is limited by the damage threshold intensity of a metasurface, I_D. In our experiments with plasmonic metasurfaces using near diffraction limited beams from either mode-locked oscillators ($\Omega = 80$ MHz, $\tau_0 = 150$ fs) or continuous wave lasers, we have found damage occurs at about 5 mW average power. For a diffraction limited area of 0.25 μm^2, $I_D \sim 10^{11}$ W cm^{-2} for pulsed operation and $I_{D,cw} \sim 10^6$ W cm^{-2} for CW. Damage here is due to sample heating, and so the lower repetition rates of amplified laser systems can allow higher intensities. Dielectric metasurfaces have slightly higher damage threshold intensities than plasmonic one, but are not immune to damage at intensities $I_D > 10^{12}$ W cm^{-2} where ionization effects occurs. We note that at these intensities, non-perturbative nonlinear process start to emerge, and the preceding analysis requires reevaluation.

The quantum efficiency and average SHG power are plotted in Figs. 7(b) and 7(c) as a function of normalized power and mode area. Along the power axis, normalization against both I_D and diffraction limited mode area, A_D, leaves the axis dimension-less. Likewise, we have also normalized the beam area against A_D. [We assumed a pump wavelength, $\lambda = 1\mu$m with a diffraction limited mode area: $A_D = \pi(0.41\lambda)^2$.]

The power independent efficiency, η_p, might seem like the most appropriate metric, but it predicts optimal conversion efficiency at low

16 July 2024 09:29:41

© Author(s) 2024

beam area. Indeed, this is where the nonlinear effect is strongest, since the beam intensity is maximized. However, the scaling of SHG with pump power squared suggests that large mode areas and high pump powers should produce optimal SHG. The quantum efficiency proves to be a more useful metric; although it varies with pump power, it can be evaluated in a way that is independent of both beam area and pulse duration, $\eta_q = \alpha_n \bar{P}_0/[2\sqrt{2}A_0\Omega\tau_0] = \alpha_n I_0/[2\sqrt{2}]$. As shown in Fig. 7(b), contours of η_q are linear and pass through the origin, so the gradient gives the intensity. If the damage threshold of the metasurface is known, its limiting performance can be completely specified at any power and beam area.

Figure 7(c) shows a plot of average SHG power as a function of average pump power and beam area. The plot confirms that optimal SHG occurs when the pump power is maximized and the mode area is minimized to operate at the damage threshold intensity. This power-area scaling presents challenges for applications of metasurfaces. The write field of electron beam lithography is typically $100 \times 100\ \mu m^2$, representing an upper limit on metasurface area. A beam area of $10^4\ \mu m^2$, at damage threshold intensity requires an average beam power of ~ 100 W!

D. Future directions of nonlinear optical metasurfaces

Metasurfaces cannot compete with phase-matched nonlinear processes in terms of efficiency, and the power-area analysis above suggests there are a few routes forward. Metasurfaces offer strong resonant nonlinearities, wave-front control and the possibility to integrate new materials. In this final section, we review applications in wave-front control, optical switching, and accessing non-perturbative nonlinear physics at reduced power.

1. Metasurfaces for nonlinear wave-front control

The capability to locally engineer optical nonlinearity in metasurfaces provides the means to engineer local nonlinear phase. Here, subwavelength nanostructures are tailored to control the phase and amplitude and direction of the nonlinear polarization.[2,199,200] Recently, nonlinear wavefront control has been demonstrated using plasmonic[144,201,202] and all-dielectric[203,204] nanostructures with specific structural symmetries from the extreme ultraviolet to terahertz.[53,180,181,205] Beam shaping based on binary nonlinear phase and holography based on continuous nonlinear phase have been demonstrated by nonlinear optical wavefront engineering techniques.[144,206,207] Currently, there are a few studies in this area and with the attention being dedicated to controlling local nonlinear phase, conversion efficiencies are relatively low. Additionally, wavefront engineering techniques for various optical beams,[53,208] such as multiple optical vortex beams (Sec. VII), have been realized using linear optical metasurfaces. Transferring these techniques developed for linear optical metasurfaces into the nonlinear regime will open a new avenue for the realization of compact and ultrafast nonlinear optical devices.

2. Metasurfaces for modulation and switching

Although nonlinear metasurfaces open new avenues in flat nonlinear optics, the majority cannot be actively tuned post-fabrication despite this being a key feature in some linear metasurfaces (see Secs. II, XIV, and XV). Dynamic control over nonlinear metasurfaces under external stimuli is highly desirable in future. The mechanisms of the tunability include but are not limited to thermo-optic effects, free-carrier effects, and phase transitions.[209] The electrical modulation of a nonlinear response based on electric-field-induced SHG or optical rectification has been investigated in both plasmonic or dielectric metasurfaces.[210–214] While this research direction is in its infancy, there are clear opportunities that play to the strengths of metasurfaces: thin films can be electrically accessed and modulated and resonant nonlinearities are more amenable to tuning with stronger modulations in material parameters.

3. Reduced power non-perturbative nonlinear optics

The intrinsic nonlinearity of materials is measured by the nonlinear susceptibility,[115] $\chi^{(n)}$. For example, SHG is governed by the value of $\chi^{(2)}$ and naturally transparent crystals have $\chi^{(2)} \sim 1$–100 pm V^{-1}. When multiplied by incident electric fields of light, the dimensionless product indicates nonlinear strength. For an n-order process, the dimensionless parameter $\chi^{(n)}|E|^{n-1}$ is a metric of nonlinearity. For example, SHG with 1 W of CW light over a $10^4\ \mu m^2$ beam area, has $\chi^{(2)}|E| \sim 10^{-8}$–$10^{-6}$. Meanwhile, strong nonlinear effects occur for $\chi^{(n)}|E|^{n-1} \sim 1$, where the perturbation description of the nonlinear polarization breaks down. Achieving this condition requires either more intense light or a more nonlinear material. For example non-perturbative effects such as high harmonic generation occur at intensities $I > 10^{13}\mathrm{Wcm}^{-2}$ in gases, and slightly lower in solids. While amplified pulsed lasers can access non-perturbative intensities, lowering the intensity at which non-perturbative effects begin is appealing for reducing cost, complexity, size, weight and power. The increased nonlinearity of metasurfaces are a promising route.

Nanostructures have been used to control non-perturbative high harmonic generation effects both in isolated structures[215–219] and metasurfaces.[149,220–224] High-harmonic generation has also been shown in ENZ based metasurfaces.[165] Such applications play to the strengths of metasurfaces and would enable an expansion of research teams able to study non-perturbative nonlinear physics across different disciplines by mitigating the need for expensive and bespoke laser systems. Metasurface nonlinearity can be extremely large: to our knowledge, $\chi^{(2)} = 1.2\ \mu m\ V^{-1}$ is the highest nonlinear response reported for a metallic metasurface coupled to inter-sub-band quantum well transitions in the mid-infrared,[52,225] yielding $\chi^{(2)}|E| \sim 1$ under CW illumination. Such giant nonlinear responses have been seen in metasurfaces combining both electromagnetic and material resonances.

IV. METASURFACES FOR BIOSENSING

William J. Peveler and Alasdair W. Clark*

*Alasdair.Clark@glasgow.ac.uk

A. Introduction

The advancement of technologies for the rapid and sensitive detection of biological macromolecules (e.g., nucleic acids, proteins, glycans) and whole organisms (e.g., viruses, bacteria, and other pathogens), are crucial to furthering our understanding of biological systems, to the development of new diagnostic tests and healthcare tools, to improved drugs and therapeutics, and for ensuring the safety of our food and water supplies. Therefore, as new developments are made in materials science, one of the first application areas of these new materials is often sensors. This is also true of nanophotonic metasurfaces.

16 July 2024 09:29:41

© Author(s) 2024

Indeed, metasurface biosensors have emerged as one of the most notable success stories in the field of nanoscale metamaterial research, transitioning quickly from an academic curiosity to practical, commercial sensing devices that are having impact in medical diagnostics, environmental monitoring, and pharmaceutical research. The term "nanophotonic metasurface" relates to devices comprised of two-dimensional arrangements of nanoscale building blocks (meta-atoms), whose collective optical properties are derived from their rational design and engineered array properties, rather than purely from their chemical composition.[199] These surfaces can be constructed using metallic or dielectric meta-atoms which have optical resonance properties defined by their size, shape, composition, spacing, and crucially for biological detection, the refractive index of their local surroundings.[226] Therefore, their resonances properties can be altered by individual biomolecules interacting with their surface. The nanoscale nature of the meta-atoms mean they are often of comparable size to these biomolecules, meaning that even single-molecular localization on a meta-atom surface can produce resonance shifts easily measurable in the far-field by simple white light illumination; shifts that can also provide information on interaction kinetics between molecules.[227] Resonant meta-atoms are also able to confine light to extremely small volumes, producing many orders of magnitude enhancement to the electric field around certain facets of the nanostructure (e.g., at sharp corners and inside small gaps). Since many vibrational spectroscopy techniques have efficiencies that scale with electric-field strength, the signals recorded from molecules within these enhanced regions is greatly improved. These two aspects of resonant meta-atoms make them excellent candidates for applications where label-free, hyper-sensitive detection is required, and for applications where the interaction strength between pairs of molecules is being assessed. It has been possible to produce structures with bespoke optical properties for decades, but recent strides in fabrication technology have greatly improved the efficiency, speed, and cost-effectiveness of producing metasurface sensors. Coupled with their ease of excitation (e.g., illumination with incandescent light bulbs, LEDS, laser diodes, etc.) and the low complexity of their optical measurement, these advancements pave the way for portable, low-power, point-of-care, and field-deployable sensing solutions. In this brief roadmap we will cover a small number of research developments in the field of metasurface biosensors (some of which appear in Fig. 8), and provide our outlook on what the future of this fast-moving field may hold.

B. Biosensors: Plasmonic vs dielectric

Metasurface biosensors can be broadly categorized in two groups: plasmonic (where meta-atoms are metallic) and dielectric (where meta-atoms are, typically, silicon). Plasmonic metasurfaces exploit localized surface plasmon resonances (LSPR), a nanoscale variant of the long-established biosensor technology of surface plasmon resonance (SPR).[1] Instead of generating surface plasmons that propagate along the air-metal interface of bulk, thin-film metals (as in SPR), LSPR is generated by the oscillatory interaction of light with the free electrons in the metal nanostructures. These structures are smaller than the wavelength of the exciting light, producing resonantly driven, highly localized electric fields. In contrast to SPR devices, LSPR metasurfaces require no special coupling schemes, meaning they are trivial to excite, and produce fields with very short decay lengths (only probing their immediate surroundings[228]—i.e., *bound molecules, not molecules in the bulk*), meaning they are not thrown off by environmental fluctuations (e.g., temperature). While plasmonic nano-resonators are decades old, new research into dielectric resonators is revealing key advantages. Metallic metasurfaces suffer from high losses, strong dispersion, and poor magnetic response, whereas dielectric resonance, the result of Mie resonances which generate oscillating displacement currents in response to the driving field polarization, exhibit low loss, sharper bandwidths, little heating, and can support strong magnetic dipoles.[229] Despite their different resonance mechanisms, the outcomes are similar: nanostructures, resonantly driven by light, with properties tunable by altering their geometry, and which are either sensitive to their surroundings (i.e., the presence of a biomolecule), or that produce a highly localized electric field that can be used to enhance existing sensing techniques. In terms of sensor production, both wide-area, relatively inexpensive techniques, like colloidal lithography, and smaller-area, relatively slow, more expensive techniques like electron-beam lithography are commonly used in the research space. However, advances in rapid nanolithography techniques, such as nano-imprint lithography and extreme UV photolithography, mean that, even for e-beam-developed geometries, there is a clear path to practical, high-throughput production of metasurface biosensors.

C. Biosensing

The resonances that unlock applications in biosensing produce highly confined field enhancements at the meta-atom surface. Therefore, only molecules resident within this near-field (typically in direct contact with the meta-atoms) are going to influence, *or be influenced by*, the resonance, and be detected. So, to function as a sensor, mechanisms are required to ensure that analytes are located within the sensing volume long enough to measure. As a result, in almost all the following biosensor examples, bio/chemical modification of the metasurface is required, usually with a receptor molecule that is complementary to the target analyte (e.g., nucleic acids, proteins, antibodies, etc.). Once located there are several techniques that allow molecular presence to be confirmed, some of which can also provide information about molecular structure and binding strength of those analytes. The examples below include technologies developed to detect biomarkers of specific diseases. In those cases, the detection limits achieved are within the range of clinical relevance.

D. Refractometric sensors

The most widely employed sensing modality involves monitoring the resonance frequency of the metasurface as it interacts with its surroundings—operating on the principle that this frequency is linked to the refractive index immediately adjacent to the nanostructure. Therefore, when biomolecules bind to or approach the nanostructure's surface, they induce an easily observable resonance shift that provides a quantitative measure of molecular presence, binding events, and interaction kinetics.[230]

E. Plasmonic refractometric sensors

As a widely used technique, there are thousands of examples of different geometries, materials, and operating frequencies that have

16 July 2024 09:29:41

© Author(s) 2024

been explored. What follows is a small selection of recent examples. Gold is the most popular material for these sensors because of its chemical stability, simplicity of modification with bio-receptors, and the ease by which visible resonances can be excited using white light.[231] For over two decades, the most popular surface geometry has been circular nanodisks, a geometry that can be produced using many different fabrication techniques. Since controlled array spacing is not necessarily required for many biosensing tasks, a number of wide-area fabrication examples (e.g., colloidal fabrication) exist. Examples include hole-mask colloidal lithography and photolithography to produce gold nanodisks for multiplexed measurement of diagnostic-relevant protein-protein binding affinity at pM concentration.[232] Similar fabrication techniques have been used to detect single-base DNA mutations,[233] and others have shown that by coating the nanodisks with molecularly imprinted polymers (MIPS) instead of traditional "complementary" receptor molecules, label-free quantification of many polyphenol-protein interactions can be made.[234] Other examples of wide-area fabrication for scalable sensor production include nanosphere lithography to produce Au nanopyramids to measure real-time protein (α–Synuclein)-small molecule interactions,[235] and the use of nanoimprinting to create indented gold structures ("nanocaves") for detecting tumor markers in human serum (carcinoembryonic antigen at 5 ng/ml).[236] Electron-beam lithography enables greater metasurface control, providing more options for geometry and layout variation (e.g., multi-layered biosensors with internal self-referencing),[237] and receptor localization (e.g., receptor "patches" *adjacent* to the meta-atoms for biomolecule-mediated metasurface reconfiguration).[238,239] As such, periodic arrays of e-beam produced gold structures have been used to detect prostate specific antigen (PSA), in serum, at 500 pg/ml.[240] In a variation of the periodic nanodisk structure, Shen *et al.* demonstrated gold mushroom arrays with high-intensity coupled resonance modes (between a gold film and elevated gold disks) for detecting alpha-fetoprotein (a liver cancer and fetal development marker) at 15 ng/ml.[241] Similarly, high-intensity fields can be produced in small gaps between discrete structures, as demonstrated with IR-resonant nanorods for detecting human antibody IgG down to 30 pM,[242] and to monitor peptide-induced neurotransmitters from synaptic vesicle mimics.[243]

F. Dielectric refractometric sensors

Recently, as the benefits of dielectric resonators has become apparent, similar functionality has been demonstrated with dielectric metasurfaces. Silicon nanodisks have been used to monitor biotin-streptavidin interaction at 10^{-10} M,[244] to detect breast cancer biomarkers at 0.7 ng/ml,[245] and to identify PSA at 1.6 ng/ml (below diagnostic requirements).[246] Low-cost fabrication has also been explored in this space, with PSA detection shown using silicon disks produced via colloidal lithography,[247] and, in efforts to produce cost-effective meta-sensors with CMOS camera compatible readouts, Triggs *et al.* demonstrated chirped silicon-nitride gratings for characterizing antibody binding.[248] More complex shapes are also emerging, with crescent structures supporting quasi-BIC (bound states in the continuum)[140] having achieved 0.16 nM protein detection,[249] and where, notably, Altug's laboratory have manipulated the angles and spacings of germanium and silicon nano-ellipse structures, and combined them with hyperspectral imaging, to fingerprint various biomolecular events at high sensitivities.[250,251]

G. Chiral sensors

Chirality is a fundamental property of many biomolecules, including amino acids and nucleotides, where molecules exist in two forms that are mirror images of each other, known as enantiomers. This characteristic is crucial in biochemistry and pharmacology because enantiomers of the same substance can exhibit vastly different biological activities, with one form potentially beneficial and the other harmful. Chiroptical spectroscopic techniques can identify and characterize chiral biomacromolecules, but their sensitivities can be greater than six orders of magnitude lower than refractometric plasmonic sensors,[252] meaning they are largely unsuitable for detection of enantiomers at diagnostically relevant concentrations (which can be pg/ml). The enhanced fields exhibited by resonant metasurfaces can significantly enhance the chiroptical response, enabling more sensitive detection of chirality. By using geometrically chiral plasmonic structures, so-called superchiral fields can be generated,[253] optimizing the selective absorption of light by chiral molecules and enhancing CD signals. This provides a more efficient means for the detection, analysis, and separation of enantiomers, offering improved sensors for pharmaceutical development and diagnostics. The quest to generate superchiral fields for these purposes has led to a number of plasmonic metasurfaces which exhibit complex meta-atom geometries. Notable examples include the use of gold shuriken indentations, fabricated by injection molding, to detect pg quantities of helical biopolymers,[252] perform multiplexed sensing of proteins and virions,[254] and record the chiro-optical response of type II dehydroquinase.[255] Another example of a chiral metasurface sensor demonstrated the use of a 3D core-shell nanohelix structure, constructed via ion beam deposition of a Pt core, surrounded by the conductive polymer P-oPD, to achieve detection of DNA binding protein 43 (relevant for neurodegenerative disease) at a concentration of 10 fM.[256]

H. Enhanced vibrational spectroscopy

The ability to confine light to incredibly small volumes make metasurfaces ideal for increasing the efficiency of vibrational spectroscopy techniques. Many techniques can benefit from these properties, with Infrared Absorption Spectroscopy, Surface-Enhanced Infrared Absorption (SEIRA), and Terahertz spectroscopy, having benefited from metasurface enhancement (using IR resonating microstructures).[257,258] However, the most common use of metasurface-enhanced vibrational spectroscopy is seen in Surface Enhanced Raman Spectroscopy (SERS).[259,260] When light passes through a molecule with certain attributes, it may undergo Raman scattering; inelastic scattering that produces a fingerprint of molecular vibrations from that molecule, elucidating chemical composition and structure. However, Raman scattering is inefficient; large concentrations are required to obtain signals. SERS amplifies scattering from molecules adsorbed on nanostructured surfaces, enabling detection of individual molecules and events. Since SERS enhancement scales with electric-field, meta-atoms are engineered to exhibit sharp edges or small gaps to concentrate the electric-field. Sensing requires the excitation laser line crossover with the (typically broad) meta-atom plasmon, making surface tuning simple, even with less-controlled techniques (e.g., colloid-mediated lithography). Indeed, the vast majority of SERS work is performed using cheap, effective, metal colloid. However, commercial and research examples of metasurface SERS systems do exist when signal reproducibility or more sophisticated functionality are required. One

16 July 2024 09:29:41

© Author(s) 2024

such example used coupled gold triangular trimer structures designed to exhibit multiple resonance modes spanning the visible and mid-IR.[261] With tip separation of a few nanometers, the trimers promoted large field in these volumes. The authors demonstrated that these multi-resonant structures were multi-functional, and could be used as SERS substrates for detecting DNA hybridization, and as surface enhanced fluorescence and SEIRA substrates.[261] DNA hybridization has also been detected via SERS using metasurfaces consisting of polarization-sensitive silver split-ring resonators[262,263] and by using the hybridization events to drive individual nanoparticle localization into the center of gold bowtie structures.[239] Combining SERS with chiral nanostructures has led to chiral discrimination of amino-acids via SERS.[263] Recent work on dielectric metasurfaces has shown that, much like for refractometric sensing, these surfaces may hold advantages over plasmonics for SERS biosensing. While plasmonic meta-atoms can require high laser intensities, leading to heating and molecular damage, dielectric meta-atoms exhibit little absorption, minimizing heat, while retaining nanoscale light confinement. However, although there is activity in dielectric SERS,[264] and some examples of dielectric SERS metasurface substrates do exist (e.g., silicon dimers to detect β-carotenal molecules)[265] the enhancement factors that can be achieved in Si systems are significantly lower than those seen in plasmonic systems (10^3 for Si vs 10^6–10^14 in metal systems),[260] meaning that their impact in biosensing may be limited.

I. Nanoholes

Surfaces that exhibit structured "negative" features, such as engineered holes and voids, also make for effective biosensors.[266] Extraordinary Optical Transmission (EOT) through plasmonic nanoapertures is a phenomenon where light passes through holes in metal films at efficiencies higher than classical theories predict. A combined effect of propagating and localized surface plasmon resonances, EOT acts to concentrate and funnel light through the nanoapertures, significantly enhancing the transmitted light intensity, in doing so generating enhanced fields within the aperture itself. Thus, if molecules can be located inside these holes, refractometric and enhanced spectroscopy sensors can be created. Gold nanohole arrays have been shown to be highly sensitive to antibody binding events,[267] capable of responding to PSA in a 96-well plate compatible metasurface format,[268] used for detecting numerous exosomes for cancer diagnostics (measurements that can also monitor treatment efficacy),[269,270] for detecting pancreatic cancer,[271] and for identifying virus-like particles and assessing viricidal drug candidates.[272] Hole structures also bring the possibility to create nanofluidic flow-through systems, where the apertures serve dual roles as both optical modulators and liquid delivery channels. Examples of these systems include circular gold apertures for label free DNA detection,[273] single base DNA discrimination using gold nanopores and electro-plasmonic trapping,[274] and bowtie shaped gold pores to detect DNA[275] and beta-amylase protein translocation.[276]

J. Future directions and outlook—cross-reactive metasurface biosensors

In all the above examples, recognition of the target and retention in the sensing volume has been achieved using a specific binding partner or interaction. For example, complementary base pairing of DNA, or a specifically chosen antibody or affinity protein for the target. Such approaches are well established and many methods of engineering metasurfaces with suitable chemistries attached have been achieved. However, there are also drawbacks to such an approach that are now becoming more widely recognized.

The first consideration is one of multiplexing and the number of targets that need to be detected. In the paradigm considered above, assuming perfect receptor or sensing element specificity, "n" functional sensing elements are required for n different targets. As the understanding and appreciation of multi-biomarker solutions for disease detection or biological systems measurement grows, particularly with advances in "omic" technologies, n can approach a very large number, rendering it impractical or impossible to build such a large number of sensors.[280] Second, again led by the increased amount of -omic data available, there is an understanding that not all biomarkers or target molecules are actually known at the outset. These "unknown-unknowns" might enable greater insight or more accurate diagnosis but simply have not yet been linked to the condition in hand. Finally, there is a question of just how specific a sensor can be, particularly when targeting small molecules or macromolecules with few features to bind.

Thus, the idea of *cross-reactive* arrays is now gaining traction. Such arrays contain multiple sensing elements, sensitive to multiple or many different targets, and, rather than generating a single target response, generate a pattern or fingerprint when exposed to a sample. The sensing fingerprint is then tied back to the sample contents by statistical analysis and pattern recognition. This cross-reactive approach breaks the n for n paradigm and enables a holistic approach to sample measurement where all biomarkers in the sample have a chance to be measured, not just those known about at the outset.[281] The sensor targeting chemistry can be tuned to be more specific or more cross-reactive as the user desires, and a "training and testing" model is used to gather representative data that informs a statistical model or machine learning for further "unknown" sample analysis.[282]

Incorporating this approach with metasurfaces allows optically addressable arrays to be created where changes in absorbance, reflectance, optical helicity, or other outputs are transduced to create a fingerprint, with spatial or wavelength based multiplexing possible for each individual part of the sensor array.[227]

There are many examples of the method using plasmonic nanoparticles in solution, deposited inside well-plates, or drop-cast onto surfaces as discrete sensing areas that display differential reactivity directly with target compounds or biomarkers to alter their plasmonic color.[283] For example, Hormozi-Nezhad and co-workers have made extensive studies in this area, differentiating pesticides,[284] measuring urinary biomarkers for neurology,[285] and also amyloid proteins among many other bio-targets.[286] Biogenic amines as markers of food spoilage can also be detected in this manner,[287] as well as the different bacteria themselves.[278] In each case, the growth, etching, and aggregation of metallic nanomaterials that leads to their color change, is influenced by the different reactive chemistry included in each part of the array (typically a well in a 96 well plate), and the chemical interactions with the sample under test. It is clear that a reactive plasmonics approach such as this could be further integrated into arrays of plasmonic materials as part of a metasurface, however, this would likely have to be a single-use sensor, so may have limited utility in practical applications.

A second approach is to functionalize the metasurface elements with different cross-reactive chemistries, less specific than an antibody

16 July 2024 09:29:41

© Author(s) 2024

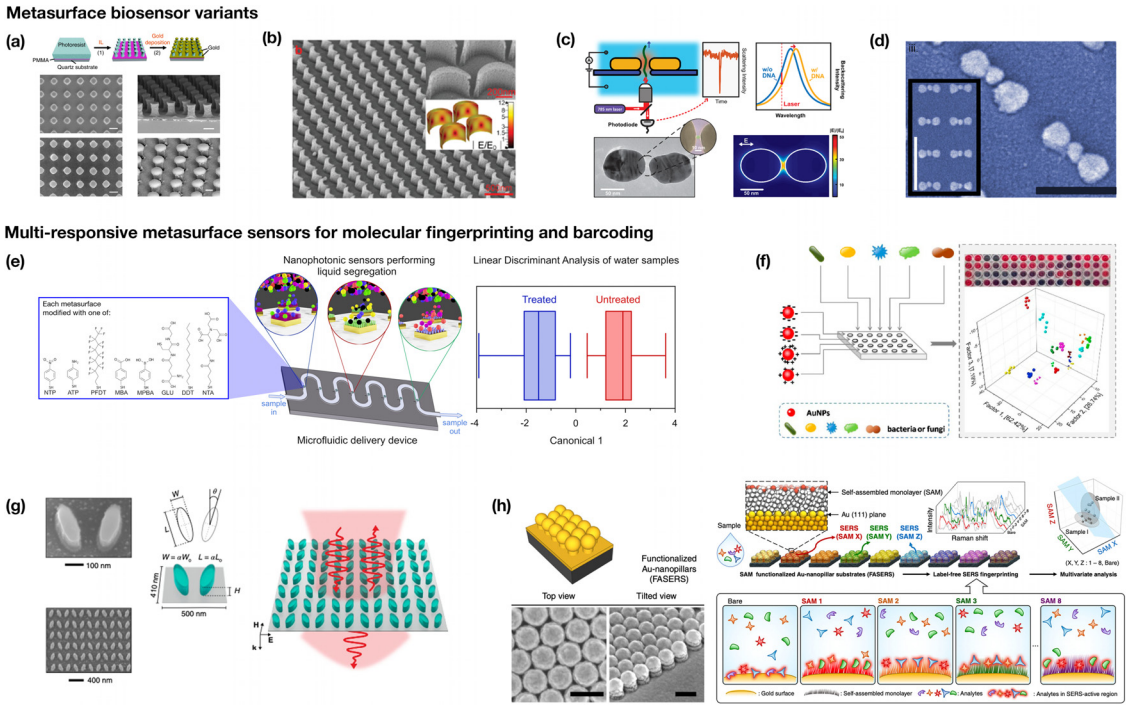

FIG. 8. Metasurface biosensing examples. (a) Gold mushroom nanostructures.[241] (b) Quasi-BIC mode supporting silicon crescent nanostructures.[249] (c) Flow-through nanohole sensor for DNA sensing.[273] (d) DNA-directed nanoparticle localization inside gold bowties, as a sensing system.[239] (e) Cross-reactive metasurfaces for monitoring water treatment sites.[277] (f) Multi-responsive, array-based nanoparticle sensor for micro-organism detection.[278] (g) Barcode-based biosensing with elliptical dielectric resonators.[251] (h) A SERS-based artificial nose sensors.[279] (a) Reprinted with permission from Shen *et al.*, Nat. Commun. **4**, 2381 (2013). Copyright 2013 Macmillan Publishers Limited.[241] (b) Reprinted with permission from Wang *et al.*, Adv. Funct. Mater. **31**, 2104652 (2021). Copyright 2021 Wiley-VCH GmbH.[249] (c) Reprinted with permission from Shi *et al.*, Nano Lett. **18**, 8003 (2018). Copyright 2018 Authors, licensed under a Creative Commons Noncommercial License (CC-BY-NC-ND).[273] (d) Reprinted with permission from Clark *et al.*, Adv. Mater. **26**, 4286 (2014). Copyright 2021 Wiley-VCH Verlag GmbH & Co.[239] (e) Reprinted with permission from Sperling *et al.*, Environ. Sci. **10**, 3500 (2023). Copyright 2020 Authors, licensed under a Creative Commons Attribution 3.0 Unported License.[277] (f) Reprinted with permission from Li *et al.*, Anal. Chem. **89**, 10639 (2017). Copyright 2017 American Chemical Society.[278] (g) Reprinted with permission from Yesilkoy *et al.*, Nat. Photonics **13**, 390 (2019). Copyright 2019 Springer Nature Limited.[251] (h) Reprinted with permission from Kim *et al.*, Nat. Commun. **11**(1), 207 (2020). Copyright 2020 Authors, licensed under a Creative Commons Attribution 4.0 International License.[279]

but still imparting a degree of selective binding to nearby biomolecules. We have already exemplified this approach with cross-reactive metasurface arrays applied to the sensing of small molecules in whiskey and water.[277,288] In each case, a sensor was produced that consisted of an array of plasmonic metasurfaces (many separate metasurfaces on the same substrate) that were each modified with a self-assembled monolayer (SAM) of a different small molecule, imparting varying local charge, acidity, nucleophilicity and hydrophobicity to each metasurface. The metasurfaces were then exposed as an ensemble to different samples, reacting with molecules in solution to alter the local dielectric environment of each metasurface differently, creating a varying plasmonic fingerprint based on color shift across the array. These fingerprints were analyzed with principal component analysis (PCA) and linear discriminant analysis (LDA) to create tools capable of either discriminating whiskeys based on their chemical content, or treated and untreated water samples based on their mineral and organic carbon content. It is clear how such an approach can now be extended to direct biosensing, and is an area of ongoing research.

In a similar approach, but with a different transduction method, Stevens *et al.* demonstrated a gold nanopillar metamaterial, where each region (sensing element) again featured a different SAM.[279] The metamaterial created strong SERS hotspots between the elements, and the interaction of the SAM with the targets (small biomolecules, extracellular vesicles, cell lysates) ensured different molecules could enter the hotspots, driving differential SERS spectra across the array. Two companion cell lines (one cancerous, one not) were easily identified based on their differential SERS spectra across select array elements, coupled with PCA and LDA analysis.

The coupling of this approach with the exquisite sensitivity of metasurfaces, their greatly improved multiplexing capacities, and advanced fabrication methods should make metasurface sensing arrays a hugely powerful tool in bioanalysis of the future, capable of operating in both liquid and gas sensing modes to deliver pattern recognition of a wide variety of targets. Key to this success will be the choice of interfacial cross-reactive chemistries to deliver the best interactions with the analytes under study, as well as exploitation of novel transduction modes possible with advanced metasurfaces, to increase the data density that can be collected. As more and more metasurface-based tools become portable, thanks to their compatibility with simple optical platforms and even smartphone read outs, there is huge potential here for delivering ultra-sensitive biomolecule detection with specific or cross-reactive sensing, at the point of need.

16 July 2024 09:29:41

© Author(s) 2024

V. METASURFACES FOR PASSIVE RADIATIVE COOLING

George Perrakis*, Anna C. Tasolamprou, and Maria Kafesaki

*gperrakis@iesl.forth.gr

A. Introduction

From a thermodynamic point of view, exploiting a ∼3 K heat sink (ultra-cold universe) of infinite heat capacity, earth objects can reach temperatures below the ambient air temperature (∼ 300 K). This is the principle behind passive radiative cooling (PRC). Specifically, PRC technology aims to exploit the coldness of the Universe for cooling purposes without any electricity input required.[289] It relies on Earth's atmosphere transparency between 8 and 13 μm. This transparency window coincides with the peak of the black-body thermal radiation spectrum of earth objects at typical temperatures (∼ 300 K). Thus, any earth object facing the sky can release heat to the outer space, in the form of thermal electromagnetic (EM) radiation, lowering its temperature.

Such a passive strategy (i.e., that cools without any electricity input) could significantly impact global energy consumption (15% decrease).[290] The use of PRC as a passive cooling mechanism in human infrastructure elements like buildings, for instance, may lead to lower indoor temperature and alleviate the need for excessive air conditioning, with potential for energy savings and improved efficiency.[290] Many other devices and technologies, such as solar cells, thermal textiles, and thermophotovoltaics, can highly benefit from PRC.[291,292]

Despite the practical benefits and high potential impact, PRC has three main limitations.[293–298] First, peak cooling demand occurs during daytime, when incident sunlight heats the objects, Fig. 9(a). Therefore, one will need a structure that reflects the entire solar spectrum, Figs. 9(b) and 9(d).[296] Second, PRC technology may be counterproductive in year-round assessments, due to provision of undesirable cooling during cold days. Therefore, adaptive PRC may be required, i.e., based on dynamic modulation techniques to tune thermal emission depending on the ambient air temperature.[297] Third, current PRC technology is highly unstable, strongly affected by climate or varying weather conditions (e.g., humidity or clouds, resulting to reduction of atmospheric transparency) and by surrounding constructions [e.g., high-rise buildings, providing additional heat or obstructing the heat release, Fig. 9(c)], causing drop of the radiative cooling power. These limitations are a direct consequence of the symmetry of absorption-emission met in most thermal emitters, owing to the fact that PRC configurations are made of reciprocal materials. Specifically, reciprocal materials, characterized by symmetric permittivity and permeability tensors, satisfy Kirchhoff's law of thermal radiation, which states that

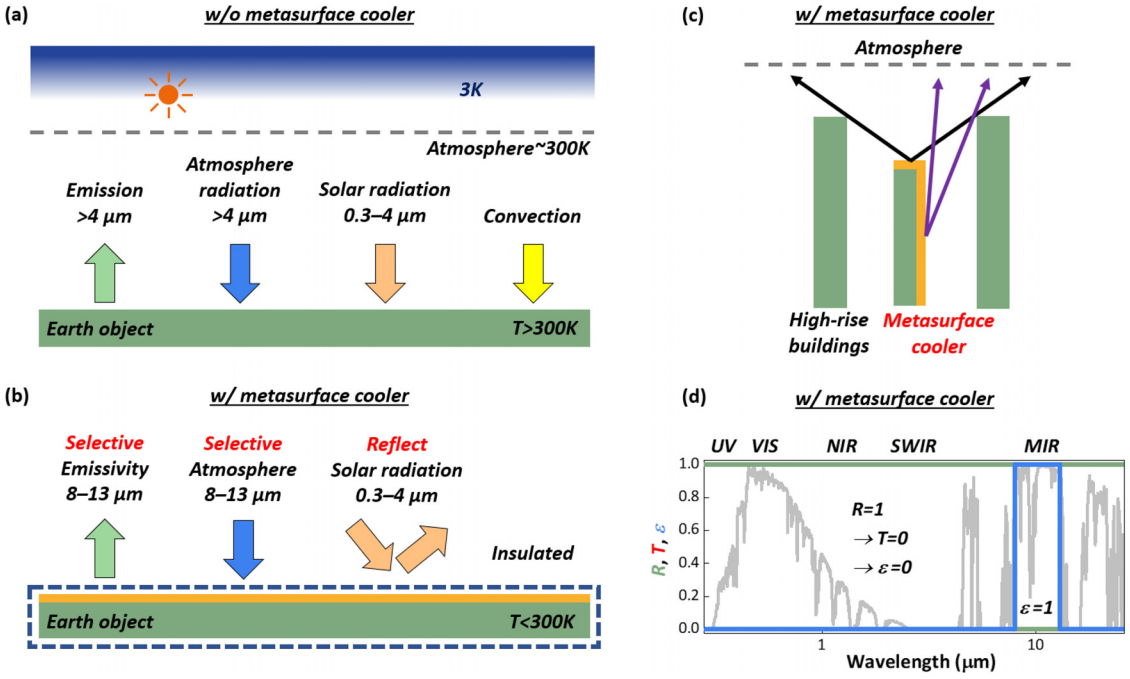

FIG. 9. (a) Solar absorption and thermal radiation properties of conventional surfaces (without metasurfaces cooler). Sub-optimal thermal emission (for $\lambda > 4$ μm) and strong parasitic solar absorption are observed resulting to object's temperature larger than the ambient (300 K). (b) With a metasurface cooler on top (yellow layer), the radiative cooling is enhanced, by enhancing emissivity at 8–13 μm and reducing atmospheric absorption, and the unwanted solar radiation is strongly reflected, leading to sub-ambient surface temperatures, T< 300 K. Note that the object is insulated in (b) to minimize non-radiative heat gains from conduction and convention (e.g., wind), i.e., besides avoiding the radiative heat gains. (c) Illustration of obstruction effect of high-rise buildings on the access of coolers to the sky. The black and purple arrows indicate top and sidewalls emission, respectively. In (b) and (c), sun and outer space are omitted for clarity. (d) Ideal reflectivity (R, green), emissivity (ε, blue), and transmissivity (T, red) in ultraviolet (UV), visible (VIS), near-infrared (NIR), short-wave-infrared (SWIR), and mid-infrared (MIR) spectra, together with the normalized AM 1.5G solar irradiance spectra (gray, <4 μm) and the infrared transmission of the atmosphere (gray, > 4 μm).

16 July 2024 09:29:41

© Author(s) 2024

their spectral, directional emissivity (ε) equals their spectral, directional absorptivity (α). To this end, the two main existing strategies to stabilize PRC (i.e., avoid fluctuations in the radiative cooling power) are (i) high spectral selectivity [maximizing the thermal radiation in the atmospheric transmission window and keeping it minimum everywhere else, Figs. 9(b) and 9(d)][299] to mitigate the sensitivity to humidity, and (ii) enhanced directionality, also to a limited solid angle (beaming), to avoid additional heat gains from the surrounds, Fig. 9(c).[300]

Conventional approaches to meet these stringent requirements, however, come with large space demands, often requiring complex shelter and shading systems, and therefore limit applicability, often reducing also the emission power.[293] For real objects in local thermal equilibrium, Kirchhoff's law of thermal radiation still holds at every combinatorial specific set of wavelength (λ), angle (θ), and polarization (p).[300] The field of photonics though, which explores the use of light molding techniques in the visible and infrared, assisted by the recent advances in nano-fabrication, is capable of engineering ε at selected λ, θ, and p, i.e., using the concepts of photonic crystals (PCs), metasurfaces, and metamaterials. Metasurfaces and metamaterials, for instance, involve structuring the material at a subwavelength scale. Relying on local and non-local resonant phenomena (as a result of proper structuring, i.e., of suitably designed building-blocks, known as meta-atoms), metamaterials and metasurfaces provide unique optical properties and enable novel ways to tailor light. The careful engineering of shape, size, and arrangement of meta-atoms can imprint the desired response, such as enhanced directionality,[300] or tune the spectral bandwidth of operation,[301] also offering extra advantages, such as ultra-low thickness and weight,[305] and flexibility. Therefore, metamaterials/metasurfaces have been employed as coatings for PRC applications in recent years [see Fig. 9(b)].[305–307] Additionally, to date, considerable attention has been paid to utilizing metasurfaces and metamaterials also to relax the constraints coming from space-reversal symmetry or by reciprocity (connected to time-reversal symmetry) via (i) breaking the time-reversal symmetry with non-reciprocal materials and gratings, e.g., magneto-optic materials, time-modulated systems, or Weyl semimetals,[308] or (ii) breaking the space-reversal symmetry of transmission with reciprocal but anisotropic or bi-anisotropic systems, such as metallic gratings with subwavelength slits, gradient metasurfaces, hyperbolic metamaterials, and chiral structures.[309,310] Consequently, it would be of paramount importance to fabricate non-reciprocal thermal emitters (coolers) or asymmetric configurations that would emit or allow heat in certain directions without absorbing or allowing incoming heat.[293,294] Currently and in recent years, there is significant research on examining different photonic strategies in terms of applicability, feasibility, and potential of enhancing and stabilizing PRC. In this perspective, we provide an overview of the recent and ongoing research on metasurfaces, metamaterials, and PCs as means to control the fundamental aspects of thermal radiation for cooling purposes. Such aspects are related to (i) spectral selectivity, (ii) tunability, (iii) directionality, and (iv) asymmetric propagation. Finally, we discuss the challenges and potential future directions.

B. State of the art

Spectral selectivity. As mentioned already, spectral selectivity is a quite important feature of a radiative cooling system, as it can allow emission/absorption only in the beneficial for cooling $\sim$8–13 μm spectral window (atmospheric transparency window) and reject the non-beneficial parts of the EM spectrum, Figs. 9(b) and 9(d). In 2015, Hossain *et al.*[301] fabricated an anisotropic, conical-shaped waveguide-metamaterial emitter composed of 14 alternating layers of aluminum (Al) and germanium (Ge) (size $\sim$2 μm, i.e., thickness and bottom diameter) to realize polarization-insensitive, highly selective PRC, Fig. 10(a). They demonstrated ultra-high emissivity (>0.85) and broadband operation at $\sim$8–13 μm, owing to the slow-light modes at different wavelengths (with peaks' emissivity >0.9) and the tapered shape. They measured a remarkably high cooling power, of 116.6 W/m^2, at ambient air temperature and a temperature of 12.2 °C below ambient.

Apparently, fabrication feasibility, scalability, and cost-effectiveness are also vital for promoting PRC as a viable energy technology. With this in mind, Zhai *et al.*,[302] two years later, demonstrated a highly transparent hybrid metamaterial cooler composed of resonant polar dielectric (silica) microspheres ($\sim$4 μm diameter) randomly distributed in a polymeric matrix (50-μm-thick), Fig. 10(b). By accessing the high-order Fröhlich resonances of the polar silica spheres, the metamaterial provided larger than 0.93 and broadband infrared emissivity across the atmospheric window. When backed with a silver coating to reflect solar radiation, the metamaterial showed a noon-time radiative cooling power of 93 W/m^2 under direct sunshine. The high significance of this work is related to the high-throughput and economical roll-to-roll manufacturing of the metamaterial combined with the high PRC performance.

Although the impact of PRC on emitters' surface temperature was early highlighted, its impact on cooling inner (enclosed) spaces (that trap heat by the greenhouse effect) remained unclear until 2020. In 2020, Heo *et al.*[299] presented a Janus thermal emitter for cooling enclosed spaces, consisting of an Ag-coated quartz grating and a polydimethylsiloxane (PDMS) layer on quartz substrate's front and rear side, Fig. 10(c). The Janus emitter acted as selective emitter on the top side, to dissipate heat to outer space, and as broadband emitter on the bottom side, to draw heat from the inner space, Fig. 10(c). The selective emitter showed a sub-ambient cooling of $\sim$6 °C, obtained by exploiting spoof surface plasmon polaritons (sSPPs) to achieve near-ideal selectivity. Notably, the temperature of an object inside the enclosure was $\sim$4 °C lower than that achieved when using a conventional radiative cooler with reflective bottom surface. These results demonstrate that metasurfaces and metamaterials can provide high-efficiency PRC (4 − 12 °C) even paired with high-throughput, economical, and scalable manufacturing, promoting PRC as a viable energy technology.

Tunability. As mentioned also earlier, the ability to tune a cooler's thermal emission depending on the environmental conditions allows for an adaptive PRC system whose cooling power switches off when not needed, e.g., in cold nights or winter times, avoiding overcooling that increases the heating cost. In 2018, Ono *et al.*[311] proposed an one-dimensional (1D)-PC consisting of two components, a spectrally reflective filter and a switchable radiative cooler. The on-top spectrally selective filter was a 11-layer stack of alternating Ge/MgF_2 layers, which served as a reflector of solar radiation and a passband filter with high transmissivity at 8–13 μm. The radiative cooler at the bottom consisted of a VO_2/MgF_2/W tri-layer, where VO_2 (material with phase transition hysteresis) was the switching component. The angle and polarization averaged emissivity (0°–90°) in the wavelength range of 8–13 μm was 0.64 in the metallic state of VO_2. On the contrary, the averaged emissivity dropped to 0.05 when VO_2 was in insulating

16 July 2024 09:29:41

© Author(s) 2024

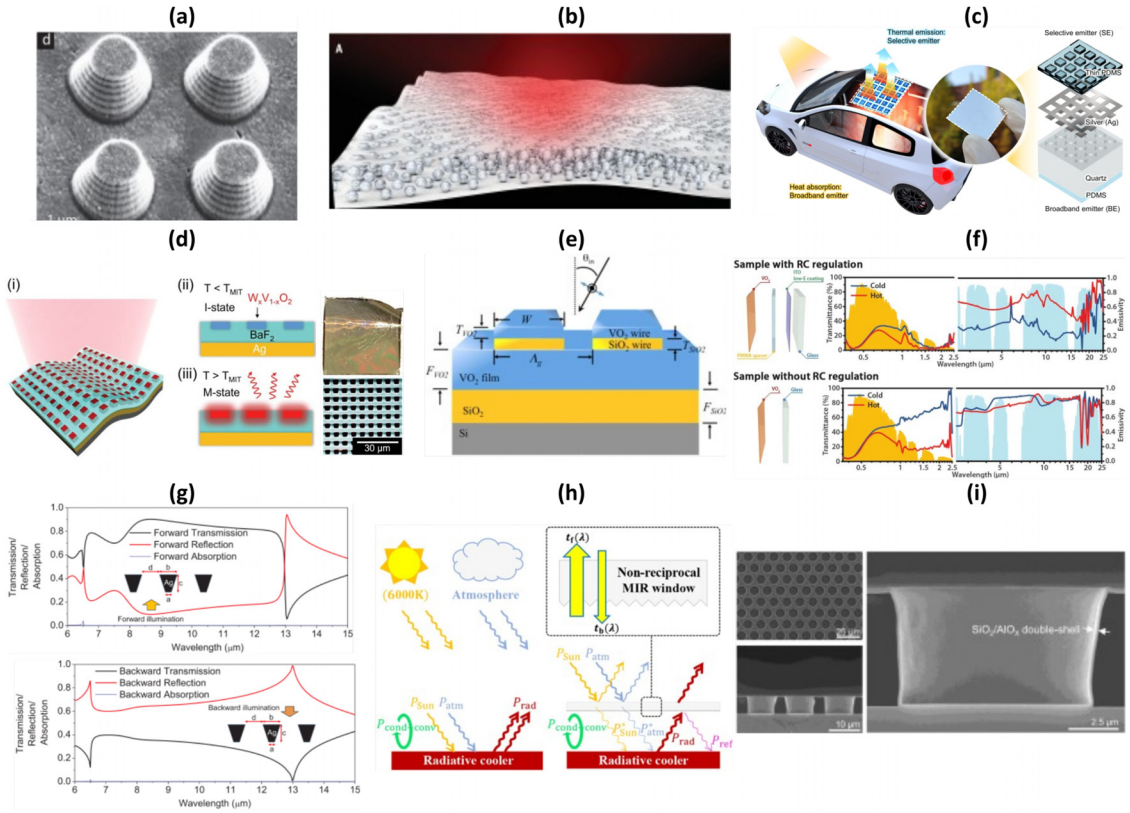

FIG. 10. Examples of PRC metasurfaces of different geometries and configurations. (a) Array of fabricated conical-shaped metamaterial pillars.[301] (b) Polymer-based hybrid metamaterial with randomly distributed SiO_2 microspheres for large-scale PRC.[302] (c) Janus emitter applied to an automobile under direct sunlight, where heat is trapped by the greenhouse effect, allowing broadband absorption of IR waves from the enclosure and selective emission to the ultracold space.[299] (d) Structure of the temperature-adaptive radiative coating and principle of operation.[297] (e) Phase change metasurface consisting of periodic $VO_2/SiO_2/VO_2$ cavities.[303] (f) Spectra of the thermochromic smart window with and without radiative cooling regulation in VIS, NIR, and MIR at 20 °C (blue) and 90 °C (red).[304] (g) Asymmetric transmission periodic micro-structure of inverted silver trapezoids and relevant forward/backward transmission, reflection and absorption over the atmospheric transparency window range and beyond.[294] (h) Schematic of the asymmetric transmission pyramidal micro-structure and principle of operation.[295] (i) Array of fabricated SiO_2/AlO_x double-shell hollow microcavities for directional thermal emission.[300] All images are reprinted (adapted) with permission from the respective Journal and copyright remains with the original publisher.

phase, leading to a 0.59 modulation performance. At "on" state, the radiative cooler reached an equilibrium temperature around 10 °C below ambient. At low ambient temperatures (≤ 25 °C, when cooling is not needed) the system switched off, accompanied by a sudden reduction of the cooling power, maintaining cooler's temperature near the critical temperature (∼25 °C). The same year (2018), Wu *et al.*[303] proposed a phase-change metasurface consisting of periodic $VO_2/SiO_2/VO_2$ cavities supporting a thermally switchable Fabry–Pérot (FP)-like fundamental resonance mode at 8–13 μm, Fig. 10(e). The thermal emissivity there switched from ∼0.2 to ∼0.65 (∼0.45) with a critical (VO_2 phase-change) temperature ∼68 °C. The cooling power was calculated 118 and 528 W/m^2 at device temperatures 67 and 69 °C, respectively, compared to 1.3 and 187 W/m^2 for a simple 300-nm-thick VO_2 film. In 2020, Zhang *et al.*[312] proposed a trapezoidal hyperbolic metamaterial (HMM) emitter composed of Ge and VO_2 for self-adaptive PRC and a MgF_2/Ge multilayer filter placed on top for reflecting solar radiation and allowing selective transparency (at 8–13 μm). When VO_2 was in metallic phase, close-to-unity, broadband (>4 μm), and angle-insensitive emission was achieved due to the slow-light waveguide mode in the trapezoidal HMM, while with the presence of the filter on the top, system's emissivity peaked (>0.95) only at three wavelengths (8.4, 9.7, and 11.8 μm), creating spectral-selective emission (at 8–13 μm). The thermal emissivity modulation performance was ∼0.67 (from ∼0.20 to 0.87), leading to a cooling power >100 W/m^2 (up to 127.8 W/m^2) when cooler's temperature was 69 °C, and 27.9 W/m^2 at 68 °C. Considering scalability, flexibility, and low cost, Tang *et al.*,[297] in 2021, fabricated a phase-change metamaterial consisting of a 2D array of thin $W_xV_{1-x}O_2$ blocks embedded in a BaF_2 dielectric layer on an Ag film, in various design configurations, for production in a roll-to-roll fashion, Fig. 10(d). When $W_xV_{1-x}O_2$ was in the insulating phase, the metamaterial was mainly transparent to the IR radiation at 8–13 μm and highly emissive when it switched to the metallic state. The thermal emissivity was further amplified by a designed photonic resonance involving adjacent $W_xV_{1-x}O_2$ blocks and by the $\frac{1}{4}$-wavelength cavity formed in BaF_2 due to the bottom ultra-thin Ag layer, Fig. 10(d). This flexible, temperature-adaptive metamaterial switched its thermal emissivity from 0.2 to 0.9 (0.7) at 8–13 μm when the surface temperature raised

16 July 2024 09:29:41

© Author(s) 2024

above ∼22 °C. The metamaterial was 2 °C warmer than two reference (non-adaptive) roof coatings when the ambient temperature was below ∼22 °C.

In addition to modulation of thermal emissivity, the simultaneous modulation also of solar heating (i.e., absorbing/reflecting near- and short-wave-IR radiation and remaining transparent or semi-transparent in the visible spectrum), e.g., in smart and/or thermochromic windows, may further improve the regulation of heat flow to maintain a system's temperature near a desired set point, increasing energy-savings. In 2020, Wang *et al.*[313] proposed a compound metasurface of large and small cross-shape resonators for realizing self-adaptive PRC and solar heating in one system. The core of the self-adaptive response is the utilization of a PVP (pNIPAM) spacer below crosses, which can expand (contract) with heat and contract (expand) with cold, increasing or decreasing crosses' spacing. The absorptivity/emissivity modulation performance in both solar and 8–13 μm spectral regimes was ∼0.8 (from ∼0.1 to ∼0.9) within a narrow bandwidth. The results showed that the compound metasurface can remain cool at 35 °C and warm at 25 °C. In 2021, Wang *et al.*[304] fabricated a scalable smart window based on W-doped VO_2 nanoparticles dispersed in a PMMA solution on top of a PMMA spacer for simultaneous thermal emissivity and solar reflectivity modulation, Fig. 10(f). Interestingly, the critical temperature was tuned through W-doping around 27.5 °C (i.e., much lower than that of pure VO_2, 68 °C). The stacking formed a FP resonator with weak resonance (at 8–13 μm) at low temperatures and strong FP resonation effect at higher temperature (due to the insulator-to-metal transition of VO_2), enhancing emissivity. The emissivity at low temperatures was 0.21 and at high temperatures 0.61 (0.4 modulation performance), combined with near-IR solar modulation of 9.3%, due to the change of the transmittance of VO_2 with temperature, Fig. 10(f). The proposed smart window yielded higher energy-saving performance than a commercial low-ε window, up to 324.6 MJ/m^2, revealing the importance of integrating PRC modulation in smart and/or thermochromic windows.

Stabilizing PRC. In 2018, Wong *et al.*[294] proposed an asymmetric EM transmission structure (ATS) placed on top of a thermal emitter/cooler to reduce its dependence on humidity and clouds that lower its radiative cooling power, Fig. 10(g). The proposed ATS, consisting of a tapered metallic grating, exhibited high-contrast asymmetric transmission at 8–13 μm (∼0.8 forward and ∼0.4 backward, ratio ∼2), Fig. 10(g). Therefore, the ATS, on one hand, permits outgoing transmission of thermal radiation emitted by the radiative cooler, and, on the other hand, it reflects incoming radiation from the sky that lies within the same wavelengths [see also Fig. 10(h)]. Theoretical predictions under humid, semi-transparent sky revealed 57% (50 W/m^2) recovery of cooling power, translating to a radiative cooler's temperature 8 °C lower than the standalone radiative cooler (without ATS). In this case, however, the metallic grating is made of silver, Fig. 10(g), which is a reciprocal material, meaning the directional absorption must equal the directional emission. Therefore, the amount of recovered cooling power should be reconsidered.[314] Two years later, Wei *et al.*[295] proposed an ATS placed on top of a thermal emitter/cooler to mitigate the combined effects of weather (humidity and clouds) and terrain [e.g., obstruction effect of high-rise buildings, Fig. 9(c)] on its radiative cooling power, Fig. 10(h). Using a glass imprinted with properly designed micro-structures [Fig. 10(h)], a high forward-backward transmissivity contrast ratio at 8–13 μm was achieved (∼0.7 forward and ∼0.1 backward, ratio ∼7). Theoretical predictions revealed that the radiative cooler integrated with the ATS has an insensitive (no matter the conditions and terrain) equilibrium temperature ∼10 °C below ambient, compared to ≤ 2 °C of the standalone thermal emitter/cooler. As in the previous case, though, the equilibrium temperature should be reconsidered.[314]

In 2023, Cho *et al.*[300] reported directional, polarization-insensitive thermal emission, which facilitates PRC from the sidewalls of buildings [Fig. 10(i)], see also purple arrows in Fig. 9(c). They fabricated hexagonally arrayed holes (12-μm pitch, 5.5-μm depth, and 10-μm diameter) realized by sub micrometer-thick SiO_2/AlO_x double shells (100/100 nm), resulting to a hollow cavity film, Fig. 10(i). The cavity film exhibited average emissivity values of 0.51–0.62 at angles (θ) 60°–75° and 0.29–0.32 at 5°–20°, yielding a parabolic antenna-shaped distribution. The angular selectivity peaked at four different wavelengths at 8–13 μm (8, 9.1, 10.9, and 12 μm), identified as Berreman modes (only in p-polarization at epsilon-near-zero (ENZ) wavelengths of SiO_2) and photon-tunneling modes (at maximum negative permittivity wavelengths of AlO_x), creating broadband (at ∼8–13 μm), angle-selective emission bands, resulting to superior directional PRC compared to an isotropic black body-like thermal emitter (up to 4 °C). We note that Wang *et al.*[315] proposed the same year that directional thermal emission can also be realized in a broader spectrum beyond the previously considered ENZ and Berreman mode region. A two-phase metamaterial emitter composed of only two materials (material 1 containing subwavelength particles of material 2 on top of a perfect electrical conductor) was proposed showing numerically strong ($\varepsilon > 0.8$) directional ($80° \pm 5°$) broadband thermal emission, where the bandwidth of directional thermal emission can be controlled through the methods of gradient ENZ and effective medium theory. These results suggest that by utilizing metasurfaces and metamaterials, PRC can be less affected by the environmental conditions and the surroundings, which promise all-weather and all-terrain applications.

Regarding non-reciprocal emitters, where Kirchhoff's law of thermal radiation does not hold, i.e., emissivity is not equal to absorptivity, their impact on PRC is not extensively examined in the literature. Two recent studies in 2023, by Liu *et al.*[316] and Shayegan *et al.*,[317] demonstrated direct observation of Kirchhoff's law violation under a moderate external magnetic field (<1.5 T). They reported inequality between emissivity and absorptivity over a broad MIR band, matching also 8–13 μm.[317] In Liu *et al.* case, they used a photonic design that supports a guided-mode resonance coupled to a magneto-optic material[316] while in the Shayegan *et al.* case, they employed magnetized gradient epsilon-near-zero thin films.[317]

C. Future directions and outlook

Using concepts coming from metasurfaces, metamaterials, and PCs research, recent studies have demonstrated tunable (>0.4) and high-efficiency PRC (∼ 4 − 12 °C below ambient) during daytime under direct sunlight, even combined with high-throughput, economical, and scalable manufacturing, Fig. 10. Here, we emphasize on flexible, roll-to-roll processing technologies that earned sufficient attention as a future contender on the PRC industry manufacturing roadmap [see Figs. 10(b) and 10(d)].[297,302] In this case, radiative coolers' reliability should be further examined in relation to integrated polymers' degradation (thermally- or light-induced due to ultraviolet (UV)

16 July 2024 09:29:41

© Author(s) 2024

radiation) or to metal reflectors' oxidation by oxygen and moisture. Employing chemical additives, coatings, or hybrid organic-inorganic ultra-thin PRC multilayers[306] may improve polymers' outdoor performance, although thin polymer films with extended outdoor lifetimes are already available.[302] Moreover, a way to avoid the metal layers or more intricate 1D multilayers (commonly used to reflect sunlight) and still strongly reflect sunlight (including UV radiation) is by integrating layers with light-scattering pores on the nano- and micro-scale.[318] Porous structures' durability, though, affected by dust or moisture, should be further examined. Alternatively, to avoid porosity and efficiently reflect solar light, paints based on a binder (e.g., polymeric) with various fillers and high-index pigments to scatter light (such as TiO_2, SiO_2, Al_2O_3, and $BaSO_4$ nano- and micro-particles) could be utilized,[318] i.e., "complementary" to porous structures. Finally, minimizing non-radiative heat gains from conduction and convention [wind, Fig. 9(b)] should also be addressed for efficient PRC below ambient air temperature (i.e., besides avoiding the radiative heat gains).[296] This could be achieved by tuning metamaterial's thermal conductivity, which can be achieved by changing its chemistry or microstructure.[319,320]

In addition to the above, great effort has been conducted to stabilize PRC subject to unideal conditions such as clouds, humid subtropical climate, and high-rise buildings [Fig. 9(c)].[294,295,300,315] Despite the demonstrated superior directional PRC (up to 4° C compared to an isotropic black body-like thermal emitter), enhanced selectivity and directionality come with reduced sky access and emission power [Figs. 9(b)–9(d)],[296] limiting heat dissipation to outer space and, therefore, cooling power. Moreover, integrating ATSs composed of reciprocal materials to break the symmetry of transmission as means to stabilize PRC [Figs. 10(g) and 10(h)][294,295] is still under consideration.[314] Theoretical studies proved that asymmetric transmission is achievable using reciprocal materials but without increasing the overall radiative cooling power.[314] Therefore, it would be interesting to experimentally examine the applicability and potential of this photonic strategy on stabilizing PRC compared to conventional approaches for enhancing directionality and selectivity, given also the plethora of photonic designs for asymmetric transmission proposed in the literature (e.g., gratings, arrays, and chiral metamaterials) for various applications, even at 8–13 μm.[321] We note that, according to recent studies,[293–295] asymmetric transmission and PRC cannot be enabled in the same component or material (e.g., one grating or metamaterial), which may increase PRC system's complexity, Fig. 10(h).

A promising route to stabilize PRC, maintaining high cooling power enabled by a single component, is to avoid the reciprocity constraints with non-reciprocal materials.[316,317] Maximal violation of detailed balance in thermal radiation (absorbed equals emitted) currently faces several challenges, as it requires a temporal or magnetically induced modulation.[322] The design, simulation, and optimization of such approaches, though, are inherently complex while the involved phenomena are typically resonant.[322] Consequently, novel solutions to achieve high-contrast asymmetric propagation with broadband operation in MIR are required.[316] Moreover, the impact of non-reciprocal thermal emission on PRC, to our knowledge, has not been experimentally demonstrated yet, also due to limited fabrication feasibility, scalability, and increased cost in standard lithographic techniques. Toward this direction, emerging low-cost, robust, and scalable approaches could be employed, such as two-photon polymerization (2PP), 3D/4D-printing, and laser-induced periodic surface structures (LIPSS) with ultrashort pulsed lasers, for nano-structuring a wide range of materials (metals, semiconductors, dielectrics, and polymers). Decoupling α and ε can lead to novel functions, ranging from reducing losses from solar radiation re-emission in solar energy harvesting systems (occurring due to reciprocity) to radiative camouflage and optimum PRC.[292,317]

ACKNOWLEDGMENTS

G.P., A.C.T., and M.K. acknowledge support by the Hellenic Foundation for Research and Innovation (HFRI) under "Sub-action 2 for Funding Projects in Leading-Edge Sectors—RRFQ: Basic Research Financing (Horizontal support for all Sciences)," Project ID 15117 (MultiCool).

VI. METASURFACES FOR PHOTOCATALYSIS

Anastasiia Zaleska, Wayne Dickson, David Richards, and Anatoly V. Zayats

a.zayats@kcl.ac.uk

A. Introduction

Chemical reactions facilitated by light are a cornerstone of clean energy conversion, environmental remediation and material synthesis. While photochemical transformations can take place when reactants are directly illuminated with light, the use of various material systems, often nanostructured, as photocatalysts, can enable a broader class of chemical reactions and can offer enhanced efficiency and selectivity in light-driven processes. Nanomaterials, particularly nanoparticles, play a crucial role in photocatalytic applications by providing large surface areas for molecular adsorption and unique electronic properties, enabling efficient light absorption and facilitating controlled photochemical transformations. The size, shape, and composition of nanomaterials and their surface chemistry can be engineered to optimize photocatalytic activity and selectivity, thereby enhancing the overall efficiency of light-driven reactions. Both semiconductor and metallic nanostructures can be used for photocatalysis, exploiting strong light absorption in the designed spectral range, resulting in electron–hole pair excitation through interband transitions in semiconductors and metals, or the generation of energetic hot electrons using surface plasmon resonances in metallic nanostructures. An additional side-effect of such electronic excitations is the rise of the local temperature of the material which influences the reactivity through thermal effects, as in conventional thermal catalysis. Overall, the integration of nanostructures with photochemistry and photocatalysis holds significant promise for advancing sustainable technological solutions.

In this respect, metamaterials and metasurfaces provide a highly flexible platform for engineering enhanced light–matter interactions which control electric field localization and its polarization as well as local temperature, while providing large surface areas important for chemistry.[323,324] The planar geometry of metasurfaces also facilitates their integration into photo-electrochemical systems, while the use of metaparticles—nanoparticles engineered using metamaterial design

16 July 2024 09:29:41

© Author(s) 2024

principles[325]—provides the combination of increased surface area and engineered optical response with the advantage of scaleable fabrication afforded by nanoparticle synthesis. Furthermore, the opportunity to engineer these nanoparticles as a coating on powders is preferred for some photocatalytic applications.

B. State of the art

Many realizations of metallic (plasmonic) and semiconductor metasurfaces and metamaterials have been recently developed and investigated for enhancing and controlling photocatalytic and photoelectrocatalytic transformations. While plasmon resonances have been widely employed in metallic catalysts, which provide enhanced light absorption and hot-carrier excitation not limited by a bandgap, semiconductor, and dielectric metastructures are also actively considered for enhancing light absorption at sub-bandgap energies and engineering strong absorption in catalytically inert dielectrics decorated with metal or semiconductor catalysts. These often exploit archetypical metasurface designs based on nonradiative high-index nanophotonics, such as multipolar Mie resonances and bound states in the continuum.

Photocatalysts based on semiconductor materials, such as titanium dioxide (TiO_2) and gallium phosphide (GaP) are traditionally attracting significant attention because of the possibility to utilize solar energy directly.[326,327] They generally benefit from high chemical stability and reactivity, are nontoxic and inexpensive. Holes in the valence band and electrons in the conduction band, excited upon interband light excitation, can then interact with molecules on the surface promoting chemical transformations. However, optical absorption in semiconductor materials is limited by their bandgap. TiO_2 has a relatively large bandgap of about 3.2 eV, which makes this catalyst predominantly active under UV light, in the wavelength range shorter than 400 nm, compared with a bandgap of around 2.2 eV for GaP. This means TiO_2 photocatalysts can harvest only a few percent of the solar spectrum energy (about 3%–5%). Additionally, the photocatalytic activity of semiconductor materials is limited by the rapid recombination of photogenerated electron–hole pairs and insufficient charge carrier transfer. Extensive research efforts have been dedicated toward the improvement of their photocatalytic performance through material modification and incorporation or doping with other functional materials for visible light utilization.

Metasurfaces patterned on TiO_2 and GaP have been designed to increase the absorption of light and broaden their working spectral range.[328–331] For TiO_2 metasurfaces, doping can be first used to introduce defect states near the bandgap edges, and the associated absorption is then increased at selected wavelengths of visible light by engineering nonradiative modes via the interplay between electric and magnetic dipoles of the individual nanostructures forming the metasurface (meta-atoms), lattice modes, or the effects of bound states in the continuum. While the defect related excitation of electron–hole pairs may have its drawbacks, primarily in lower carrier mobility, the enhanced absorption at the resonances in the visible spectral range can be sufficient to demonstrate photocatalytic transformations at wavelengths where reactivity would be negligible without the metasurface. The impact of patterning also increases the surface area available for photocatalytic activity, which may be the dominant effect, as was demonstrated for NO degradation, when a 20-nm-thick TiO_2 film was conformally coated onto a photonic crystal, with some contribution also from the waveguided mode excitation enabled by the photonic crystal.[332] This approach can be applied to various types of semiconductor material systems by varying the active materials, leading to substantial improvements in air/water contamination, water splitting or artificial photosynthetic processes (Fig. 11).

The engineered enhanced light absorption and planar geometries of metasurfaces enable their use as a photo-electrode material,[333] demonstrating, in the case of a GaP-nanodisk-based metasurface, an overall photocurrent enhancement by more than fivefold compared to a planar GaP film under hydrogen evolution reaction conditions [Fig. 11(c)].[331] Nanoimprint lithography techniques and electrochemical approaches enable the rapid development of large-area nanopatterned surfaces of various materials necessary for industrial applications as a new generation of highly efficient solar metaelectrodes.

Dielectric (catalytically inactive) metasurfaces decorated with metal catalytic nanoparticles can be employed as an antenna-reactor photocatalyst where the virtually lossless metasurface funnels light to efficiently drive a chemical reaction.[334] By combining a Si_3N_4 metasurface exhibiting strong quasi-bound states in the continuum (quasi-BIC) resonances and large electric field enhancements, with Ni nanoparticles as reactors, this hybrid metasurface-based catalytic system was demonstrated to efficiently drive H_2 dissociation under the resonant illumination [Fig. 11(d)]. The experimental and theoretical analysis suggest that both photothermal heating and electronic transitions at the quasi-BIC-Ni surface facilitate catalytic chemistry (the thermal effect also cannot be ruled out in the above-discussed semiconductor metasurfaces when defect-related transitions are considered). This approach, based on engineered dielectric metasurfaces combined with otherwise weak absorbing metal catalysts, provides a universal platform which can be exploited for various combinations of dielectrics and catalytic metals.

In contrast to dielectric and semiconductor materials, plasmonic nanostructures provide the unique possibility to engineer light absorption throughout visible and near-infrared spectral ranges with spectral selectivity as well as strong electromagnetic field enhancement. Surface plasmons excited in metal nanostructures by light absorption decay either radiatively through re-emission of photons or non-radiatively via, e.g., Landau damping on a femtosecond timescale, resulting in hot carriers with energies comparable to the energy of the exciting photons.[337] These highly energetic hot carriers generated from the nonradiative decay of surface plasmons can either directly interact with molecular adsorbates on the metal surface or be transferred into adjacent semiconductor or metal co-catalysts efficiently inducing chemical transformations.

Plasmonic hot-electrons can be harvested in metal-semiconductor Schottky barriers, by combining the semiconductor catalyst with plasmonic nanostructures to achieve efficient electron–hole pair separation to prevent their direct recombination, thus increasing the lifetime of the hot-carriers and prolonging their opportunity to interact with adsorbed molecules. One drawback of metal–semiconductor heterostructure catalysts is the low charge mobility from the Schottky contacts. Many designs use a combination of plasmonic metasurfaces on or in a catalytic semiconductor layer simply to increase the local temperature and enhance thermal catalysis.

Alternatively, by incorporating strong plasmonic effects from metallic (Au, Cu, Al, etc.) nanostructures with highly catalytic active

16 July 2024 09:29:41

© Author(s) 2024

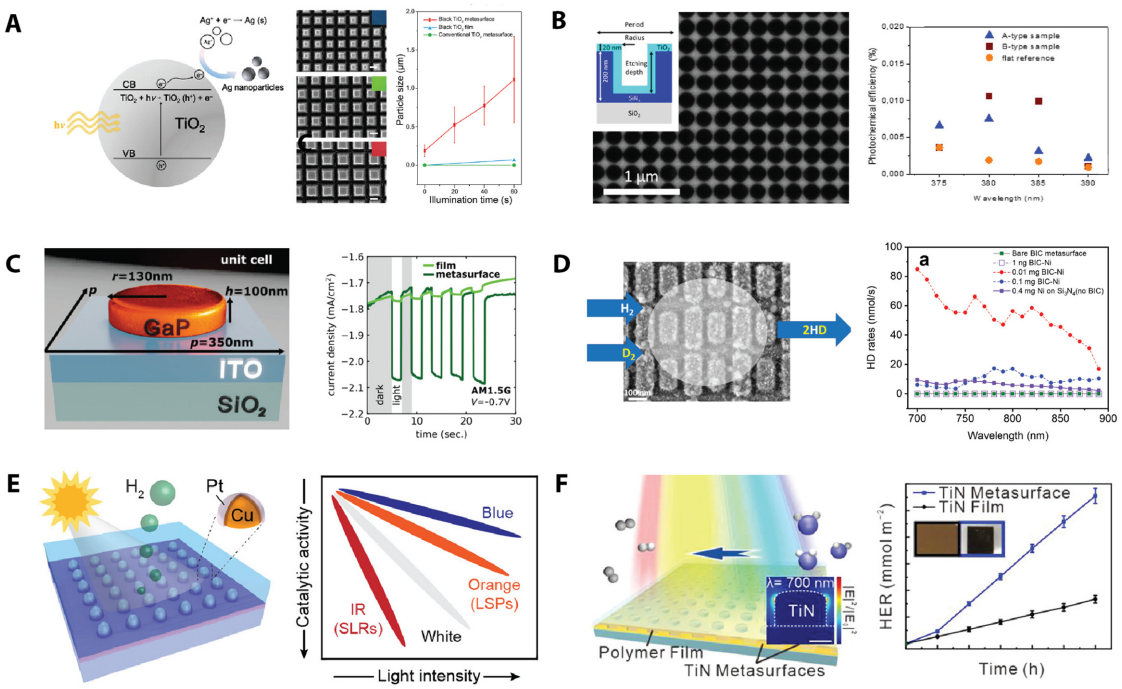

FIG. 11. (a) SEM images of the TiO_2 metasurfaces for the photoreduction of Ag nanoparticles and the dependence of the obtained mean particle size as a function of illuminating time for the black TiO_2 metasurface (red square line), the black TiO_2 film (blue triangle line), and the conventional TiO_2 metasurface (green dot line). Scale bar: 200 nm. The insets show the corresponding structural colors under a bright-field microscope. A schematic of the electron transfer process is shown on the left.[328] (b) An active metasurface based on a periodically patterned SiN_x coated with TiO_2 photocatalyst. The spectra of the photochemical efficiency for the flat sample and the two different structured samples.[332] (c) Enhancement of hydrogen evolution reaction (HER) under simulated solar illumination from a dielectric metasurface made of amorphous a-GaP on an ITO-covered glass slide, compared to that with a 100 nm thick continuous a-GaP film.[331] (d) Wavelength-dependent reactivity for photocatalytic H_2 dissociation using a quasi-BIC metasurface with and without Ni nanoparticle loading.[334] Adapted with permission from.[334] Copyright 2024 American Chemical Society. (e) Photo-electrocatalytic HER performances of core–shell Cu/Pt lattices combining individual LSPs and collective plasmonic SLRs under different illumination wavelengths.[335] Adapted with permission from Deng *et al.*, Nano Lett. **21**, 1523 (2021).[335] Copyright 2021 American Chemical Society. (f) Plasmon-enhanced visible-light-driven hydrogen production from water using a TiN plasmonic metasurfaces (blue line) and compared with a TiN film (black line).[336] Adapted with permission from Yu *et al.*, ACS Photonics **8**, 3125 (2021).[336] Copyright 2021 American Chemical Society.

materials, core-shell or decorated nanostructures can be employed for various types of reactions. Plasmonic metasurfaces decorated with transition metals (Pd, Pt) can enable efficient coupling of light energy into a catalyst through strong electromagnetic field enhancement, hot-carrier generation and photothermal effects. Such metaparticles (or hetero-nanoparticles) have demonstrated a significant increase in photocatalytic activity over monometallic particles by efficient transfer of hot carriers to the catalytic surface for various reactions.[338–341]

As an alternative to conventional plasmonic metals, titanium nitride (TiN) has started attracting significant attention for photocatalysis. TiN metasurfaces can be designed to exhibit broadband optical absorption in the visible range (i.e., an average of more than 92% in the 400–750 nm spectral range).[336] When coated with a polymeric photocatalyst, plasmon-enhanced hydrogen production from water under visible-light illumination was achieved, with the hydrogen evolution rate increased by 300% compared to a smooth TiN film [Fig. 11(f)]. The increased efficiency is attributed to a combination of enhanced light absorption, carrier separation, hot carrier transfer and thermal effects induced by the plasmonic metasurface. Refractory plasmonic TiN metasurfaces were also used for driving heterogeneous photothermal catalytic reactions. Self-assembled TiN cylindrical nanocavities act as plasmonic "nanofurnaces" capable of reaching temperatures above 600 °C under moderately concentrated solar irradiation (~20 Suns). Upon decoration with catalytic Rh nanoparticles, the obtained photothermal metasurface achieved a high rate of CO_2 production under solar-spectrum-simulated light intensities[342] as well as in the reverse water gas shift reaction.[343]

Metasurfaces based on arrays of strongly coupled bimetallic core–shell nanoparticles were also exploited to enhance photoelectrocatalytic activity for hydrogen evolution reactions.[335] Large-area Cu–Pt nanoparticle lattices fabricated by combining top-down lithography and solution-based chemistry support two different types of plasmon modes, localized surface plasmons from individual particles and surface lattice resonances (SLRs) from the 2D lattice, that increased the catalytic activity under white-light illumination up to 60% [Fig. 11(e)].

In addition to optical excitation by light illumination, hot electrons can also be generated electrically by excitation with tunneling electrons in tunnel junctions.[344] Recent realization of an electrically driven plasmonic nanorod metamaterial provides the opportunity to use an electron tunneling effect for the simultaneous excitation of hot electrons and surface plasmons, providing the means to realize a new

16 July 2024 09:29:41

© Author(s) 2024

kind of hot-electron-activated nanoreactor. By constructing a high-density array of plasmonic tunnel junctions at the top surface of a plasmonic metamaterial composed of vertically oriented gold nanorods, the efficient electrical excitation of the plasmonic modes of the metamaterial by inelastic electron tunneling can be realized. During the tunneling process, the majority of electrons (~99.9%) tunnel elastically in the electrically driven nanorod metamaterials, appearing as energetic hot electrons in the nanorod tips. The highly efficient and confined hot-electron generation makes the tunnel junctions highly reactive and opens up opportunities for the precise activation of chemical reactions in the junctions, which can be further detected with high sensitivity by observing the light emission from the tunnel junction or by observing changes in the tunneling current due to the extreme sensitivity of this highly confined tunneling process to any changes in the junction.

C. Future directions and outlook

Photonic metasurfaces have emerged as a promising platform for driving photocatalytic reactions. To develop a highly efficient photocatalyst with a photonic metasurface, several key design concepts need to be considered (Fig. 12). First of all, scalability of the fabrication method. For commercial exploitation, high durability, low unit cost, and efficient use of materials are undoubtedly the most appealing criteria for economic viability and sustainable chemical/energy production. Most of the aforementioned metasurfaces were fabricated using EBL or lithographic techniques which are relatively expensive fabrication processes and do not offer a large catalytic surface area. Nanoimprint lithography and self-assembled techniques can be used instead to reduce the fabrication cost.

To justify the use of metasurfaces, it will be advantageous to move from expensive noble metals and employ sustainable earth-abundant materials. For example, plasmonic metasurfaces made of transition metal nitrides and phosphides, CuS, MXenes, copper, and aluminum nanostructures need to be further investigated as a platform for engineering light absorption for photocatalysis and photo-electrocatalysis. The quality of semiconductor and plasmonic materials is of utmost importance. For plasmonic photocatalysts, different applications in photocatalytic metadevices may favor either rough or monocrystalline and ultrasmooth interfaces depending on the requirements of hot electron transfer to either molecules or semiconductor co-catalysts.[345]

In this regard, geometries and constituent materials can be optimized by using numerical simulations to tailor the desired engineering optical response for reactions that require specific energies. Furthermore, advanced *ab initio* numerical methods could help deepen understanding of reaction mechanisms under specific light illumination conditions (intensity, light polarization) and optimize optical properties to create a database of photonic metasurfaces suitable for photocatalysis. Electron and thermal effects of the metasurface illumination under both solar and pulsed laser illumination, as well as hot-electron transfer processes to reactants, need to be optimized. Machine learning and deep neural networks (DNNs) have recently been demonstrated to be powerful tools for designing efficient light-harvesting metasurfaces due to their extraordinary capability to find solutions from a large data set or parameter space.[346]

Product selectivity is a crucial aspect of any photocatalytic reaction that remains an ongoing concern and challenge. By engineering the synergetic effects of electron transfer and temperature, as well as the choice of the materials for adsorption, there is an opportunity to explore the prescribed modification of the energy reaction landscape to steer reactions toward the desired products. Many tests of the catalytic properties of plasmonic metastructures are performed under pulsed laser illumination which favors plasmonically derived hot-electron generation, and the peculiarities of CW illumination need to be taken into account. Selectivity in the synthesis of chiral molecules is the utmost challenge for pharmaceutical industries, and chiral metasurfaces may play an important role in steering the chiral reactions under circularly polarized light illumination.

Significant attention has been paid recently to the control of the chemical reactions through optical cavity modes, addressing specific vibrational modes of the molecules to influence selectivity.[347] These studies have been performed until now in optical cavities which select

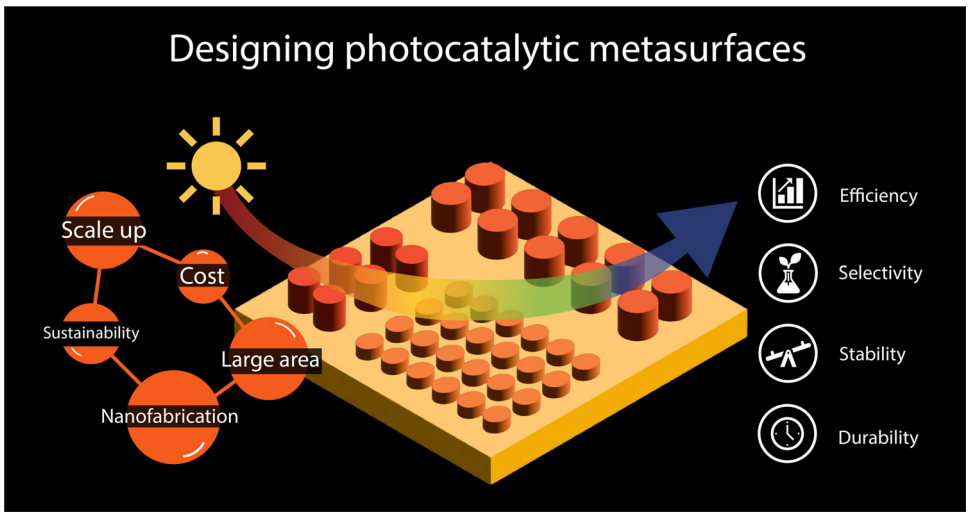

FIG. 12. Challenges (left) and requirements (right) for practical applications of optical metasurfaces in photocatalysis.

16 July 2024 09:29:41

© Author(s) 2024

the spectrum of the electromagnetic modes available for strong-coupling to vibronic modes of the reactants. Metasurfaces and metaparticles may play an important role in these photochemical transformations as they can be engineered to provide high quality-factor vibrational modes for coupling to molecular vibrational states.[348]

D. Concluding remarks

Metasurfaces and metamaterials providing precisely designed light–matter interactions offer an exquisite platform for understanding the mechanisms of light-induced chemical transformations, hence revealing routes to optimization. Through targeting either electron-induced and/or thermal effects via the design of the composition and structure of metamaterials, understanding of the role and interplay between electronic and thermal contributions in the reaction can be achieved, and their relative weight can be adjusted to control reaction pathways. Beyond fundamental research, metasurfaces can be readily applied in synthesis of high-value chemicals where small quantities of products, cost and femtosecond laser illumination are not prohibitive issues. Similarly, they provide an excellent platform for multiplexed functionalities, such as sensing and photochemical transformations, useful for environmental applications and pollution remediation.

In order to advance metamaterial-based catalysis concepts into mainstream photocatalysis, the problem of scalable production must be addressed together with a reduction of the associated costs, which can be achieved by moving away from top-down approaches toward self-assembly, electrochemistry, laser printing, or nanoimprint lithography for roll-to-roll fabrication. The planar nature of metasurfaces and metamaterials is advantageous for photo-electrochemical reactors and generally for photochemistry, where light-management issues are important considerations. Beyond these, the transfer of the light-harvesting properties designed for metasurfaces into a metaparticle platform holds much promise for the application of these designs in a scaleable manner compatible with chemical industry standards.

Harnessing metasurfaces and metamaterials as photocatalysts has emerged in the catalysis community because of their ability to harvest sustainable solar energy to promote chemical reactions. It is a comparatively new area of photonics and metamaterial research that is growing rapidly and showing promising results. Due to the ongoing climate and energy crisis, much research effort is currently focused on finding catalysts to combat environmental problems such as CO_2 reduction, NOx decomposition, and ammonia production to name but a few, and to provide renewable and clean energy with sustainable input through water splitting, etc. Metasurfaces, metamaterials and metaparticles have an important role to play in achieving net-zero pollution.

ACKNOWLEDGMENTS

This work was supported by the UK EPSRC under Project No. EP/W017075/1.

VII. ORBITAL ANGULAR MOMENTUM AND WAVEFRONT CONTROL

Haoran Ren, Yuri Kivshar, and Stefan Maier*

*stefan.maier@monash.edu

A. Introduction

Structuring light in multiple degrees of freedom, from spatial to temporal, holds great promise for advancing modern photonics from both fundamental and applied aspects. In particular, structured-light fields have proven useful for numerous photonic applications, including super-resolution microscopy,[349] optical trapping,[350] multimode imaging,[351,352] and holography,[32,208,353] optical communications,[354,355] nonlinear light conversion,[356] chiral sensing,[357,358] and quantum information processing.[359–361] Conventional generation of structured light typically relies on multiple cascaded phase and wave plates in bulky form, imposing major challenges for their practical applications. Over the past decade, flat optics, also known as ultrathin metasurfaces,[5] have become a new topic in the photonics community. Recently, such metasurfaces have been largely developed for the generation, manipulation, and detection of structured light. Here we summarize the key physical concepts demonstrated for generation of various kinds of structured light with metasurfaces. Apart from the generation, we highlight some exciting applications of metasurface manipulation of structured light, including but not limited to metasurface lasers with tailored spatial modes, metafibres capable of transforming arbitrary vector beams, vectorial metasurfaces that can create optical skyrmions, high-bandwidth twisted light holography, vortex metalens for edge enhancement, and metasurface-structured quantum emission. We also discuss some of the major challenges that lie ahead for the large deployment of structured-light metasurfaces. Finally, we provide some insights into recent new advances in metaphotonics that could potentially mitigate these challenges and push the field forward by creating more research impact.

B. State-of-the-art

In meta-optics, both plasmonic antennas and dielectric pillars have been used for the metasurface generation of different structured light fields in real space. For instance, a helical phase profile that carries the orbital angular momentum (OAM) has been imprinted by a phase-only metasurface, with the use of a set of meta-atoms that offer a complete phase modulation (from 0 to 2π). Ultrathin plasmonic metasurfaces based on near-field mode hybridization have been designed to implement the OAM phase [Fig. 13(A-a)].[5] High-index dielectric nanopillars with strong mode confinement, operating as truncated waveguides, have also been used to realize different phase vortices [Fig. 13(A-b)].[85] Huygens' metasurfaces of high transmission efficiency offer an alternative platform to realize phase vortices through spectrally overlapping electric and magnetic Mie resonances [Fig. 13(A-c)].[362,363] Apart from the use of phase-sensitive elements for creating phase vortices, plasmonic and dielectric nanostructures can be designed to possess strong polarization birefringence, exhibiting different phase accumulations for the polarization along the long and short axes [Fig. 13(B)].[16,20,364] Geometric metasurfaces based on the Pancharatnam–Berry phase principle have been used to create polarization-encoded phase vortices through the in-plane rotation of an identical asymmetric nanostructure. Meta-atoms with both varying orientation and size have been further developed to control arbitrary orthogonal polarizations in an independent manner.[365] As such, the output phase response for orthogonal polarization incidence can be decoupled from each other, leading to the generalized spin-to-OAM conversion of light that

16 July 2024 09:29:41

© Author(s) 2024

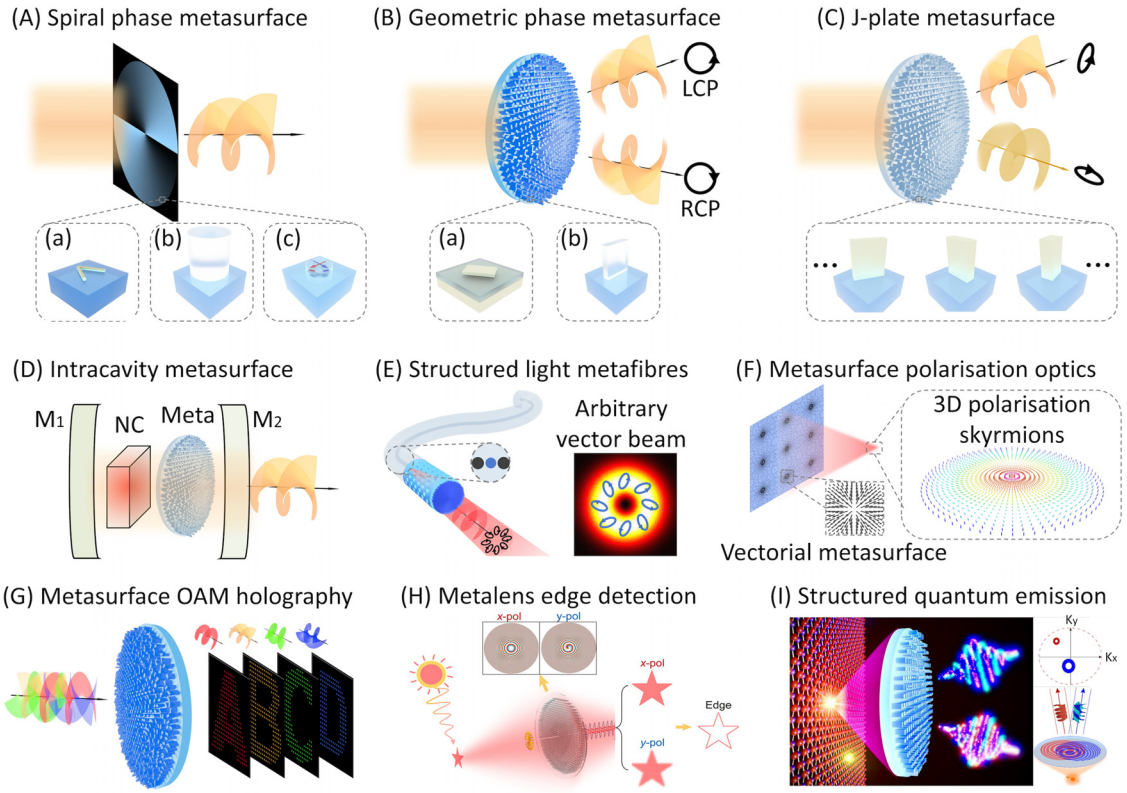

FIG. 13. Illustration of the metasurface generation of structured-light fields and their use for various photonic applications. (A) Spiral phase metasurfaces directly imprint a spiral phase profile via phase-sensitive elements made of (a) hybrid plasmonic antennas, (b) high-aspect-ratio dielectric nanopillars, and (c) flatter dielectric nanopillars satisfying the first Kerker condition. (B) Geometric phase metasurfaces encode the spiral phase profile onto the cross-polarization component from the metasurface by using birefringence (a) plasmonic and (b) dielectric nanostructures. (C) J-plate metasurfaces exploit the complete and independent phase and polarization control, capable of creating different OAM modes at arbitrary orthogonal polarization outputs. (D) An intracavity metasurface enables coherent laser emission with tailored structured-light modes. (E) Structured-light metafibres interfaced on the fiber end-faces can transform the fiber output into arbitrary selected structured-light fields on the hybrid-order Poincaré sphere. (F) Vectorial metasurfaces enable the creation of free-space optical skyrmions carried by topologically nontrivial 3D vectorial textures. (G) Metasurface OAM holography allows the multiplexing of a range of OAM-selective holographic images. (H) A spiral metalens can perform a 2D spatial differentiation operation and achieve isotropic edge detection under ambient sunlight illumination. (I) A polarization-beam-splitting metalens has been used for structuring quantum emission in multiple degrees of freedom from ultra-bright defects in hexagonal boron nitride at room temperature.

creates different OAM modes at orthogonal polarization outputs.[366] Such metasurfaces are designed by exploiting the complete and independent phase and polarization control by single meta-atoms based on the Jones calculus, named as J-plate metasurfaces [Fig. 13(C)]. Notably, J-plate metasurfaces pave the way of using a single metasurface for creating arbitrary structured light on the hybrid-order Poincaré sphere.[367]

Unlike traditional refractive or diffractive optics constrained from a limited access to multi-dimensional wavefront shaping, meta-optics has offered an unprecedented opportunity for structuring light fields in multiple degrees of freedom, from transverse to longitudinal (propagation direction) planes, as well as from spatial to temporal domains. Propagation-invariant or non-diffracting light beams, such as caustic beams whose transverse intensity distribution remains invariant over a significant propagation distance, exhibit high robustness and a self-healing behavior.[368] This has inspired metasurface generation of multiple phase vortices[369] as well as on-demand polarization transformations[370] along the optical path, which may inspire new directions in singular optics toward 3D space. In addition, temporal shaping of light, especially in the ultrafast domain, has benefited wide-ranging photonic applications.[50,371] Spatio-temporal metasurfaces have thus been created by combining a frequency comb source with a passive metasurface, capable of steering optical beams with a wide steering angle in just a few picoseconds.[50] In addition, metasurface-enabled pulse shapers have been demonstrated by embedding a dielectric metasurface in the focal plane of a Fourier-transform pulse shaping setup.[371] Such a Fourier-transform pulse shaper has recently allowed the generation of spatiotemporal optical vortices carrying previously unexplored transverse OAM modes.[372,373]

Over the last decade, structured-light metasurfaces have found many applications in the optics-related fields. Here we present only a few highlights, including but not limited to intracavity metasurface lasers, metafibers harnessing structured-light fields, generation of optical skyrmions in free space, metasurface holography using twisted light

16 July 2024 09:29:41

© Author(s) 2024

modes, vortex metalenses for edge detection, and the manipulation of quantum emission. Incorporating structured-light metasurfaces in a solid-state or fiber laser cavity has enabled coherent light emission with tailored spatial mode profile, such as high-purity vortices[374] and vortex arrays,[375] in a compact form factor [Fig. 13(D)]. This paves the way for the development of the next generation of miniaturized laser sources with tailored spatiotemporal mode control. The current use of structured light in optical fiber science and technology is limited by mode mixing, and hence generation of structured light is most usually handled outside the fiber via bulky optics in free space. A new meta-fiber platform has been introduced for implementing ultrathin metasurfaces directly on the end face of optical fibers.[376,377] Polymeric metasurfaces, with unleashed height degree of freedom, were 3D laser nanoprinted and interfaced with polarization-maintaining single-mode fibers. Multiple metasurfaces were interfaced on the fiber end-faces, capable of transforming the fiber output into arbitrary selected structured-light fields on the hybrid-order Poincaré sphere [Fig. 13(E)].[377]

Allowing subwavelength-scale-digitization of optical wavefronts to achieve complete control of light at interfaces, metasurfaces are particularly suited for the realization of planar holograms that promise new applications in high-capacity information technologies. Recent advances in metasurfaces and Fourier holography have offered an unprecedented opportunity to control optical wavefront in the spatial-frequency domain. Metasurface holograms have shown the independent control of both the 3D polarization[378] and the OAM states[32,208,353] of individual spatial-frequency components, represented by different image pixels reconstructed from the metasurface holograms in the Fourier plane. It opens the door to the use of a single metasurface for creating optical skyrmions with topologically nontrivial 3D vectorial textures[379] [Fig. 13(F)], as well as for reconstructing distinctive images from different OAM states [Fig. 13(G)].[32,208] Meanwhile, structured light has fueled many photonic applications in imaging, microscopy, and optical communications. For instance, the donut-shaped OAM beam in the focal region of a microscopic objective lens can deactivate fluorophores, minimizing the effective area of illumination and leading to super-resolution imaging. In addition, a spiral phase metasurface incorporated in a Fourier filtering optical setup can perform a 2D spatial differentiation operation and achieve isotropic edge detection.[380] A recent polarization-multiplexed metalens integrated with a polarization camera has allowed single-shot edge detection of indoor and outdoor scenes under ambient sunlight illumination [Fig. 13(H)].[381] Practical OAM communication systems suffer from turbulence-induced phase distortions to the propagating beams, decreasing the orthogonality of OAM modes through introduced modal crosstalk. An ultrathin OAM mode-sorting metasurface was recently used for characterizing the OAM orthogonality breakdown under different turbulence conditions.[382] It allows the measurement of the whole OAM spectrum at the same time, suggesting that metasurfaces with a small form factor can be integrated with practical communication systems for compact, fast, and efficient detection of twisted light in turbulence environments.

Structured photons in the quantum regime promise enhanced security by harnessing structured light as high-dimensional quantum states. An ultrathin polarization-beam-splitting metalens was demonstrated for arbitrary structuring quantum emission at room temperature [Fig. 13(I)].[359] The quantum metalens can collect the quantum emission from ultra-bright defects in hexagonal boron nitride (hBN), as well as enable simultaneous manipulation of multiple degrees of freedom of a quantum light source, including directionality, polarization, and the OAM of light. Dielectric metasurfaces can also be used for the manipulation and even direct generation of entangled photon pairs.[383] A geometric metasurface was first used in a spontaneous parametric downconversion setup for the nonlocal spin and OAM correlations on entangled biphoton states.[361] In this context, quantum state engineering mainly relies on the nonlinear optical effects, including spontaneous parametric downconversion and four-wave mixing, where one or two pump photons spontaneously decay into a photon pair. These nonlinear effects typically require the use of bulky nonlinear crystals by matching the momentum of the participating photons. Nonlinear metasurfaces have subwavelength thickness and allow the relaxation of this constraint,[34] opening new possibilities of quantum state engineering. Recently, metasurface generation and manipulation of entangled photons via spontaneous parametric downconversion have been demonstrated by high-quality-factor nonlinear metasurfaces made of lithium niobate[137] and gallium arsenide[384] materials. These results suggest that metasurfaces can offer a versatile platform for creating complex photon quantum states toward high-dimensional photonic quantum processing.

C. Future directions and outlook

Structured light, with many millions of spatial modes in a tiny cross section area of light, has shown great potential in transforming the landscapes of a wide range of photonic applications, from classical to quantum regimes. Meanwhile, metasurfaces have provided scientists and engineers with versatile tools to generate, manipulate, and sculpt optical fields. Although numerous advancements have been made in both the structured light and metasurface fields, there remain certain challenges in the science and technical aspects of structured-light metasurfaces. Even though metasurfaces benefit from the use of subwavelength meta-atoms to digitize optical wavefronts, the accuracy and efficiency of their amplitude, phase, and polarization modulations still need to be improved. For instance, for a phase-type metasurface, increasing the number of gray levels is important to reach near-unity diffraction efficiency, but this is indeed challenging for metasurfaces that rely on size-varying meta-atoms to realize the phase modulation. Recent developments in 3D laser-nanoprinted metasurfaces,[208,376,377,385] multilayer,[386] and cascaded metasurfaces,[387] as well as in hybrid metasurfaces that combine both refractive and diffractive optical elements[388] may alleviate this major challenge by unlocking 3D design degrees of freedom.

Current structured-light metasurfaces still require external source excitation, making them difficult to be integrated on-chip. Integration of metasurfaces with on-chip light sources, waveguides, and detectors will provide an exciting opportunity for future metasurface systems-on-a-chip. Recently, generation of free-space structured light with programmable integrated photonics was demonstrated.[389] More complications of using structured-light fields include strong modal coupling and intermodal crosstalk, due to free-space turbulence, large beam divergence, and misalignment in the detection process. Despite a great success has been made in the metasurface generation and manipulation of structured-light fields, metasurface-based selective detection of complex spatial modes, for instance, arbitrary selected states on the hybrid-order Poincaré sphere, is still elusive today. Nonlinear

16 July 2024 09:29:41

© Author(s) 2024

metasurfaces have been developed to observe high-order nonlinear optical spin–orbit interactions,[390] as well as non-reciprocal asymmetric generation of visible images.[391] Owing to the use of subwavelength meta-atoms, nonlinear metasurfaces hold tremendous promise for enhancing the toolkit for structured light–matter interactions beyond the limits of linear optics. While major challenges still exist on both science and technical aspects of structured-light metasurfaces, we believe these challenges are rather likely the driving forces to inspire more innovations and push the field forward.

ACKNOWLEDGMENTS

The authors acknowledge financial support from the Australian Research Council DECRA Fellowship DE220101085 (H.R.) and Australian Research Council Discovery Project DP220102152 (H.R., S.A.M.). S.A.M. additionally acknowledges the Lee-Lucas Chair in Physics.

VIII. METASURFACES FOR HOLOGRAPHY AND STRUCTURAL COLOR

Xianzhong Chen* and Muhammad Afnan Ansari

*X.Chen@hw.ac.uk

A. Introduction

Optical holography has been used for several decades for reconstructing 3D images by shaping the wavefront of a light beam. Unlike multiview parallax and photography techniques, a hologram consists of complete information of an object. The recording in the holographic technique is not an image itself, rather it contains random patterns of varying phase or intensity.[392] The holograms can be reconstructed either by the interference of a reference light beam with a scattered light beam from a real target or by calculating the phase profile of the light beam at the interface of a hologram. The phase profile can be encoded into the spatial light modulators or surface structures using lithography. The process involving the computer-generated phase information is known as computer-generated holography (CGH).[393] In the traditional holography and diffraction optics, the light field is regarded as a scalar field with two parameters, i.e., intensity and phase of the light beam.[394] With the ongoing advancements in nanofabrication techniques, the last decade has witnessed the rapid development of ultrathin and flat optical devices with unique degrees of freedom. One degree of freedom is the independent control of polarization distribution in the engineered light path, which remains the cornerstone for multifunctional holography, e.g., vectorial holography.[395] The traditional bulky optics were also used to a certain extent to introduce the concept of polarization holography for two-channel orthogonal polarization control using birefringent materials.[396] These polarization-dependent computer-generated holograms are sensitive to the polarization state of the incident light beam and capable of separating readout light through its polarization to generate distinct holographic images. This led to various novel applications such as multi-optical switching and image processing.[397,398] However, the conventional holographic recording medium and diffraction optics suffered from a limited degree of freedom and were unable to achieve simultaneous control of polarization state and spatial light field distributions. The form and magnitude of such type of birefringence were limited to naturally occurring crystals. On the other hand, materials with structures smaller than working wavelengths provided an alternative method to enhance the controllability of birefringence.[399,400] The drawback of materials with subwavelength structures was their extreme anisotropic requirement with very high aspect ratios.

B. Optical field manipulation in polarization-based holography

To tackle the challenges in conventional optics, metasurfaces have provided more degrees of freedom and better performance, particularly manifesting polarization-dependent physical channel multiplexing.[401–405] Initial demonstration of polarization multiplexed holograms based on plasmonic metasurfaces suffered from poor quality and low efficiency.[5,406] Wen *et al.* proposed and experimentally demonstrated highly efficient helicity multiplexed metahologram with good image quality in the near-infrared and visible range.[407] In this work, the issues of poor image quality and low efficiency were resolved by leveraging the high efficiency and broadband property of reflective metasurfaces.[20] Two off-axis holographic images were reconstructed under the illumination of a circularly polarized (CP) light beam. The images were symmetrically distributed and interchangeable by controlling the helicity of the CP light beam as shown in Fig. 14(a).[407] The right panel of Fig. 14(a) shows the change of holographic images (bee and flower) when the polarization of the input light beam is changed from left circular polarization (LCP) to right circular polarization (RCP). The helicity multiplexed property for CP light was attained by interleaving two metasurfaces comprised of plasmonic nanorods. Polarization-sensitive metaholograms for input light beams with elliptical, linear, and arbitrary orthogonal polarizations have also been reported in the literature.[365] Helicity multiplexed metaholograms have attracted various exciting applications in optical field manipulation such as stimuli-responsive (e.g., pressure, voltage, temperature, and gas) and tunable metaholograms.[408–410] For example, a volatile gas sensor based on helicity multiplexed metahologram integrated with liquid crystals was presented to sense isopropyl alcohol gas by generating a visual alarm.[408] In this work, the response of gas was recorded with different geometries of the designer liquid crystal (nematic and isotropic) by integration with an asymmetric metasurface. The proposed non-interleaved asymmetric metasurface[411–413] employed both geometric and propagation phase for the phase modulation. The overall phase retardation was controlled by controlling the cell order of liquid crystals through the external stimulus, i.e., the presence of gas. The tunable phase retardation adjustment of output light beam with desired polarization state using asymmetric metahologram and liquid crystals have opened new avenues to detect chemical and biomedical/biological substances in real-time for public health and environmental monitoring.[408,409] Recent studies on optical polarization multiplexing have further demonstrated the ability of metasurfaces to realize independent amplitude and phase modulations with non-orthogonal polarizations, which further expanded the ability of metaholograms for the full vectorial holography.[407,414,415]

Furthermore, holography has been widely used to achieve beam shaping,[416] surface plasmon holographic displays,[417] data storage,[418] optical trapping,[419] diffractive laser tweezers,[420] and digital holographic microscopy.[421] Although two-dimensional (2D) holograms were experimentally reported using metamaterials and metasurfaces, none of them have achieved 3D image reconstruction using CGH in the visible domain. To fulfill the essence of holography in 3D space, Huang

16 July 2024 09:29:41

© Author(s) 2024

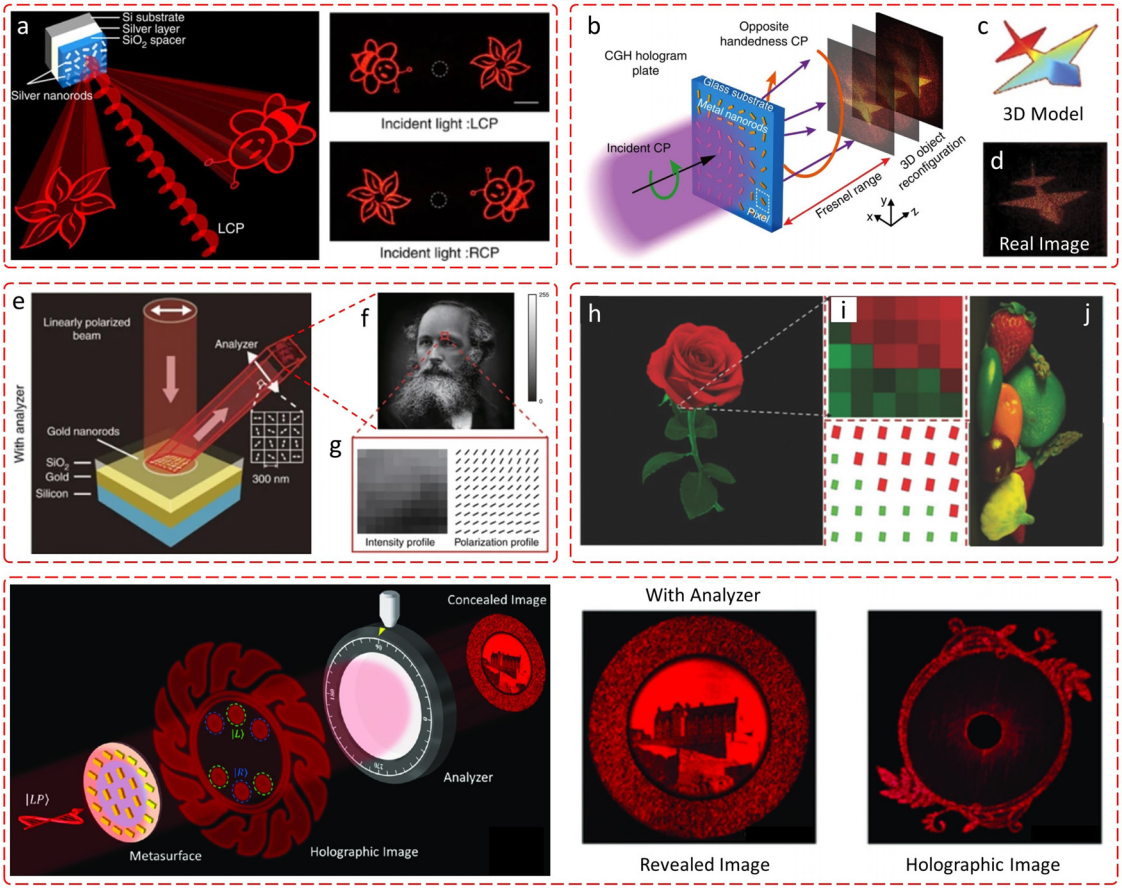

FIG. 14. Polarization sensitive metasurface holograms, 2D polarization structures and their combination. (a) Helicity multiplexed holograms. Two central symmetric helicity-dependent holographic images are reconstructed under the illumination of LCP (bee and flower) and RCP light beams (flower and bee). (b)–(d) Schematic diagram of a 3D metasurface hologram. (c) A 3D object (jet) and (d) Experimentally obtained a real holographic image of the jet at an observation plane under the illumination of an RCP light beam. (e)–(g) Schematic for hiding a gray-scale high-resolution image in a laser beam through metasurface based on Malus' law. (f) The hidden image of James Clerk Maxwell is revealed with a linear polarizer (analyzer). (g) Detailed information in the eyebrow area (10 × 10 pixels). The right and left FIGS show the polarization distribution and the corresponding intensity profile. (h)–(j) Mechanism of polarization encryption for encoding a color image. (h) The target image of flower (red) and leaves (green). (i) Detailed information in the selected region (6 × 5 pixels) of the target image (top panel) and the corresponding orientation angles and feature sizes of dielectric nanopillars (bottom panel). (j) Results of metasurfaces for hiding a color image based on color mixing, which is realized with a metasurface consisting of supercells. (k)–(m) A metasurface that can simultaneously realize polarization sensitive and insensitive holograms and 2D polarization profiles for hiding a high-resolution image (a castle), which can increase information channels and information density. Panels (a) reproduced with permission from Wen *et al.*, Nat. Commun. **6**, 1 (2015).[407] Copyright 2015 Springer Nature. (b)–(d) Reproduced with permission Huang *et al.*, Nano Lett. **13**, 3559 (2013). Copyright 2013 Springer Nature.[426] (e)–(g) Reproduced with permission from Yue *et al.*, Light **7**, 17129 (2017).[423] Copyright 2017 Springer Nature. (h)–(j) Reproduced with permission from Zang *et al.*, Adv. Mater. **30**, 1707499 (2018). Copyright 2018 Wiley-VCH.[424] (k)–(m) Reproduced with permission from Intaravanne *et al.*, Adv. Photonics Res. **2**, 2000046 (2021). Copyright 2020 Wiley-VCH.[425]

et al. presented a relatively simpler approach to realizing 3D holography using ultrathin metasurface consisting of subwavelength metallic resonators with varying orientation as shown in Fig. 14(b).[392] The phase information of the 3D object was calculated using commercially available CGH algorithm.[422] In the CGH algorithm, the 3D target object [Fig. 14(c)] was considered as a collection of many point sources. The complex amplitude at the hologram interface was numerically calculated through the superposition of the wavefronts of all point sources. Upon the illumination of the CP light beam, the metasurface reconstructed a real 3D holographic image within the Fresnel range of hologram as shown in Figs. 14(b) and 14(d). As explained earlier, the incorporation of spatially varying polarization along with the phase distribution is essential to fully unlock the potential of metasurfaces for increased information storage. Yue *et al.* proposed such a technique to encrypt a 2D grayscale image (of James Clerk Maxwell) in a structured laser beam with inhomogeneous polarization distribution using metasurface based on Malus' law as shown in Fig. 14(e).[423] The result of the intensity profile of the encrypted grayscale image was revealed with an analyzer (linear polarizer) as shown in Fig. 14(f). To further explain the technique, a selected portion from the eyebrow area (10 × 10 pixels^2) is enlarged in Fig. 14(g) to show the intensity and its corresponding pixel-level polarization distribution. It is noted that the resultant

16 July 2024 09:29:41

© Author(s) 2024

beam exhibited a subwavelength resolution. Similarly, metasurfaces can also be used to encode colorful images in inhomogeneous polarization profiles based on Malus's law. Zang *et al.* experimentally demonstrated simultaneous encryption of intensity and color information into a wavelength-sensitive polarization distribution.[424] This technique was used to embed high-resolution color images with precisely controlled contrast and brightness onto a dielectric metasurface as shown in Figs. 14(h)–14(j). The target high-resolution color image of a rose was selected which encompassed green and red pixels with the variation of spatial brightness as shown in the top panel of Fig. 14(i). The corresponding wavelength-dependent polarization distributions were different for both colors and mapped by controlling the orientation and the feature size of the dielectric nanopillars as shown in the bottom panel of Fig. 14(i). Vivid red petals and green leaves were revealed with the right transmission axis of the analyzer under the illumination of 660 and 550 nm wavelengths. The same method was also used to produce polarization-encrypted colorful images using additive color mixing of the primary colors as shown in Fig. 14(j). In this work, a supercell contains nanopillars with different feature sizes, which respond to different wavelengths.[424] By integrating such high-resolution polarization encryption techniques with holography, many diverse applications can be realized in information security, anticounterfeiting, and high-density data storage. For example, an application of optical information security was experimentally demonstrated by integrating an arbitrary polarization distribution for image concealment and a hybrid CGH as shown in Fig. 14(k).[425] The functionality was achieved by simultaneously concealing a high-resolution image in the polarization distribution and encoding holographic images through the superposition of two-phase profiles for orthogonal CP light beams. As a result, a metasurface was used to reconstruct holographic images at the observation plane either under the illumination of linearly polarized light beam without the analyzer or under the illumination of RCP light beam as shown in Fig. 14(m). The desired concealed image was revealed with a predesigned angle combination of the analyzer and input linear polarizer as shown in Fig. 14(l). In contrast, the other transmission axis combination of the analyzer and input linear polarizer could not generate meaningful information. The work also investigated the simultaneous incorporation of polarization-sensitive and insensitive holograms with high-resolution image encryption in the polarization distribution, which further enhanced the information capacity and hence can be utilized for high-level anticounterfeiting.

C. Toward 3D polarization structures: challenges and future directions

2D high-resolution image encryption based on spatially varying polarization distributions has been realized with metasurfaces.[423–425] However, in addition to the phase, intensity, and color, the encryption of spatially varying polarization distribution in a 3D space remains a challenge. To generate the desired wavefront and dynamically manipulate the polarization distribution in a 3D space, an independent pixel-level control of phase and polarization is simultaneously required along the light's propagation. The biggest challenge to achieve such functionality is the limited degree of freedom in the current metasurface design. Although few studies have shown unprecedented abilities to break the conventional limits to some extent,[415,427–429] they are still unable to address the complete and dynamic control of light fields in a 3D space. Therefore, a solution is required to address this problem at the fundamental level where new control variables can be incorporated into the metasurface design procedure. The required control variables for an arbitrary 3D polarization structure include wavelength, wavefront positioning (x, y, z), and dynamic polarization rotation in a 3D space. Much work has been done to address one control parameter at a time,[407,412,425,426,430] however, simultaneous control of all parameters is scarce and challenging. The combinational control of more than one parameter is also expected to yield unique optical field manipulation. Recently, Zang *et al.* proposed a metalens with polarization functionality through the superposition of both RCP and LCP components of the light beam at each focal spot under the illumination of linearly polarized incident light beam.[431] The authors started from a simple lens model by incorporating an additional term for the polarization rotation ϕ in the phase profiles of LCP and RCP components. Since a linearly polarized incident light beam can be divided into LCP and RCP light components, therefore, a portion of the transmitted wave is converted to LCP light to focus with an additional phase shift $-\phi$, and the other portion is converted to RCP light with an additional shift of ϕ. The idea was then extended to realize multiple focal points using the superposition method with independent polarization rotations as shown in Fig. 15(a). Wang *et al.* presented an off-axis multi-foci metalens model to incorporate polarization rotations in four different focal points at different locations on the observation plane as shown in Fig. 15(b).[432] Unlike the previous work where only linear polarization rotations are created, Wang *et al.* introduced RCP, LCP, and linear polarization rotations for the application of polarimetry to detect the polarization of arbitrary incident light beams. The ellipticity, handedness, and major axis of the polarization state of the incident light beam were determined through the measured intensities of the four focal points.[432] Both designs have provided a unique insight into a pixel-level simultaneous control of wavefront along with the independent polarization rotations. More specifically, both unique ideas of polarization rotation at different focal lengths (f1 and f2) along the z-direction[431] and the off-axis (xi, yi) multi-foci metalens[432] have led to the generation of 3D polarization structures. An optical focal curve can be regarded as a continuous structure if the number of focal points along the curve becomes infinite. Wang *et al.* started from a muti-foci metalens with discretized focal points to a continuous optical curve along an arbitrary trajectory by increasing the number of focal points.[433] In the next step, the 2D polarization curve model was transformed to 3D polarization knot design by introducing the longitudinal parameter (z) as an additional control variable in the phase terms using the superposition method. As a result, 3D light fields along with spatially varying inhomogeneous polarization distributions and intensity patterns were generated in the form of 3D optical knots as shown in Fig. 15(c).[433] The predesigned polarization distribution was confirmed through the modulated intensity patterns with an analyzer (linear polarizer). In addition to the predefined inhomogeneous polarization distribution, the polarization rotation at each point on the 3D trajectory was dynamically modulated by changing the polarization state of the incident light beam. The complete evolution of the 3D structure was also observed and measured using a CCD camera as shown in Fig. 15(d). Intaravanne *et al.* introduced a new control variable (wavelength λ) in the design procedure along with polarization rotation ϕ and 3D focal position (u, v, f) to demonstrate wavelength selective 3D polarization structures as shown in Fig. 15(e).[434,435] At a given observation plane,

16 July 2024 09:29:41

© Author(s) 2024

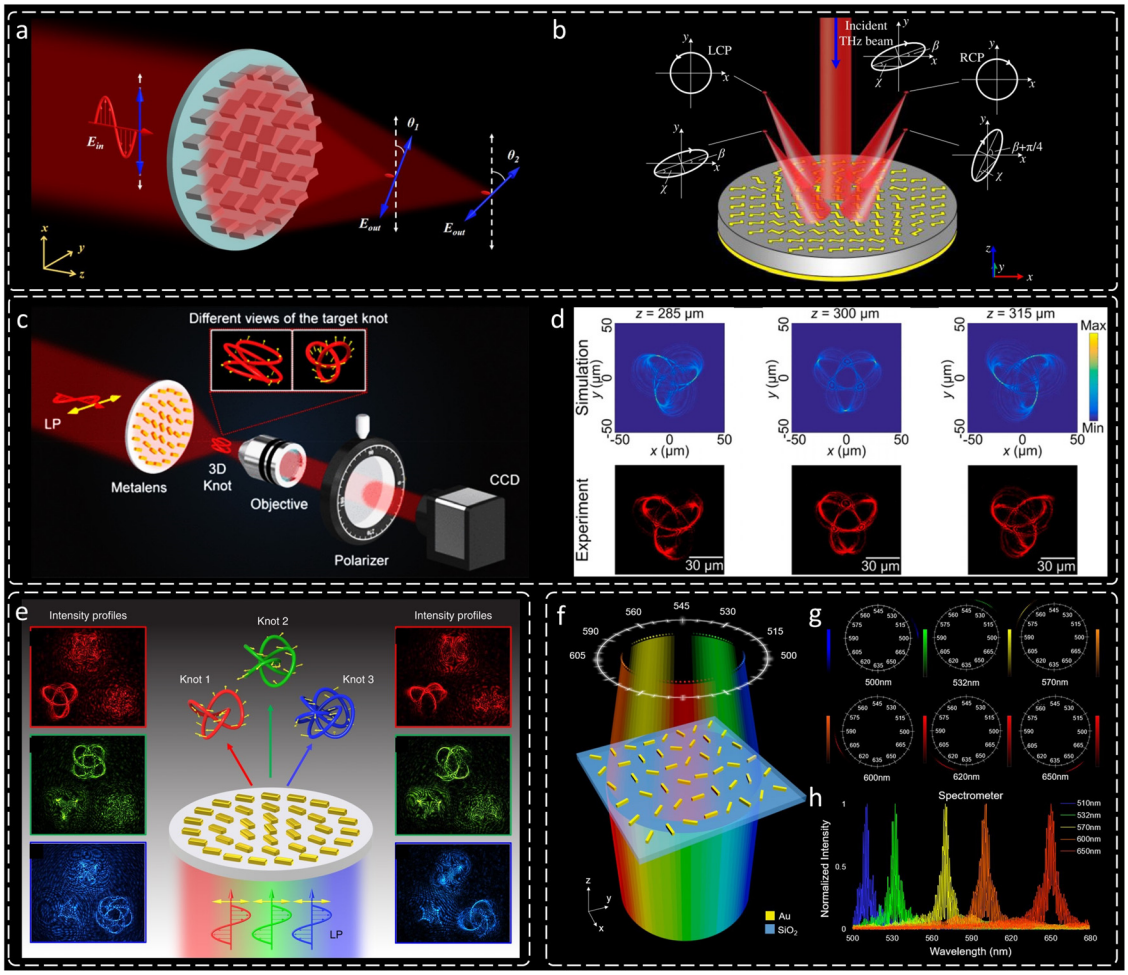

FIG. 15. Metalenses for realizing polarization rotation, 3D polarization structure manipulation and a compact spectrometer. (a) A multi-foci metalens with a polarization rotation functionality. (b) Application of multi-foci metalens for the polarization detection in the THz range. (c) Customized 3D polarization structures based on multi-foci metalens. (d) Simulated and experimental intensity distributions of 3D structures at different observation planes under the illumination of an RCP incident light beam. (e) Metasurface for color-selective 3D polarization structures. The left panel and right panel show the light intensity distributions without and with an analyzer, respectively,. (f) A compact metasurface spectrometer based on multi-foci metalens. (g) Light intensity distribution under the illumination of different monochromatic incident light beams. (h) Spectrum detected by the metasurface spectrometer under the illumination of the polychromatic incident light beam. Polychromatic light beam contains five different wavelengths. Panels reproduced with permission from: (a) reproduced with permission from Zang *et al.*, Laser Photon. Rev. **13**, 1900182 (2019).[431] Copyright 2019 Wiley-VCH. (b) Reproduced with permission from Chang *et al.*, J. Vac. Sci. Technol., B **21**, 2755 (2003). Copyright 2020 Optica Publishing Group (formerly OSA).[432] (c) and (d) Reproduced with permission from Wang *et al.*, Nano Lett. **21**, 2081 (2021). Copyright 2021 American Chemical Society.[433] (e) Reproduced with permission from Intaravanne *et al.*, Light Sci App **11**, e302 (2022). Copyright 2022 Springer Nature.[434] (f)–(h) Reproduced with permission from Intaravanne *et al.*, Adv. Opt. Mater. **12**, 2203097 (2024). Copyright 2023 Springer Nature.[435]

different 3D polarization knots were generated by changing the wavelength of the incident light beam as shown in the left and right panels of Fig. 15(e). The right panel and left panels present the intensity distribution of corresponding 3D polarization structures with and without the analyzer, respectively.

The ability to generate arbitrary wavelength-dependent 3D polarization structures with ultrathin metasurfaces can be of interest to many pragmatic applications such as integration optics for compact spectrometers, and longitudinally variable structures for 2D and 3D optical image steganography. For example, motivated by the intrinsic dispersion property and ability of metalens to generate multiple focal points at will, the wavelength of the incident light beam can be detected accurately by mapping the wavelength information to the intensity distribution. A compact spectrometer was realized by tailoring the dispersion based on the model of multi-foci metalens as shown in Fig. 15(f).[436] The metasurface-based spectrometer can focus and split the monochromatic [Fig. 15(g)] and polychromatic light beams [Fig. 15(h)] of different wavelengths to desired positions on an observation plane with 1 nm resolution. This unique dispersion control and high nanometer spectral resolution were achieved over a broadband range in the visible domain. The application of the proposed multi-foci metalens-based spectrometer proved that this technology has clear potential for

16 July 2024 09:29:41

© Author(s) 2024

development in on-chip integrated photonics where wavelength detection, information processing, and spectral analysis are required in a compact platform. Like other emerging technologies, further improvements in the current design are required and new challenges need the attention of the research community. For example, the demonstrated metasurfaces have a low conversion efficiency, which is associated with the symmetric spin–orbit interactions and can be resolved by employing the nanoresonators with asymmetric spin–orbit interactions.[411–413] Furthermore, the polarization manipulation can be extended to incorporate arbitrary polarization states, including linear, elliptical, and circular polarization states. The integration of metasurfaces with materials such as 2D transition metal dichalcogenides,[437] conducting oxides,[438] liquid crystals,[408,409,439] and active materials[209] can add the extra degree of freedom and perform complicated optical tasks that are impossible or extremely challenging only with passive metasurface design.

IX. META-OPTICS FOR AUGMENTED REALITY APPLICATIONS

Yuhui Gan, Arseny Alexeev, Thomas F. Krauss, and Andrea Di Falco*

*adf10@st-andrews.ac.uk

A. Introduction

Augmented reality (AR) superimposes computer-generated content onto a transparent medium such that the user can perceive the real world augmented with the artificial content; this contrasts with virtual reality (VR), whereby a computer generates all the content. In AR applications, the need for a transparent medium precludes the use of conventional displays. This requirement for transparency poses challenges, but it also promotes widespread acceptance of the technology. It benefits specialized applications such as assisted surgical operations or equipment maintenance, as well as end-user applications such as smartphones.

The main elements of an AR system are the image projector, which creates the digital image, and the optical combiner, which blends digital and real images before delivering the combined picture into the user's eyes.[440] Depending on the system architecture, the image projector consists of a light source (laser or LED), a spatial light modulator that modulates the light to create an image, e.g., based on liquid crystals or digital micro-mirrors, and image-forming optics such as lenses and mirrors. The optical combiner has been the subject of intense research over the last few years and is the focus of this paper. Combiners started as bulky and irregularly shaped glass elements,[440] as shown in Fig. 16(a), they then evolved into sophisticated photonic devices, usually involving nanostructures [Figs. 16(b) and 16(d)].

The most common configuration used for optical combiners to date is an optical waveguide that delivers light toward the observer via a Holographic Optical Element (HOE)[441] or a Surface Relief Grating (SRG)[442] [Fig. 16(b)]. Both HOEs and SRGs are manufactured using nanoscale lithographic techniques. Another type of optical combiner uses metalenses [Fig. 16(c)],[443] which are actively being explored for AR applications due to their low weight and their ability to imprint any desired phase distribution onto the incoming wave; therefore, metalenses can replace freeform optical elements due to their advantageous form factor and functionality. We note that several reviews describing AR systems using both waveguide combiners and metalenses are already available,[444] which this perspective article aims to

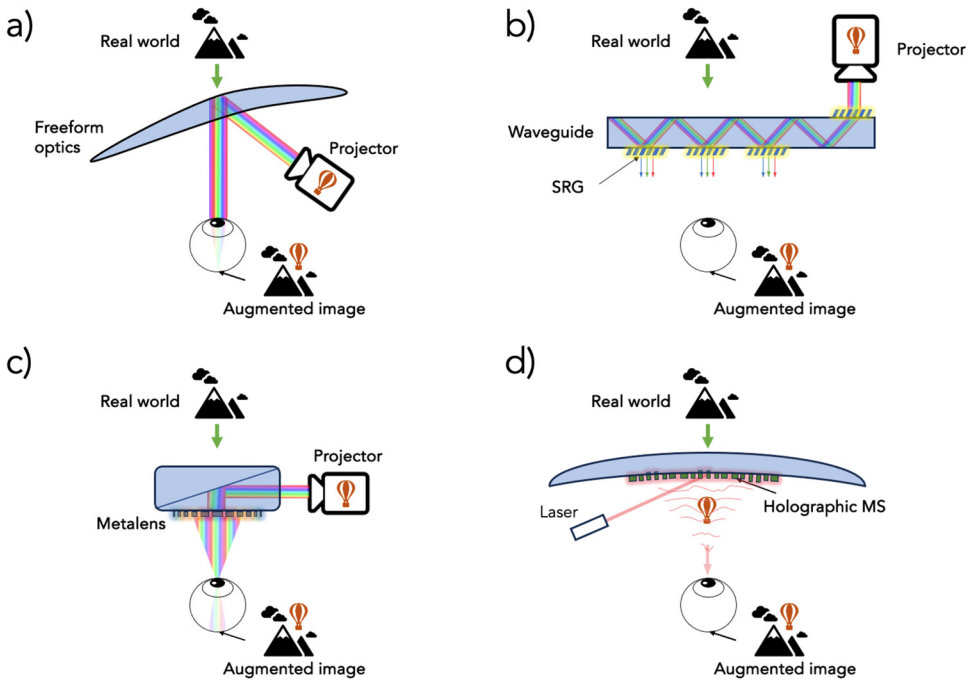

FIG. 16. Four AR architectures: (a) freefrom optical combiners; (b) waveguide combiners with metagratings; (c) prism combiners with a metalens; (d) holographic metasurface combiners. (a)–(c) use full-color projectors to generate virtual image; and (d) uses plain laser beams and the virtual image is encoded in the metasurface.

16 July 2024 09:29:41

© Author(s) 2024

complement. Here, we first introduce the key parameters and figures of merit of an AR near-eye transparent display and then briefly review the state-of-the-art of various meta-optical technologies that are being used in consumer-grade AR glasses. Finally, we discuss the performance tradeoffs of each approach, including the use of transparent holographic displays based on metasurfaces. The holographic approach eliminates the need for an image projector, thus achieving a minimalistic form factor while delivering superior optical performance, as shown in Fig. 16(d).

B. State of the art

1. Parameters

AR display systems must meet a variety of performance metrics, which can sometimes conflict one another. For example, the field of view (FoV) describes the range of angles at which optical rays are delivered to the human eye to form an image on the retina. The FoV is critical, as it defines the perceived size of the virtual object generated by the AR glasses. A typical value for heads-on AR displays is around 60° (diagonally)[444] while, for reference, the human eye's FoV is approximately 120°;[440] thus, it is desirable to extend the FoV of AR glasses. However, such an extension poses real challenges for the display brightness and resolution, as the properties of the image are determined by the luminous source. If the FoV increases, the luminous energy must be distributed over a larger range of solid angles, so the luminous energy per solid angle will suffer. Similarly, for a larger FoV, the resolution decreases, as there is only a fixed number of pixels available. A large FoV also has an impact on the eyebox, which describes the geometrical region of eye positions that contribute to image formation without vignetting. AR glasses must have a large eyebox to ensure tolerance to eye movements and to accommodate different users. The size of the eyebox is measured in mm in the x and y directions in the plane coinciding with the plane of the eye hole, where a minimum of 6 mm is required to accommodate inter-pupil distance variations of 95% of the human population. High-performance displays achieve >10 mm in both directions. The product of the FoV and the eyebox is comparable to the etendue of an optical system, as it represents the product of an area and an angle; this product is fixed by the image projector. For a given projector, an increase in the FoV directly results in a decrease in the eyebox size. As discussed further below, this conservation of etendue can be overcome by the method of "pupil replication"—which replicates the image source over the surface of the optical combiner, which is why the waveguide approach is so attractive. Finally, images must be created with good color and brightness uniformity, irrespective of FoV and eyebox, so this requirement cannot be traded off.

2. System architectures and technological platforms

Freeform Optics—The simplest way to deliver light from a projector to the eye is to reflect the projector signal toward the eye by a suitably shaped, partially reflective mirror, as shown in Fig. 16(a). This approach has the advantage of requiring minimal image preprocessing and results in a relatively simple system architecture while delivering good FoV (90°) and eyebox (>10 mm) as well as producing high-quality images. The main disadvantage of this approach is the need for a bulky, inconvenient headset that imposes an unnatural look on the user due to the shape and weight of the freeform mirror and its tilt. Additionally, this design is fundamentally restricted by the conservation of etendue, as discussed before.

Waveguides—Currently, the most popular implementation of the AR optical combiner function consists of an imaging waveguide with diffractive elements. In a typical arrangement, three linear diffraction gratings are used, (i) to deliver the image rays created by the projector into the first diffracted order below the angle of total internal reflection of the glass-air interface, thus in-coupling image rays into the waveguide; (ii) split the image rays into higher diffraction orders, thereby replicating the image pupil; and (iii) diffract the image rays at multiple points into the user's eye, thus, outcoupling the image rays from the waveguide. The key advantage of this approach is that the waveguide produces copies of the image pupil, thereby surpassing the fundamental trade-off between the FoV and the eyebox imposed by the conservation of etendue, achieving FoV > 60° and eyebox > 10 mm without the need to use bulky free-form optics. The gratings are typically Bragg gratings recorded in holographic media or Surface Relief Gratings—SRGs. The technology of holographic Bragg gratings is very mature but this solution only offers low refractive index contrast. This intrinsically leads to a high selectivity of the diffraction process in terms of angle and wavelength, therefore limiting the FoV of the entire system.[444] Despite these shortcomings, this approach is well suited for applications that do not require large FoV (for example, displaying notifications or giving instructions for navigation, for automotive

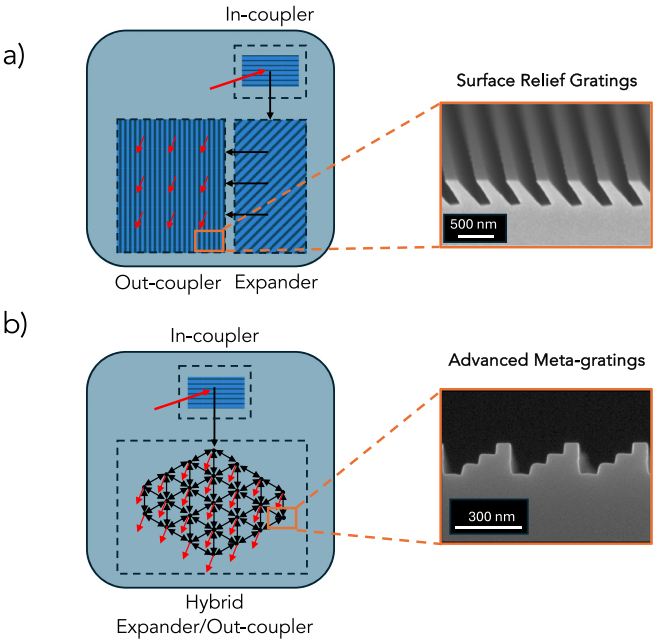

FIG. 17. (a) Side view of a waveguide combiner consisting of three elements, i.e., to in-couple, spread, and out-couple the image rays. The inset shows an example of a Surface Relief Grating (Reproduced with permission from Levola and Laakkonen, Opt. Express **15**, 2067 (2007). Copyright 2007 OSA Publishing).[445] (b) Top view of a waveguide combiner with two grating elements. The inset shows the cross section of an advanced etched metagrating which constitutes the hybrid element of the waveguide combiner which simultaneously spreads and out-couples the image rays, with a pitch of 300 nm.

16 July 2024 09:29:41

© Author(s) 2024

applications). SRGs are, in turn, fabricated by nano-structuring waveguide surfaces and possess higher refractive index contrast. Therefore, SRGs support larger FoVs. Such gratings can now be fabricated with high accuracy and high manufacturing yield because of advances in nanofabrication, including the use of nanoimprint lithography [see Fig. 17(a)].[445] This classical three-element grating scheme was pioneered by Nokia[440] and then adopted by other companies, including Microsoft, Magic Leap, Vuzix, and others. A more advanced version of the waveguide combiner scheme (e.g., that introduced by WaveOptics uses two-dimensional SRGs to combine the expander and the outcoupler elements in one hybrid unit). In this configuration, a larger area of the combiner is available for the outcoupling, resulting in an increased eyebox of >10 mm in both directions. Realizing these advantages is, however, a challenging task. The grating must not only have minimal dependence of the diffraction efficiency on the wavelength and incident angle, but also balance the contributions from the image rays that are incident from different directions, as specific optical rays can reach a given extraction point via multiple routes and not just through a single geometrical path as in the classical configuration, see Fig. 17(b). In this way, the chromatic and angular aberrations can be minimized to produce a uniform virtual image. These requirements can only be met with the introduction of further degrees of freedom, which has led to the development of 3D metagratings—true nanophotonics objects sculpted into complex 3D shapes.[446] Each element of such a 3D metagrating acts as a sub-wavelength antenna. The full response of the grating is then defined by the convolution of the interference pattern of the entire grating with the radiation profile of each grating element.[447] While traditional SRGs are patterned at scales greater than the wavelength, these advanced metagratings require a lithography resolution below 50 nm and high-precision alignment.

Metalenses—Metalenses utilize subwavelength structures to manipulate light at the nanoscale. With their ultra-thin size, sub-wavelength modulation scale, and ability to imprint any desired phase front onto the incoming signal, metalenses can be used to make flat versions of traditional lenses[448] reducing the size, complexity, and cost of the optical system.[449,450] Remarkably, metalenses can also be engineered to respond differently to light with specific polarization, wavelength, or angle of incidence.[451,452] This flexibility makes them very attractive for AR applications.[453–455] In the example of Fig. 16(c), metalenses are used in the Maxwellian configuration, whereby the image is focused on the pupil and the virtual image is always in focus, independent of the accommodation of the eye lens.[456] This approach offers advantages in terms of FoV. However, the eyebox for the Maxwellian configuration is very small.[444] While metalenses offer superior control over the wavefront of the transmitted light, they are characterized by intrinsic tradeoffs.[457] The main trade-off is the fact that a typical metalens design strongly depends on the wavelength. The choice of thin film thickness, meta-atom size and unit cell, as well as the use of Fresnel zones to accommodate multiple 2π phase shifts, are all wavelength-dependent. Moreover, the unit cell size depends on the numerical aperture (NA) according to the Nyquist criterion as a $<\lambda/(2\,\mathrm{NA})$, which means that the higher NA required for AR systems to achieve reasonably large FoV also demands a smaller unit cell size. This quickly becomes very challenging in terms of lithographic requirements, especially for operation in the visible. All these requirements trade-off against each other; for example, the wavelength dependence can be addressed by controlling the dispersion in each meta-atom by substructuring the unit cell and using two meta-atoms instead of one.[458] This is an elegant solution which, however, restricts the unit cell size for lithographic reasons, so only a low NA or longer wavelength operation can be achieved. Another example is the control of aberrations, where in particular, designed phase profiles have been used to demonstrate a very large FoV,[459] but only for a single wavelength.

When it comes to AR applications, metalenses face the same challenge as standard freeform optical elements in terms of balancing a sufficiently large FoV (>60°) with a wide enough eyebox (>10 mm), while possessing a small form-factor for the convenience of the user. However, the main limitation is that due to the design and manufacturing challenges we mention above, modern metalenses are yet to become suitable for image-forming optical systems. As a result, many metalenses are designed for security camera operations that do not require multiple colors and that work best in the near-infrared.

Holographic Metasurfaces—In the scheme shown in Fig. 16(d), the microdisplay projector is replaced by a simple laser or an LED. This choice shifts the physical location of the digital information from the image projector to the optical combiner, which is much simpler, but restricts the system to fixed images stored in the hologram.[35,460] While some degree of image multiplexing is possible, the number of independent images that can be stored in the combiner is then rather limited. A solution would be the deployment of dynamically tuned metasurfaces to create AR glasses capable of displaying dynamic images. Such a dynamic holographic display could be achieved using a variety of material platforms and actuation mechanisms, as discussed in Sec. IX C.

C. Future perspectives

Waveguides and *Metalenses*—Metalenses and metagratings used in AR optical combiners exhibit noticeable similarities in terms of controlling a given wavefront and producing a desired optical response. Both approaches utilize engineered patterns of sub-wavelength antennas to create a desired functionality. Likewise, both in metalenses and metagratings, the complexity of the meta-atom design is now surpassing initial simplistic designs by shaping or substructuring the meta-atoms. By exploiting all the degrees of freedom of metaoptics design, it is now possible to improve the brightness and color uniformity of AR systems.

While the design complexity of the meta-atoms and the manufacturing of metalenses and metagratings have already merged, these two approaches employ fundamentally different architectures. Given the advanced technology readiness level reached by the waveguide-style combiner, it is anticipated that waveguide combiners will be the choice for the next few generations of commercially available AR systems. The main advantage that motivates this choice is that the waveguide architecture addresses the issue of the FoV—eyebox trade-off, through the pupil replica mechanism. Importantly, from an engineering point of view, in metagratings, it is also possible to manage the extraction efficiency and thus maximize the extracted energy along the propagation path of the image rays. The main challenge for waveguide-based combiners remains to achieve good color and brightness uniformity. These parameters are still limited by chromatic and angular aberrations. Regardless of the coupling mechanism, it is extremely challenging to in-couple and out-couple all the image rays with the same efficiency, independently of their wavelength and incident angle. To this end, the shape of the 3D meta-atoms will require further optimization. Importantly, this development will need to

16 July 2024 09:29:41

© Author(s) 2024

include consideration of the manufacturing at the scale of the metagratings, e.g., using nano-imprinting technologies and using materials with a sufficiently high index of refraction. Current efforts in this direction tend to fabricate gratings with a refractive index greater than 2.5 by imprinting patterns into polymers and using them as an etching mask.[461] This approach can employ a wide range of conventional optical materials but possesses the challenge of accurately translating complex metagrating shapes into dielectric materials through a single-step etch process [see, e.g., Fig. 17(b)]. Alternative approaches include imprinting into a polymeric matrix with added nanoparticles, which have been used to create 3D nano-structures with a refractive index greater than 2[462,463] avoiding the etching step.

While waveguide combiners will likely remain the standard approach, they will improve on their limitations by incorporating some of the benefits of metalenses. Next-generation combiners will likely exploit the polarization-dependent response of meta-atoms, implement pupil replica schemes, be achromatic, and offer a high level of sophistication of response. In the process, they will also tackle other key issues like the unwanted scattering of external light, known as the "rainbow effect," and the outcoupling of the digital image away from the user's eyes, referred to as "glowing eye." This will be achieved by designing metagratings that have an asymmetric optical response depending on the direction of the incident light.

While the intrinsic limitations of metalenses make it harder to see them prevailing as combiners in AR glasses, we see potential in their use as AR technology integrated with LiDAR and Time-of-Flight sensors, and as optics for facile recognition applications.[464] These applications have much less stringent achromatic requirements, as they solely need to operate at a predetermined wavelength and exclusively within the near-infrared (NIR) spectrum. This has the additional benefit of enabling the use of silicon technology, such as nanolithography, which is readily compatible with scaled-up manufacturing processes with high precision in extra small feature size.[465,466]

Freeform combiners with metasurfaces—Another possible direction in the development of metasurfaces for AR glasses is their use to enhance freeform optical elements.[467] This type of hybrid freeform-meta optics uses both the controlled phase response typical of metamaterials and the geometry of the freeform elements to fix both the image quality and the aberrations. Patterning curved substrates is challenging, but recent results have shown that this is a practically viable solution.[467] Alternative approaches include the use of conformable metasurfaces, which have the advantage of decoupling the fabrication constraints from the shape of the substrate to which they are applied.[468,469] This manufacturing approach could also be used to create curved waveguide combiners to mimic curved lenses used in most modern spectacles by first manufacturing diffraction gratings on a transparent flexible film and then transferring this film onto a curved waveguide combiner. This type of combiner would be less bulky than conventional freeform combiners and have a more natural look, however, still be constrained by the conservation of the etendue. It is, therefore, more likely that freeform optics enhanced by metasurfaces will find better use in the image projector, working on a broadband range with a wide field of view.

Holographic metasurfaces—Finally, we would like to imagine ultimate AR glasses based on holographic metamaterials. Current solutions only offer static images, at best multiplexed in the same device, using e.g., polarization, wavelength, the direction of the incoming light, and their shape.[470,471] Future solutions would deploy active tuning mechanisms. The most promising solutions include the incorporation of liquid crystal cells coupled to metasurfaces filters,[472,473] metasurfaces based on phase change materials[474,475] and variants of transparent conductive oxide modulators.[476,477] Ideally, the holographic metasurfaces should be tuned electrically, at the level of the single meta-atom, over a sufficiently wide modulation range, and reversibly over a meaningful number of cycles, cycle number still being an issue with phase change materials. Despite the fast and meaningful progress,[478] at the time of writing this article, it is not clear which, if any, of these approaches will yield the magnitude in change of the optical response required by AR applications, with low dispersion and low loss. If this important issue could be solved, however, such glasses would be lightweight with a form factor barely different from modern spectacles. Their frame would be thin yet contain all the electronics and the light source. The degree of freedom available in the design would also enable the implementation of pupil replica strategies, thus surpassing the etendue constraints. By scanning a laser over various areas of a holographic metasurface and dynamically altering the optical response of specific meta-atoms, it becomes possible to generate wavefronts in any desired shape and direction. This approach could realize the goal of consumer-grade AR glasses that seamlessly integrate digital and real-world visuals.

To conclude, there have been major developments in AR systems over the last few years. Traditional methods have evolved to incorporate more sophisticated strategies to manage the delivery of light to the eye, incorporating nanopatterned optical interfaces. In their evolution, these systems have crossed paths and aligned with the progress made in the various areas of meta-optics, which is indeed one of the most versatile nanophotonic platforms available to optical engineers. Here, we have discussed both the differences and the similarities between the different platforms and practical solutions. While some considerations are unavoidably speculative, and AR systems of the future may look very different from current implementations, meta-optics has already carved a place for itself in this future.

X. METASURFACES FOR QUANTUM STATES GENERATION

Sylvain D. Gennaro, Tomás Santiago-Cruz, Igal Brener, and Maria V. Chekhova*

*maria.chekhova@mpl.mpg.de

A. Introduction

In the early 20th century, the understanding of light underwent a significant transformation through the discovery of the photoelectric effect and the development of quantum theory.[479] Pioneering physicists of the time postulated the existence of quanta of light called photons—a term coined by the American physicist Gilbert N. Lewis in 1926 from the Greek word "phōs," meaning "light."[480] However, it was not until the 1970s that physicists learned to generate single photons and even more fascinating states—pairs of such photons that behave as a single quantum object, and exhibit entanglement. Subsequent advancements enriched the toolbox of quantum optics with other quantum states of light, such as squeezed states, Schrödinger cat states, cluster states, and many others, whose description in terms of classical

16 July 2024 09:29:41

© Author(s) 2024

electromagnetic theory leads to paradoxes. These quantum states of light are now pivotal instruments for quantum photonic technologies, including quantum information processing, communication, metrology, sensing, and imaging.[481]

Over the years, scientists have developed a plethora of single-photon sources[482] using atoms,[483,484] trapped ions,[485] single molecules in solids,[486] epitaxially grown[487] and colloidal[488] quantum dots, carbon nanotubes,[489] color centers in diamond,[490] and defects in two-dimensional materials.[491] The most convenient sources of entangled photons are created using nonlinear optical effects: spontaneous parametric downconversion (SPDC) in second-order nonlinear crystals[492–497] and spontaneous four-wave mixing (SFWM) in fibers.[498,499] SPDC and SFWM can also produce single photons if one photon of a pair is used to herald the presence of the other photon. However, the most significant application of these nonlinear effects is to generate and engineer entanglement between the two photons, whether in polarization or continuous variables, such as time/frequency and position/momentum. With stronger pumping, both SPDC and SFWM produce higher fluxes of photon pairs, forming different kinds of squeezed vacuum states. Being brighter than single- or few-photon states, squeezed vacuum and other squeezed states are especially useful for quantum measurement and sensing.

In recent years, optical metasurfaces have been developed to manipulate and control the amplitude, phase, and polarization of light.[1,13,500–502] The latter manipulation combined with enhanced efficiencies due to engineered resonances has been used to promote the classical process of harmonic generation at the nanoscale.[53,130,135,503–519] More recently, metasurfaces have evolved into platforms for the generation and manipulation of quantum light. Thanks to their flexibility in engineering high-quality optical resonances, metasurfaces can control and amplify various forms of spontaneous emission—from the emission of single photons by solid-state emitters[58,100,395,489,520–525] to the generation of photon pairs through nonlinear optical effects.[137,384,526–529] In addition to their compact nature, metasurfaces are multifunctional, capable of combining the generation of quantum light with tasks like sorting,[530] filtering,[531] polarization transformation,[532,533] sensing,[534] and engineering photon entanglement.[535,536] Metasurfaces thus present a promising avenue to generate and control complex quantum states of light at the nanoscale. In this short perspective, we direct our focus toward the unique abilities of optical metasurfaces at enhancing the emission of single photons or photon pairs through the engineering of optical resonances.

B. Single-photon generation

One of the fundamental building blocks of optical quantum technologies consists of single-photon sources. A prominent challenge in this field is thus the search for single-photon sources that emit indistinguishable photons with well-defined polarization, high purity, and high emission rates. Many traditional quantum emitters (QEs) typically face issues such as low quantum yields and emission rates, a broad emission spectrum, and omnidirectional emission.[525]

Recently, metasurfaces have facilitated the enhancement of spontaneous emission rates,[58,100,395,489,520–525] beam steering,[48,88,537,538] and polarization control of emitters[370,539] using optical resonances. According to the Fermi golden rule, the emission rate of a QE increases with the local electromagnetic density of states in its environment. As demonstrated by Purcell in 1946, the spontaneous emission rate in an optical cavity is proportional to the ratio between the quality (Q) factor of the cavity and the optical mode volume.[540] Consequently, optical resonances with high quality factors and/or small optical mode volumes are sought after for this purpose. From a quantum optical perspective, effects of spontaneous emission—such as single-photon emission by atoms or solid-state emitters, and the generation of photon pairs through SPDC and SFWM—can be elucidated as being stimulated by the vacuum field. Despite the vacuum field having an average value of zero, it exhibits non-zero fluctuations around this mean. The spectral density of these fluctuations is uniform across all states in the k-space and is equal to one photon per state (per mode).[479] A resonance augments the density of states for the resonant mode. Given the uniform population of states due to quantum vacuum fluctuations, the resonance intensifies the spectral brightness of these fluctuations at its wavelength and for the corresponding orientation of the optical field. This explains the enhancement of all spontaneous emission effects for resonant modes of optical metasurfaces.

Similar enhancement of emission can be obtained using plasmonic nanoantennas and metasurfaces. Plasmonic metasurfaces harness the power of surface plasmons—collective electron oscillations at interfaces between metals and dielectrics—to amplify single-photon emission. By tailoring light–matter interactions within nanoscale mode volumes, these structures improve the efficiency of QEs. For instance, plasmonic metasurfaces were shown to enhance the spontaneous emission rate of embedded InAs quantum dots, as illustrated in Fig. 18(a).[523] The quantum dot entered a superlinear photoluminescence regime, which was attributed to the excitation of surface plasmon polaritons (SPPs) and the subsequent room-temperature generation of hot electrons. Plasmonic metasurfaces can also enhance the spontaneous emission of isolated defects in 2D materials, such as hexagonal boron nitride (hBN), that are known to emit single photons at room temperature. For instance, Fig. 18(b) depicts a metasurface composed of gold nanoparticle arrays that support localized surface plasmon resonances. The strong confinement of the electric field near the nanoparticle surface intensifies the spontaneous emission, aligning with the Purcell enhancement in the weak coupling regime.[521]

Plasmonic metasurfaces, while offering remarkable opportunities for enhancing single-photon generation through their ability to concentrate light in small volumes, face limitations in achieving high-Q resonances. These limitations arise due to the inherent Ohmic loss of plasmonic materials. Researchers are thus actively exploring alternative high refractive index dielectric materials to achieve higher Q-factors. All-dielectric metasurfaces offer a promising route to enhance single-photon generation at visible and near infrared wavelengths through the excitation of Mie-type resonances and high-Q bound states in the continuum (BIC). For instance, as depicted in Fig. 18(c), an early experimental demonstration shows an all-dielectric metasurface, made of arrays of high-index nanoresonators supporting magnetic dipole modes, modifying the single-photon emission of oxygen-doped single-walled carbon nanotubes (SWCNTs), by a moderate factor of $0.8 - 4.0$. Moreover, single-dopant polarization experiments show an anomalous photoluminescence polarization rotation due to coupling

16 July 2024 09:29:41

© Author(s) 2024

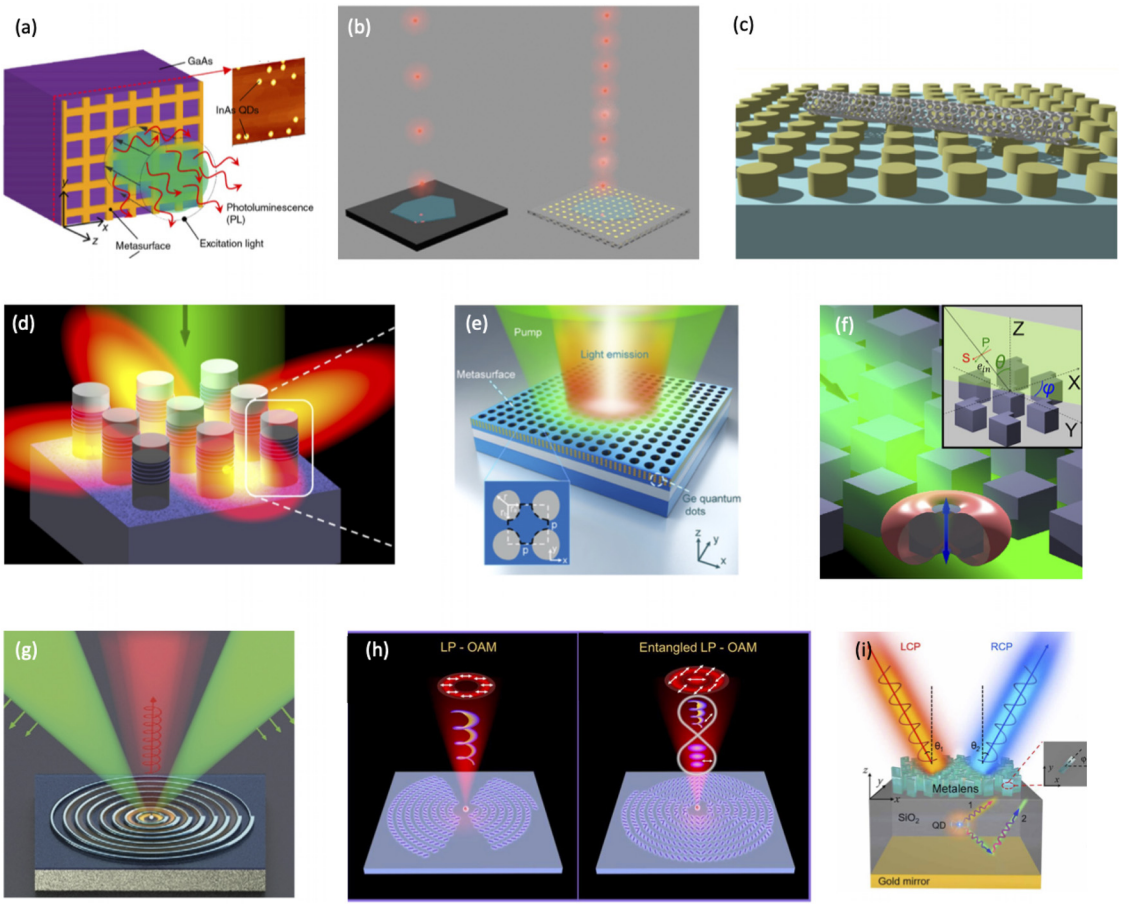

FIG. 18. Single-photon generation in metasurfaces. (a) Super-linear photoluminescence dynamics in SPP- quantum-dot coupling systems in a plasmonic metasurface.[523] (b) Deterministic coupling of quantum emitters in 2D materials to plasmonic nanocavity arrays.[521] (c) Solitary oxygen dopant emission from carbon nanotubes modified by dielectric metasurfaces.[489] (d) Mie-resonant GaAs nanocylinders incorporating five layers of InAs quantum dots.[100] (e) and (f) All-dielectric metasurface exhibiting quasi-BICs due to (e) lattice deformation (Si)[58] or (f) resonator deformation (GaAs).[522] On-chip single-photon sources coupled to (g) concentric dielectric rings[539] or (h) anisotropic nanobricks[541] enabling linear polarization and OAM control. (i) Dielectric bifocal metalens enabling the emission of single photons along one of the two different directions depending on their polarization.[542] (a) Reprinted with permission from Iwanaga *et al.*, ACS Photonics **5**, 897 (2018).[523] Copyright 2018 American Chemical Society. (b) Reprinted with permission from Tran *et al.*, Nano Lett. **17**, 2634 (2017).[521] Copyright 2017 American Chemical Society. (c) Reprinted with permission from Ma *et al.*, ACS Nano 11, 6431 (2017). Copyright 2017 American Chemical Society.[489] (d) Reprinted with permission from Vaskin *et al.*, Opt. Express **29**, 5567 (2021).Copyright The Optical Society.[100] (e) Reprinted with permission from Yuan *et al.*, ACS Nano **11**, 10704 (2017). Copyright 2017 American Chemical Society.[58] (f) Reprinted with permission from Liu *et al.*, ACS Photonics **5**, 1365 (2018). Copyright 2018 American Chemical Society. (g) Reprinted with permission from Kan *et al.*, Adv. Mater. **32**, 1907832 (2020). Copyright 2020 Authors, licensed under a Creative Commons Attribution Noncommercial License4.0 (CC BY-NC).[539] (h) Reprinted with permission from Purcell, Proc. Am. Phys. Soc. **69**, 674 (1946). Copyright 1946 Authors, Creative Commons Attribution Noncommercial License4.0 (CC BY-NC).[540] (i) Reprinted with permission from Bao *et al.*, Sci. Adv. **6**, 8761 (2020). Copyright 2020 Authors, Creative Commons Attribution Noncommercial License4.0 (CC BY-NC).[542]

individual SWCNTs to silicon nanoresonators, showcasing the exciting potential of dielectric metasurfaces to control the polarization of QEs.[488]

Using optical modes with higher Q-factors, single-photon generation can be further enhanced. For instance, consider a metasurface composed of Mie-resonant GaAs nanocylinders embedding five layers of InAs quantum dots [Fig. 18(d)[100]]. Although the primary objective of this study was to modify the photoluminescence polarization and directionality through the outcoupling of quantum dots emission to the magnetic quadrupolar modes, the authors also observed a noteworthy 19-fold enhancement in the emission rate when compared to an unstructured surface. This improvement in the spontaneous emission rate aligns with expectations, given the diminished Q factors associated with the resonances involved.

All-dielectric metasurfaces can capitalize on high-Q optical resonances such as symmetry-protected quasi-BICs.[506–508] BICs are discrete-energy modes that do not radiate and possess energy levels that coincide with a continuous spectrum of radiating modes.[141] Leveraging their high-Q resonances can lead to increased spontaneous emission. For instance, as depicted in Fig. 18(e), a 1000-fold enhancement of photoluminescence was observed for four layers of self-assembled Ge quantum dots (QDs) embedded within a metasurface

16 July 2024 09:29:41

© Author(s) 2024

composed of a periodic lattice of asymmetric air holes in a silicon-on-insulator (SOI) slab. This metasurface exhibited quasi-BICs with a Q-factor of approximately 1000.[58]

Similarly, a metasurface employing broken-symmetry GaAs resonators, arranged in a square lattice, showcased a several-hundred-fold enhancement in the photoluminescence of monolithically embedded, self-assembled, near-infrared InAs/InGaAs QDs [Fig. 18(f)]. Notably, the symmetry protected quasi-BICs reshaped the emission of the QDs, making it unidirectional along the normal to the metasurface.[522]

Optical metasurfaces can go beyond the mere enhancement of spontaneous emission and tailor its polarization and orbital angular momentum properties. Examples are metasurfaces designed in the configuration of a bullseye target through concentric dielectric rings [Fig. 18(g)][539] or anisotropic nanobricks [Fig. 18(h)],[541] allowing the emission of single photons with controllable polarization. Consider a nitrogen-vacancy (NV) center at the center of concentric dielectric nanoridges positioned above a silver film, as shown in Fig. 18(g). This arrangement emits single photons with well-defined circular polarization (chirality >0.8) and remarkable directionality (collection efficiency reaching up to 92%), a result of the tailored phase of the field scattered from the QE and the corresponding excited surface plasmon polaritons.[539] Similarly, Fig. 18(h) illustrates how a metasurface composed of dielectric anisotropic nanobricks, enveloping a room-temperature single-photon emitter—germanium vacancy center (GeV-ND) positioned on a silica (SiO_2) spacer-covered silver (Ag) substrate—excites radially diverging SPP waves. In this manner, metasurfaces can confer topological charges to emitted single photons, thus enabling the emission of linearly polarized vortex beams. The authors additionally demonstrated the realization of multiplexing single-photon emission channels with orthogonal linear polarizations carrying distinct topological charges and demonstrate their entanglement.[541] A further application of this concept involves the construction of a dielectric bifocal metalens atop a SiO_2 and gold film, housing a quantum dot within the SiO_2 layer [Fig. 18(i)]. The metalens is designed with its two foci aligned with the positions of the quantum dot and its mirrored image. Consequently, each photon can be emitted along one of the two distinct directions, depending on its polarization.[542]

To conclude, we have surveyed some of the recent work in using metasurfaces to improve the performance of quantum emitters embedded within them, achieved through optical resonance engineering. In addition, metasurfaces can also tailor the emission direction and polarization. Shifting our focus, we will now turn to showcasing how nonlinear metasurfaces can facilitate the generation of photon pairs via SPDC.

C. Biphoton generation

Quantum state engineering largely relies on SPDC[492,493,496,497] and SFWM.[498,499] These processes lead to the spontaneous emission of entangled photon pairs, known as biphotons, while adhering to principles of energy and momentum conservation. SPDC and SFWM serve as the foundation for generating a diverse range of quantum states, spanning from heralded single photons and higher-order Fock states to squeezed states and multiphoton non-Gaussian states like Schrödinger cat states or NOON states.

In contrast to bulk crystals, SPDC at the nanoscale relaxes the requirement for longitudinal momentum conservation,[543] resulting in a broad range of frequencies and angles for emitted photon pairs. For instance, the broad frequency-angular spectrum of SPDC in ultrathin nonlinear films [Fig. 19(a)][543] leads to a heightened degree of frequency and angular entanglement, along with short correlation times and sub-wavelength correlation distances.[116] Moreover, the relaxation of momentum conservation offers the potential for tunable polarization entanglement,[544] thereby expanding the possibilities for quantum state engineering. However, in optical antennas and metasurfaces, resonances serve to select the wavelengths, directions, and polarizations of enhanced photon emission. Through meticulous selection and design of optical modes and resonances, the generation of entangled photons with improved efficiency can be achieved with control over their emission direction and creation of intricate quantum states.[116,137,384,527–529]

Observing SPDC at the nanoscale presents challenges. SPDC is inherently a weak parametric process, and experiments with nanophotonic samples require prolonged data acquisition to detect a signal. To find suitable materials and structures, one can use classical processes such as second harmonic generation (SHG) and sum frequency generation (SFG).[527] These processes share the same phase matching condition and effective nonlinearity as SPDC. Alternatively, difference frequency generation (DFG) can be employed within stimulated emission tomography (SET) to investigate the efficiency of SPDC and the entanglement of biphotons.[116,543,545,546]

For instance, SFG was used to predict the enhancement of SPDC from a nonlinear plasmonic metagrating made of periodic silver nanostrips atop a thin lithium niobate ($LiNbO_3$) film and a silver substrate. Through optical excitation, localized surface and gap plasmon resonances were formed around the edges of the nanostrips and within the nanogaps. This amplified the optical field in the nonlinear $LiNbO_3$ layer.[547] However, because plasmonic-based systems have high Ohmic losses, they also emit incoherent light, which would reduce the signal-to-noise ratio of the generated biphotons.[548]

Compared to their plasmonic counterparts, metasurfaces crafted from materials with high second-order susceptibility, such as GaAs,[509,510,518,549] AlGaAs,[503,513,550] and other materials,[512,551,552] are attractive alternatives. The initial endeavor to observe SPDC created within nanostructures was centered around a single crystalline AlGaAs nanocylinder, characterized by Mie-like resonances at both the fundamental and down-converted wavelengths [Fig. 19(b)].[553] The histogram of the photon arrival time difference revealed a minor peak above the background of accidental coincidences. However, the peak-to-background contrast (referred to as CAR, coincidences-to-accidentals ratio) was insufficient to confirm the emission of SPDC pairs. Given that thermal light can also lead to a peak at zero arrival time difference,[554] a signature of two-photon emission is the peak exceeding the background (CAR > 1). Another hallmark of biphoton emission is the reciprocal relationship between the CAR and the pump power. The first demonstration of nanoscale SPDC using this approach emerged in the context of a nonlinear film.[116] Very recently, SPDC was achieved in a single $LiNbO_3$ nanoresonator of height 500 nm and diameter 1 μm, which is, perhaps, the most compact 3D source of biphotons to date.[555]

One approach to achieve higher biphoton rates involves using resonances in optical metasurfaces, which enhance the vacuum field and hence the spontaneous emission of photon pairs via SPDC. This

16 July 2024 09:29:41

© Author(s) 2024

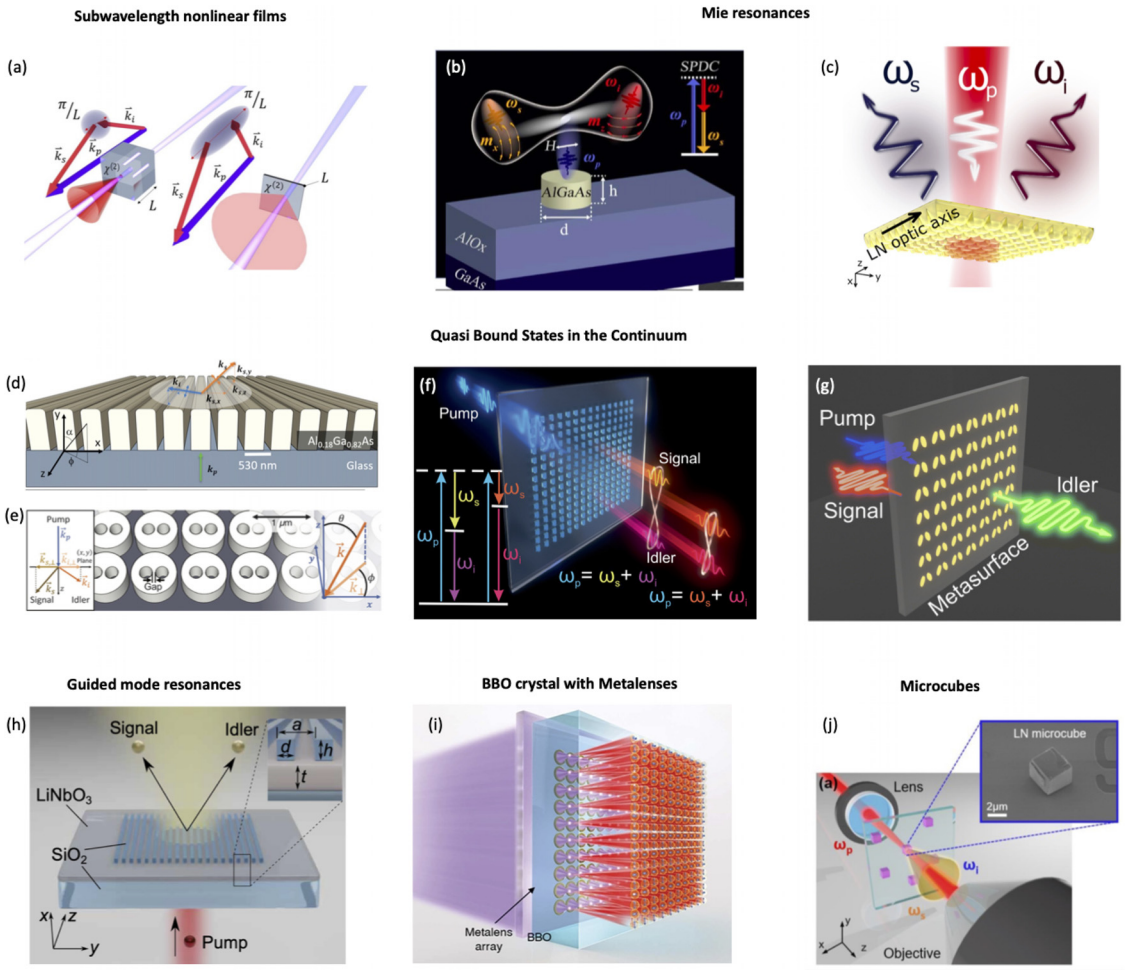

FIG. 19. Photon pairs generation in optical antennas, metasurfaces, and other nanoscale structures. (a) Relaxed momentum conservation in SPDC for thin crystals (right) compared to thick ones (left).[543] (b) and (c) The excitation of electric and magnetic dipole resonances in (b) an AlGaAs nanoantenna[553] and (c) a lithium niobate metasurface enhances the emission of photon pairs.[526] (d)–(g) Quasi-BIC optical modes drastically enhance the generation of photon pairs, predicted (d) in meta gratings made of nanofins,[528] (e) in AlGaAs metasurfaces made of nanocylinders with two holes in them,[527] measured in (f) a metasurface made of broken symmetry GaAs nanoresonators,[384] and (g) in tilted ellipses nanoresonators.[529] (h) Spatially entangled signal and idler photons from a $LiNbO_3$ nonlocal metasurface with guided-mode resonances.[137] Other notable approaches of photon pairs generations via SPDC in (i) metalens arrays combined with a BBO crystal[190] and (j) $LiNbO_3$ microcubes.[557] (a) Reprinted with permission from Okoth *et al.*, Phys. Rev. Lett. **123**, 263602 (2019). Copyright 2019 American Physical Society.[543] (b) Reprinted with permission from Marino *et al.*, Optica **6**, 1416 (2019). Copyright The Optical Society.[553] (c) Reprinted with permission from Santiago-Cruz *et al.*, Nano Lett. **21**(10), 4423–4429. Copyright 2021 American Chemical Society.[526] (d) Reprinted with permission from Mazzanti *et al.*, New J. Phys. **24**, 35006 (2022). Copyright 2022 Authors, Creative Commons Attribution Noncommercial License 4.0 (CC BY-NC).[528] (e) Reprinted with permission from Parry *et al.*, Adv. Photonics **3**, 550011 (2021). Copyright 2021 Authors, Creative Commons Attribution Noncommercial License 4.0 (CC BY-NC).[527] (f) Reprinted with permission from Santiago-Cruz *et al.*, Science **377**, 991 (2022).[384] Copyright 2022 The American Association for the Advancement of Science. (g) Reprinted with permission from Son *et al.*, Nanoscale **15**, 2567 (2023).Copyright 2021 Authors, Creative Commons Attribution 3.0 Unported License.[529] (h) Reprinted with permission from Zhang *et al.*, Sci. Adv. **8**, 4240 (2022). Copyright 2022 Authors, Creative Commons Attribution Noncommercial License 4.0 (CC BY-NC).[137] (i) Reprinted with permission from Aouani *et al.*, Nat. Nanotechnol. **9**, 290 (2014).[190] Copyright 2014 The American Association for the Advancement of Science. (j) Reprinted with permission from Hanh Duong *et al.*, Opt. Mater. Express **12**, 3696 (2022). Copyright 2022 The Optical Society.[557]

was first realized in 2021 using arrays of truncated $LiNbO_3$ nanopyramids [Fig. 19(c)]. These arrays exhibited Mie-like electric dipole resonances at telecom wavelengths.[526] Given the high reflectivity of the metasurfaces at resonance wavelengths and their low reflectivity elsewhere, an amplified emission of frequency-degenerate biphotons was observed in the backward direction. Notably, the rate of pair generation surpassed that of an unpatterned $LiNbO_3$ film of equivalent thickness and crystalline orientation by two orders of magnitude. Remarkably, there was no discernible indication of biphotons emitted in the forward direction.[556] The resonances characterizing the metasurface were adjustable by altering the size and period of the pyramidal nanoresonators, thereby enabling the tuning of the biphoton emission wavelength. However, we note that that only frequency degenerate SPDC exhibited a noticeable rate enhancement.

16 July 2024 09:29:41

© Author(s) 2024

The enhancement achieved in SPDC due to Mie resonances is generally moderate. For more substantial enhancements in biphoton generation rates for specific directions, optical resonances with higher Q-factors, such as photonic quasi-BIC[384,527,528] and guided-mode resonances,[137] come into play. Symmetry-protected BICs can prevent, via design, the outcoupling of radiation in the direction normal to the metasurface.[546] However, a symmetry-breaking perturbation of a resonator or the metasurface lattice can convert a symmetry-protected BIC into a quasi-BIC. Quasi-BIC resonances,[525] with their elevated Q-factors, can lead to significant enhancements of biphoton generation rates compared to those obtained from traditional Mie metasurfaces. For example, this enhancement was expected in a meta-grating configuration comprising (110)-cut $Al_{0.18}Ga_{0.82}As$ nanofins atop a dielectric substrate [Fig. 19(d)],[528] and within an array of AlGaAs nanocylinders with pairs of holes [Fig. 19(e)].[527] Experimentally, tunable biphoton generation mediated by quasi-BIC has been observed in a metasurface consisting of GaAs nanoresonators arranged in a square lattice [Fig. 19(f)]. The shape of each nanoresonator was designed to disrupt the rotational C2 and C4 symmetries of the lattice.[384] This metasurface facilitated not only degenerate, but also non-degenerate SPDC, with the photons of a single pair emitted at different wavelengths. The wavelength separation between the two photons reached almost 200 nm without significant efficiency loss. By coherently exciting this metasurface at various wavelengths, photons at multiple distinct wavelengths can be entangled via pairwise coupling, offering the potential for generating more intricate quantum states. These methods of quantum state engineering, made feasible by the relaxation of momentum conservation and the exploitation of high-Q resonances, thus hold tremendous appeal.

Metasurfaces can also impart distinct directionalities to SPDC. Despite the relaxation in phase matching constraints, even within ultrathin layers, the probability of both photons being emitted backward remains exceedingly low. However, metasurface resonances engineered to exhibit enhanced reflectivity enable such backward pair emission.[526] Conversely, resonances configured for enhanced transmissivity result in the forward emission of biphotons.[384] By strategically designing a metasurface to possess high reflectivity at the resonance of a quasi-BIC and high transmissivity elsewhere, bidirectional emission of photon pairs was observed[529] [Fig. 19(g)]. In this work, the photon at the resonant wavelength was predominantly emitted backwards, while its entangled partner was emitted forwards. The integration of quantum- and nanophotonics thus presents a promising avenue for generating complex photon states encompassing more than two entangled photons. Additionally, as exemplified in Fig. 19(h), guided-mode resonances have facilitated the creation of spatially entangled photon pairs with a degenerate narrowband emission spectrum spanning approximately 3 nm around 1570 nm.[137] This achievement was realized using a metasurface comprised of a silica metagrating atop a $LiNbO_3$ film. Notably, the biphoton generation rate was amplified by over 450 times in comparison to an unpatterned film.

Finally, we note other avenues for generating photon pairs at the nanoscale. These alternatives include the incorporation of a metalens—constructed from a 10×10 array of GaN nanopillars—onto the surface of a 0.5 mm β-barium borate (BBO) crystal,[190] which enables the generation of pairs in multiple modes as shown in Fig. 19(i). Additional methods encompass the utilization of $LiNbO_3$ microcubes[557] [Fig. 19(j)] and GaAs nanowires,[558] to amplify the biphoton rate while retaining a certain degree of engineering flexibility offered by nanophotonics. In a different vein from SPDC, some groups are investigating SFWM in doubly resonant gold plasmonic nano-antennas and metasurfaces.[158,511,546]

D. Future directions

Optical metasurfaces have significantly improved the emission of single and entangled photons, offering unprecedented control over polarization and directionality. For single-photon emission, optical metasurfaces have enabled efficient coupling of QEs to closely located optical resonances, resulting in substantial enhancements in emission rates. Two promising directions have thus emerged in this context.[58] First, exploring anisotropic quantum metasurfaces has the potential to revolutionize the design of hybrid plasmon-QE coupled metasurfaces. Composed of anisotropic nano-scatterers as elements, these metasurfaces promise greater versatility in controlling photon properties, including polarization. This advancement could facilitate the realization of on-chip single-photon sources with high polarization purity. Second, the development of tunable quantum metasurfaces presents an exciting avenue for actively manipulating emitted photon properties, encompassing emission rate, direction, wavefront, and polarization. Inspired by dynamic optical metasurfaces used for classical light, the incorporation of phase-changing materials into metasurfaces that shape single-photon emission can provide tunability through temperature variation or voltage application, thereby unlocking transformative possibilities for quantum information technologies.

Efficiency remains a critical challenge in the generation of photon pairs using quantum optical metasurfaces (QOMs). State-of-the-art QOMs, due to their extremely thin profile, exhibit very low photon pair-generation rates: tens of Hertz at moderate pump powers.[384,529] However, practical quantum optical applications demand pair-generation rates on the order of 100 kHz, a benchmark that is still significantly distant from achieving with current QOMs. Several research directions to enhance the pair-generation rate predominantly rely on elevating the Q-factors of the optical mode at play, improving mode overlap between pump, signal, and idler wavelengths, and involving materials with high second-order susceptibilities, such as (110)-oriented GaAs or van der Waals crystals like niobium oxide dichloride ($NbOCl_2$).[559] In this context, polaritonic metasurfaces featuring resonant susceptibilities present a promising avenue as well.[518,560,561] Another challenge is the generation of tunable, polarization-entangled photon pairs, including Bell states, with recent advances in thin films[544] and optical metasurfaces,[562] offering promising design approaches.

SPDC is also a source of squeezed states of light. However, the low parametric gain ($G \propto E\chi^{(2)}L$, with E being the electric field amplitude of the pump, and L the length of the nonlinear medium), makes it rather challenging to observe light squeezing in metasurfaces. It might be possible to reach a parametric gain $G \sim 1$, which is needed for squeezing, in optical nonlinear metasurfaces using pulsed pumping. Incidentally, the use of pulsed excitation could help to distinguish between SPDC and photoluminescence, as the latter is orders of magnitude stronger than the former.[563]

Finally, the generation of quantum states via third-order nonlinear processes, such as SFWM and third order SPDC (TOSPDC)[564] has yet to be observed in optical metasurfaces. Importantly, the values of

16 July 2024 09:29:41

© Author(s) 2024

third-order susceptibility $\chi^{(3)}$ differ in various materials by up to four orders of magnitude; therefore, the freedom to choose any material due to relaxed momentum conservation is crucial for third-order effects. The use of strongly nonlinear materials like Si or Ge may facilitate the observation of new nonlinear effects such as TOSPDC.

ACKNOWLEDGMENTS

I.B. and S.D.G. acknowledge support from the U.S. Department of Energy, Office of Basic Energy Sciences, Division of Materials Sciences and Engineering. This work was performed, in part, at the Center for Integrated Nanotechnologies, an Office of Science User Facility operated for the U.S. Department of Energy (DOE) Office of Science. This article has been authored by an employee of National Technology & Engineering Solutions of Sandia, LLC under Contract No. DE-NA0003525 with the U.S. Department of Energy (DOE). The employee owns all right, title and interest in and to the article and is solely responsible for its contents. The United States Government retains and the publisher, by accepting the article for publication, acknowledges that the United States Government retains a non-exclusive, paid-up, irrevocable, world-wide license to publish or reproduce the published form of this article or allow others to do so, for United States Government purposes. The DOE will provide public access to these results of federally sponsored research in accordance with the DOE Public Access Plan https://www.energy.gov/downloads/doepublic-access-plan. This paper describes objective technical results and analysis. Any subjective views or opinions that might be expressed in the paper do not necessarily represent the views of the U.S. Department of Energy or the United States Government.

XI. METASURFACE LASERS

Ren-Min Ma

renminma@pku.edu.cn

A. Introduction

The definition of metasurface lasers can be arguably derived from the conceptual framework of metamaterials. Metasurface lasers exhibit a fundamental similarity to metamaterials by employing artificial functional "atoms" to tailor the properties of the composite matter formed by these constituent atoms. In the realm of metasurface lasers, individual nanolasers serve as the fundamental atoms. The eigenmode of a nanolaser can be deliberately shaped to synthesize the inner laser cavity field and/or emission beam in a highly controlled manner. Furthermore, coordinated ensembles of nanolasers can generate a macroscopic response surpassing the capabilities of conventional lasers. Within the near field, manipulation of the polarization and profile of each nanolaser eigenmode is possible, and additional control over the ensemble can be achieved through coupling, relative phase, symmetry, and topology. This approach has the potential to provide unprecedented control over the macroscopic laser field, offering diverse applications in the far field.

The definition of metasuface lasers proposed in this article aims to capture the essential characteristics of metamaterials and metasurfaces, combined with the features of lasers. We hope this definition offers a stimulating perspective for studying lasers from the standpoint of metamaterials. We note that some lasers discussed in the article do not strictly meet this definition because their individual units cannot achieve lasing independently. However, the concept of those lasers can indeed be applied to arrays of coupled nanolasers. Therefore, to maintain a broad scope and inspire potential future research, we have included discussions of some metasurface-like, cutting-edge laser studies that do not strictly conform to our definition of metasurface lasers.

Nanolaser research gained traction around 1990 when it was discovered that the threshold and modulation rate of lasers are influenced by their size.[565–568] First, miniaturized lasers with a smaller gain material volume and a larger spontaneous radiation coupling factor exhibit lower thresholds. Simultaneously, miniaturized lasers can achieve faster rates of spontaneous and stimulated emission, resulting in faster modulation rates. Since then, achieving miniaturized lasers with smaller mode volumes, lower threshold power consumption, and faster modulation rates has been a focal point of research in the relevant field. Innovations such as the microdisk laser, photonic crystal defect-state lasers, and nanowire lasers have significantly reduced the characteristic dimensions of lasers to the order of a vacuum wavelength.[569–571] In 2009, the experimental realization of plasmonic nanolasers achieved characteristic scales one-tenth of a vacuum wavelength, approaching the characteristic scales of electronic devices.[572–575]

In recent years, novel methods of controlling optical fields have continually been introduced into the micro and nanolaser domain, creating the development of metasurface lasers. These encompass plasmonic lattice lasers,[576–579] topological lasers,[91,113,580–616] bound-state in the continuum (BIC) lasers,[617–619,624,625] non-Hermitian parity-time symmetric lasers,[624–637] supersymmetry lasers,[638–640] and moiré lasers,[641–644] injecting renewed vitality into the advancement of micro and nanolasers. In this article, we first briefly discuss the significance of metasurface lasers in the context of laser development, specifically addressing why these mode control methods are introduced from a laser perspective. Following that, we delve into the mode engineering of individual nanolasers. Finally, we explore the characteristics of metasurface lasers formed by the coupling of multiple nanolasers.

B. Key performance parameters

The key performance parameters of a laser include threshold power density, lasing linewidth, external quantum efficiency, modulation speed, power consumption, emission directionality, emission power, and side mode suppression ratio, among others. These parameters are intricately linked, often imposing constraints on one another. For example, the pursuit of reduced size to achieve lower threshold power and enhanced modulation speed may inadvertently lead to a broadening of the lasing linewidth, increased divergence angles, and diminished output power. However, the silver lining lies in the fact that various applications necessitate the fine-tuning of specific parameters, making the optimization process application-dependent. Consequently, the performance of lasers is contingent upon the unique requirements of a given application context.

To illustrate, industries employing lasers for precise material processing, such as cutting, welding, and marking, demand higher power. In contrast, applications like data communication or consumer electronics necessitate lower output power to achieve energy efficiency.

Beyond these traditional laser characteristics, the incorporation of novel optical field control introduces a transformative dimension to metasurface lasers, endowing them with features not inherent in

16 July 2024 09:29:41

© Author(s) 2024

conventional counterparts. This includes the attainment of higher radiation field dimensions, superior single-mode characteristics, relative phase control, and reconfigurability.

C. Eigenmode engineering in a single microscale laser cavity

In the domain of microscale lasers centered on individual cavities, the impetus for eigenmode engineering manifests through three primary objectives.[645] First, the focus is on advancing laser performance by reducing lasing thresholds and accelerating modulation speeds. Second, there is a concerted effort to generate a strong local field. Finally, the goal is to control field properties of a nanolaser in near and far field.

1. Enhance laser performance

The lasing threshold power can be categorized into two components. The first involves achieving population inversion of the gain material, essentially rendering the gain medium transparent. The second requires compensation for cavity loss, ensuring the condition of having one real photon in the cavity mode is met. The quest for smaller lasers has been a persistent research goal, striving for a more compact size and reduced power consumption. Whispering-gallery-mode microlasers, photonic crystal defect nanolasers, nanowire lasers, plasmonic nanolasers, bound states in the continuum nanolasers, magic angle nanolasers have been invented to miniaturize lasers and consequently lower their threshold power. In both dielectric and plasmonic cavities, cavity loss increases as the volume decreases.[646,647] Therefore, the exploration of materials with higher optical gain and the meticulous design of nanocavities with lower cavity loss are pivotal for the advancement of nanolasers.[648] In the case of a small laser cavity with a large free spectral range, the meticulous design of the lasing resonance wavelength becomes crucial in lowering the total cavity loss. This is due to the wavelength dependence of gain material loss, emphasizing the importance of aligning the resonance wavelength of the cavity for optimal performance. Additionally, it is important to carefully balance the radiation rate and the cavity loss rate to ensure that microscale lasers have a high external quantum efficiency.[607,649]

2. Enhancing local field

The interaction between light and matter is generally a weak process owing to the disparity in wavelength between photons and electrons. Over the decades, artificial microstructures have been employed to enlarge and manipulate the density of states of photons, thereby enhancing light–matter interaction.[645,650–662] In this context, the ratio of quality factor to mode volume (Q/V) emerges as a crucial figure of merit, signifying the strength of light field confinement on both spatial and spectral scales. Various localization mechanisms, including total internal reflection,[655,663–670] photonic bandgap,[671–680] plasmonic resonance,[681–686] and bound states in the continuum (BICs),[151,177,624,687,688] have been developed over the years to craft optical cavities with high Q/V. However, in photonics, a persistent trade-off exists between confining a light field in space and in frequency due to the limitations of the applicable finite potential well. Recent innovations of twisted lattice nanocavities can overcome this trade-off by enabling a mode volume approaching to diffraction limit, accompanied by an exceptional quality factor exceeding 2.9×10^{11} (Ref. 689). A cavity with an extremely large Q/V enables exploration of light–matter interaction in extreme conditions, facilitating tests of fundamental physics. Moreover, it can be used in nanolasing, ultrasensing, nonlinear optics, optomechanics, and quantum-optical devices.

3. Controlling radiation field

The advantage of nanoscale lasers lies in the minimal number of modes permitted within the cavity, facilitating the targeted design of eigenmodes for controlling the near-field and far-field properties.[645] Each laser mode represents a specific eigenmode of the cavity. The estimated number of eigenmodes (N) allowed in a cavity is given by the expression $N = \rho V_{PHY} \Delta\nu_E$, where ρ denotes the density of states of the cavity, V_{PHY} is the physical size of the cavity, and $\Delta\nu_E$ is the gain spectrum bandwidth. As typically $\Delta\nu_E$ spans a few tens of terahertz for conventional organic dyes and semiconductor materials, only a few eigenmodes generally coincide spectrally with the gain spectrum when the laser cavity size is subwavelength scale in all three dimensions. This characteristic enables precise engineering of the eigenmode in a nanolaser in a controllable manner, leading to novel inner laser cavity fields and/or emission beam synthesis. Various eigenmode engineering mechanisms have been proposed to control the optical field distributions inside and outside nanoscale laser cavities, including parity-time symmetry, exceptional point, supersymmetry, topological nanocavity, among others. Optical fields exhibit rich dimensions,[690] providing a vast development space for eigenmode engineering.

D. Eigenmode engineering in arrayed lasers

We can classify arrayed lasers into two categories: those originating from photonic crystals and those stemming from individual nanolasers. While there is no fundamental difference between the two, the approaches and methods employed to construct arrayed lasers differ. Both strive for characteristics such as large-area single-mode lasing, higher laser field dimensions, and reconfigurability (Fig. 20), emphasizing similar performance goals despite the varied methodologies.

1. Large area single mode

Semiconductor lasers, valued for their compactness, efficiency, and controllability, play vital roles in information technology. However, achieving semiconductor lasers with single-mode operation over a large area presents a significant challenge. The attainment of single-mode operation in a spacious region is essential for semiconductor lasers to exhibit high output power and superior beam quality, crucial attributes for various applications such as laser processing, remote sensing, and long-range free-space communications.

Achieving a semiconductor laser with a large-area single mode using photonic crystals involves two primary physical aspects. First, to enable surface emitting, it is necessary to utilize the lattice momentum formed by the photonic crystal to scatter a portion of the guided modes within the photonic crystal into the light cone, preferably at the Gamma point. Second, to achieve a large-area single mode, it is essential to enhance the contrast between the lasing thresholds of the fundamental mode and higher-order modes.

Photonic-crystal surface-emitting lasers: Photonic-crystal surface-emitting lasers (PCSELs) currently stand as the most mature

16 July 2024 09:29:41

© Author(s) 2024

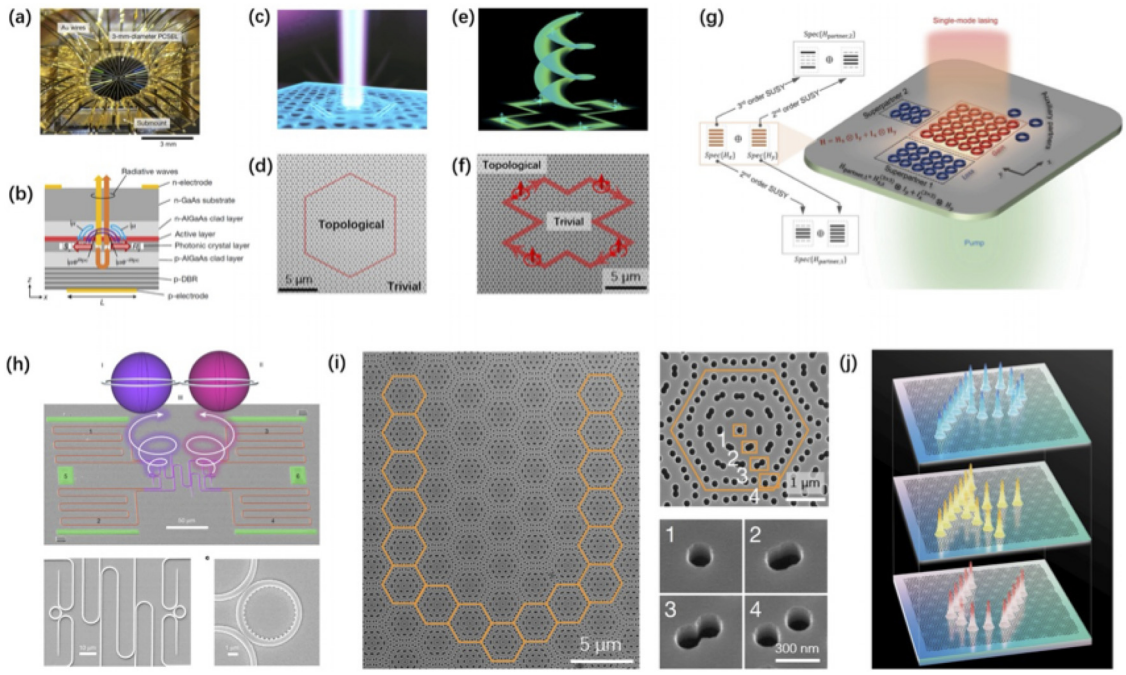

FIG. 20. Metasurface lasers. (a) and (b) Photograph (a) and schematic of the cross-sectional structure (b) of a 3-mm-diameter photonic-crystal surface-emitting laser (PCSEL).[110] (c) and (d) Schematic (c) and SEM image (d) of a surface emitting topological bulk laser based on band-inversion induced reflection.[590] (e) and (f) Schematic (e) and SEM image (f) of a topological vortex laser based on spin-momentum-locked edge mode.[591] (g) Schematic of a supersymmetric microlaser array.[640] (h) SEM image of a hyperdimensional spin–orbit microlaser.[691] (i) and (j) SEM images (i) and schematic of reconfigurable moiré nanolaser array.[642] Reproduced with permission from Yoshida *et al.*, Nature **618**, 727 (2023). Copyright 2023 Springer Nature. Reproduced with permission from Shao *et al.*, Nat. Nanotechnol. **15**, 67 (2020). Copyright 2020 Springer Nature. Reproduced with permission from Yang *et al.*, Phys. Rev. Lett. **125**, 13903 (2020). Copyright 2020 American Physical Society. Reproduced with permission from Qiao *et al.*, Science **372**, 403 (2021). Copyright 2021 AAAS. Reproduced with permission from Luan *et al.*, Nature **624**, 282 (2023). Copyright 2023 Springer Nature. Reproduced with permission from Zhang *et al.* Nature **612**, 246 (2022). Copyright 2022 Springer Nature and Copyright Remains with the respective publishers.

system for realizing semiconductor lasers with single-mode operation. PCSELs achieve single-mode oscillation across expansive areas through careful tailoring of the photonic crystal's unit cell design. Recent research outcomes showcase the capability of PCSELs to achieve 50 W continuous-wave operation in a single mode, even in areas with diameters exceeding 3 mm.[110] Notably, these lasers boast a very narrow beam divergence angle of 0.05° and an impressive brightness of 1 GW cm^{-2} sr^{-1}.

Plasmonic surface lattice nanolasers: Plasmonic surface lattice nanolasers leverage collective coupling among metal nanoparticles in a lattice to establish the resonance mode for lasing.[76] This coupling involves the localized surface plasmon mode and lattice-defined diffraction mode, resulting in sharp Fano lines with reduced radiative loss. The integration of dye molecules within a polymer matrix or organic solvent with plasmonic nanoparticles in a surface lattice enables lasing, with the wavelength tunable by modifying the refractive index, nanoparticle size, interparticle spacing, or lattice geometry. Plasmonic surface lattice nanolasers can achieve a small divergence angle ($<0.5°$) and provide a robust platform for mode control.[578,692] Modifying the shape or symmetry of plasmonic NP lattices allows for precise control over lasing emission properties. Low-symmetry lattices exhibit polarization-dependent lasing, while multiscale plasmonic superlattices support multiple plasmon resonances for controlled multimodal nanolasing. The spatial organization of photoactive materials around plasmon nanocavities leads to nanoscale exciton-plasmon coupling and mixed photon modes.

Topological surface-emitting lasers: In recent years, significant progress has been achieved in the field of topological lasers, with the integration of a novel degree of freedom linked to band topology in photonic crystals. This integration holds the promise of providing topological protection characteristics and introducing innovative optical feedback mechanisms for laser cavity design. Such advancements prove particularly beneficial for driving the development of surface emitting semiconductor lasers with large-area single-mode. Effective mechanisms in this context include topological bulk modes, topological insulator edge modes, topological vortex defect modes, and open-Dirac modes. Surface-emitting topological bulk lasers have been realized through band-inversion-induced reflection, emitting vertically with divergence angles less than 6%, despite their microscale cavity size.[590]

The topological bulk laser achieves high-performance single-mode lasing due to the exclusive operation of band-inversion-induced reflection around the Γ point, where the band inversion occurs. This topology-induced mode selection not only restricts the number of cavity modes with efficient confinement but also enhances the quality factor of the mode closer to the band edge. Furthermore, an array of vertical-cavity surface-emitting lasers (VCSELs) has been strategically arranged to form photonic crystals featuring topological insulator edge modes for collective array lasing.[599] Additionally, the utilization of the

16 July 2024 09:29:41

© Author(s) 2024

topological vortex defect mode has led to the creation of a surface-emitting topological laser with a device diameter of 500 μm and a sub-1° divergence angle.[606] In open-Dirac cavities, surface-emitting lasing has been achieved, demonstrating that single-mode lasing can be maintained as the cavity size is scaled up.[604]

Supersymmetry lasers: Recently, leveraging concepts from supersymmetric quantum mechanics has led to the development of scalable laser arrays with the distinctive features of single-mode operation. In a supersymmetric laser array, the linear spectrum of the superpartner is meticulously constructed to mirror that of the primary array, with the exception of the fundamental supermode. The operating principle of the supersymmetric laser array is derived from the deliberate coupling of the main array with its dissipative superpartner, strategically reducing supermode competition by limiting the available lasing modes. The mode matching between the supersymmetric partners guarantees the suppression of all except for the fundamental supermodes. This fundamental supermode, confined solely in the main array without a superpartner, exhibits the lowest threshold and is conducive to lasing under suitably applied pumping. The initial realization of a supersymmetric laser array was based on a one dimensional waveguide structure.[638,639] Subsequently, two-dimensional supersymmetry lasers were developed, exemplified by a two dimensional five-by-five supersymmetric microlaser array.[640]

Moiré lasers array: The utilization of a moiré nanolaser array can result in extensive single-mode operation over a large area.[642] The synchronization of emission within the moiré nanolaser array is contingent upon the flatness of the band structure in momentum space. The use of a moiré superlattice with a predetermined twisted angle ensures the necessary periodicity for the formation of a flatband, thereby facilitating the scalability of the moiré nanolaser array. However, practical limitations may arise due to nonuniformities induced during the fabrication process. Enhancing the uniformity of the fabricated devices, the fabrication of the moiré nanolaser array onto a SiO_2 substrate eliminates any deformations that may occur when suspending the membrane. Through this process, more than 160 nanolasers have been synchronized to achieve single-mode lasing with a divergence angle of only about 3°.[642]

2. High dimensional radiation

The optical field is a transverse wave field with two polarization degrees of freedom, which can also be transformed into two spin degrees of freedom. In addition to polarization, spatial modes provide a promising avenue for creating high-dimensional Hilbert spaces. In 1992, the orbital angular momentum degree of freedom of optical fields was discovered.[693] Optical vortex beams, carrying orbital angular momentum, are distinguished by a helical phase front and a phase singularity at the beam center. The number of phase front twists around the axis of propagation within one wavelength determines the beam's topological charge. Vortex beams with different topological charges are orthogonal, implying the potential for high-dimensional multiplexing. This property has been leveraged in applications such as optical communication and quantum information processing. Various methods, including the use of spiral phase plates, metasurfaces, synthesized holograms, plasmonic nanostructures, and photonic crystals,[694] exist to convert a normal laser beam into a vortex beam. A compact vortex emitter can be constructed by engineering the eigenmode of a microscale laser. Chiral eigenmodes of a whispering gallery mode resonator serve as a natural source, sharing the azimuthal phase factor of a vortex beam propagating in free space and controlling the topological charge of the emitted vortex beam.[695]

However, constructing a robust chiral whispering gallery mode that circulates only in one direction has been a long-standing challenge. Typically, at a resonant frequency, two degenerate chiral modes travel in opposite directions, leading to potential coupling caused by backscattering, bending, or defects. This coupling transforms circling waves into standing waves, resulting in zero orbital angular momentum in the emission. To overcome this challenge and directly generate a vortex beam, the symmetry of whispering gallery mode lasers needs to be broken.

In recent years, the introduction of new physics such as exceptional points,[631,632,696–698] unidirectional topological edge states,[591,597] and spin–orbit coupling[691] has enriched the capability of laser cavity eigenmode engineering. This enables the direct use of chiral whispering gallery modes in a microscale laser to directly generate radiation fields carrying high-dimensional information.

3. Reconfigurable phased array nanolasers

One of the ultimate objectives in nanolaser research is to develop reconfigurable coherent nanolaser arrays. This advancement will broaden the applications of nanolasers, encompassing areas such as coherent computing and communication, laser displays, and LiDAR (light detection and ranging). Recently, reconfigurable moiré nanolaser arrays with phase synchronization has been realized.[642] This device is based on moiré-angle nanolasers, whose modes are highly localized within a single moiré unit cell.[641]

The optical moiré superlattice structure is formed by processing two sets of twisted photonic crystal lattices in the same layer of a semiconductor membrane. Non-local Bloch modes in the structure are coupled through moiré reciprocal vectors, resulting in spatially localized eigenmodes in real space. In the band structure, these localized eigenmodes correspond to Moiré flat bands. The wavefunction localized in a single moiré unit is employed to construct single-cavity moiré nanolasers.

When moiré-angle nanolasers are arranged in an array, the localized wave functions of individual moiré-angle nanolasers form Moiré flat bands. These bands ensure the degeneracy of frequencies, enabling coherent emission of nanolaser arrays in arbitrary shapes. Building upon this principle, synchronized nanolaser arrays have been realized, demonstrating high spatial and spectral coherence across various distinct patterns, including P, K, and U shapes, as well as the Chinese characters "中" and "国" ("China" in Chinese). Furthermore, the introduction of spatially varying relative phases has enabled the realization of phased-array nanolasers, facilitating the manipulation of emission directions.

E. Future directions

Navigating the current landscape of metasurface lasers and their evolving mode engineering capabilities reveals a field in continuous evolution, characterized by emerging concepts and innovative approaches. Looking ahead, several promising directions stand out, guiding the trajectory of future research in this dynamic domain.

In the realm of single cavity microscale lasers, the most crucial future research direction remains miniaturization. Much like the

16 July 2024 09:29:41

© Author(s) 2024

miniaturization of transistors for electronic chips, miniaturizing lasers is pivotal for optoelectronic technology. Efforts should be directed toward constructing lasers with smaller volumes, lower power consumption, and faster speeds. This dual focus aims to explore the limits of coherent light sources in various dimensions while promoting their applications in integrated photonics, super-resolution imaging, high-resolution displays, and beyond. Simultaneously, constructing stronger local fields is a crucial research direction, particularly for investigating light–material interactions and developing coherent light sources with atomic-scale characteristics in extremely localized optical fields. Finally, further development and exploration of single nanolaser mode control are advantageous for the advancement of nanolaser arrays.

For photonic crystals or nanolaser arrays, achieving large-area single-mode outputs to realize kilowatt-level or even higher output powers in semiconductor lasers remains a crucial research direction, poised to extend the current application scope of semiconductor lasers. Integrating new physics concepts into the toolbox for laser cavity eigenmode engineering is another promising avenue. By leveraging recent advancements in physics, researchers can enhance the capabilities of metasurface lasers, potentially unlocking new possibilities for high-dimensional information processing and communication.

The realization of the reconfigurable moiré nanolaser arrays highlights the potential to construct phased array nanolasers with significantly enhanced information capacity and functionality. Through phase synchronization, nanolaser arrays can achieve large-area, high-power single-mode lasing. Precise adjustment of relative phases enables accurate control of the emission direction of the laser array. Complete control of the intensity and phase of individual nanolasers within an array will enable the customization of the outgoing wavefront of metasurface lasers, resulting in outputs such as holograms, focused beams, or other desired emission patterns. Simultaneously, the coherence between nanolasers can be utilized for coherent computing and communication. In the realm of fundamental physics research, the extreme localization of the optical field in a twisted lattice nanocavity provides an excellent platform for studying cavity quantum electrodynamics, nonlinear optics, quantum optics, and other related phenomena.

F. Summary

In summary, the field of metasurface lasers has witnessed significant progress and diversification in recent years, marked by the integration of innovative methods to control optical fields in micro and nanolasers. Metasurface lasers, stemming from the conceptual framework of metamaterials, utilize individual nanolasers as artificial functional atoms to tailor the properties of the composite matter they form. This approach enables unprecedented control over the macroscopic laser field. The future of metasurface lasers presents exciting prospects for groundbreaking discoveries and advancements that can further push the boundaries of laser technology, opening up new possibilities for applications in communication, computing, sensing, and beyond.

ACKNOWLEDGMENTS

This work was supported by the National Natural Science Foundation of China (Grant Nos. 12225402, 91950115, 11774014, and 62321004) and the New Cornerstone Science Foundation through the XPLORER PRIZE.

XII. SOLUTION-DERIVED NANOFABRICATION FOR NONLINEAR METASTRUCTURES

Helena C. Weigand, Ülle-Linda Talts, Irene Occhiodori, Viola V. Vogler-Neuling, and Rachel Grange*

*grange@phys.ethz.ch

A. Introduction

Miniaturization of optical components without compromising functionality or scalability is a main challenge for deploying compact photonic solutions in current and future technologies, such as telecommunication with fast data transmission, imaging with small mobile cameras, or light sources with quantum features. Nonlinear materials used in telecommunication, lasers, and quantum applications are typically bulk metal–oxide single crystals.[699] Those high-quality bulk crystals are neither integratable, due to limited compatibility with top-down nanofabrication methods compared to typical semiconductors, nor scalable, due to the low generated signals, especially in frequency conversion at small scale. Current material platforms rely on a top-down fabrication approach with standard semiconductors (Si, InP, GaAs), which is limited to the available wafers, crystalline orientation, and transparency range. To access more sophisticated features such as parametric or electro-optic effects, metal-oxides thin films, i.e., lithium niobate on insulator have been commercially available for a few years.[700] However, they come at high wafer cost and huge constraints to master the smart-cut technique and etching process flow of a thin layer of metal-oxides to obtain the best photonic integrated chip performances.[701]

The quest for a material or fabrication method to harvest their functional response at the nanoscale that will favor energy requirements and simplify their production is still widely open. Recent advances based on photonic assemblies of randomly oriented nanocrystals instead of bulk crystals have shown excellent tailored optical properties in the linear regime.[703] More rarely, also frequency doubling and electro-optic responses have been demonstrated, mainly in isolated nanoparticles,[516] individual microstructures,[552] and rare-earth doped nanoparticles for the quantum regime[704]—all not very well suited for integration in large surface areas with fully controlled design.

These limitations are key motivations for exploring bottom-up polycrystalline nonlinear assemblies of metal-oxides for miniaturized photonic components, which, in fabrication complexity, energy consumption, footprint, and functionalities, can compete with the performance of bulk crystals or top-down thin films. Overcoming the intuitive, yet disproven, perception that nonlinear optical effects are limited or even completely eradicated in random assemblies of nanocrystals gives rise to puzzling questions and new functionalities that we aim to address. Hence, bottom-up assembly of nonlinear materials may potentially become the most agile technique for classical and quantum devices.

B. Nanoimprint and solution derived principles and advantages

Nonlinear optical metal-oxides such as lithium niobate ($LiNbO_3$ or LNO) or barium titanate ($BaTiO_3$ or BTO) are chemically inert due to

16 July 2024 09:29:41

© Author(s) 2024

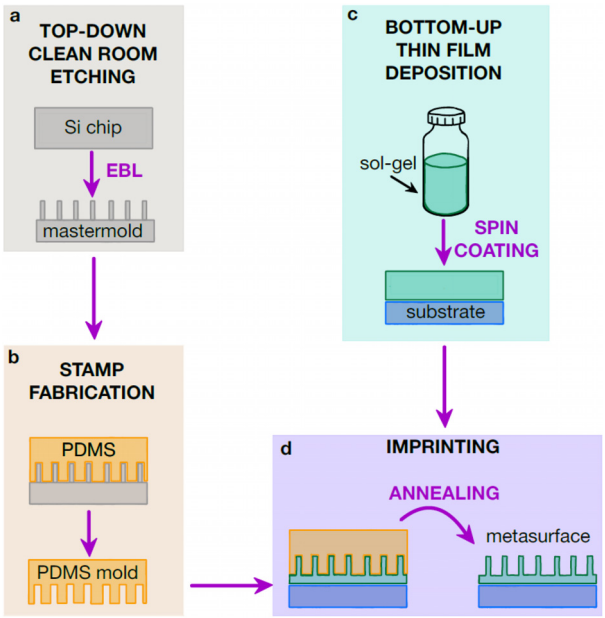

FIG. 21. Process flow of the direct soft nanoimprint lithography (SNIL). (a) The only step with top-down approach is to produce the master mold by EBL. (b) Stamps (daughter molds) are used to transfer the pattern from the Si master mold to the PDMS daughter mold. (c) Preparation of the nonlinear material sol-gel liquid film for (d) imprinting and annealing to obtain the metasurface.

their oxide character, which prohibits chemical wet etching techniques for nanostructuring these materials.[705] They possess strong nonlinear susceptibility ($d_{33,\max,\mathrm{LNO}} = -34\,\mathrm{pmV}^{-1}$, $d_{15,\max,\mathrm{BTO}} = 17\,\mathrm{pmV}^{-1}$) and electro-optic tensor components ($r_{33,\max,\mathrm{LNO}} = 31.8\,\mathrm{pmV}^{-1}$, $r_{42,\max,\mathrm{BTO}} = 730\,\mathrm{pmV}^{-1}$) at around 1060 nm.

Nevertheless, nonlinear metasurfaces have been top-down fabricated using, e.g., gallium-based focused-ion beam milling, to realize nano-gratings for second-harmonic generation and electro-optically active metasurfaces.[706–708] Alternatively, electron-beam lithography (EBL) and physical dry etching were employed for pillar-based metasurfaces from LNO thin films.[709] Finally, nonlinear thin films can serve as a substrate on which nanostructured metasurfaces from e.g., plasmonic materials have been fabricated.[710,711] BTO top-down second-harmonic metasurfaces have been achieved by pulsed-laser deposition (PLD) of polycrystalline BTO thin films, EBL, and physical etching.[551] These top-down processes are limited in footprint, typically in the range of a few hundreds of $\mu\mathrm{m}^2$, in aspect-ratio and sidewall angles. However, they allow the processing of monocrystalline materials.

An alternative and upscalable process is soft-nanoimprint lithography (SNIL) combined with solution-derived metal-oxides. Direct SNIL, also known as substrate conformal imprint lithography, is a bottom-up fabrication method that utilizes a polydimethylsiloxane (PDMS) elastomer intermediate mold to replicate nanostructures from a silicon master mold (Fig. 21). Applying this highly scalable and cost-efficient technique to form nanostructures directly from solution-derived metal oxides has shown to drastically reduce the embossing temperatures and pressure while being compatible with various substrates. Furthermore, the elastomer molds are permeable to trapped air and solvent vapors, enabling higher conformity to the design and lower remaining organic residues.[712,713] The latter is essential for ensuring dense and uniformly filled metal-oxide unit cells. This etchless method entails dispersing or synthesizing the material of interest in a liquid and malleable solvent. Nanoparticle solutions may be used, but this can result in limited conformity to the design and increased porosity, which reduces the quality of the effective material and causes unwanted scattering effects. However, specific metal-oxide sol-gels optimized for imprint lithography can overcome these limitations and provide a flexible material platform based on chemical synthesis protocols. Third-order nonlinear optical effects can be investigated in metasurfaces fabricated using binary sol-gel recipes, which have been relatively well-established for silica and titanium dioxide.[712] Second-order nonlinear optical effects arise from the non-centrosymmetric crystalline properties of ternary metal oxides. This means the sol-gel precursors for nonlinear metal–oxide photonic devices must be tailored to incorporate two metal elements in a defined stoichiometry. This makes the synthesis more complex and sensitive to small environmental or composition variations. Nevertheless, sol-gel derived non-centrosymmetric crystalline films and assemblies have been shown to exhibit nonlinear optical properties for example in potassium titanyl phosphate,[714] barium titanate,[715,716] or lithium niobate.[717,718]

Solution deposition for crystalline materials requires the removal of organic solvents and stabilizers by pyrolysis steps and final annealing at high temperatures to enable the formation of dense crystallites from the cross-linked xerogel matrix. Material characterization techniques, such as x-ray and Raman spectroscopy, can be used to verify the final composition after imprinting and annealing. The chemistry-based approach enables adjusting the chemical composition to account for the evaporation of volatile precursors. Considerable research has been dedicated to enhancing ternary metal–oxide sol-gel formulas for creating thin film transistors or capacitors,[719] and bridging this interdisciplinary research field with developing materials for nonlinear optics has significant potential, particularly when combined with SNIL nanofabrication. The advantages of the SNIL process over the top-down fabrication of quadratic nonlinear metasurfaces are the large surface areas up to full wafer scale [Fig. 22(a) shows imprints over approximately 5 mm], high-aspect-ratio more than 10 [Fig. 22(b)], the potential to increase the dimensionality of the system to three-dimensions, the ability to avoid material redeposition-caused artefacts such as slanted sidewalls [Fig. 22(b)], access to more diverse geometries and more economical processing.[720] Metal-oxides such as BTO and LNO also have a high refractive index in the visible to IR spectrum and are transparent over the whole visible range down to the UV [Fig. 22(c)], resulting in sufficient refractive index contrast for resonant structures even with sol-gel processing. Applying SNIL for metasurfaces, second-harmonic enhancing nanohole arrays,[716] second-harmonic generating nano-gratings,[721] and imprinted metalenses with a broadband focus[722] have been demonstrated so far.

C. The challenges of solution-based processing of metasurfaces

While the advantages of sol-gel-based fabrication can be primarily found in the flexibility due to the initial liquid solution, there are

16 July 2024 09:29:41

© Author(s) 2024

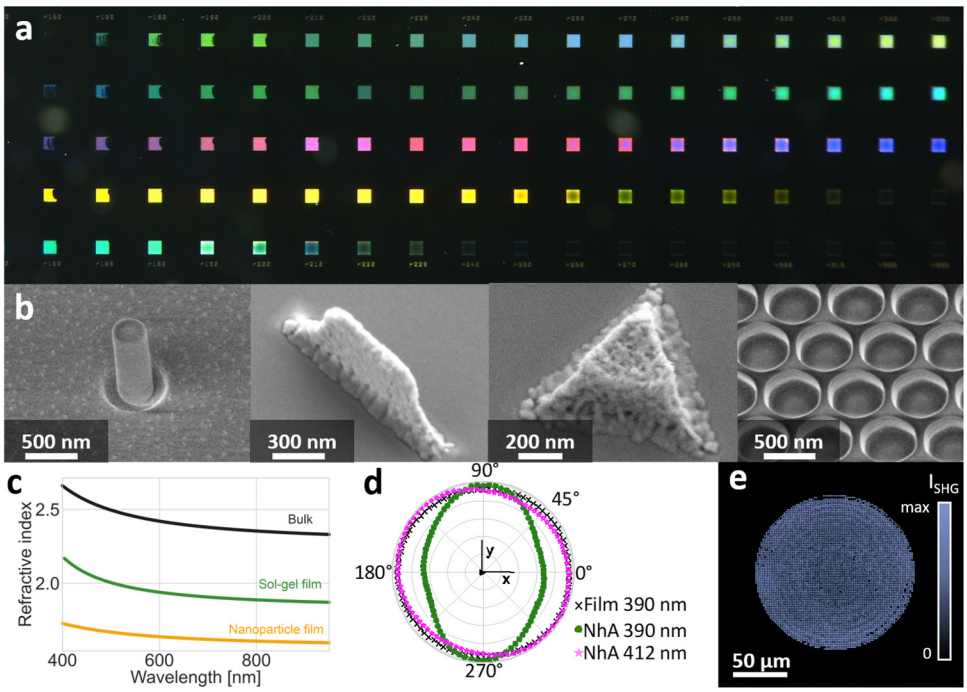

FIG. 22. SNIL metasurfaces and their properties (a) metasurface array with color responses over the whole visible spectrum (b) Overview of different achievable metaatom geometries with maximum aspect ratios included in brackets: (i) pillars (4), (ii) fins (16), (iii) triangles, (iv) nanoholes, (c) refractive index comparison for barium titanate for bulk, sol-gel derived and a nanoparticle film. (d) Polarization-dependence of second-harmonic generation for a thin film (gray) and off resonance (pink) nanohole array (NhA) showing an isotropic response. The nonlinear behavior becomes however polarization dependent at the structures optical resonance (green). (e) Two-photon microscopy image of the second-harmonic response of an imprinted metalens with a large surface area (diameter 100 μm).

challenges regarding the material composition. Solution-based techniques do not give monocrystalline material structures as opposed to ion-slicing thin films used for, e.g., LNO thin films. The crystallization process starts from numerous nuclei in the solution, yielding a polycrystalline yet very dense material structure.[723] While polycrystallinity, especially with random domain orientation, can be exploited for its advantageous properties,[724] it could also, if needed, be mitigated by aligning the domains with an external (e.g., electric) field.[725] However, the overall effectiveness of nonlinear processes, be it SHG or electro-optic modulation, will be decreased compared to a monocrystalline material.[726] It is attributed not only to the polycrystallinity of the sol-gel-based material, which might not result in fully pure crystals but also to the formation of voids during the annealing process [see Fig. 22(b), e.g., in the triangle]. In the context of signal modulation via an applied electric field, these voids decrease modulation efficiency, as any voltage drop will occur over the air inclusions instead of the sol-gel material. In addition to that, scattering of light currently limits, e.g., sol-gel-based waveguides, but slightly rough surface profiles do not pose a problem for imprinted metasurfaces as can be seen in some of the SEM images of Fig. 22(b). Furthermore, the crystallization results in a decrease of the total nanostructure volume due to the restructuring of the material into a crystal lattice and the evaporation of organic materials present in the solution. This implies, on the one hand, the formation of cracks in large structures (such as thin films or waveguides), while on the other hand, it restricts the parameter space available for metasurface designs, as volume shrinkage needs to be taken into account from the initial master mold design and can be as large as 80%.[712] Annealing conditions need careful engineering, as the temperature, ramping rate, atmosphere, and pressure can be used to optimize the density, domain size, and crystalline phase of the nonlinear material. For example, the electro-optic properties of BTO sol-gel were enhanced by a factor of 3 under oxygen annealing.[715] Keeping in mind the restrictions of high annealing temperatures (up to 800 °C), chemical compatibility, or transparency requirements, the choice of substrate can additionally enhance the formation of pure crystalline phases (e.g., by choosing lattice-matching MgO for BTO sol-gel[727]). Finally, the presence of solvents or organic stabilizers in the sol-gels induces void formation and poses a technical challenge for SNIL, as the imprint with the PDMS mold needs to happen while the spin-coated sol-gel is still in a liquid phase. This adds significant time constraints to the process, limiting complicated multilayer imprints with precise alignment.[728] However, considerable progress has been made to develop specialized SNIL tools for imprinting volatile sol-gel solutions.[713]

D. Roadmap towards high-performing solution-based metasurfaces

Overcoming the mentioned challenges will be key to the success of this material platform for future metasurface-based devices. There

16 July 2024 09:29:41

© Author(s) 2024

are several handles for optimization. One key parameter will be the quality of the crystalline domains in terms of increased size and preferred crystalline structure. This will improve the nonlinear properties of the material and minimize void formation for reduced scattering and smooth surfaces. Handles for these improvements range from controlling the nucleation by chemical composition engineering to optimizing the annealing conditions and substrates. In addition, one could use hybrid systems of sol-gel and nanoparticles, which could serve as crystallization nuclei and prevent the nanostructure shrinkage. The nanoparticles could be derived from the same sol-gel in a separate process to ensure identical chemical composition.[729] However, applications might directly use the sol-gel shrinkage, for instance, to increase the aspect ratio of the structures. The same holds for the roughness of the surface of SNIL devices, as it also increases the surface area, which is a property commonly sought for and exploited in sensing or electrochemical applications. The randomly distributed domain orientation is also a factor that one can try to mitigate (poling after or during the annealing) or exploit, e.g., with respect to quasi-random phase matching.[552] In addition, it offers the freedom to engineer the nonlinear susceptibility components based solely on the geometrically chosen symmetries thereby imprinting an artificial tensor structure on an otherwise unpolarized SHG-emitting material. For example, an imprinted nanohole array was shown to exhibit SHG orientation at the resonance compared to off-resonant behavior [Fig. 22(d)].[716] Specifically considering the efforts of the metasurface community to overcome unfavorable tensor parameter orientations by beam steering,[730] this would be an exciting approach to follow up on, as crystal-symmetry considerations would not restrict the freedom in design due to the effectively isotropic $\chi^{(2)}$ of the polycrystalline material. Particular attention should be given here to the field of Pancharatnam–Berry phase-based nonlinear structures [e.g., metalenses emitting SHG as shown in Fig. 22(e)], as they are commonly thought to follow specific symmetry-selection rules.[53] To what extent these can be influenced by unoriented but intrinsically emitting $\chi^{(2)}$-materials remains unclear. To ease the imprint process, engineering the chemical composition of sol–gels with selected precursors or solvents that have lower vapor pressure would allow more time for precise alignment to enable large-scale stacking of imprints. Further technological advancements can be made in the imprint process itself. Different daughter mold materials with, e.g., hybrid PDMS stacks (hPDMS/sPDMS) or polyvinyl alcohol (PVA) can be used to achieve high-aspect ratio structures.[722,731] Employing degassing processes, curing in a vacuum or under high pressures, or inverse application of sol-gel on the PDMS could reduce residual layers and improve uniformity. Alternative imprint techniques like hard imprints from the master, microcontact printing, capillary force-based or microfluidic-based imprinting, or eventually roll-to-roll imprinting will pave the way for higher quality or larger-scale nonlinear photonic devices, similar to developments in the field of photovoltaics.[713,732,733] An asset not discussed so far is also the possibility of extending this imprint technique to non-flat substrates like curved lens surfaces or fiber facets. Already the possibility of these applications demonstrates the resilience of this fabrication technology toward defects like dust particles.

E. Future directions

1. Exploration of other materials and processes

Soft-nanoimprint lithography relies on capillary forces, and the infiltration works best if the solution is still liquid. Still, the density of the final material will be less than in bulk crystals. Aging the sol-gels could be a solution to densify the materials and avoid shrinking, leading to higher linear and nonlinear properties. However, the aged sol-gels cannot be structured with SNIL. Therefore, one should start investigating other templating methods: (i) hard nanoimprint lithography might be an option as the imprinting relies on the applied external forces and not on the capillary forces; (ii) block copolymer self-assembled templates in which the sol-gels could be infiltrated, already been demonstrated with titanium-dioxide sol-gels;[734,735] and (iii) controlled dewetting of optical glass thin films could be adapted for nonlinear optical materials.[736]

Interdisciplinary collaboration between the fields of material sciences, chemistry, and nanosciences will play a crucial role in the future not only to help the optimization of the soft-nanoimprint process and the nonlinear properties of the sol-gel derived metal-oxides but also in the development of new materials with very high nonlinear optical properties.[737] Existing sol-gel recipes for other nonlinear materials, e.g., KTP, could be further developed.[714] By using more sophisticated alignment tools for soft nanoimprint lithography, one could stack several metasurfaces on top of each other to compensate hereby the lower electro-optic and nonlinear material intrinsic coefficients.

2. Nonlinear applications with high scalability, transparency ranges, robustness, and dimensionality

One clear advantage of solution-processed nanofabrication of nonlinear metasurfaces compared to standard top-down protocols is the upscalability. Soft-nanoimprint lithography has been demonstrated on the wafer scale and roll-to-roll fabrication.[738] From an economic viewpoint, the bare material cost of quadratic nonlinear thin films is at least two orders of magnitude higher than that of the solution-derived materials. The only expensive part for the latter is determined by what substrate wafer is required for the intended device.

Recently, metalenses have been realized on the length scales of 10 cm in diameter with which the moon and nebulae could be imaged.[739,740] Nonlinear metalenses based on frequency conversion could allow access to other wavelength ranges, e.g., up to the mid-infrared and down to the ultraviolet wavelength ranges, thanks to their high transparency window. Metasurface sensors from these materials could be used in harsh environments. They would be easy to clean, increasing their reusability and decreasing waste by exploiting the intrinsic inertness of metal oxides. Furthermore, the inherent material robustness also results in a high optical damage threshold, making these photonic devices more sustainable and long-lasting. The second-harmonic generation mechanism, combined with photonic crystal design, could add to the linear responses in advanced security features. In addition to flat devices, three-dimensional metasurfaces could be applied, e.g., if stacked to realize electrically tunable metalenses for fast switching that might be an alternative to membrane-type liquid lenses, which suffer from gravitational lag.[741]

16 July 2024 09:29:41

© Author(s) 2024

3. Unexplored properties and more fundamental aspects

We focused on the classical nonlinear and electro-optic properties of LNO and BTO, though both materials belong to the class of ferroelectrics, which also exhibit other compelling effects such as piezoelectricity and pyroelectricity. Therefore, the potential of further exploring the functionalities of this type of compound is enormous, mostly unexplored at the nanoscale and in the polycrystalline form of those materials.

Finally, spontaneous parametric downconversion, used in the early sources of entangled photons for quantum cryptography from periodically poled LNO,[742] remains to be demonstrated in polycrystalline sol-gel. In doing so, the miniaturization of quantum sources may benefit from a new type of fabrication process that can further help the integration of current bulky quantum systems.

ACKNOWLEDGMENTS

The authors acknowledge ScopeM and D-MATL X-Ray Service Platform at ETH Zurich for providing instrumentation for characterization, nanofabrication support from the operation team of the Binning and Rohrer Nanotechnology Center (BRNC) and the operation team of FIRST–Center for Micro and Nanoscience at ETHZ. This work was supported by the Swiss National Science Foundation SNSF (Consolidator Grant Nos. 2022 213713 and 179099), the European Union's Horizon 2020 research and innovation program from the European Research Council under the Grant Agreement No. 714837 (Chi2-nanooxides). H.C.W. acknowledges financial support from the Physics Department at ETH Zurich.

XIII. SEMICONDUCTOR METASURFACES: MATERIALS AND NANOFABRICATION APPROACHES

Mohsen Rahmani and Lei Xu

∗mohsen.rahmani@ntu.ac.uk

A. Introduction

Metasurfaces consist of artificial atoms, also referred to as subunits, with dimensions and separations much smaller than the light wavelength. The light passing through the metasurfaces interacts with the material's effective parameters, such as permeability (μ) and permittivity (ε). In other words, in addition to the lattice constant, i.e., separation, the refractive indices ($n^2 = \mu\varepsilon$) of the atoms and their surrounding environment also play an essential role in stimulating and controlling the light interactions with metasurfaces. Meanwhile, to obtain strong light confinement in these atoms and enhance the optical effects produced by the metasurfaces, fabricating metasurfaces on low-refractive-index insulators, such as glass and sapphire, has become an important factor in designing the geometry of metasurfaces.[743]

In the past decades, advanced nanofabrication techniques have enabled complicated assemblies of nanoscale structures that can be employed for engineering the metasurfaces. Metals were among the first exploited materials for producing nanoscale particles and metasurfaces,[5] mainly employing the oscillation of free electrons on the surface, so-called surface plasmons.[744–746] Fabrication of metallic nanostructures is relatively straightforward by using electron beam lithography (EBL). As a result, many high-quality metallic nanostructures have been proposed, fabricated, and studied. Despite numerous advantages allowing for near-field enhancement, metallic nanostructures suffer from Ohmic losses at optical frequencies, leading to light absorption. Hence, metallic nanostructures can be irreversibly damaged under illumination by high-power lasers, which is not preferable in many applications, particularly nonlinear metasurfaces.[53,747,748] Subsequently, a quest has taken place to employ other materials with more intrinsic and extrinsic properties to offer more versatile degree of freedom to produce metasurfaces with exotic properties.[510] As a result, materials' intrinsic and extrinsic properties have been employed as a versatile degree of freedom to produce metasurfaces with exotic properties. Several scenarios, such as solution-drive nanofabrication or nanofabrication on flexible metasurfaces are discussed in this roadmap. This section focuses on recently demonstrated approaches for fabricating semiconductor metasurfaces on insulators—a task that has been deemed challenging for decades.[510]

B. Semiconductor metasurfaces and fabrication challenges

Semiconductor metasurfaces, driven by their high refractive index and wide bandgap, have attracted significant attention in the photonics community recently. In addition to their loss-free nature, which distinguishes them from metals, semiconductor metasurfaces benefit from exotic electronic properties and controllable crystalline structures that provide vast and new opportunities to engineer light–matter interaction.[749] Therefore, semiconductors have been deemed as major building blocks for the development of advanced optical devices such as meta-lenses, holograms, displays, sensors, and more.[15] As a result, precise control of the geometry of sub-unit nanoparticles via top-down nanofabrication approaches has gained remarkable importance. However, unlike metallic nanostructures, regular lithographic and liftoff processes cannot be exploited for fabricating semiconductor metasurfaces, as discussed below.

The major categories of semiconductor metasurfaces include: (a) Group IV semiconductors, such as silicon or germanium, which are widely explored using the complementary metal–oxide–semiconductor (CMOS) processes, (b) III–V compound semiconductors, like GaN, GaAs, or AlGaAs, renowned for their high intrinsic nonlinearity, or (c) recently emerging materials, such as perovskites, with strong light absorption, high charge-carrier mobilities and long lifetimes.[750] The common challenge for fabricating metasurfaces out of these semiconductors is the high-temperature requirements for the growth of a thin film. Therefore, the regular liftoff process (i.e., patterning, film deposition, and liftoff) cannot be exploited, as photo/electro resist is vulnerable against high temperatures. In addition, each category comes with its own set of fabrication challenges, including but not limited to lattice mismatch between film and substrate (particularly insulators), controlling the crystalline orientation, or resistance against dry or wet etching, etc.,[510] highlight a need for innovative approaches for fabricating semiconductor metasurfaces. This section reviews the community's effort to balance these fabrication challenges with the inherent properties of different semiconductor materials to advance both the fabrication techniques and the applications of these versatile materials in metasurface design.

16 July 2024 09:29:41

© Author(s) 2024

C. Group IV semiconductor metasurfaces

Group IV semiconductor nanostructures and metasurfaces, especially those made of silicon and germanium, have come to the forefront as viable alternatives to traditional metallic nanostructures, largely motivated by their ability to mitigate the Ohmic losses prevalent at optical frequencies in metal materials.[146,751–754] High-refractive index materials offer a promising platform for different nanophotonics applications in the visible and infrared regions, such as flat optics, sensing, computing, imaging, etc.[15] They support both electric and magnetic resonant optical modes, facilitating enhanced linear and nonlinear optical effects.[755] Notably, the ability to finely tune these materials through sophisticated fabrication methods allows for the precise manipulation of their optical properties, making them even more promising for the aforementioned applications.[15]

Given that germanium can be deposited with standard evaporation techniques, Germanium nanostructures can be fabricated through the standard top-down techniques, involving EBL for patterning hard masks, transferring the masks to the germanium film via inductively coupled plasma (ICP)/reactive ion etching (RIE), and mask removal via dry or wet etching.[146] On the other hand, silicon films cannot be deposited through evaporation or sputtering. Therefore, the fabrication of silicon nanostructures often leverages silicon-on-insulator (SoI) technology, which was initially developed for electronic applications. However, SoI wafers, benefiting from a crystalline silicon film, have been recently employed in photonics, as well. SoI enables planar waveguides that strongly confine light, thanks to the high refractive index contrast between the silicon core and a SiO_2 substrate.[756]

More recently, the use of amorphous silicon (a-Si), which can be grown directly on any substrate by plasma-enhanced chemical vapor deposition (PECVD), has opened up new possibilities in fabrication.[757] a-Si films can then be converted to any complicated metasurfaces via EBL patterning followed by ICP/RIE etching.[758] PECVD allows for the growth of thin films of hydrogenated amorphous silicon under lower temperatures compared to crystalline silicon, making it suitable for a broader range of substrates, including fully transparent ones, e.g., SiO_2 or quartz. This method involves the decomposition of silane gas in a plasma environment, where the ions and radicals facilitate the deposition of silicon on the substrate. The ability to control the deposition parameters, such as gas flow rates, power, and temperature, allows for tuning the properties of the amorphous silicon layer, such as its optical bandgap and conductivity. This control is crucial for tailoring the materials to specific applications, such as absorbers, holograms, metalenses, and other optical components. Amorphous silicon's flexibility in deposition and adaptability to different substrates have significantly broadened its applicability in the nanophotonics field, making it an invaluable material in the fabrication of advanced semiconductor metasurfaces.[758]

D. Group III–V semiconductor metasurfaces

As explained in Sec. IV (Nonlinear Optical Metasurfaces) above, nonlinear metasurfaces have great potential to revolutionize modern photonic devices, including optical signal processing, control over the frequency spectrum of laser light, ultrafast switching and generation of ultrashort pulses.[759] However, weak nonlinear optical responses of metasurfaces have guided the community's attention to materials, which naturally possess large nonlinearities. III–V semiconductor nanoantennas and metasurfaces, comprised of materials such as Gallium Arsenide (GaAs), Gallium Phosphide (GaP), Indium Phosphide (InP), benefit from the non-centrosymmetric crystal structure, large second-order susceptibilities,[503] and fast carrier recombination times.[760] The strong second-order bulk susceptibility of III–V materials would, therefore, intrinsically increase the nonlinear conversion efficiency as compared to silicon or germanium. Furthermore, like IV semiconductors, III–V semiconductors also exhibit high refractive indices that allow the use of strong Mie resonances to amplify the nonlinear signals. Moreover, III–V semiconductors are pivotal in various advanced technological areas in optoelectronic applications due to their direct bandgap and high electron mobility. Therefore, the unique electronic and optical properties of III–V semiconductors enable superior performance for various applications ranging from high-efficiency solar cells, light-emitting diodes, and photodetectors to quantum computing and photonic integrated circuits.

Unfortunately, the full fruition of III–V metasurfaces in photonics has been bottle-necked because of the absence of good-quality dielectric-semiconductor interfaces. The main challenge is that III–V semiconductors, which are generally grown epitaxially, must be grown on a substrate with a minimal lattice mismatch to avoid defects.[761] Over the years, various techniques for fabricating III–V semiconductor nanostructures and metasurfaces on insulators have been developed. Recently, a solution was achieved by Cambiasso *et al.*, who introduced a novel approach to circumvent the challenges associated with growing III–V films on mismatched substrates. Instead of using conventional film growth, they directly fabricated GaP nanoantennas on a GaP wafer. This technique involves using EBL to create highly precise and intricate patterns on the GaP wafers. Following the EBL process, these patterns are transferred into the wafer using ICP etching. Eventually, GaP nanopillars with a height of 200 nm were created and optimized for visible light applications, demonstrating enhanced SHG characteristics as described in Ref. 762.

Pioneering a novel approach in III–V semiconductor fabrication, Person *et al.* focused on creating GaAs nanoantennas on glass substrates.[763] Initially, they grew a thin film of GaAs on a GaAs substrate using molecular beam epitaxy (MBE). This was followed by an epitaxial liftoff process, where the GaAs film was separated from its substrate and then transferred onto a fused silica substrate via a water-bounding procedure. Subsequently, by using RIE, the thickness of the film was reduced to the desired value, and then the nanoantennas were patterned onto the film through EBL, followed by another RIE process. This technique marks a significant step in fabricating GaAs nanostructures on transparent substrates.[763] Although it was the first of its kind, the relatively low quality of resonators and the rough side walls restricted its performance for nanophotonics applications, such as the obtained field confinement for nonlinear enhancement. In the pursuit of efficient nonlinear optical materials, Gili *et al.* introduced an AlGaAs-based monolithic platform. Their process starts with growing a layered structure on a non-intentionally doped GaAs wafer through MBE. This structure includes a layer of AlGaAs on the top an aluminum-rich layer for later oxidation. Following the growth, the sample then undergoes patterning using the EBL, and the resultant patterns are etched into the substrate using nonselective ICP-RIE. Subsequently, the aluminum-rich layer was oxidized to create a uniform AlOx substrate. Such a substrate with a low refractive index plays a crucial role in enabling effective optical confinement within the

16 July 2024 09:29:41

© Author(s) 2024

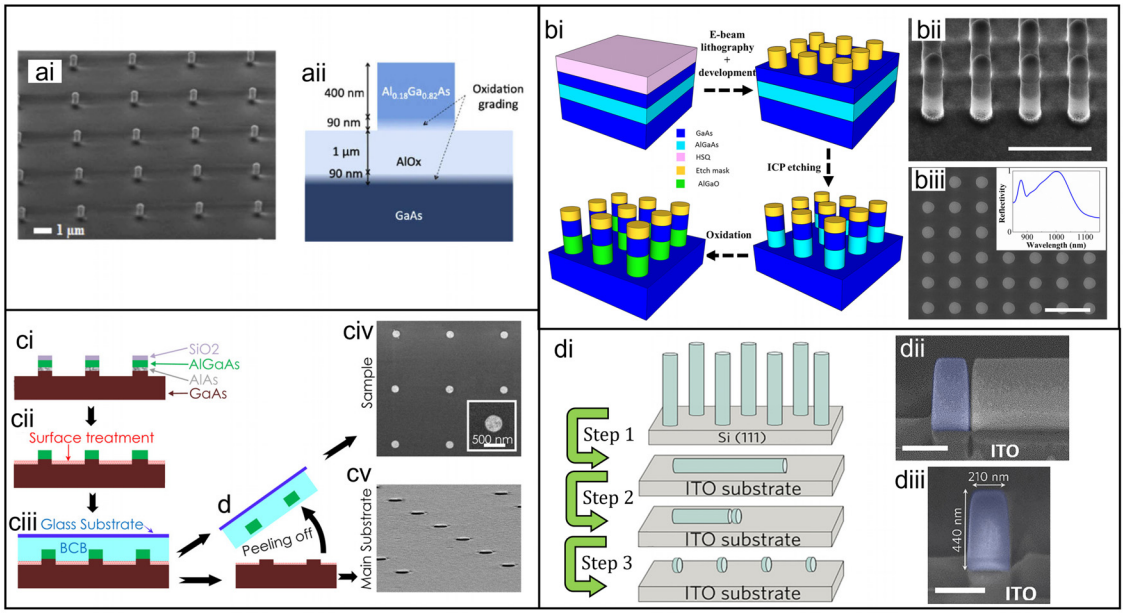

FIG. 23. (a-i) SEM image of an array of monolithic AlGaAs-on-AlOx nanoantennas. (a-ii) Schematic of a single monolithic AlGaAs-on-AlOx nanoantenna. Adapted from Ref. 504. (b-i) Steps illustration for fabricating GaAs metasurfaces, proposed by Adapted from Ref. 764. (b-ii) A side view and (b-iii) top view SEM images of the fabricated GaAs metasurfaces. The inset gives the reflectivity spectrum of the GaAs metasurface. Liu *et al.*, Nano Lett. **16**, 5426 (2016). Copyright 2016 American Chemical Society. [(c-i)–(c-v)] Fabrication procedure for the AlGaAs nanoresonators in a transparent media Rocio *et al.* Adapted from Camacho-Morales *et al.*, Nano Lett. **16**, 7191 (2016). Copyright 2016 American Chemical Society.[197] (d-i) Fabrication process flow for slicing the nanowires. (d-i) SEM image of one nanowire sliced by FIB into standing disks (highlighted in blue). (d-ii) SEM image of the resulting single standing disk (blue) on an ITO substrate. Scale bars are 300 nm. [(d-i)–(d-iii)] Adapted with permission from Timofeeva *et al.*, Nano Lett. **18**, 3695 (2018). Copyright 2018 American Chemical Society.[512]

AlGaAs nanocylinders to facilitate strong nanoscale light–matter interactions, as shown in Fig. 23(a).[504]

Shortly afterward, Liu *et al.* demonstrated a similar approach for creating nonlinear metasurfaces composed of a square lattice of GaAs nanodisk resonators.[764] These resonators were placed on a low refractive index AlGa oxide spacer layer, formed by selectively oxidizing high-Al content AlGaAs layers. It began with the growth of alternating layers of AlGaAs and GaAs on a GaAs substrate via MBE. A negative hydrogen silsesquioxane (HSQ) mask was then applied for patterning. The shapes of the SiOx nanodisks were transferred onto the GaAs and AlGaAs layers using ICP etching. Finally, via the selective wet oxidation process, the AlGaAs layer has converted into a low refractive index (AlxGa1-x) layer. In parallel with these studies, Camacho *et al.* implemented a recipe for III–V in insulator fabrication, enabling the production of metasurfaces on fully transparent substrates like glass or sapphire. Their approach includes metal-organic chemical vapor deposition (MOCVD) growth of AlGaAs or GaAs on a thin sacrificial AlAs layer, pre-grown on a semi-insulating GaAs substrate. The process was followed by EBL patterning and RIE etching to imprint the designs onto the top and AlAs layer. Subsequently, the AlAs layer was removed by wet etching, and loosely bound nanostructures are embedded in a benzocyclobutene (BCB) polymer layer that can be transferred to a glass substrate. As a result, high-quality AlGaAs nanoresonators were obtained on a fully transparent matrix [see Fig. 23(c)].[197] Furthermore, several alternative approaches were reported for fabricating III–V metasurfaces on insulators. Timofeeva *et al.* proposed free-standing III–V disks, by slicing nanowires with focused ion beam (FIB) milling to create disk-based configurations on any substrate, as shown in Fig. 23(d).[512] Another promising technique is to grow GaP on GaAs substrate with an AlGaInP buffer layer, then bond it to a sapphire substrate after depositing SiO_2 layer on top of both surfaces. By removing the AlGaInP/GaAs layer with wet etching, one can obtain GaP film on an insulator that can be used to produce high-quality nonlinear metasurfaces.[152,765] Depositing GaN on sapphire by MOCVD is another exciting technique enabling many applications of both linear and nonlinear metasurfaces in the visible range, particularly meta-lenses.[737] Overall, all these advances in fabricating III–V metasurfaces on a wide range of substrates open many doors to make them compatible with CMOS technologies in the near future.

E. Multi-layered semiconductor metasurfaces

Stacking several metasurfaces on each other, to benefit from several functionalities simultaneously, is an important step forward for realizing multi-functional end-user devices. This concept was first studied in plasmonic bilayered chiral structure,[766] and stacked metamaterials, so-called Stereometamaterials.[767] The concept of multi-layered semiconductor metasurfaces is a recently developing field, with the vision of integrating multi-functions, such as linear, nonlinear, passive, and active metasurfaces, into a single, compact device.[768,769] This approach promises significant advancements in optical technology, enabling more sophisticated and versatile functionalities.[770]

16 July 2024 09:29:41

© Author(s) 2024

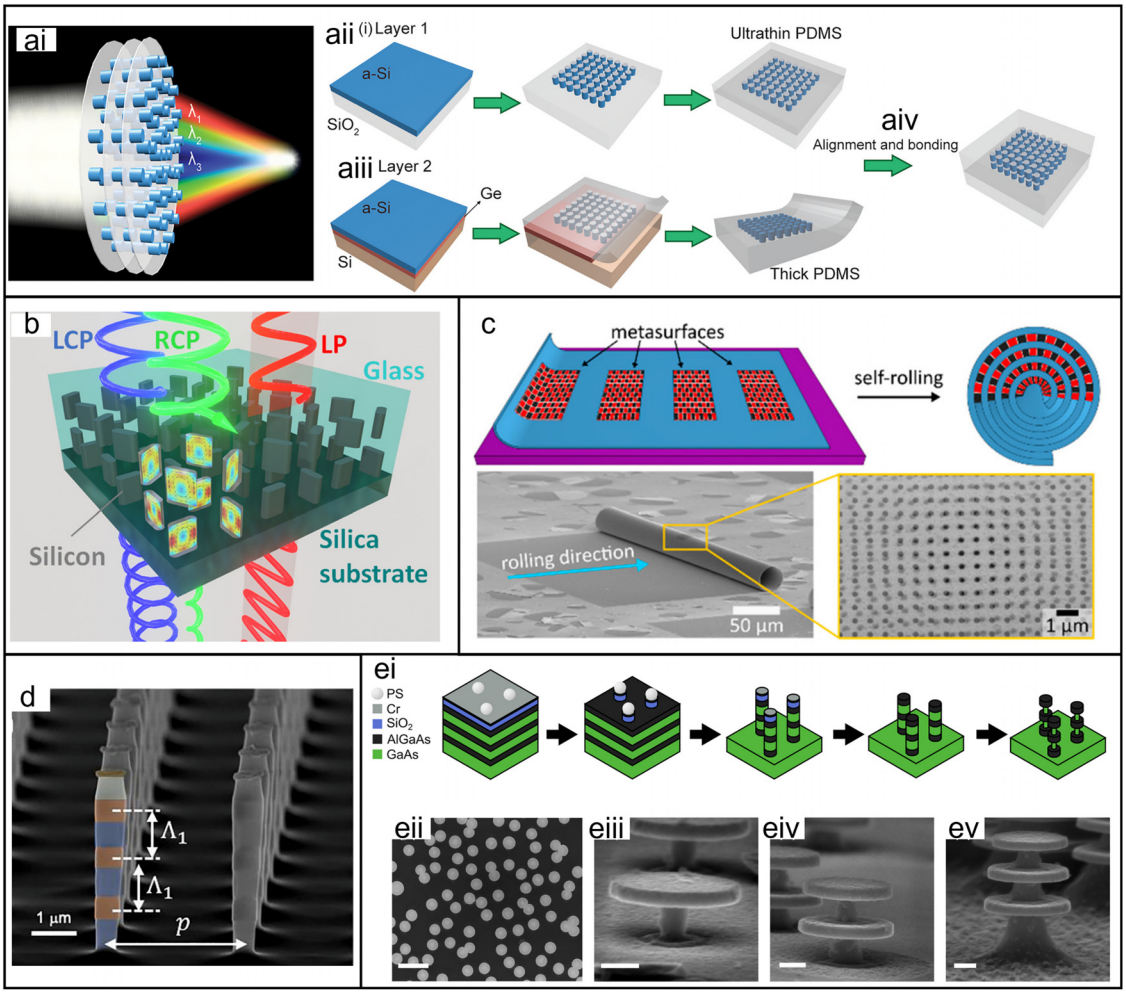

FIG. 24. (a-i) A schematic of a three-layered silicon metasurface triplet lens. (a-ii)–(a-iv) Illustration of the fabrication of layered silicon metalens doublet. Adapted with permission from Zhou *et al.*, Nano Lett. **18**, 7529 (2018). Copyright 2018 American Chemical Society.[771] (b) Schematic illustration of a chiral bilayer dielectric metasurface. Adapted with permission from Tanaka *et al.*, ACS Nano **14**, 15926 (2020).[773] Copyright 2020 American Chemical Society. (c) Sketch illustrating the evolution from the design of independent 2D metasurfaces to a multi-layer stack exploiting a single-shot thin film self-rolling mechanism. Side-view (bottom left) and top-view (bottom right) SEM images of self-rolled microtubes after the sacrificial layer removal, revealing the two nanohole array stacks in the microtube walls. Adapted with permission from Bermudez-Urena and Steiner, ACS Photonics **6**, 2198 (2019). Copyright 2019 American Chemical Society.[774] (d) SEM image of the fabricated three-layer AlGaAs metasurface. Adapted from Ref. 775. (e-i)–(e-v) Illustration of the steps for fabricating stacked AlGaAs/GaAs alternating multi-layer resonators. (e-ii) A top view image of the final pillar structures, scale bar 1 μm. (e-iii)–(e-v) Tilted views of the finalized one, two and three AlGaAs nanodisk stacks. The scale bars are 100 nm in (e-ii)–(e-v). (e-i)–(e-v) Adapted from Ref. 778.

Recently, Zhou *et al.* demonstrated tightly spaced multi-layer metasurfaces for multiwavelength focusing.[771] They fabricated two a-Si meta-lens embedded in PDMS, separately. The two layers were bounded by heating and curing the PDMS. As a result, they demonstrated a multiwavelength metalens doublet ($NA = 0.42$) with focusing efficiencies of 38% and 52% at wavelengths of 1180 and 1680 nm, respectively [see Fig. 24(a)]. Later, the same group extended this fabrication technique to realize bilayer metasurfaces for multiwavelength holograms, multiwavelength waveplates, and polarization-insensitive 3D holograms.[772] A similar technique, shown in Fig. 24(b), but using a spin-on-glass layer instead, has been proposed for the creation of bilayer semiconductor chiral metasurfaces.[773] Figure 24(c) demonstrates another approach proposed by Bermudez-Urena and Steiner. It involves a thin film self-rolling technique to fabricate multi-layered semiconductor metasurfaces.[774] During the fabrication process, the semiconductor materials primarily used include Ge and SiO_2, along with gold, for certain steps. When the sacrificial underlayer (Ge) is selectively removed, these strained layers naturally roll up, either upwards or downwards, creating a microtubular structure with multi-layered surface walls, depending on the number of turns completed. This method reduces the number of steps required for creating multi-layer metasurface devices.

16 July 2024 09:29:41

© Author(s) 2024

In 2021, Marino *et al.* employed a novel fabrication technique for a three-layer metasurface in the AlGaAs-on-insulator platform designed to enhance the optical performance in applications like ultrafast optical switching and high harmonic generations.[775] As depicted in Fig. 24(d), the metasurface features three AlGaAs layers separated by a low-index AlOx spacer, all resting on an AlOx optical substrate. The fabrication process involves MOCVD growth of the epitaxial structure on a GaAs wafer, PECVD deposition of a SiO_2 hard mask, EBL, Electron-Beam Physical Vapor Deposition (EBPVD) nickel deposition, liftoff, ICP-RIE etching, and selective oxidation of AlGaAs layers, resulting in a deeply etched, high-efficiency metasurface. The lower refractive index contrast between the resonator and the spacer layers (AlOx) reduces the energy confinement within the resonators. To maximize the index contrast and field confinement, later in 2022, Vennberg *et al.* proposed another approach to fabricate vertically stacked AlGaAs/GaAs nanodisk resonators with a fast and scalable patterning method using charged sphere colloidal lithography, where they have under-etched the spacer layer (GaAs), as illustrated in Fig. 24(e).[776]

F. Metasurfaces made of hybrid and emerging materials

Despite the recent progress in semiconductor metasurfaces, there is still a quest to explore new materials for various applications to address the major issues hampering the full-scale development of metasurface technology, such as high loss, cost-ineffective fabrication, and challenging integration.[3,777–779] Some research works have demonstrated that combining the advantages of the metal and semiconductor approaches can address such issues. Various types of hybrid nanoantennas, consisting of metallic resonators embedded in semiconductor media or vice versa, have been proposed and realized in recent years, such as hybrid metal-oxide nanostructures[191] or nanopatterned plasmonic films filled with GaAs,[780] metal/dielectric core-shell nanoparticles,[781] plasmonic ring filled by concentric lithium niobate,[782] silicon,[148] or AlGaAs.[783] The fabrication technique for hybrid nanostructuring is generally a combination of the techniques discussed above, consisting of multiple EBL steps, requiring precise alignment of every subsequent mask to the previous steps.

2D materials, ranging from WS_2, MoS_2, $MoSe_2$ to WSe_2 with semiconducting band gaps on the order of 1–2.5 eV, to hexagonal boron nitride (h-BN) with a wideband gap of 6 eV, are recently proposed materials for semiconductor metasurfaces, particularly in nonlinear regime,[784,785] Chemical vapor deposition (CVD) technique is the most employed method that has enabled the synthesis of large area and uniform thickness 2D layer of metal and insulating surfaces for the large-scale device fabrication including electronic and flexible optoelectronic devices.[786] II–VI compound semiconductors, such as ZnS or CdHgTe, with a large range of electronic energy bandgaps, have also been considered for optoelectronic metasurfaces,[787] and Cd–Te helices have been proposed for chiral nonlinearity.[788] More recently, perovskite materials with a large ability of tunability have been proposed for reconfigurable semiconductor metasurfaces[91,789–794] The optical properties of perovskite metasurfaces can be tuned by changing the composition of the perovskite material or the thickness of the perovskite film. All these emerging materials are already subjects of heavy studies in the community of semiconductor metasurfaces.

G. Conclusions and future perspectives

Today, semiconductor nanoscale devices are routinely used in the electronics industry. The possibility to engineer their bandgap and electrical conductivity has made them an ideal platform for making transistors and integrated circuits.[795] Alongside this, the optoelectronic properties of semiconductor nanomaterials, mainly based on quantum mechanical effects of light on electronic materials, have also been employed to find, detect and control the light via photo-diodes, solar cells, plasma displays, nano-lasers, etc.[796] However, engineering and exploiting purely optical properties of semiconductor nanostructures, including metasurfaces on insulators, is a relatively new field of research that has recently flourished via developing novel fabricating techniques.[510] As briefly summarized in this section, despite challenges for growing semiconductor films, including high-temperature deposition and lattice mismatch, which forbid regular liftoff nanolithography, many innovative techniques have been recently proposed for fabricating high-quality semiconductor metasurfaces. It is worth noting that this concept differs from fabricating quantum dots via the synthesis of sub-30-nm semiconductor nanoparticles. Quantum dots employ semiconductors' optoelectronic properties, which is beyond the scope of this section.

Given the recent development in the fabrication techniques of semiconductor metasurfaces, there is a promising perspective on the capability to fabricate more complex and hybrid metasurfaces. As a result, significant interest has grown in integrating metasurfaces in photonics chips and tunable metasurfaces, two areas requiring well-controlled and precise nanoscale devices. Recently, the incorporation of metasurface principles into integrated photonics has grown rapidly. This capability opens opportunities to control the off-chip emission of customized free-space wavefronts and on-chip manipulation of light.[797] Similarly, a great interest has appeared in tunable metasurfaces where external tools, such as mechanical force, heat, applied voltage, etc., can be used to control the light emission, propagation direction, polarization, phase, or wavelength.[798–801] These developments are not only enhancing the performance and efficiency of existing applications for semiconductor metasurfaces but also paving the way for future applications of nanostructures ranging from advanced imaging and signal processing to sensing and energy harvesting, unlocking more potential in nanotechnology and photonics fields.

ACKNOWLEDGMENTS

M.R. and L.X. acknowledge support from the UK Research and Innovation Future Leaders Fellowship (No. MR/T040513/1). M.R. appreciates the support of the Royal Society and the Wolfson Foundation.

XIV. CONFORMAL AND FLEXIBLE METASURFACES: A BRIEF PERSPECTIVE

S. M. Kamali, E. Arbabi, and Andrei Faraon

faraon@caltech.edu

A. Introduction and brief history

Metasurfaces designed for, and fabricated on, flexible substrates enable very interesting concepts and have potential for applications in conformal optics where a thin metasurface can vastly alter the optical

16 July 2024 09:29:41

© Author(s) 2024

function of an optical element with a given shape,[467,468,802,803] or a stretchable metasurface can act as a compact tuning element in an optical system.[804–806] Nevertheless, despite the attention and advances made over the past decade, this technology has not been adopted beyond academic and research efforts. In this Perspective, we give a short account of the history of conformal and flexible metasurfaces, briefly discuss their design, fabrication, and potential applications, and share our view of their opportunities and the challenges that must be overcome before those opportunities can be realized.

The applications of gratings fabricated on curved surfaces goes back more than a century where concave gratings have extensively been used in spectroscopes to reduce the optical aberrations and improve spectral resolution.[807–810] Since then, diffractive structures patterned on non-planar surfaces have also been used to mitigate the chromatic aberrations of lenses[811,812] or enhance the power of optical system without compromising size and weight.[813] Independently, conformal RF and microwave phased array antennas[814,815] and metasurfaces[816–818] have been developed over the past many decades to fit certain functionalities in structures dictated by other factors such as aerodynamics, stealth, or physical constraints of the host structure.

Over the past decade, the increased availability and reduced cost of advanced nano-fabrication and computational resources have allowed for the design and fabrication of conformal metasurfaces at optical length scales, see Figs. 25(a) and 25(b).[821–823] As intrinsically quasi-2D structures (i.e., having a third dimension much smaller than the first two), metasurfaces are suited for conforming to non-planar structures and can be directly fabricated on the target surface.[802] Direct fabrication, however, is only possible if the target surface has small curvature (i.e., a very large radius of curvature) and very small height variation overall (in the tens of micrometers, maximum).[802] Otherwise, pattern generation machines with special capabilities are needed to define the metasurface pattern, and the utility of regular planar techniques that are widely developed and used for electronics will be very limited in fabrication of conformal metasurfaces. The requirement of special equipment and methods for their fabrication severely limits the types and shapes of structures that could be directly made as well as the shape and material of the target non-planar surfaces, and would thus hinder the development and scaling of conformal metasurfaces. To circumvent these issues, the idea of transferring metasurfaces to flexible substrates, that could later conform to a non-planar surface, was developed.[468] Using this method, flexible metasurfaces can be fabricated separately and later fitted to the target structure, altering its optical function to one that does not match its form, or adding totally new functionalities.[467] For instance, a specially designed metasurface can be used to make a diverging cylindrical lens work like a converging spherical one,[468] or metasurfaces can be added to regular eyepieces and turn them into visors for near eye displays.[467]

Since many flexible substrate materials are also stretchable, transferring of metasurfaces to these substrates enables other lines of applications utilizing this property.[806,822,823] For instance, a main property of optical gratings is their period, which would change proportional to the local strain if a metasurface on a flexible material is stretched. This would in turn change the grating momentum and thus can be used to tune the diffraction angle at a certain wavelength of light, or change the color appearance at a given angle.[824] The focal length of diffractive and metasurface lenses can also be tuned through radial stretching [albeit with introduction of additional geometric abberations, see Fig. 25(c)].[822] The deformations of the substrate, such as stretching, can significantly alter the optical function of flexible metasurfaces, providing an opportunity to tune their functionality. Various tunable and

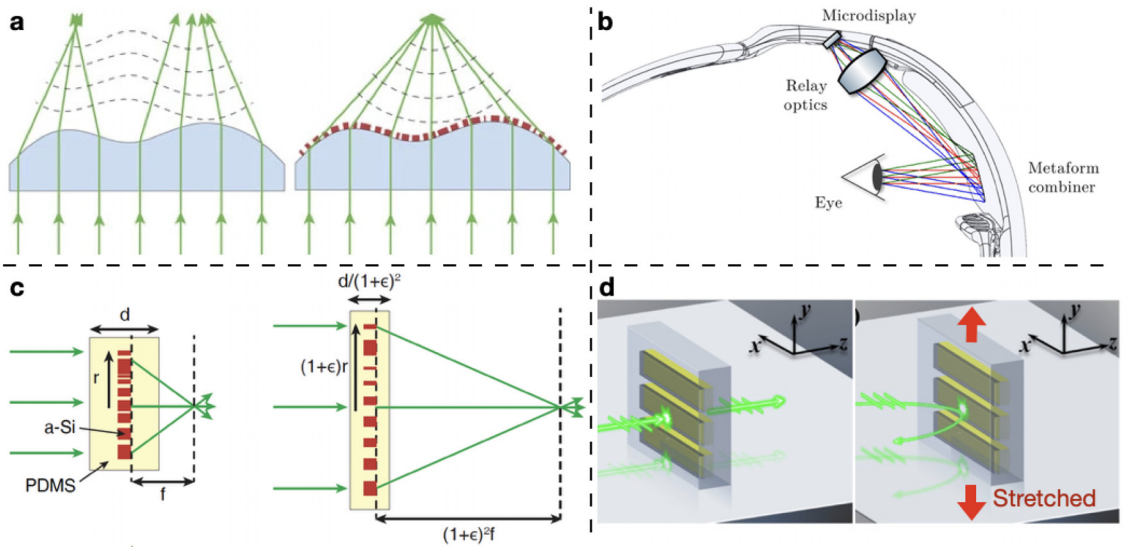

FIG. 25. Conformal and flexible metasurface concepts. (a) A metasurface conforming to an optical elements modifies the optical function of the element in a desired way.[468] (b) Concept of a flexible metasurface conformed to an eyeglass's eyepiece to redirect display light from the micro-display to the eye. Similar to holographic optical elements, metasurfaces can implement a grating and wavefront control functions simultaneously in a single layer, allowing for the thin metasurface to both correct for the eyepiece shape and redirect light.[467] (c) Schematic illustration of a flexible tunable metasurface. Upon stretching, the focal length of the metasurface changes proportional to strain squared.[822] (d) Schematic of a stretch tunable filter, where the transmission and reflection spectra can be modified upon stretching the metasurface.[825] All images are reprinted (adapted) with permission from the respective Journal and copyright remains with the original publisher.

16 July 2024 09:29:41

© Author(s) 2024

stretchable metasurface lenses and gratings have been demonstrated using different metasurface platforms (see Fig. 25),[806,824] in addition to tunable filters and color tuning in metasurfaces.[825–827]

It is worth noting here that fabrication of diffractive optical elements (e.g., surface relief optics like blazed gratings, Fresnel lenses, diffusers, etc.) using non-rigid materials such as polymers and resins is relatively mature and multiple companies (Luminit, Viavi, etc.) have already commercialized these technologies for many years now. While these technologies, and devices fabricated using them, are in many aspects similar to metasurfaces fabricated on or transferred to flexible substrates, we would like to distinguish and separate them for the purposes of this paper by the effective volume thickness (i.e., wavelength and subwavelength scale thickness for metasurfaces vs multiple to several wavelengths for these more conventional devices), and the critical dimensions of the structures involved (i.e., subwavelength for metasurfaces and single to multiple wavelength scales for the conventional ones). Each of these technologies have their own benefits and drawbacks and the specific choice of which one to use depends on many technical and non-technical factors involved. Nevertheless, in the rest of this chapter we will focus on metasurfaces

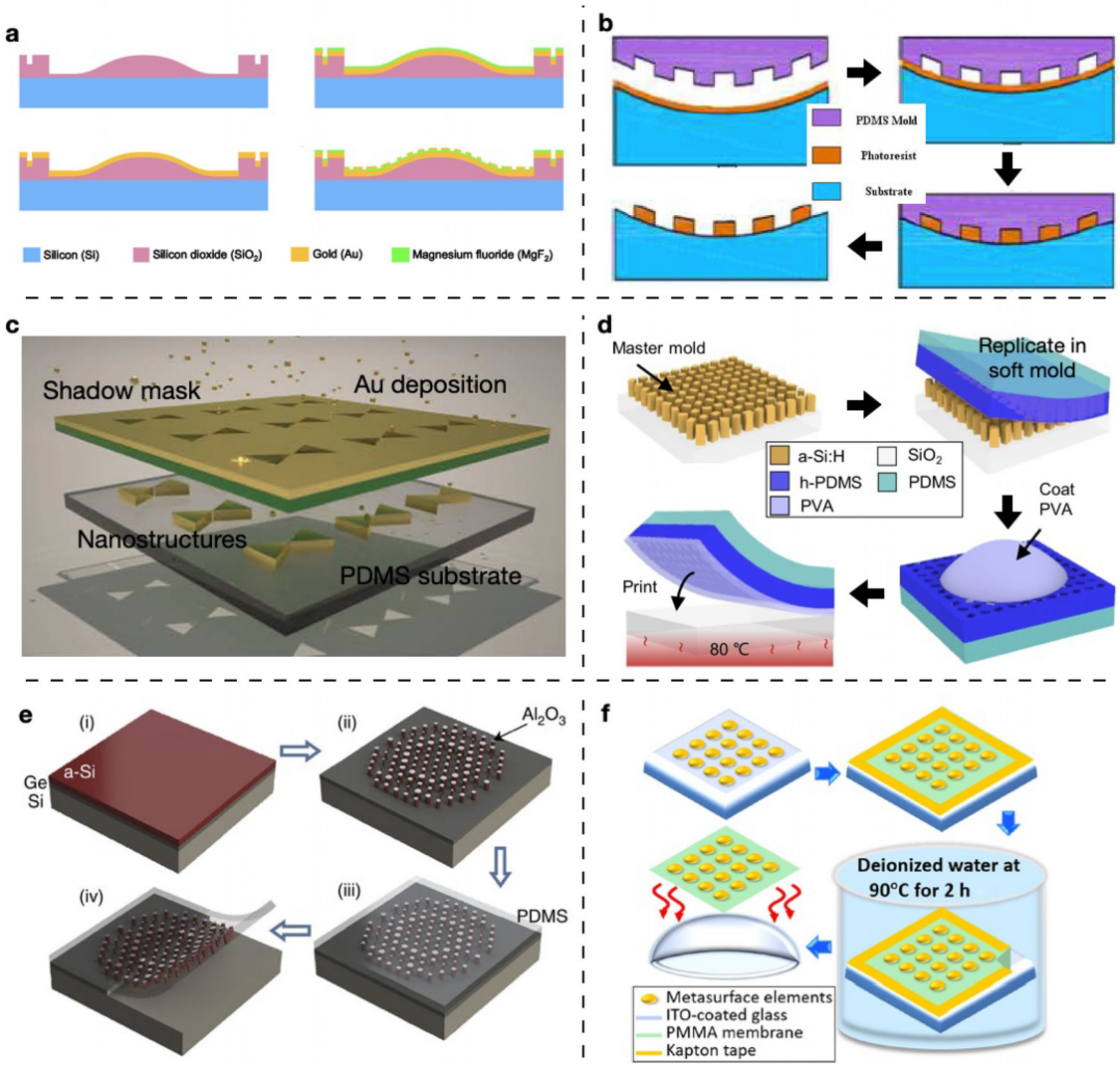

FIG. 26. Fabrication methods for flexible metasurfaces. (a) For non-planar surfaces with small bumps (i.e., a few tens of micrometers of height variation and slopes smaller than a few degrees) the pattern can be directly generated on the non-planar surface using electron-beam lithography, and then transferred to the active metasurface layer using etch or liftoff processes.[802] (b) Metasurface can be patterned directly on the non-planar surface using nano-imprint lithography. The patterned layer can then be used as an etch mask or liftoff agent to transfer the pattern to the metasurface layer material.[821] (c) A pre-patterned layer can be used like a stencil shadow mask to transfer a pattern to a flexible substrate using a directional deposition method.[831] (d) The metasurface pattern can be generated using master and soft molds and a nano-imprint lithography process.[832] (e) The metasurface structure can be fabricated on a conventional rigid substrate, and then transferred to a flexible substrate using spin and cure and a sacrificial layer.[468] (f) Spin-coat and peel-off method can be used to transfer plasmonic metasurfaces fabricated on conventional rigid substrates to a flexible layer.[803] All images are reprinted (adapted) with permission from the respective Journal and copyright remains with the original publisher.

16 July 2024 09:29:41

© Author(s) 2024

and will not discuss these more conventional techniques and devices any further.

In Sec. XIV B, we will briefly discuss the design methods, fabrication techniques, and demonstrated applications of conformal and flexible metasurfaces, and in the third section we will layout some perspectives, opportunities, and challenges facing the development and scaling of this field moving forward.

B. Design, fabrication, and applications

1. Optical design

The optical design of conformal and flexible metasurfaces is for the most part similar to that of planar ones on rigid substrates as in most practically relevant cases the radii of curvature of the involved surfaces are significantly (i.e., thousands to million times) larger than the wavelength of the light. As such, most of the techniques used for designing planar metasurfaces can also be applied in the design of non-planar ones.[468] In the simplest methods, the nano-scatterers can mostly be treated independently from each other and their impact on the transmitted/reflected light can be estimated as such. Due to the large radius of curvature of the surfaces, locally we can assume that the nano-scatterers are arranged on a planar surface and therefore the scattering properties estimated from simulations of planar versions can be used. Even more complicated design and optimization methods, that are usually based on optimizations at grating period or Fresnel zone length scales instead of single scatterer ones, can still be applied to the conformal metasurfaces the same way.[828]

While mostly the same, there are still considerations and design practices that are specific to conformal and non-planar metasurfaces. The most important difference is the role of the optical function of the substrate on determining the desired scattering properties of the metasurface. In the case of wavefront shaping metasurfaces, the phase imparted by the metasurface added on top of the wavefront transmitted/reflected by the substrate should produce the desired total wavefront. To be more precise and reduce optical aberrations, even the role of flat substrates should be taken into account in the design of optical metasurfaces (e.g., in the case of a lens where the incoming beam passes through the metasurface first and substrate second, and is then refracted by the boundary between the substrate and the environment). Nevertheless, the impact of substrate form is much larger in the case of conformal metasurfaces, necessitating the utilization of ray-optics or physical optics to estimate the impact of the substrate in addition to the full-wave simulations needed to model the metasurface locally. For various types of non-planar surfaces like spherical and cylindrical ones the combined functionality of the substrate and metasurface (modeled as a thin phase surface) can already be simulated using commercial software packages like Zemax OpticStudio, allowing a concurrent optimization of the two.

Another factor to consider in the design of conformal metasurfaces is the impact of incidence and/or diffracted angle on the phase and polarization of transmitted/reflected light. Generally the scattering properties of the nano-scatterers are functions of incidence angle, and therefore it is important to take this into account for an improved design. For instance, in order to make a metasurface grating really polarization independent at non-zero incidence angles it might be necessary to make the nano-scatterers themselves asymmetric.[829,830] In the case of conformal metasurfaces, each part of the metasurface should be designed around the actual local nominal incidence angle that is generally different for separate areas.

For tunable metasurfaces based on flexible substrates, it is usually the local strain of the substrate and metasurface that is used to tune the function. In these devices, the changes in the metasurface lattice caused by this strain (or the actual length scale used in the local full-wave simulations) should be taken into account. Additionally, a solid mechanics simulation might be required to predict the local strain of the metasurface, especially if the stretching force is not completely symmetric. It is also worth noting here that our focus has been consciously on optical wavelengths, not microwave frequencies where generally the structural length scales of the non-planar surfaces are comparable to the wavelengths involved, and therefore some sort of full-wave simulation or more advanced approximation technique is required for the design.

2. Fabrication techniques

Generally we can separate the fabrication methods used to make conformal and flexible metasurfaces into three categories: (1) direct fabrication on the rigid non-planar substrate [Figs. 26(a) and 26(b)], (2) fabrication done on a flexible substrate and transferred to the non-planar surface if needed [Figs. 26(c) and 26(d)], and (3) fabrication done on a rigid flat substrate, transferred to a flexible medium and fitted to the non-planar substrate [Figs. 26(e) and 26(f)]. Methods 2 and 3 can be utilized to fabricate tunable metasurfaces based on flexible substrates too.

In the direct fabrication method, usually the metasurface pattern should be generated via electron beam lithography (with a depth of focus greater than the surface height variation or an adjustable beam focus system), holographic pattern generation, or nano-imprint lithography. The main challenge with this method is that the steps after the pattern generation are limited to conformal processes (i.e., methods like atomic layer deposition and wet etching, as opposed to directional methods like plasma enhanced chemical vapor deposition or deep reactive ion etching). This limits the material, shape, and aspect ratio of the nano-structures that can be fabricated by this method. For instance, this method has been used to fabricated thin plasmonic metasurfaces thorough liftoff, or low aspect-ratio low-index contrast gratings.[821]

Metasurface patterns can also be generated on the flexible substrate itself either via nano-imprint lithography,[465,833] spin/cast and cure, or through optically or electronically sensitive resins. The flexible substrate and whether it is compatible with high-temperature or high-vacuum processes could be a major limiting factor in this technique. Therefore, devices fabricated with this method have mostly been limited to plasmonic metasurfaces made through liftoff[831] or imprinted substrates back-filled with a high-index resin.[832] When nano-imprint or spin and cure patterning plus high-index filling method is used, this technique is well-suited for high volume and low-cost roll to roll manufacturing.

Finally, metasurfaces can be fabricated on regular planar rigid substrates (e.g., silicon or glass wafers), and then transfer printed to a flexible one like PDMS [Fig. 27(e)].[822] The main advantage of this method is its compatibility with most conventional planar nano-fabrication techniques including high temperature and high vacuum deposition and etching. Thus, it is relatively versatile and can be used

16 July 2024 09:29:41

© Author(s) 2024

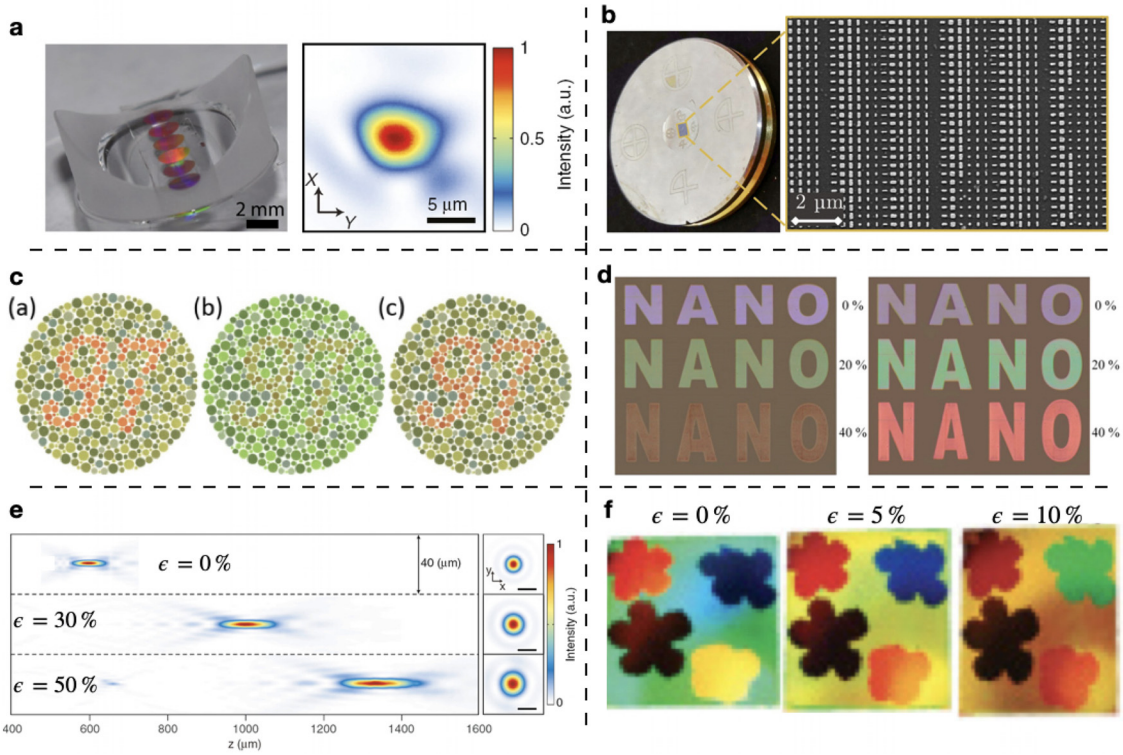

FIG. 27. Potential applications for flexible metasurfaces. (a) Image of a flexible metasurface conformed to a concave cylindrical lens, and the measured focal spot intensity of the combined optical system.[468] (b) A free-form metasurface optical element with wavefront shaping and grating deflection ability combined, fabricated on a non-planar substrate.[467] Metasurfaces designed and fabricated with the same mindset could be integrated on eyepieces of headmounted displays. (c) Simulated performance of a metasurface spectral filter proposed as a mitigating solution for deuteranomaly. Original image (left), simulated image without correction (middle), and simulated image after correction (right) are shown.[803] (d) A stretchable metasurface with tunable reflection spectrum showing full spectral tuning from blue to red for both linear polarizations of light.[804] (e) Focal length tuning using a stretchable tunable metasurface singlet. The change in focal length is proportional to strain squared.[822] (f) A tunable grating with enhanced first order diffraction efficiency used to achieve color tuning. As the grating period changes when stretched, the appearing color varies with it.[826] All images are reprinted (adapted) with permission from the respective Journal and copyright remains with the original publisher.

to fabricate and transfer most types of metasurfaces. The transfer step to the flexible substrate can be done through simple transfer printing in cases where adhesion to the flexible substrate can be higher than the rigid one, or using a sacrificial layer that can be dissolved away from underneath the metasurface and release the metasurface inside the flexible substrate.[822] The main disadvantage with this method is the complication and number of process steps involved that could increase the process cost and lower the total yield.

3. Applications

In a coarse division, we can categorize the applications of conformal metasurfaces to modify/improve performance of a non-planar object, or add a totally new functionality to an optical element. One example of the first category was wavefront shaping plasmonic reflective metasurfaces used to compensate for phase distortions caused by height variations on a reflective surface [Fig. 25(a)].[802] While called cloaking, the phase compensation only works over a narrow band and the direct fabrication method utilized limits the application to small surfaces with bumps in the few micrometers, also requiring very precise alignment between the non-planar surface and the metasurface.

Dielectric conformal metasurfaces have been used to alter the optical function of conventional refractive optical elements [Fig. 27(a)].[822] The phase profile of the metasurfaces were chosen to change the function of diverging and converging cylindrical lenses to converging spherical ones. In practice, this method can be useful when there is need for optical windows through transparent surfaces whose shapes are dictated by factors other than optics. Similar to other metasurfaces and diffractive optics wavefront shaping elements, chromatic aberrations limit the bandwidth of the light that can be used. Another main challenge with this line of application is that it requires high accuracy alignment between the metasurface and the target surface, which doesn't necessarily have suitable alignment marks, or might require deformations in the flexible substrate that cause non-uniform strain throughout.

As mentioned in the first section, adding gratings and diffractive optical elements to non-planar surfaces has had a long line of applications, for instance in spectroscopes that use it to reduce aberrations and improve resolution.[808] More recently, the use of metasurfaces as the combining element on near eye display systems has been proposed where the metasurface would be integrated onto the visor or eyepiece element in lieu of a holographic optical element and work either as a pure grating or a grating with wavefront

16 July 2024 09:29:41

© Author(s) 2024

shaping [Fig. 27(b)].[467] This is an interesting line of applications, yet cost, scalability, and worse see-through compared with volume holographic elements are challenges (among others) that should be overcome for it to become promising.

Apart from wavefront shaping, metasurfaces have shown other functionalities like spectral filtering.[500] Similarly, conformal metasurfaces integrated on contact lenses have been used as spectral filters to improve color separation for colorblind users [Figs. 27(c) and 27(d)].[803] When the substrate is stretchable, the transmission/reflection spectra can be tuned with stretching as well, and therefore flexible metasurfaces can be used as tunable color filters.

Stretching has also been used to tune grating pitch and deflection angle to steer beams[822] or generate variable color structures [Figs. 27(d) and 27(f)][826] or tune lenses and make lenses with tunable optical power [Fig 27(e)].[822] In both cases, the tunable range is significantly larger than what is possible with other methods like liquid crystal integration or electro-optic modulation, but the tuning speed is very limited, the tuning mechanism is relatively large, and the long term reliability and number of cycles are very limited compared to those alternative methods. Due to these limitations, it might be more appropriate to call these devices *reconfigurable* rather than *tunable*.

C. Challenges, opportunities, and future perspectives

Flexible and conformal metasurfaces have some similarities with flexible electronics (mostly in fabrication processes and materials), and therefore the vast body of knowledge developed around flexible electronics can be (and has been) utilized here. Nevertheless, there are both fundamental and technical differences between flexible metasurfaces and flexible electronics (or even integrated photonics). First, functionality and form are tightly correlated in optics, and as such the shape of the structure and the conforming metasurface should remain controlled and known during operation, unlike flexible electronics where the capability to operate under various deformations is usually a key characteristics. One exception where flexible metasurfaces might be fine with deformations is the case of arrays of small elements (e.g., a micro-lens array). In such cases, it is possible that the metasurface remains functional under deformation as long as the deformation in each element remains small. One potential application could be for a micro-lens array integrated with a flexible OLED panel.[403,834,835]

On the technical side, the target substrate of a conformal metasurface should be well-known and well characterized, and the conforming metasurface should be aligned with it to the regular opto-mechanical alignment accuracy of the system. In addition, if the conformal metasurface goes through a planar deformation or local stretching during the alignment and fitting steps (e.g., due to a finite Gaussian curvature of the target surface), these deformations need to be well-controlled and understood, and their impacts need to be considered in the design and fabrication steps.

Tunable flexible metasurfaces can be very light and compact by themselves (e.g., they can be as thin as a few tens of micrometers). However, the mechanical system required to stretch the metasurface can be relatively large and heavy as the stretch generally should be very uniform and well-controlled. This necessitates close attention to the design and implementation of the mechanical tunable system for the benefits of low weight and volume to be realized. Reliability and cycle count are other important factors that need improvement, requiring the exploration and use of better flexible substrates.

Finally, conformal and tunable metasurfaces have a chromatic dispersion similar to other diffractive optical elements that could severely limit their useful operation bandwidth, unless the dispersion is useful for the application (like in spectrometers), or could be compensated for (e.g., in diffractive-refractive combinations, or augmented reality waveguides).

A major opportunity for flexible substrates is in roll-to-roll fabrication of metasurfaces. Whether the flexibility and conforming ability of the metasurface is critical for an application or not, nano-imprint or cast-and-cure methods of fabricating metasurfaces can provide significant cost reduction over other methods that rely on lithography and etch.

With the growing interest in wearable and head mounted displays in recent years (and potentially over the coming decade), metasurfaces in general, and flexible metasurfaces in particular, face a great opportunity. With stringent requirements on weight, volume, and power consumption, while demanding high performance optics for various parts of the system like cameras, eye tracking, and the display system all in a fashionable form factor, conformal metasurfaces pose many appealing properties that could make them suitable for sensor optics, holographic elements on visors, or diffractive optics on waveguides.

In addition to wearable displays, various types of compact consumer electronics (e.g., smart watches, wireless headphones, etc.),

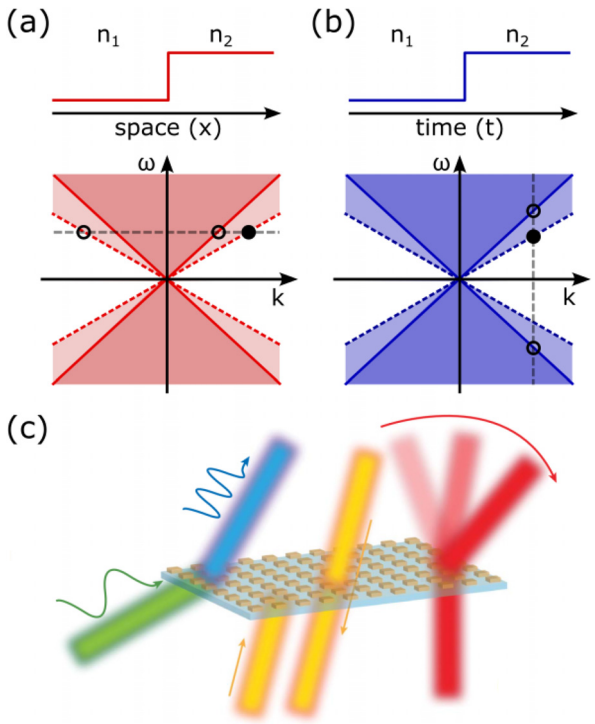

FIG. 28. Scattering of light traveling in the x direction at a (a) spatial and (b) temporal interface can be illustrated with dispersion diagrams, where the full and dashed lines denote the dispersion cones for the two media. (c) An illustration of a device that combines advanced structuring of both spatial and temporal inhomogeneities to provide dynamic control over the momentum and frequency of scattered light, adapted from Ref. 48. Copyright remains with the original publisher.

16 July 2024 09:29:41

© Author(s) 2024

smart appliances, medical imaging systems, and many other smart and electronic systems are becoming ubiquitous with an ever increasing push for integrating more sensors and machine vision cameras. If the challenges facing flexible metasurfaces are overcome or circumvented for the relevant applications, these areas could become significant growth opportunities for flexible metasurfaces, in particular if low-cost and scalable fabrication pipelines are developed.

Optical metasurfaces, in general, and flexible metasurfaces, in particular, have gone through a major cycle of attention and research growth in the past decade. We believe over the coming years there are many opportunities for them to enable consumer level applications, but they have to overcome the multiple barriers and challenges outlined above.

XV. TIME MODULATED METASURFACES

A. C. Harwood, S. Vezzoli, and R. Sapienza

a.harwood22@imperial.ac.uk

A. Introduction

Traditional, bulk optical components are ubiquitous in modern day life, providing a means to transform light into an essential technological tool through the use of engineered spatial inhomogeneities. This framework for light manipulation is underpinned by Noether's theorem, which dictates that light scattered at a spatial interface between two media must conserve energy, and thus frequency, as the system is invariant in time [Fig. 28(a)]. Conversely, a system exhibiting homogeneous and instantaneous changes in its optical properties scatters light in time through non-conservative processes. This temporal scattering modifies the frequency of light while maintaining the conservation of its momentum [Fig. 21(b)]. These novel processes of light scattering are known as time reflection and refraction, the temporal counterparts to the familiar, spatial reflection and refraction derived from Fermat's principle. The parallels between scattering in space and time can be readily visualized by using a phase diagram Figs. 21(a) and 21(b). As a consequence, the arrangement of temporal inhomogeneities in time-varying media serves as a mechanism through which a device may effectively manipulate the spectral content of light.[836,837]

Initial studies into time-varying phenomena were undertaken in the field of plasma physics,[838] as well as systems of mechanical waves[839] and low frequency electromagnetic waves.[840,841] These systems facilitated high-efficiency time-varying experiments, as the desired high-contrast modulations could be easily manipulated at frequencies equal to that of the propagating waves using convenient electronic or mechanical driving mechanisms. On the other hand, systems that demonstrate high-contrast, sub-period modulations in the optical regime rely upon Kerr-like processes, which are exclusively mediated by powerful femtosecond lasers. Consequently, the exploration of time-varying photonics has been dependent upon the development of ultrafast laser science and compatible material platforms for nonlinear optics. Since its conception this decade, time-varying photonics has been studied across a broad range of systems, such as 2D materials,[842] ultracold atoms,[843] and quantum wells.[844] However, the discussion herein will concentrate on systems that have demonstrated the most profound capabilities and potential—time-varying optical metasurfaces.

Time-varying optical metasurfaces emerge through temporal modulations of the optical properties of a sub-wavelength medium, forming an interface characterized by time-varying reflectivity and transmissivity. The scattering of light from the temporal inhomogeneities of such an interface inherently deviates from the temporally switched medium illustrated in Fig. 1(b), where propagation may lead to complications from effects such as self-broadening.[836] The control obtained with a temporally modulated interface mimics the approach employed by spatial metasurfaces, which leverage sub-wavelength structuring of high-contrast inhomogeneities to efficiently manipulate the momentum of scattered light. Likewise, high efficiency time-varying metasurfaces require a mechanism which acts on sub-period timescales and provides a large modulation contrast between the time-varying structure and its unmodulated surroundings.[845] Furthermore, the framework of temporally structured interfaces lends itself to the development of space-time structured devices that combine the matured science of spatial metasurfaces with complex temporal modulations. This envisioned device, a space-time metasurface [XXI(c)], would utilize engineered spatial and temporal inhomogeneities to provide simultaneous and dynamic control of the momentum and spectral content of scattered light from a nanoscale component. This versatile device holds promise for a wide range of applications, spanning from temporal aiming and antireflection coatings to the exploration of photonic time crystals and the development of magnet-free nonreciprocal devices.[50,846]

To explore the extensive and varied research avenues concerning time-varying optical metasurfaces, the current state-of-the-art for temporally engineered metasurfaces will first be reviewed in Sec. XV B. This section will discuss the prevalent experimental systems that have illustrated the great potential, alongside challenges that must be resolved to be able to realize more complex temporal structures. In extension to this paradigm, Secs. XV C and XV D will proceed to investigate the use of structuring in space and time simultaneously to provide enhanced time-varying interactions and 4D control over scattered light, via spatially static and varying modulations. To conclude, the current state of the field will be summarized, alongside the prevailing obstacles that will determine the future of time-varying optical metasurfaces.

B. Time-varying metasurfaces

To identify a suitable material for a time-varying optical metasurface, one must first examine electronic state transitions that may give rise to large changes in permittivity and occur over sub-picosecond timescales. A familiar example of such a mechanism is the virtual-state transition of electrons induced by nonlinear polarizations, giving rise to oscillating regions of permittivity. Although this modulation process meets the ideal requirement of being ultrafast, the change in permittivity induced by such processes is conventionally minimal. Alternatively, one may consider the modulation of a material's refractive index via real-state transitions of electrons, for example the excitation, and subsequent relaxation of electrons via photoexcitation. These real state transitions are typically linked to substantial changes in permittivity; however, they predominantly unfold over time periods exceeding picoseconds.[847] Consequently, traditional nonlinear materials do not provide an efficient platform for time-varying photonics. However, this paradigm is notably disrupted by transparent conductive oxides, a variety of epsilon-near-zero materials. Although constricted to the

16 July 2024 09:29:41

© Author(s) 2024

region about their near-infrared epsilon-near-zero wavelengths, indium tin oxide and aluminum zinc oxide in particular, have been used to demonstrate vastly enhanced, non-perturbative nonlinearities,[848] as well as interband and intraband transitions of electrons in sub-picosecond timescales.[184,185,849] It is this latter characteristic, arising from their non-parabolic band structure, which distinguishes them from most semiconductors and dielectrics, where real-state transitions occur over nanosecond periods.[850]

In wake of their discovery, sub-wavelength films of transparent conductive oxides have facilitated the fundamental explorations of time-varying photonics. By pumping these films with high intensity, ultrafast pulses of light, it is possible to inhibit ultrafast changes in permittivity via both the real and virtual electronic transitions. Through the utilization of the fast, virtual transitions, these systems have been used to demonstrate negative refraction[851] and time reflection,[852] as predicted a decade earlier.[853] Congruently, the ultrafast, real-state transitions have enabled investigations into temporal interfaces, characterized by unity changes in refractive index with ultrafast rise and decay dynamics, see Fig. 21(a).[854] Temporal scattering from these temporal interfaces has been studied extensively via pump-probe experiments, demonstrating a novel method of frequency control via the ultrafast dynamics of the transition's rise and decay time, leading to red and blue shifted light respectively.[855] Moreover, these phenomena not only provide innovative approaches for nanophotonic frequency control but also serve as diagnostic tools for inferring the temporal dynamics of the material's ultrafast response.[855] However, the spectral control obtained from these simple responses is limited. Thus, the natural evolution of time-modulated metasurfaces involves exploring more complex temporal inhomogeneities. In the case of the aforementioned system, this would materialize as designing the pump pulse's temporal profile. Through the pursuit of this avenue, it would be possible to investigate the eigenpulses of a time-varying system—temporal modulations related to the Fresnel coefficients for the dispersive, time-varying interface in question, which leaves scattered light spectrally unchanged.[856] Conversely, through careful design of the temporal profile of the modulation, one would also be able to design the spectral profile of the scattered light, offering applications across the fields of optical switching and computing.[857] Moreover, promising theoretical investigations into systems that exhibit isotropic-to-anisotropic switching have motivated the concurrent pursuit of compatible media capable of hosting unique temporal phenomena.[858–860]

Another direction of research regarding increased complexity of temporal structuring, is the generation of periodic modulations. A first step toward this goal has been the investigation of double slit time diffraction a study which utilized two temporally adjacent modulation responses to obtain the characteristic diffraction response in the spectra of scattered light [Fig. 29(b)].[861] A challenging extension to this framework of patterning numerous responses in time is the generation of a photonic time crystal. By mimicking the configuration of photonic space crystals in the time domain, periodic temporal modulations, generated with a frequency comparable or greater than the probe frequency, create bandgaps in momentum. The relative width of these bandgaps is dependent on the contrast of the temporal interfaces induced. Light propagating within these momentum bandgaps does so with an energy that exponentially grows in time, comprising a non-resonant amplification system.[114,862] Additionally, periodic temporal modulations have been proposed as mechanisms for realizing surface-wave excitation in the absence of any surface structure,[863] advanced absorption systems that surpass their static counterparts[850] and the temporal analogue to Bragg gratings.[864] In the case of transparent conductive oxides, the realization of such temporal structures is resisted by the problem of heat accumulation and dissipation due to high intensity optical pumping. Thus, the discussion as to whether or not transparent conductive oxides may offer a platform to explore photonic time crystals is an open one that hinges on the limits of the materials and the demand for power densities on the order of TWs/cm^2.[845] As a result, the realization of a periodic modulation may demand a sacrifice in magnitude of the momentum bandgap, or duration of the periodic temporal modulation. More clarity regarding the future of photonic time crystals generated with transparent conductive oxides will come from comprehensively theoretical model of these materials, including electronic and lattice temperature and their effect on the optical properties.[865] As a result, the realization of a periodic modulation may demand a sacrifice in magnitude of the momentum bandgap, or duration of the periodic temporal modulation, possibly led by use of the ultrafast virtual transitions.[866] Moreover, the observation of momentum bandgap characteristics, induced by $\chi^{(3)}$ nonlinear phenomena may also be marred by the presence of undesirable nonlinear processes, a concern that has begun discourse into the use of $\chi^{(2)}$ processes[845] and investigations into new media.

C. Time-modulation in spatial metasurfaces

As detailed throughout topics Secs. III and X in this roadmap, metasurfaces are great resonance-hosting systems capable of increasing the efficiency of nonlinear interactions, via increased field localization, offering control over the directionality and propagation of emitted light. The increased localization of electric field and thus energy has allowed for time-varying systems that enhance effects engineered by spatial structures. For example, in semiconductor-based metasurfaces, temporal boundaries have been studied as tools for the enhancement and control of nonlinear spectral effects induced by resonance-hosting structures.[867–872] Notably, the utilization of gold nanoantennas has been central to numerous studies that observed reduced intensity requirements for significant frequency shifts based on temporal refraction by localizing energy in a transparent conductive oxide structure.[851,876] In these spatially structured devices, resonances are leveraged to provide increased modulation amplitude at the expense of an increased interaction time. Hence, while these structures significantly enhance nonlinear efficiencies, temporal phenomena are constrained due to increased modulation timescales and the diminished optical damage threshold.[875] Yet despite the presence of these deleterious characteristics, this paradigm offers a route to realizing low-power technological applications of these phenomena. In addition, the 1D temporal modulation of a resonant structure that hosts an effective lattice of states, constructed via the structure's supported modes, provides a method for accessing synthetic frequency dimensions. By using a time-varying modulation with a configurable amplitude, modulation frequency or phase, one can utilize the temporal domain as a method to navigate the system's synthetic dimensions.[876] The realization of these synthetic dimensions promises to uncover a wealth of higher-dimensional topological effects, as well as a potential route toward N dimensional control, alongside the benefits of conventional time-varying.[836,876]

16 July 2024 09:29:41

© Author(s) 2024

Alongside the amplification of nonlinear processes, static structures offer systems from which the momentum of scattered light may be configured. This framework, embodied by the pioneering metasurface work of the early 2000s,[877,878] in conjunction with temporal modulations, enables frequency and momentum control over scattered light. By temporally modulating a gold gradient metasurface upon a transparent conductive oxide substrate, pioneering work by Karimi *et al.*[879] demonstrated simultaneous, dynamic control over the spectral content of light that has been diffracted [Fig. 21(c)]. Moreover, the process of frequency translation via temporal refraction leads to beam steering, via the conservation of the forward momentum, and thus dynamic control over the angle of the generated diffraction orders. It can be envisioned that this framework offers a logical extension to the impressive metalens work of the past decade,[880] providing an all-optical method of fine-tuning the focal distance through beam steering or offering simultaneous spectral control. At present, these systems for 4D optical control offer potential applications across the field of dynamic metasurface designed for sensing and beam steering, however, they also present a stepping stone toward unlocking the potential of simultaneous frequency and momentum control.[846]

D. Space-time metasurfaces

In the previous section, spatially static, yet temporally varying, optical metasurfaces were initially discussed as the most mature method of structuring a device in space and time. Herein, *space-time* metasurfaces are differentiated by their use of a modulation mechanism that is configured in both space and time in order to exhibit control over the momentum and frequency of scattered light. In the context of photocarrier excitation in transparent conductive oxides, the modulation can be controlled in space and time by manipulating the intensity and shape of the pump beam in both domains. This premise relies heavily on the profound advancements made throughout digital micromirror devices and spatial light modulators and has been effectively applied to the fields of ultrafast beam steering,[88] electron optics,[881] reconfigurable metasurfaces,[882] and the generation of reconfigurable integrated photonic circuits.[883] Following in this vein, pursuit of such a modulation strategy would reveal all-optical, reconfigurable metasurfaces capable of also harnessing temporal frequency generation.[50,884] In 2023, Fan *et al.* demonstrated ultrafast wavefront control via the all-optical structuring of a thin film's refractive index in both space and time [Fig. 21(d)].[885] This work used the induced space-time modulation to provide a spatially dependent response of temporal refraction, resulting in the focusing of probe light due to the subsequent beam steering. In extension to this work, one can easily envisage simultaneous control over spatial diffraction from configurable diffraction-limited transient structures alongside this time-varying control. This paradigm of simultaneous structuring in space and time for ultrafast control of light lends itself straight-forwardly to 4D optics but also the advancement of optical holography,[886] analogue optical computation,[46] and neural networks.[887] However, the generation of space-time modulations using photocarrier excitation in transparent conductive oxides will encounter the constraint of the material's high intensity requirements for high contrast modulations (≈ 100 GW/cm^2 for 100 fs pulses[184]) limiting their complexity and size. This represents an avenue that may greatly benefit from the use of efficiency-increasing gold nanoantennas in order to not only reduce power requirements but also as a method of localizing modulations to non-diffraction-limited regions. Thus, in

16 July 2024 09:29:41

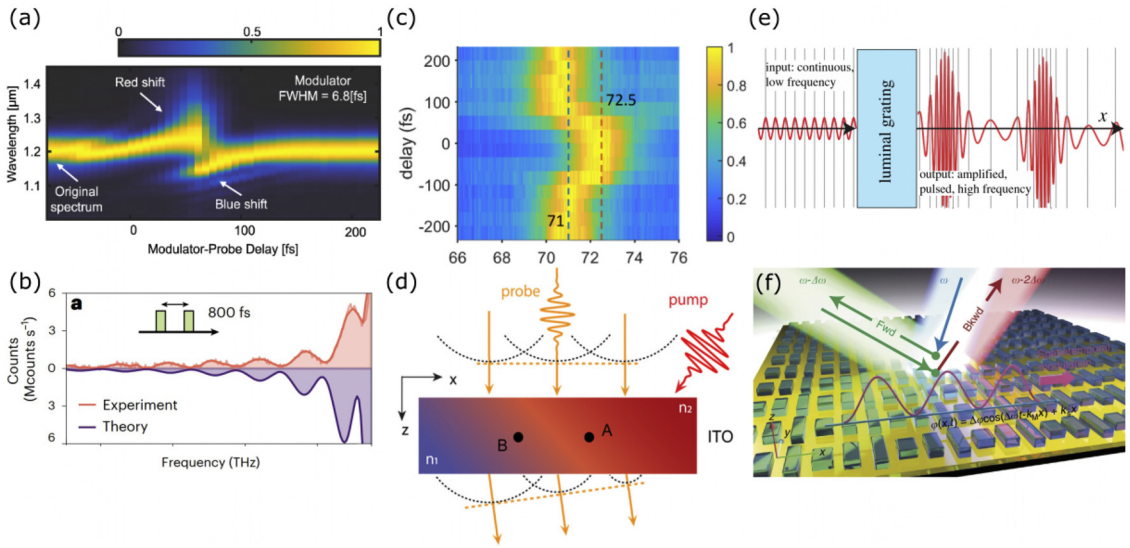

FIG. 29. (a) A spectrogram of negative and positive frequency translation via sub-cycle pumping of ITO.[854] (b) Full experimental and theoretical interferograms for diffracted light from a temporal double slit as a function of slit separation and frequency.[861] (c) Spectrogram showing the ultrafast beam steering of light diffracted by a temporally modulated static gradient metasurface.[879] (d) Schematic displaying wavefront manipulation from a material structured in space and time.[885] (e) A schematic illustrating the theoretical demonstration of amplification and compression of light incident upon a luminal grating.[888] (f) An illustration of non-reciprocal beam steering generated by a space-time modulated metasurface based upon the illumination of a static, dielectric metasurface.[889] Figures adapted from Refs. 854, 861, 879, 885, 888, and 889 and copyright remains with the respective publishers.

© Author(s) 2024

closing, achieving simultaneous spatial and temporal structuring of inhomogeneities is a significant milestone for space-time metasurfaces, but unlocking their full potential requires the development of new and improved time-varying systems.

The exploration of traveling modulations of permittivity within dielectric media signifies this report's concluding frontier in the investigation of optical time-varying metasurfaces, presenting experimental challenges beyond the previously discussed space-time metasurfaces. Systems which host traveling regions of modulated permittivity are generally referred to spatiotemporal metasurfaces. These traveling regions can be defined by a permittivity (and corresponding permeability) that is described by $\delta\varepsilon(x,t) = \delta\varepsilon(gx - \Omega t)$, where g and Ω are the spatial and temporal reciprocal lattice vectors. Spatiotemporal modulations have promised to result in a broad variety of phenomena and are thus defined by the modulation's speed of travel $\nu_m = \Omega/g$. By consequence of this traveling modulation, physically realized through the conjunction of a modulation and the material response, probing light will observe synthetic motion of the modulation. This phenomenon has been explored as a method to exert control over the spectrum of scattered light via an artificial Doppler shift,[890] capable of compensating for the Doppler shift of moving objects.[891] Furthermore, slab structures that host a traveling wave modulation offer unique applications throughout beam splitting[892] and recombination.[893] Moreover, there has been broad research into the phenomena demonstrated by such spatiotemporal synthetic motion, including Fresnel drag,[894] Čerenkov radiation,[895] and Hawking Radiation.[896] Discussions into the demonstration of these phenomena have remarked the viability in low frequency regimes, as well as potentially the terahertz regime in graphene, however, their demonstration in the optical regime is closely linked to the discussion of hosting period modulations in time alone (Sec. XV B).

In parallel, linear or rotational traveling modulations have been investigated throughout numerous wave domains as novel systems for leveraging non-reciprocal responses. Notably, the inherently non-reciprocity of luminal synthetic motion represents a platform capable of the amplification and compression of incident light [Fig. 21(e)].[888] Moreover, such mechanisms have been heralded as a method for efficiently breaking the constraints of a system's reciprocal symmetry and thus offering a route toward compact, non-reciprocal devices without need for magnetic bias, see Fig. 21.[889,897] Consequently, a core motivation of research in this direction of spatiotemporal modulations is the pursuit of phenomena that do not rely upon high modulation frequencies that are difficult to realize in physical systems.[898] Moreover, could spatiotemporal modulations substitute for modulations in time alone, resulting in more feasible realizations of the temporal woods analogy or Bragg grating? Unlike periodic temporal modulations, the material limitations imposed upon the exploration of spatiotemporal modulations have not been theoretically characterized—leaving the door open to a rich experimental future.

E. Conclusion

Research into time-varying systems has reshaped the way we perceive and control the propagation of waves. The last decade has brought time-varying physics to the optical regime with seminal studies being performed upon the framework of photocarrier excitation in transparent conductive oxides. As discussed herein, the multitude of pathways to enhance the complexity of current straightforward temporal and spatial modulations unveils a plethora of exciting research avenues in the field. Modulations in time alone provide a theoretical research destination of prophesied photonic time crystals, while complex space-time modulations unlock the potential of 4D optical components and synthetic motion. However, most advanced discussions and explorations have predominantly existed within the realm of theoretical and computational physics. In order for a majority of these phenomena to be fully realized, the restrictions of the current systems must be overcome. It is possible that many applications may be realized, in a less efficient form, via a compromise with regard to the desired modulation strength or frequency. However, in order to observe many advanced temporal or spatiotemporal phenomena, new systems or mechanisms will be required. These considerations have begun to occupy an increasing presence in modern discussions of time-varying optical experiments, applying pressure on this direction of research. Nevertheless, the future of the field still promises to offer great potential to light-based technologies and studies of novel physics.

XVI. DISORDERED OPTICAL METASURFACES: PHYSICS, THEORY AND DESIGN

Philippe Lalanne,* Alexandre Dmitriev, Carsten Rockstuhl, Alexander Sprafke, and Kevin Vynck

*philippe.lalanne@institutoptique.fr

The use of coherent wave phenomena to enhance device performance is a cornerstone of modern optics. In juxtaposition to (locally) periodic metasurfaces, their disordered counterparts exhibit an interplay of destructive and constructive interferences occurring at the same spatial and spectral frequencies. This attribute provides disorder with many degrees of freedom. Recognizing and comprehending their utility across diverse applications is invaluable. Hereafter, we provide a concise overview of the cutting-edge developments and offer insights into the forthcoming research in this dynamic field.

A. Introduction

Disorder has often been viewed as a constraining element in nanophotonics, which might explain the limited coverage of the subject of disordered metasurfaces in the existing literature.[524,899] Nevertheless, there exist plenty of reasons to delve into this area. Let us highlight just a few. The presence of disorder is ubiquitous across manifold complex structures. Leveraging disordered metasurfaces, as opposed to their meticulously ordered counterparts, holds promise in realizing extensive, cost-effective devices. It also paves the way to a wealth of specialized applications, such as anti-reflection coatings,[900] augmented absorption,[901] surface-enhanced Raman scattering,[902] alongside contemporary applications to be discussed below.

This article aims to survey the current state of research and offer a forward-looking perspective on the topic. We highlight a few promising future applications and anticipate forthcoming advancements in design and fabrication.

B. State-of-the-art

The general problem of light scattering by disordered metasurfaces made of resonant nano-objects (a.k.a. meta-atoms) is very complicated due to multiscale effects, namely the multipolar

16 July 2024 09:29:41

© Author(s) 2024

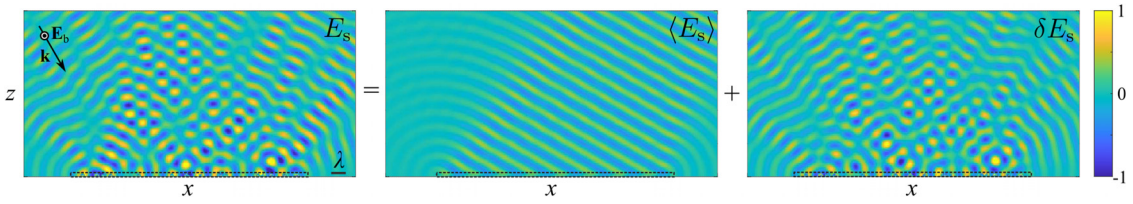

FIG. 30. Illustration of the average (coherent) and fluctuating (incoherent) components of the scattered field [Eq. (4)] with fully vectorial simulations for a finite-size disordered metasurface composed of identical Si nanocylinders in air. The incident (background) field $\mathbf{E}_b$ is a plane wave ($\lambda = 440$ nm) polarized along the *y*-direction. It is incident from the top with an angle of 30° with respect to the surface normal. The rods are parallel to the *y*-axis and are placed using a random sequential addition algorithm with a non-overlapping condition. The 2D simulations are made for assemblies of 15 infinitely-long nanocylinders (140 nm diameter, $n_{\mathrm{Si@440nm}} = 4.793 + 0.109i$), resulting in a side length of 7.0 μm ($\approx 16\lambda$) at a surface coverage of 30%. The *y*-component of the scattered field (component parallel to the cylinder *y*-axis), E_s, is normalized to the amplitude of the background field $|E_b|$.

resonances of the individual particles, their interaction with the substrate, and their mutual interaction.[903,904] In this section, we start by outlining some fundamental concepts on coherent vs incoherent scattering. We then familiarize the reader with computational tools and approximate models that predict the scattering properties of disordered metasurfaces, and finally examine recent advances in fabrication techniques.

1. Diffuse (incoherent) vs. specular (coherent) light

Within the context of wave scattering by rough surfaces—a long-standing topic with many applications[905–907]—, the distinction between diffuse (incoherent) light and specular (coherent) light emerges as a pivotal consideration. These two components have different physical origins, as we will see below, and have significant implications for optical effects—for instance, their relative weight play a decisive role in determining the glossiness or matteness of a surface.

This distinction can be understood from the statistical properties of the scattered light. In this framework, one considers separately the average and fluctuating values of physical parameters, with the averages computed among a large statistical ensemble of independent realizations. The quantities of main interest in the present case are electromagnetic field characteristics, including the field itself, its intensity or root mean square, along with auxiliary quantities such as the Poynting vector and the energy density that a wave carries.

Formally, the electric field $\mathbf{E}_s$ scattered by a disordered system can be expressed as the sum of its ensemble average (the specular light), calculated among many disorder realizations, and a fluctuating term (the diffuse light) that varies from configuration to configuration,

$$\mathbf{E}_s = \langle \mathbf{E}_s \rangle + \delta\mathbf{E}_s, \tag{4}$$

with $\langle \delta\mathbf{E}_s \rangle = 0$.

Figure 30 illustrates this decomposition using fully vectorial simulations conducted on a finite metasurface composed of parallel infinitely long silicon nanocylinders in air. The metasurface is illuminated at a 30° angle of incidence by a plane wave polarized parallel to the cylinder *y*-axis. In the rightmost panel, the fluctuating field $\delta\mathbf{E}_s$ showcases a complex pattern known as speckle,[908] which arises from the intricate interplay of near-field interactions among many monochromatic waves scattered by multiple scatterers. In contrast, the central panel presents the average field $\langle \mathbf{E}_s \rangle$ that readily takes the form of a directional reflected light beam indicated by black arrows. This average field describes the diffracted light from a homogenized metasurface characterized by effective parameters that vary non-uniformly in both the *x* and *z* directions due to boundary effects.

Given $\langle \delta\mathbf{E}_s \rangle = 0$, we can readily demonstrate that the averaged intensity $\langle |\mathbf{E}_s|^2 \rangle$ of the light scattered by the metasurface can be decomposed into two components,

$$\langle |\mathbf{E}_s|^2 \rangle = |\langle \mathbf{E}_s \rangle|^2 + \langle |\delta\mathbf{E}_s|^2 \rangle, \tag{5}$$

in which we identify the squared norm of the average field, which corresponds to the specular intensity (first term), and the average of the squared norm of the fluctuating field, i.e., the diffuse intensity or the averaged speckle intensity (second term).

The properties of statistically translationally invariant (i.e., infinite) disordered metasurfaces are fully determined by the Bidirectional Scattering Distribution Function (BSDF), a radiometric quantity introduced in the 1960s, which describes how surfaces scatter light for all possible plane wave illuminations. Formally, the BSDF relates an incoming irradiance E_i (in W m^{-2}) to a scattered radiance L_s (in W m^{-2} sr^{-1}),

$$\mathrm{BSDF}(\hat{\mathbf{k}}_s, \hat{\mathbf{e}}_s, \hat{\mathbf{k}}_i, \hat{\mathbf{e}}_i, \omega) = \frac{\mathrm{d}L_s(\hat{\mathbf{k}}_s, \hat{\mathbf{e}}_s, \omega)}{\mathrm{d}E_i(\hat{\mathbf{k}}_i, \hat{\mathbf{e}}_i, \omega)}, \tag{6}$$

where ω is the frequency, $\hat{\mathbf{k}}_i$ and $\hat{\mathbf{k}}_s$ are the (unit) wavevectors of the incident and scattered plane waves, and $\hat{\mathbf{e}}_i$ and $\hat{\mathbf{e}}_s$ are the polarization (unit) vectors of those waves. Following the previous considerations, the BSDF can then be conveniently decomposed into two terms, $\mathrm{BSDF} = \mathrm{BSDF}_{\mathrm{spec}} + \mathrm{BSDF}_{\mathrm{diff}}$, the specular and diffuse components.

2. Full-wave analysis

Predicting the BSDF of statistically translationally invariant metasurfaces featuring resonant particles on layered substrates stands as an outstanding challenge.[909,910] Two complementary strategies are employed. The first approach involves solving Maxwell equations with utmost precision, while the second approach (Sec. XVI B 3) relies on approximate models.

In the former approach, the strategy is twofold: first, solving Maxwell equations for larger and larger metasurfaces, and second, inferring the BSDF of infinitely large metasurfaces by extrapolation. In contrast to traditional general-purpose solvers such as the finite-difference time-domain method, disordered metasurfaces benefit significantly from specialized numerical techniques. The latter harness

16 July 2024 09:29:41

© Author(s) 2024

the unique morphologies of these structures and enhance their efficiency by precomputing light scattering by the individual scatterers that compose the metasurface.

In the widely used T-matrix method, the field outside the scatterer is expanded using spherical vectorial wave harmonics and a T-matrix is utilized to describe how each scatterer transforms incident into scattered multipolar fields. The method has been extensively explored over decades[911] and is now available through multiple open-source implementations.[911,912] Alternative methods account for multiple scattering using vectorial Green functions and treat scatterers as ensembles of equivalent electric and magnetic surface currents,[913,914] or employ numerical non-local dipoles[915] obtained by numerically solving an inverse scattering problem. A detailed comparative analysis of these methods strengths and limitations is beyond this roadmap's scope and is deferred to a comprehensive future review.[916]

Two approaches exist for the extrapolation step. In the field stitching approach, Maxwell equations are solved for numerous small square subdomains, each corresponding to an independent realization. These subdomains are then stitched together to artificially expand the metasurface area, with field discontinuities smoothed at subdomain boundaries to mitigate artifacts.[917] In the supercell approach, identical subdomains are "stitched" with pseudo-periodic boundary conditions. As the artificial period increases, both approaches generally yield stable numerical outcomes for specular and diffuse light.[918,919] Although finite-size computations unavoidably introduce boundary effects,[919] the observed relative errors are often encouragingly below 10%.

However, the two approaches necessitate numerous computations to assess statistical convergence, and they offer limited physical insights. The challenge of effectively simulating infinite metasurfaces remains, highlighting the need for approximate models.

3. Approximate models

There are a few available models for predicting the BSDF of disordered metasurfaces. Similar to research conducted on metamaterials, advanced studies have primarily focused on homogenization, i.e., on the specular contribution to the BSDF.[883,884,922,923] To our knowledge, there has been no research on diffuse light, despite its critical significance in our context. An exception to this is the independent scattering approximation (ISA), which assumes that each constituent particle scatters light independently, thus neglecting multiple scattering effects. Although the ISA may appear simplistic to readers, it holds substantial value. This approximation plays a significant role in investigations on the physics of waves in complex media. It also largely facilitates a transparent interpretation that is beneficial during the initial design phases and is amenable to more accurate models relying on mean fields.[916] For a monolayer comprising N identical particles randomly positioned at coordinates $\mathbf{r}_p = [x_p, y_p, z_p = 0]$, $p = 1, \ldots, N$, the ISA simply leads to

$$\langle I_s \rangle(\hat{\mathbf{k}}_s, \hat{\mathbf{e}}_s, \hat{\mathbf{k}}_i, \hat{\mathbf{e}}_i, \omega) = I_0 N \frac{\mathrm{d}\sigma_s}{\mathrm{d}\Omega}(\hat{\mathbf{k}}_s, \hat{\mathbf{e}}_s, \hat{\mathbf{k}}_i, \hat{\mathbf{e}}_i, \omega) S(\mathbf{q}), \quad (7)$$

for the total radiant intensity $\langle I_s \rangle$ (measured in W sr^{-1}), encompassing both coherent and incoherent components, scattered by the particles. In Eq. (7), $\mathrm{d}\sigma_s/\mathrm{d}\Omega$ (measured in m^2 sr^{-1}) is the differential scattering cross section of individual particles—a quantity directly related to the so-called form factor in condensed matter physics. I_0 is the incident intensity (measured in W m^{-2}). $S(\mathbf{q})$ is the structure factor, which incorporates the effect of far-field interference between pairs of particles on the scattered intensity, and is defined as

$$S(\mathbf{q}) = 1 + \frac{1}{N}\left\langle \sum_{m \neq n}^{N} \exp\left[i\mathbf{q} \cdot (\mathbf{r}_m - \mathbf{r}_n)\right] \right\rangle, \quad (8)$$

where $\mathbf{q} = \omega/c n_b(\hat{\mathbf{k}}_i - \hat{\mathbf{k}}_s)$ is the wavevector difference between the incident and scattered waves and n_b is the refractive index of the background medium.

The structure factor can be readily evaluated through statistical averaging. On the other hand, accurate determination of the form factor involves iteratively solving Maxwell equations for multiple wavelengths, incidences, and polarizations, followed by applying a near-to-far-field transformation to obtain the radiation pattern. Alternatively, a quicker approach with deeper insights can be achieved by expanding the differential scattering cross section using the resonance modes of the nanoparticles.[923]

Exploiting Eq. (7), one can derive straightforward expressions for the BSDF of infinite metasurfaces with $N \to \infty$. However, due to the inherent limitations of the ISA, the model's predictions exhibit notable inaccuracies for high particle densities, grazing incident angles, or large angles. These inaccuracies prompt the need for further refinements and extensions. For readers seeking a more comprehensive understanding, let us note that advanced models for the diffuse contribution in the BSDF have been presented in Ref. 918. For the specular contribution, an overview of various models can be found in a recent book chapter[920] and the references therein. Noteworthy is the remarkable efficacy demonstrated by the quasi-crystalline approximation.[921,925]

4. Fabrication

Several techniques exist for fabricating disordered metasurfaces. Top-down patterning methods, which make use of electron-beam or optical lithography, facilitate the precise positioning of the meta-atoms with nanometer-level precision and a fine-tuned control over meta-atom size and shape. Furthermore, with the advent of nanoimprint lithography[924] and soft lithography,[925] they have opened up new avenues for cost-effective fabrication.

Conversely, bottom-up approaches prioritize scalability and cost-efficiency over precision. Although they may not match top-down techniques in shaping and arranging nano-objects, their utility remains unequaled.

Among metasurfaces fabricated by scalable and cost-effective techniques, semicontinuous colloidal films composed of metal nanoislands stand out. These films naturally arise from deposition techniques that interrupt metal film growth before percolation threshold is reached.[926] Originally investigated for enhanced Raman scattering,[927] these ultra-affordable films can be mass-produced by the glass industry on extensive scales, spanning tens of square meters. Because island dimensions and interspace distances are much smaller than visible wavelengths, nanoisland metasurfaces act as coherent layers, absorbing rather than scattering incident light. Alternatives, such as utilizing block copolymer templates for self-assembly,[928,929] also facilitate monolayer creation with such tiny particles.

Producing disordered configurations with larger particles involves assembling pre-synthesized particles onto surfaces. Various techniques fit within this category:

16 July 2024 09:29:41

© Author(s) 2024

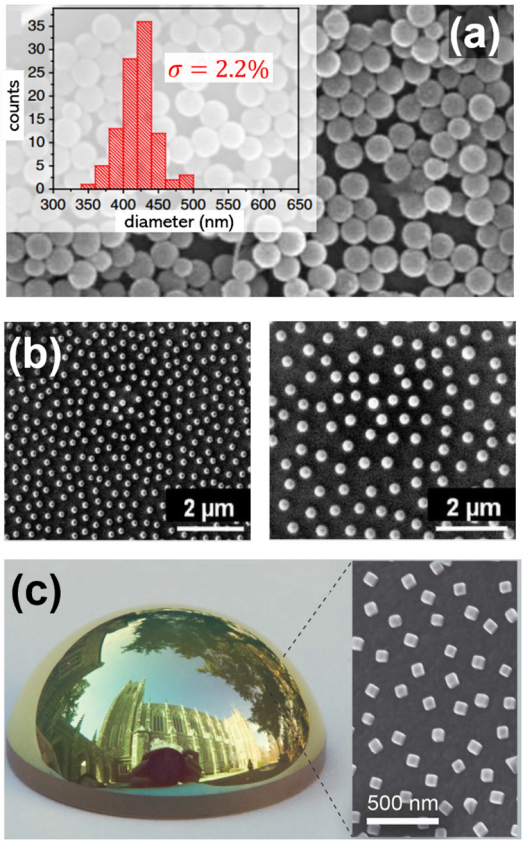

FIG. 31. A few selected examples of disordered metasurfaces fabricated with colloidal chemistry. (a) Availability of almost monodisperse nanospheres in various dielectric materials, e.g., PMMA, high-index Si nanospheres in the present figure.[930] (b) Amorphous colloidal monolayers of polystyrene nanospheres with sizes of 170 and 270 nm with short-range order.[931] (c) Monolayer of Au nanocubes with correlated disorder on a 2.5 cm-diameter half sphere.[932] All images are reprinted (adapted) with permission from the respective Journal and copyright remains with the original publisher.

- Colloidal lithography: This method hinges on nearly uniform in size colloids in solutions of materials like polystyrene, PMMA, or Si nanospheres[930] [Figs. 31(a) and 31(b)]. After drop-casting and drying, a monolayer forms,[931] subsequently serving as a mask to imprint patterns into underlying substrates. Since the sizing of polymer beads and strategies for self-assembly—utilizing repulsive and attractive forces for instance—are well-mastered [Fig. 31(b)], the transferred patterns, often arrays of nanodiscs or nanoholes in various materials, are fabricated on large scales with high fidelity and few aggregates.
- Self-assembly: With this method, colloidal nanoparticles, initially stabilized in solution, arrange on surfaces via methods like blade coating, dropcasting, and dip coating.[932] Diverse particle shapes, sizes and materials are commercially available, and controlled short-range arrangements can be achieved through nanoparticle and substrate surface functionalization [Fig. 31(c)].

For deeper insights, recent comprehensive reviews provide substantial information regarding the subject. They additionally cover deposition methods enabling the creation of densely packed monolayers. These monolayers exhibit high sensitivity to electromagnetic near-field interactions. They offer complex and possibly rich optical responses due to enhanced particle couplings and spatial dispersion. Future research directions should, therefore, include a more thorough investigation of these dense configurations, extending modeling approaches far beyond the limits of ISA and mean-field theories.[99,933–936]

C. Future directions and outlook

Disordered optical metasurfaces have unveiled a plethora of applications, some of which can be traced back to historical contributions, such as porous film-based anti-reflective coatings by Fraunhofer in 1887,[900] and observations of ultra-strong Raman signals from semicontinuous nanoisland metal films in the 1970s.[902] Over the past two decades, the field of disordered optical metasurfaces has experienced remarkable activity, encompassing a diverse array of applications. These include wide-angle broadband absorption,[932,937,938] anti-counterfeiting measures,[939] anti-reflection

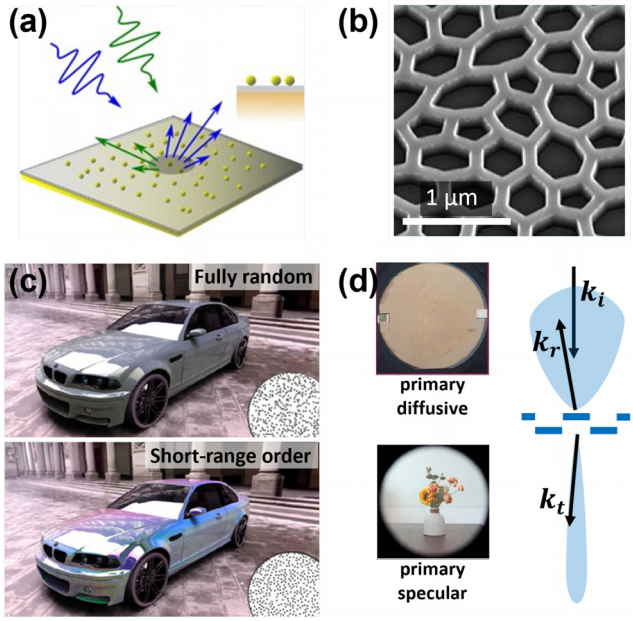

FIG. 32. (a) Harnessing the BRDF toward full manipulation of diffuse and specular light. In the sketchy example, the surface color varies abruptly, differently from the continuous color variation of classical iridescence, when the light source and/or the observer position move. (b) Hyperuniform metasurface for light trapping in solar cell application. After Ref. 968. (c) Rendered images showing the visual appearances of a car coated with disordered arrays of identical Ag nanospheres with a density of 4 μm^{-1}. Top: no structural correlation. Bottom: short-range correlated disorder. Adapted from Ref. 918. (d) Transparent display made of a bilayer metasurface which offer completely different properties in reflection and transmission. The rightmost images are camera pictures of a flower bouquet taken in reflection (top) or in transmission (bottom). After Ref. 945. All images are reprinted (adapted) with permission from the respective Journal and copyright remains with the original publisher.

16 July 2024 09:29:41

© Author(s) 2024

coating,[900,917,940] wavefront manipulation,[701,941,942] transparent displays,[943,944] chiral films,[945] fade-resistant structural coloring,[938,946–950] visual effects,[918,923] plasmonic electronic paper,[951] solar radiation management in architectural and consumer products glazing,[952–955] radiative cooling,[956] photocatalysis,[957] light trapping in solar cells,[931] and light extraction in LEDs.[958–961]

As nanofabrication capabilities continue to advance, these applications are progressively moving closer to industrial-scale production. In the subsequent sections, we delve into emerging applications that are poised to inspire numerous studies and emphasize two prospective avenues for enhancing manufacturing flexibility and reducing manufacturing costs.

1. Prospective applications

Anticipating the forthcoming wave of research, we expect a concerted effort to tackle the enduring question of how to master the nanopatterning of surfaces for shaping the far-field radiation across both spatial and spectral frequency domains. The ultimate ambition is to attain comprehensive command over both specular and diffuse light. It encompasses manipulating independently these two components, sculpting the directional patterns of diffuse light, monitoring alterations in light color for varying viewing and illumination angles, and, in essence, molding the BSDF at will [Fig. 32(a)].

Two key physical parameters that play pivotal roles can be used for design [see Eq. (7)]. Through the form factor, an assortment of shapes and high-index materials may be used to manipulate the resonances of the meta-atoms at the nanoscale. These resonances may be further enriched through mode hybridization at the wavelength scale to achieve wavelength-selective control over the directionality of scattered light.[471,962,963] Through the structure factor, we may engineer intricate mesoscale interferences. This engineering encompasses a vast landscape of arrangements,[524,964] ranging from full periodicity to entirely uncorrelated disorders. This gamut includes quasicrystals, weakly defective crystals, hyperuniform configurations, and more. For example, enforcing greater inter-particle distances engenders a short-range amorphous-type correlation that mitigates the presence of diffuse light around the specular direction,[918,965] regardless of the angle of incidence.

This effect is even more pronounced within stealthy hyperuniform metasurfaces, which entirely suppress scattering within an angular range centered on the specular direction.[524] Ongoing endeavors in the domain of hyperuniform disordered scattering structures, particularly for solar cells, are only just emerging.[965–968] A particularly remarkable recent achievement is the 2.5-fold enhancement in absorption of a 1 μm-thick silicon slab, thanks to a hyperuniform metasurface [Fig. 32(b)] meticulously designed to trap incident light into the slab guided modes.[968]

Disordered optical metasurfaces also hold significant promise for applications in applied and fine arts. Metasurfaces offer the potential to manipulate the visual characteristics–such as color, glossiness, haze, transparency, and iridescence–of macroscopic objects of any conceivable shape.[918] A recent breakthrough in this domain introduced a multiscale numerical tool capable of generating lifelike images of diverse macroscopic objects covered with disordered metasurfaces [Fig. 32(c)]. This tool not only forecasts subtle effects resulting from the interplay between diffuse and specular light but also unveils entirely new visual effects.

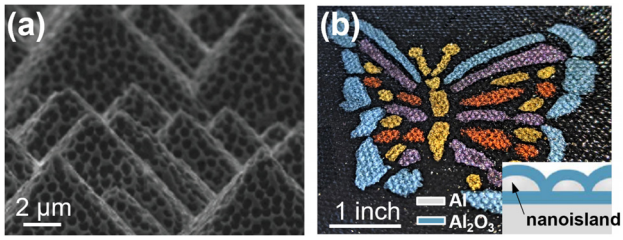

FIG. 33. (a) Metasurfaces fabricated on curved substrates: air holes etched in pyramid-textured Si surfaces. Adapted from Ref. 975. (b) Production of vivid colors despite a strong polydispersity in the size and shape of Al nanoislands used to resonantly absorb light. The resonance is due to nanogap plasmons supported by the capped nanoislands obtained by dewetting on Al_2O_3/Al substrate (inset). The photography shows a black canvas painted with oil–based plasmonic paints obtained by dispersing metasurface flakes in commercial paint oils. Adapted from Ref. 950. All images are reprinted (adapted) with permission from the respective Journal and copyright remains with the original publisher.

Future exploratory directions may capitalize on the monolithic integration of multiple metasurface layers. A compelling feature of these surfaces is their distinct behavior concerning diffuse light in transmission vs reflection. This contrast can be readily comprehended by examining the structure factor, $S(\mathbf{q})$ in Eq. (8), in which $\mathbf{q}$ signifies the difference in wavevector between the scattered direction and incident directions. It becomes evident that $(\mathbf{k}_i - \mathbf{k}_s).(\mathbf{r}_m - \mathbf{r}_n)$ in the exponential term remains independent of the normal coordinate z around the specular transmitted direction (where $\mathbf{k}_s \equiv \mathbf{k}_t \approx \mathbf{k}_i$). In contrast, this term does vary with the normal coordinate around the specular reflected direction (where $\mathbf{k}_s \equiv \mathbf{k}_r \approx -\mathbf{k}_i$). This intrinsic property has recently been ingeniously harnessed to create a transparent display[944] that selectively scatters reflected light while preserving transmitted light integrity [Fig. 32(d)].

2. Metasurfaces on curved substrates

An overwhelming number of nanopatterning methods, including optical and electronic lithography, nanoimprint lithography,[924] soft-lithography,[925] DNA-templating,[969] and functional block copolymers,[970] are available nowadays. They often function on 2D and atomically flat surfaces.

In general, adapting methods tailored for flat surfaces to curved ones necessitates significant changes to mitigate curvature-induced variations in feature attributes like size, orientation, and spacing. While some fabrication methods can accommodate relatively simple curvatures, the adaptation challenge grows as curvature intensifies. This puts severe limitations onto the use of metasurfaces in a variety of every-day-use or advanced technologies, where materials with non-planar, rough, soft, mechanically agile, or chemically sensitive surfaces are used.[971–973]

Recently, several transfer protocols have been proposed to overcome the limitations.[932,973–975] Figure 33(a) shows the example of a pyramid-textured Si surfaces which has been patterned with air holes to lower reflection at the Si-air interfaces and enhance the total absorption. The hole pattern is obtained from a template manufactured with colloidal lithography (other bottom-up or top-down approaches may be used as well). In many instances, the key is the use of a 10 nm-thin carbon film deposited on a sacrificial layer for the template. Such a

16 July 2024 09:29:41

© Author(s) 2024

thin film combines extreme strength with a large degree of flexibility that facilitates conformation of the transferred pattern to nearly any macroscopic or microscopic 3D object.

3. Striving for ultra-low costs with augmented resilience to fabrication imperfections

Optical metasurfaces, which harness resonant nanostructures at subwavelength scales, impose strong constraints on the nanofabrication precision. These constraints are growing in significance, as metasurfaces progress toward practical applications that require large sample areas. In this evolving landscape, the emergence of metasurfaces designed to exhibit resilience against imperfections becomes increasingly crucial. Recent studies have converged to provide compelling evidence that disordered arrays of nanoparticles, when placed on a transparent dielectric spacer above a metallic substrate, exhibit an extraordinary resilience to variations in material, size, and nanoparticle shape. One fundamental mechanism that imparts resilience is through the process of mode hybridization.[923] In scenarios where plasmonic nanoparticles are situated on low-index substrates without undergoing hybridization, the electromagnetic field becomes profoundly confined around the individual particle. Consequently, even slight variations in material composition or shape induce significant shifts in resonance frequencies. For context, even a minor alteration of 10 nm in the dimensions of a metal nanoparticle leads to a resonance wavelength shift of 10–20 nm. In contrast, within hybridized modes, the field localization diminishes as it extends into the transparent layer. Consequently, hybridization inherently mitigates sensitivity to size and material polydispersity. This general attribute of hybrid modes has facilitated the discovery of a remarkable diffuse iridescence phenomenon, in which a mere two distinct and vivid colors are discernible across all angles of illumination and viewing, even when confronted with significant variations in nanoparticle size and shape across the metasurface.[923]

An alternative resilience mechanism emerges when nanoparticles are substantially smaller than the wavelength. This scenario is exemplified by semicontinuous nanoisland films on a dielectric spacer atop a metal substrate, where empirical observations reveal that the pivotal factor shaping the specular reflectance spectrum is the spacer thickness,[947] rather than the typical expectation of the nanoparticle material choice. This material-independent response has been experimentally verified for various materials like Ag, Au, Pt, Pd, and numerically for Al, Cr, Cu, Ni, among others, under normal incidence.[947] Thus commonly accessible materials such as Cu or Al could substantially mitigate costs related to nanostructure-based coloration.

This striking property can be attributed to the amalgamation of localized plasmonic resonances at the nanoisland scale, hot spots within the interstitial gaps, and delocalized modes, irrespective of the metal used for the nanoislands. This synergy results in broad absorption, further enhanced by the diversity in island size and shape. Consequently, the film uniformly absorbs the incident light, except for the Fabry–Pérot resonance of the thin transparent spacer, for which the field is nearly null within the semicontinuous film.

Yet another illustration of resilience against manufacturing defects is observed in a recent work on ultralight plasmonic structural-color paints[950] with a notably low-cost morphology shown in the inset of Fig. 33(b). Impressively, vibrant colors are attainable despite the substantial variance in nanoisland sizes. While plasmon hybridization leading to a confined gap-plasmon resonance within the alumina film stands as a logical explanation, it is important to acknowledge the influence of other mechanisms as well. Among these, the generation of subtractive color through the absorption of a "homogenized" film emerges as a noteworthy consideration, deviating from the diffusion-based coloration observed with larger nanoparticles.

ACKNOWLEDGMENTS

P.L. and K.V. acknowledge financial support from the French National Agency for Research (ANR) under the project "NANO-APPEARANCE" (No. ANR-19-CE09-0014). A.D. acknowledges the Swedish Research Council for Sustainable Development (Formas) (Project No. 2021-01390). P.L. acknowledges financial support from the European Research Council Advanced grant (Project UNSEEN No. 101097856). C.R. and A.S. acknowledge financial support from the Deutsche Forschungsgemeinschaft (DFG) (Nos. 413644979, RO 3640/11-1, and WE 4051/26-1).

XVII. FROM PRINCIPLES TO PERFORMANCE: EPSILON-NEAR-ZERO METASURFACES FOR NONLINEAR OPTICAL DEVICES

Jeremy Upham, M. Zahirul Alam, Israel De Leon, Robert W. Boyd, and Sebastian A. Schulz*

*sas35@st-andrews.ac.uk

Epsilon-near-zero (ENZ) materials, particularly thin films of transparent conductive oxides, exhibit a variety of intriguing optical phenomena, two of which should be of particular interest to the metasurface community: (1) ENZ materials of sub-wavelength thicknesses can exhibit large and very fast nonlinear optical responses, including significant nonlinear phase shifts; (2) the nanoantenna of a metasurface can strongly couple to long-range surface plasmon polariton modes of these low index thin films, making these nonlinear optical responses even stronger. In this article, we examine how these enormous nonlinearities are currently understood and highlight examples of how this functionality is already being exploited for applications in nonlinear optics, such as frequency conversion, self-phase modulation, time-refraction, and beyond. Looking forward, the current limitations on ENZ-metasurface performance appear to be predominantly engineering challenges rather than physical limitations. We argue that through creative metasurface design and intuitive materials science optimization, ENZ-metasurfaces are poised to transform from compelling proofs of principle to high-performance, all-optical devices.

A. Introduction: The physics of ENZ

Exciting subsets of current metasurface research include the development of dynamic, temporally varying devices and the enhancement of nonlinear optical responses to expand metasurface functionality. Fortunately, this has proven to be achievable simply by incorporating thin film layers of a class of materials with vanishing permittivity known as epsilon-near-zero (ENZ) materials. A material is said to have ENZ properties if its dispersion curve features a spectral region where $-1 < \mathrm{Re}(\varepsilon) < 1$, typically with the ENZ-crossing being the wavelength where the real part of the permittivity crosses from

16 July 2024 09:29:41

© Author(s) 2024

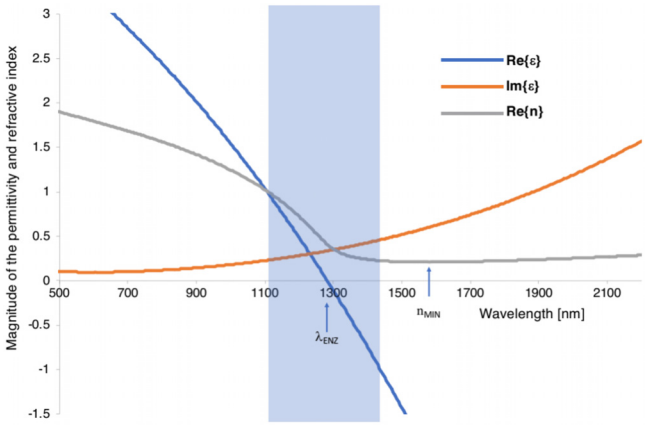

FIG. 34. Dispersion of the real and imaginary components of the permittivity, as well as the real part of the refractive index, for a typical ENZ material. λ_{ENZ} indicates the wavelength where the real part of the permittivity crosses zero. The shaded region indicates the ENZ spectral range where $-1 < \mathrm{Re}(\varepsilon) < 1$. Because the real part of the refractive index also depends on the imaginary part of the permittivity, the refractive index minimum is near, but not necessarily within the ENZ spectral range.

positive to negative. This effect leads to a wide variety of unconventional optical behaviors in both the linear and nonlinear regimes.[977,978] For example, waveguides formed from ENZ materials can feature coupling through arbitrary shaped channels, phase-matching free nonlinear processes or manipulation of radiation from nearby or embedded emitters.[977] In other platforms more relevant to metasurface technologies, ENZ films have shown enhancement of nonlinear effects such as harmonic generation[979] and the nonlinear refractive index.[184,185]

To clarify, while the ENZ condition typically has the real part of the permittivity cross from positive to negative, the imaginary component need not change sign, nor does the permeability. Therefore, the refractive index need not become negative as in the case of negative index metamaterials[980,981] or even reach zero as in near zero index materials.[982,983] The ENZ condition often occurs naturally in Drude materials simply by the impact of the plasma frequency on the dispersion curve, delineating where a material crosses from metallic to dielectric behavior. One can also obtain ENZ conditions in a Lorentz-type material for a sufficiently large value of the oscillator strength. While a near-zero real part of the permittivity can also be achieved for values of the refractive index larger than one in such materials at absorption resonances, these are typically accompanied by high imaginary permittivity values. In these cases, such excessively high losses prohibit the observation of the desired ENZ effects. Therefore, we generally consider ENZ materials to be Drude-type materials where both the absolute real part of the refractive index and the permittivity are less than unity over some range of frequencies. The schematic of Fig. 34 shows the dispersion of permittivity and refractive index for a typical ENZ material. The spectral range where the real part of the permittivity has a magnitude less than one is the ENZ range. The real part of the refractive index can be below 1 in this same region, but this also depends on the imaginary component of the permittivity.

1. Materials with ENZ properties

Depending on what part of the EM spectrum is being considered, there are multiple ways to achieve this ENZ condition. At radio frequencies well-established metamaterials such as arrays of split ring resonators can easily achieve this state,[984,985] and similarly, ENZ behavior has been shown in microwaves[986] and through phononic resonances in the THz spectral region.[987,988] Within the deep UV, many metals have ENZ crossings (e.g., silver near $\lambda = 320\,\mathrm{nm}$[989]) For the visible and near- to mid-infrared spectral regions, two solutions exist. The first is to engineer structures, either photonic crystal-like band structures[982] or multi-layer materials, with an effective index[990–993] such that their effective permittivity is near zero. However, in the context of metasurfaces, the prevailing solution has been to use transparent conductive oxides (TCOs).[994,995] These non-stoichiometric materials are typically transparent dielectrics such as indium oxide, aluminum oxide, or cadmium oxide that are degenerately doped so that the Fermi level moves to the conduction band. These TCOs hit a sweet spot for ENZ performance in the near to mid-infrared range: they feature sufficient free carriers to achieve a crossing of the real part of the permittivity from positive to negative, but still fewer than noble metals, and hence the crossing occurs at longer wavelengths. Furthermore, the concentration and mobility of the carriers (the key factors determining the plasma frequency) can be controlled during TCO deposition, e.g., by tuning the doping concentration.[996–999] Together with the naturally slightly different plasma frequency depending on the dopant (e.g., indium, gallium, aluminum), this means that TCOs can place this epsilon near zero condition anywhere within a wide range of the near- to mid-IR spectrum, covering important regions for optical communications and sensing.[1000]

Certain TCOs, such as indium tin oxide (ITO) and aluminum zinc oxide (AZO), have become reasonably mature fabrication materials because they can be deposited as transparent yet conductive thin films that enable touchscreen and solar cell technology.[1001,1002] Driven by these applications to be transparent to visible light (dielectric in the visible spectrum) but also as conductive as possible (lots of free carriers), they are readily available materials for thin films with a plasma frequency just past the visible spectrum in the near-infrared. As a result, these thin films typically exhibit ENZ behavior between 1 and 2 μm, with the additional benefit of a reasonably small absorptive loss.[996] Because the real part of the permittivity crosses zero at a wavelength where the imaginary component is also small, the refractive index is less than 1 as well.

2. ENZ induced behavior in TCOs

A consequence of the refractive index falling below 1 is that the wavelength of light within that material is stretched compared to that of free space. Equivalently, as the index approaches zero, spatial phase variation within the ENZ medium also goes to zero. Because light in a zero index medium can only radiate away normal to the bounding interfaces, this leads to interesting linear optical effects,[977] such as light propagating through arbitrary channels,[1003] or wavefront shaping at interfaces.[1004]

However, from the point of the original motivation, i.e., the desire for large, dynamic modulation of metasurface behavior, the nonlinear enhancement in ENZ materials is of more interest. Many conventionally held equations for nonlinear optical phenomena, such as the Kerr

16 July 2024 09:29:41

© Author(s) 2024

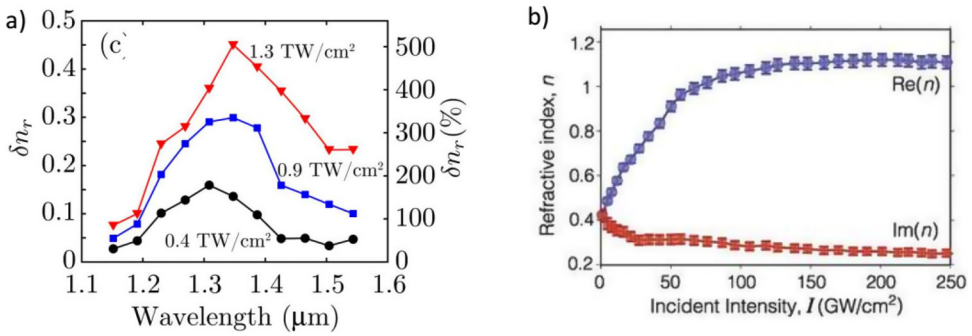

FIG. 35. First experimental demonstrations of large, optically driven changes of refractive index of TCOs in their ENZ spectral regions. (a) Pump-probe measurement of $\Delta n = 0.45$ for AZO at 1390 nm. Reproduced with permission from Caspani *et al.*, Phys. Rev. Lett. **116**, 233901 (2016). Copyright 2023 American Physical Society.[185] (b) Z-scan measurements of ITO showed a $\Delta n = 0.72$ at 1240 nm.[184] All images are reprinted (adapted) with permission from the respective Journal and copyright remains with the original publisher.

effect, are written to be inversely proportional to the real part of the linear refractive index, e.g., $n_2 = \frac{3\chi^{(3)}}{4\varepsilon_0 c n_0 R(n_0)}$ (where n_2 and n_0 are the nonlinear and linear refractive indices, $\chi^{(3)}$ is the third order susceptibility and ε_0 is the vacuum permittivity), suggesting that such phenomena would be enhanced or even diverge within an ENZ material.[1005] This led to the prediction[1006] and demonstration[1007] of ENZ materials boosting the nonlinear generation of harmonic frequencies.

In 2016, two studies on nonlinear optics in TCOs investigated the effect of all-optical nonlinear interactions on light propagation and reflection within ITO[184] and AZO films.[185] Both studies demonstrate very strong enhancement of the nonlinear refractive index, see Fig. 35, with values of $\Delta n = 0.72$ and $\Delta n = 0.45$, respectively, corresponding to up to 500% of the linear refractive index,[184,185] reaching the regime where the nonlinear response exceeded the linear component of the refractive index. We thus note that the conventionally held equations of the Kerr and other nonlinear effects that are based on perturbative descriptions are no longer appropriate. ENZ materials feature such a strong nonlinear response that the equations of nonlinear optics must be reconsidered, specifically the assumptions of $n \leq 1$ and $n \ll \Delta n$ are no longer valid, making a compelling case for the use of ENZ materials in nonlinear optics.[1008]

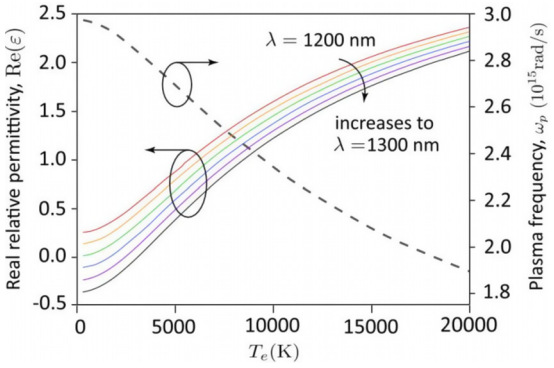

FIG. 36. Modeling changes to the real part of the permittivity of ITO as a function of the electron temperature. The green curve (1240 nm) has a real permittivity of 0 when T_e is at room temperature, but increases with electron temperature. When heated up to 4000 K, the black curve (1300 nm) becomes ENZ crossing wavelength. Reproduced with permission from Baxter *et al.*, Adv. Photonics Res. **4**(3), 2200280 (2023). Copyright 2023 Wiley.[1013] All images are reprinted (adapted) with permission from the respective Journal and copyright remains with the original publisher.

While other, non-perturbative nonlinear effects have been demonstrated before (e.g., the semiconductor-to-metallic light- or heat-induced phase transition in vanadium dioxide[1009]) such strong effects are typically slow, as such thermo-optic or thermochroic responses occur on the ms timescale or longer. In contrast to this, the nonlinear effects in the TCO materials occur on an ultrafast timescale.[184,185,1010] Often the onset seems to match the temporal width of an ultrafast pump pulse and relaxation times are on the scale of a few-hundreds femtosecond.[184,185,1010] This holds potential for THz switching speed operation of ENZ-based devices. The underlying nonlinear response of the TCOs is dominated by the free carriers, resulting in a hot electron-dominated effect. When optically pumped, the available carriers in the conduction band experience intraband transitions that significantly change their distribution and consequently the plasma frequency of the material. Because the transitions are principally intraband, the electrons cool quickly, explaining the rapid onset and relaxation of the index change. These transitions are so fast that light witnessing changes of the refractive index will undergo an equivalent change of frequency through adiabatic frequency conversion, otherwise known as time refraction[852,1011,1012] discussed further in Sec. XV.

Interestingly, the magnitude of the observed index change stems from the fact that the response is free carrier dominated, even though these are present in low concentrations. Because of the significantly lower carrier concentrations in the conduction band (compared to conventional metals), the excitation of even a modest amount of carriers is enough to significantly alter the overall carrier distribution, the Fermi level, and consequently the effective carrier mass and plasma frequency. The Drude model can thus explain the change of the TCO's dispersion curve almost entirely as a change of the electron effective mass due to the changed effective electron temperature[1013] (see Fig. 36). The observed response is all the more dramatic in the ENZ region, where the initially low linear index can be effectively tripled by the magnitude of the nonlinear index change.

While these rapid and robust index changes show significant potential for rapidly modulated optical components, the transitions are not efficient. As a low-index material and a conductor, the index contrast or impedance mismatch with optical modes in free space

16 July 2024 09:29:41

© Author(s) 2024

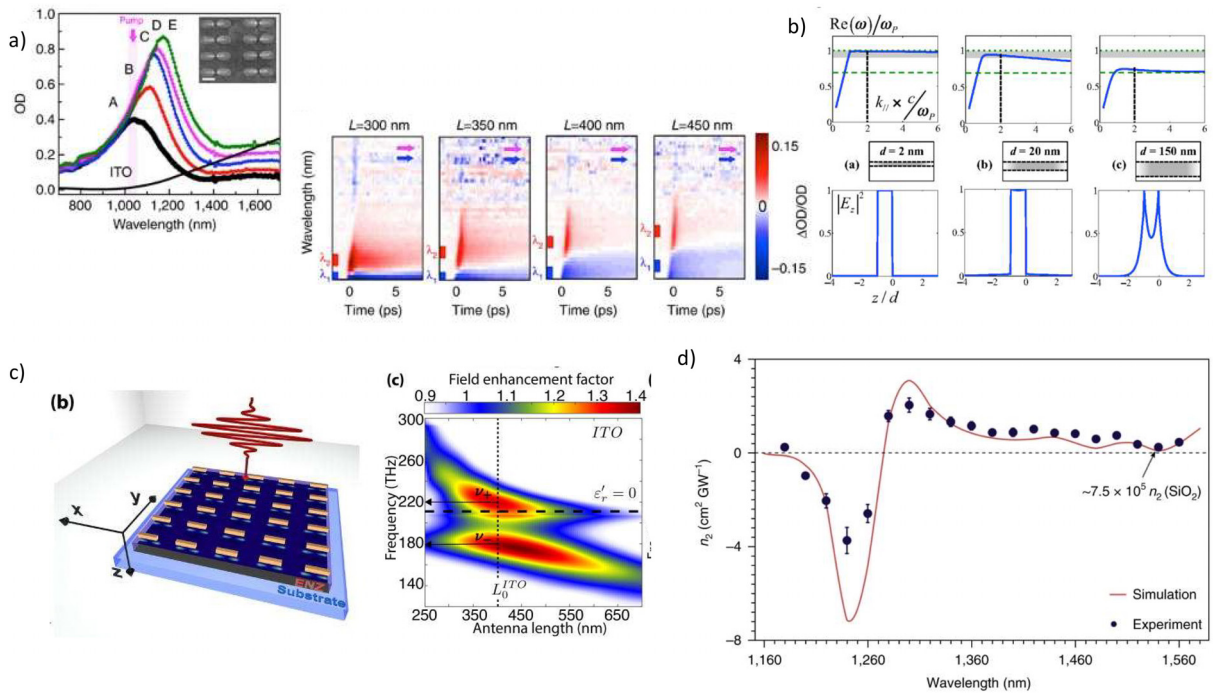

FIG. 37. Experimental demonstrations of plasmonic metasurfaces enhancing the nonlinear response of TCOs. a) Plasmonic dimers on ITO show a large, fast (sub-picosecond) modulation of optical density when exciting antenna resonances, suggesting a strong, fast Kerr-type nonlinearity.[1018] (b) A sufficiently thin, bare layer of ENZ material will support a Berreman (LR-SPP) mode with high field enhancement, but cannot easily couple to light in free space.[189] (c) Nanoantennas with resonances in the ENZ region of a thin TCO layer exhibit mode splitting from strong coupling between the metasurface and the LR-SPP mode.[1016] (d) When a metasurface enables optical pumping of this LR-SPP mode, it not only shows an enhanced nonlinear response but can also extend this nonlinear enhancement well beyond the narrow spectral range where ε is near zero.[184] All images are reprinted (adapted) with permission from the respective Journal and copyright remains with the original publisher.

makes coupling light into ENZ materials difficult. For this to be a truly useful optical component, we must overcome this challenge.

3. Incorporating metasurfaces with ENZ materials

Fortunately, metallic nanoantennas can effectively couple light between propagating and localized modes. If a plasmonic nanoantenna is placed on the surface of an ENZ material, the incident light can efficiently couple to the local surface plasmon resonance and then have the fields of this resonance penetrate the TCO and excite free carriers[1014] [Fig. 37(a)]. Excitation of free carriers is further enhanced if the ENZ material can support a Berreman mode, which is a Long Range Surface Plasmon Polariton (LR-SPP) mode traveling in the low index medium of a sufficiently thin ENZ material with field enhancement inversely proportional to its thickness[189] [Fig. 37(b)]. In fact, plasmonic metasurfaces of appropriately designed nanoantennas can even exhibit strong coupling with the LR-SPP mode of a thin film of TCO,[1015,1016] which greatly improves energy transfer into the TCO through near-field interaction [Fig. 37(c)]. Critically, this strong coupling between modes in the ENZ material and the nanoantenna enhances the nonlinear response of the metasurfaces well beyond what the bare ENZ material could achieve: Light couples through the antenna into the ENZ film, changing the latter's refractive index. This change modifies the dispersion of the TCO's LR-SPP modes, which in turn modifies the coupled resonance spectrum. As a result, light of high intensity experiences a dramatically different refractive index compared with that experienced by low-intensity light[154] [Fig. 37(d)]. Therefore, pairing an array of plasmonic nanoantenna with an ENZ thin film will not only improve energy transfer to the free carriers within the material but can further increase the nonlinear phase shift of the metasurface by its shifted resonance. Significantly, the broadening of the split resonance also extends the spectral range over which a large nonlinear phase shift can be achieved to be well beyond the ENZ region of the bare TCO material.

This synergistic interaction enables a faster, larger, and potentially more flexible nonlinear optical response from a sub-wavelength ENZ metasurface than can be achieved otherwise, significantly outperforming thicker layers of TCOs or even highly nonlinear bulk materials.[1017] Having established that a metasurface not only gains a large, dynamic optical response from incorporating an ENZ material but in fact can magnify the size of this response through strong coupling to the LR-SPP modes, we next consider how this functionality can be put to use by metasurface design.

4. Metasurfaces exploiting the nonlinear ENZ response

Having motivated the potential of ENZ-based metamaterials for nonlinear optics, we next consider some recent, exciting examples of devices where this strategy has been put into practice.

16 July 2024 09:29:41

© Author(s) 2024

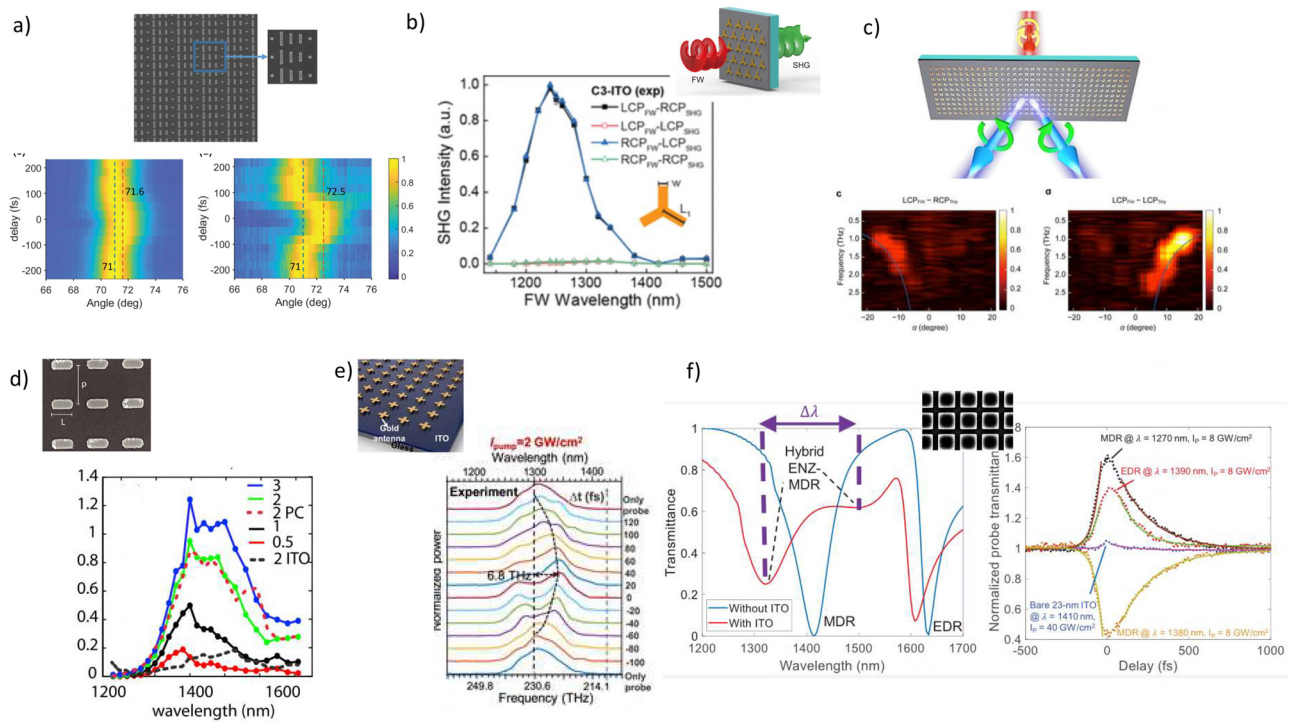

FIG. 38. Compelling results in ENZ metasurfaces: (a) dyamically changing the direction and optical frequency of light diffracting from an ENZ-metasurface is different for diffraction orders.[879] (b) SHG is enhanced by a factor of 10^4 and is polarization selective.[1019] (c) Enhanced THz generation from an ENZ-metasurface that also dictates polarization and wavefront.[1020] (d) Four wave mixing enhanced by dynamic metasurface-ENZ strong coupling.[851] (e) Enhanced adiabatic frequency conversion.[875] (f) Strong coupling and dynamic modulation of a dielectric metasurface on a thin TCO layer, for both the electric or magnetic dipole Mie resonances.[1021] All images are reprinted (adapted) with permission from the respective Journal and copyright remains with the original publisher.

An example of time-refraction in an ENZ metasurface was realized in a system consisting of a plasmonic blazed diffraction grating on an ITO thin film with a pump-probe excitation. In this instance, the pump pulses cause the diffracted probe to undergo a change of central wavelength while interacting with the metasurface and therefore have the diffraction angle dictated by the probe's new wavelength. Interestingly, the light diffracting into the -1 diffraction order (the order suppressed by the blazing) appears to interact with the metasurface longer than light diffracting to the $+1$ order. Consequently, light in the -1 diffraction order experiences about twice as much wavelength shift and thus twice as much change to the diffraction angle as it's counterpart[879] [Fig. 38(a)].

Both the previously demonstrated large refractive index change, as well as the time refraction are demonstrations of the Kerr-type effect, i.e., an intensity-dependent refractive index change. However, ENZ-metasurfaces can enhance a wide range of other nonlinear effects. For example, Deng *et al.* used a hexagonal array of Y-shaped nanoantennas to enhance the second harmonic conversion from an ITO thin film.[1019] In this work the antenna array once again overcomes the issue of coupling light into the ENZ film, resulting in an experimental observation of a 10 000-fold enhancement of the SHG efficiency. Furthermore, this work demonstrates the multi-functionality of ENZ metasurfaces, as the symmetry properties of the antennas are used to control the polarization of the second harmonic light. For example, the metasurfaces can be configured such that excitation with a right-hand circularly polarized pump results in left circularly polarized SHG emission. SHG enhancement has also been demonstrated in other ENZ-metasurface geometries, such as through gap-plasmon enhancement, based on square-shaped antennas coupled to ENZ films.[1022]

ENZ metasurface enhancement has also been demonstrated for other frequency conversion processes. For example, split ring resonators (SRRs) on ITO metasurfaces have been shown to result in orders of magnitude enhancement in the THz generation efficiency, compared to the same SRRs on glass,[1020,1023,1024] which allows the generation of single-cycle THz pulses. This enhancement can be directly linked to the hot-electron dynamics in the ENZ film, also altering the spectral properties of the emitted THz pulse, with spectral broadening being observed.[1023]

A wide range of other nonlinear processes are enhanced in such ENZ-metasurfaces, with the geometry of both the ENZ film (e.g., thin films featuring the LP-SPP mode vs thicker films not featuring this guided mode) as well as the antenna shape and dimensions together with the excitation scheme controlling the achieved nonlinear effect. For example, an array of rectangular antennas on an ENZ film was examined in a pump-probe configuration, however, with the pump at double the probe frequency.[851] This results in a number of nonlinear optical processes, including four-wave-mixing and negative refraction.

Furthermore, ENZ-metasurfaces retain the design freedom of linear metasurfaces. For example, through rectangular antennas we can design the strong coupling—and hence nonlinear enhancement—to be present for only one polarization,[154,851] or through the use of antennas with a 90°

16 July 2024 09:29:41

© Author(s) 2024

rotation symmetry, e.g., + shaped antennas, we can obtain polarization independent nonlinear enhancement.[875,1025] In a polarization-dependent setting, we can use the dynamic nature of the device to obtain controllable polarization rotation.[1026] Here for a given incident polarization featuring components both parallel and perpendicular to the antenna—e.g., of axis linear polarization or circular/elliptical polarization—the two polarizations will experience a different delay due to their varying interaction with the metasurfaces. However, this interaction will change for the parallel polarization as the antenna is excited nonlinearly (and its resonance shifts), while the cross-polarization retains the same interaction as in the linear case. We thus have the ability to control the delay of one polarization component relative to the other.

While ENZ-metasurfaces based on plasmonic nanoantennas are used in the majority of nonlinear optical investigation efforts at this time, it is important to also consider how other nano-resonances could be integrated with ENZs as well. Dielectric metasurfaces and their corresponding Mie resonances do not provide the same field enhancement in the TCO by the simple fact that their mode volumes lie principally within the dielectric material of the resonator rather than at the edges. Nevertheless, experiments have shown strong coupling between an LR-SPP mode and either electric or magnetic dipole resonances,[1021] as well as confirming that these resonances can be optically tuned in a pump-probe set-up with sub-picosecond recovery time. Just as with plasmonic metasurfaces, strong coupling between the Mie resonances and the ENZ mode of a TCO thin-film appears to enable large, rapidly tunable modulations of the optical modes and should thus facilitate a broad range of dynamic, nonlinear optical responses.

It is evident from these examples that ENZ-metasurfaces enable strong and fast nonlinear optical responses while still maintaining the tremendous design freedom available to metasurfaces. There is a significant opportunity for devices that rapidly manipulate the phase, direction, polarization, and even mode of propagating light, all within flat, sub-wavelength structures.

5. Future of applications

Going forward, there are still several outstanding research questions that need to be addressed for the nonlinear response of ENZ materials in general and optimizing the potential of ENZ-metasurfaces in particular.

a. Speed of modulation. For the experiments presented here, the nonlinear optical response of the ENZ-metasurfaces is clearly faster than the short (sub picosecond) pump pulses can resolve. Knowing it can be faster than 100 fs supports the working understanding that rapid heating and intraband transitions of the free carriers are driving the index changes in the TCO. However, a more direct investigation into the onset time of this response, how it saturates, the thermalization time as well as how each of these is affected by coupling to plasmonic nanoantennas could provide insight into devices that modulate at rates beyond GHz. The speed and magnitude of the nonlinear phase shifts are likely large enough to enable non-adiabatic transitions, which could have significant implications for applications in which mode degeneracy or spectrum engineering are important.

b. Absorptive losses. While the imaginary component of TCOs refractive indices are typically smaller than for properly conductive materials,[996] there is still a significant amount of absorptive loss seen through sub-wavelength layers and this is exacerbated by coupling with plasmonic resonances. Material science research into TCOs intends to strike a balance between strong nonlinear response and absorption[1027] and be able to produce materials tuned for specific applications. However, there must always be some absorption remaining for TCOs, making them ineffective for most low-light sensing or quantum optics applications where loss management is critical.

c. Saturation and damage threshold. The majority of the above examples of ENZ-metasurfaces are based on gold nanoantennas. It is well known[1028] that many metallic nanostructures and gold particles in particular, are very sensitive to absorption-induced heating and melting, with the melting point significantly lower than for the bulk metal. However, more thermally robust materials such as TiN have higher absorption losses. This therefore presents an interesting research area, where materials and antenna design can be optimized to allow higher optical powers and operating temperatures. This low damage threshold, together with the increased design freedom of the ENZ metasurfaces means that nonlinear saturation effects have not yet been studied extensively in these systems.

d. Alternative modulation mechanisms. In this paper we have focused on the ultra-fast, all-optical response of ENZ metasurfaces. However, the underlying tuning mechanism is much more general. We recall that the mechanism is based on a shift of the ENZ dispersion, induced by a change in the free carrier properties. Such changes can be induced in an alternative fashion, for example through electro-optic modulation[1029,1030] or thermo-optic tuning,[1031] creating the potential for dynamically reconfigurable metasurfaces. Here we note that the sign of the nonlinear response can differ compared to the hot-electron nonlinearities discussed earlier, as some of these tuning mechanisms, can include interband transitions, or extraction or addition of carriers, hence allowing either a blue or redshift of the plasma frequency.

e. Pushing back technical limits. Given the unprecedented large changes of refractive index observed in ENZ-metamaterials, a natural question is how much further such devices be engineered before reaching a new limit? Some examples still needing exploration include, can an ENZ-metamaterial be engineered to produce a rapidly modulating nonlinear phase shift of $\Delta\phi = \frac{\pi}{2}$? In the electro-optic modulation scheme, this full phase shift has been achieved, however, at the cost of a highly reduced efficiency[1030] and limited to the tuning speed of the control electronics. Reaching the $\Delta\phi = \frac{\pi}{2}$ limit all-optically would make it possible to create a sub-wavelength, THz-speed switch.

In adiabatic frequency conversion work, it's been shown that large changes of the carrier frequency can be achieved in TCOs[1011] and that plasmonic metasurfaces can manipulate this response more efficientl.[875,879] However, in time refraction the fractional wavelength shift is proportional to the refractive index change witnessed by the photons, which so far has been far less than the full index shift of the TCO ($\Delta n \sim 1.0$). If ENZ-metasurfaces could be designed to increase this interaction time, it should in principle be possible to shift the carrier frequency of light by an octave.

B. Perspective on future work

We can imagine that ENZ metasurfaces could be designed for a much wider set of nonlinear interactions. For example, some of the

16 July 2024 09:29:41

© Author(s) 2024

most widely used interactions in commercial devices featuring nonlinear optics are the sum and difference frequency generation in optical parametric amplifiers and oscillators. Similarly, the field of attosecond science relies on efficient high-harmonic generation. As ENZ metasurfaces have shown enhancement of second harmonic light it would be a natural next step to investigate and extend this to higher nonlinear orders. Furthermore, the broad response of ENZ metasurfaces could also be of interest to other processes such as supercontinuum generation and cascaded nonlinearities. However, these applications typically require nonlinear interactions over an extended propagation length. How this could be replicated in a metasurface geometry requires further research.

As the combination of metasurface resonances with TCO thin films shows such potential, a natural next question is what functionality can arise from patterning the metasurface directly into the TCO thin film itself? Initial investigations suggest sufficiently good coupling and field enhancement to produce significant nonlinear optical effects and non-reciprocal radiation patterns,[1032] so further experimentation could be fruitful.

The majority of the nonlinear optical work on ENZ metasurfaces has been performed in the near-infrared (1100–2000 nm) spectral region. Naturally, these same effects hold promise for other pump wavelength regions, such as visible light, but also mid-infrared through to THz spectral regions. Implementing these effects across different wavelength regimes will likely require different ENZ materials or at least wide tuning of the ENZ wavelength.

Perhaps most intriguing, the field of photonic metasurfaces is rapidly becoming more sophisticated, as is readily demonstrated by this roadmap. As new materials, resonance structures and metasurface principles are being introduced, there are opportunities to investigate each of their interactions with ENZ thin films. For instance, incorporating bound states in the continuum, disordered metasurfaces or active emitters with ENZ thin films could demonstrate the enhancement or quenching of various light–matter interactions.

C. Conclusion

In this perspective, we have summarized the physics governing nonlinear optical interactions in ENZ metasurfaces, consisting of antenna arrays coupled to thin films of ENZ materials. The strong coupling results in huge nonlinear enhancements, exceeding the perturbative regime, on sub-picosecond timescales. We then highlighted some recent key contributions to this rapidly growing field, well aware that an even broader body of work exists. Considering the potential future directions for this field and identifying opportunities across physics, engineering, and materials science, there is clearly a strong potential for novel nonlinear optical applications. In effect, almost any application based on the mentioned nonlinear processes could benefit from the enhancement in ENZ metasurfaces. Finally, as there remains an even wider set of nonlinear optical interactions to which ENZ metasurfaces have not yet been applied, we leave them as an exercise to the reader to make their own mark on this exciting and growing field.

XVIII. DEEP LEARNING FOR PHOTONIC METASURFACES

Willie J. Padilla* and Jordan M. Malof

*willie.padilla@duke.edu

Deep learning (DL) is a specific type of artificial intelligence and has recently garnered tremendous attention within science and engineering, including for the design and study of photonic metasurfaces. However, there is a tendency to overvalue the current capabilities of DL, often attributing powerful reasoning skills to it. Here we aim to clarify the current strength of DL methods for photonic metasurface research and development. We highlight two major successful use-cases. First, DL has been highly effective at automatically constructing models that accurately predict the properties of complex metasurfaces based upon their experimental parameters (e.g., geometric structure, or illumination). Additionally, DL models has been used to build accurate models allowing users to predict the experimental parameters needed to yield some desired behavior, significantly accelerating metasurface design. Despite these successes it is important to recognize that DL primarily serves as a collection of advanced regression methods, which represent a relatively rudimentary form of intelligence compared to, for example, human scientists. The fundamentally limited reasoning capabilities of DL manifest as key practical limitations that undermine its current value and impact, such as DL's need for large quantities of training data, and their limited generalization to new scenarios that were not represented in training data. We discuss several promising acute and long-term strategies for addressing these limitations, which may ultimately lead to DL models that fulfill more of their current promise.

A. Introduction

Photonic metasurfaces have demonstrated great utility as a materials platform for the demonstration of numerous exotic electromagnetic (EM) phenomena in both applied[1033] and fundamental[1034–1036] settings. A common objective of photonic metasurfaces is to tailor the EM field to achieve a desired configuration which may constitute various forms, including free-space scattered states, surface wave conditions,[1037] or localized field concentrations.[682] Moreover, metasurfaces enable this control over diverse dimensions of space,[1038] time,[1039] and frequency.[1040] Although design constraints including material choice, physical restrictions, and operational environmental limitations are unavoidable, there is otherwise great design flexibility in the type of photonic metasurface utilized. This rich history of EM design, evolving through distinct theoretical, computational, and now artificial intelligence (AI)-driven eras, informs our understanding of the interplay between design freedom and practical limitations in photonic metasurfaces, opening new avenues for exploration and optimization.

In stark contrast to the vast EM design tools available today, at the end of the 19th century scientists relied on manual calculations to perform EM analysis[1041] using the newly established Maxwell equations of 1864 (Ref. 1042) and the refined set in 1873.[1043] The initial focus was on finding closed form solutions to Maxwell's equations and by 1910 there were a dozen or so including those of Sommerfeld,[1044,1045] Lord Rayleigh,[1046] Mie,[1047] Hondros,[1048] Nicholson,[1049] Debye,[1050] and Hondros and Debye.[1051] During the first half of the 20th century more complex EM problems were solved by generalization of these explicit solutions. EM problems involving Sommerfeld integrals were more challenging to solve and benefited from the development of asymptotic methods including stationary phase and the method of steepest descent. Perturbation and

16 July 2024 09:29:41

© Author(s) 2024

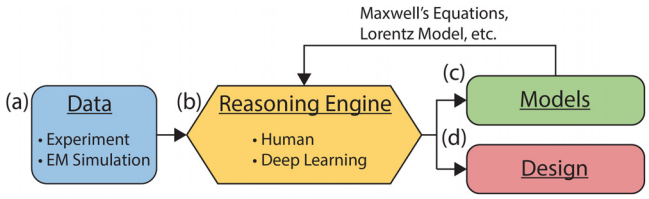

FIG. 39. Illustration depicting a conventional scientific workflow wherein a human scientist acts as a reasoning engine, denoted (b); in this capacity, a scientist synthesizes empirical data, denoted (a), and existing scientific knowledge, in the form of models/theory, denoted (c), to develop novel scientific models, or perform design of physical systems, denoted (d). In many modern branches of science, empirical data are often collected through both physical experiment and electromagnetic (EM) simulations. The promise of deep learning is to automate the process of reasoning that is currently fulfilled by humans; however the reasoning capabilities of deep learning are currently far more limited. Note that, in general, the relationships between these components can be more complex than indicated here.

approximation methods were also developed to solve more complex problems, and these are generally termed high frequency methods, to which geometrical and physical optics belongs.[1052]

A key component of scientific inquiry is empirical observation, or *data*, which is crucial to guide theoretical investigations, and ultimately to validate them. Prior to the advent of computational EM solvers (CEMS), the primary means to collect data were the construction of physical experiments, which was relatively slow and costly, severely limiting progress. The computational era began in the 1940s with the development of the computer, but it was not until the 1960s, when various numerical methods emerged to solve Maxwell's equations, that the field really gained momentum. The CEMS developed were those of the finite-difference time-domain (FDTD) method,[1053] the method of moments (MOM),[1054] and the finite element method (FEM).[1055] In contrast to physical experiment, these approaches essentially allowed scientists to conduct experiments by writing and executing software, which is generally much faster and cheaper.

The evolution of CEMS has continued in earnest, and in the past few decades, we have witnessed the emergence of many accurate and efficient options. Today, we have commercial computational EM tools

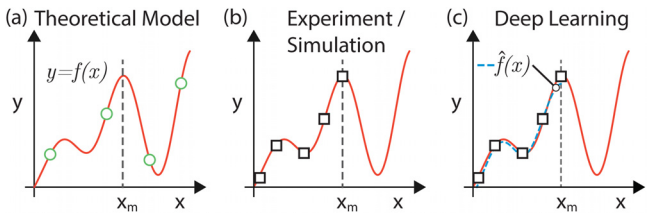

FIG. 40. Illustration depicting the relationship between DL, theoretical findings, and experimental results (e.g., CEMS). Given some EM system we often have experimental parameters x, and observed experimental results y. (a) The true relationship underlying these data (red curve), denoted $y = f(x)$, can sometimes be uncovered via observation (open green symbols) and theoretical deduction. (b) Physical experiments and CEMS (open black squares) can be used to sample this function, providing pairs of data (x, y) for specific settings of x. (c) Deep learning methods can utilize empirical data (open black squares) to automatically construct models, denoted $\hat{f}$ and shown as the dashed blue curve, that accurately approximate the true underlying relationships (solid red curve) over the domain of available data.

available including full-wave approaches based on either integral equations (both time and frequency domain) or on differential equations (both time and frequency domain), or alternatively high frequency methods based on either EM fields (geometrical optics) or currents (physical optics). With modern commercial software, programs can be created much faster, and a single program can be used to collect data over a wide variety of physical settings.

The last decade has witnessed the emergence of deep learning (DL), which has received significant attention in the literature. In the modern academic milieu, it is reasonable to ask whether this attention is justified. To address this question, it is helpful to understand the fundamental role of DL in the EM scientific workflow: for example, how does DL relate to CEMS, human scientists, and the theoretical models they develop? DL is a specific type of artificial intelligence (AI) technique, and the long-term objective of AI is to enable machines to achieve human-like intelligence.[1056] In this regard DL occupies the same role in the scientific process as human scientists, which is to reason about empirical observation and existing knowledge (e.g., theory and models) to develop new knowledge, or to perform EM material or device design. This broad scientific workflow is illustrated in Fig. 39. The prospect of automating the role of humans—or even enhancing it—using machines is enticing, and understandably garners tremendous attention.

While DL represents an important step toward automated reasoning, at present, DL methods are quite limited in their reasoning capabilities. In their current form, the term "Deep Learning" most often refers to a collection of machine learning (ML) methods—namely, deep neural networks (DNNs)—which are broadly designed construct models that *approximate* the relationships present in observed data, e.g., CEMS.[1057,1058] This capability is illustrated and described in Fig. 40. DL does, therefore, automate an important reasoning task that has historically been accomplished by human scientists—building models of the physical world from data. However, DNNs do not efficiently integrate knowledge of the physical world, or perform deductive reasoning. Nonetheless, DL does present a significant advance over prior machine learning approaches in nanophotonic metasurfaces and has enabled the analysis of far more complex materials than previously possible,[1059–1062] justifying some of the attention they have received.

Figure 40 depicts the current state of EM design approaches, including (a) theory, (b) computational EMs (simulation), and (c) deep learning. A theoretical approach strives to represent observations mathematically, aiming for closed-form solutions or, less favorably, accurate approximations. In EMs, Maxwell's equations are derived from the experimental observations of Faraday, Ampère, Ørsted, Gauss, and others, and verify the soundness of this method. We depict this theoretical approach in Fig. 40(a) where the open green symbols are points of observations which have given rise to the exact theory, $y = f(x)$, represented by the solid red curve. We next consider an EM design problem where the theory is not known, i.e., no exact solution exists. This may arise due to the complexity of the problem or the incorporation of some newly discovered material. Although no exact solution to our problem exists, CEMS, which are based on Maxwell's equations, are able to model the problem accurately and we are able to determine $f(x)$ at some discrete values, shown as the black squares in Fig. 40(b). However, since CEMS are limited by computer memory and calculation time, the problem is usually restricted to some range, denoted by x_m in Fig. 40(b). The deep learning approach to EM design permits the

16 July 2024 09:29:41

© Author(s) 2024

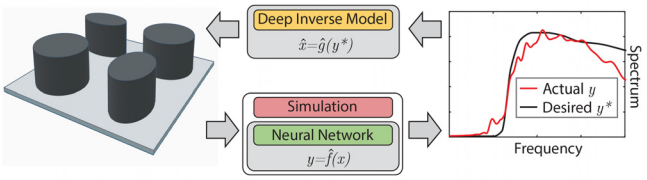

FIG. 41. Illustration of forward modeling (bottom) and inverse modeling (top) illustrated using a metasurface comprised of repeating 2×2 supercells of cylindrical resonators. Each resonator in the supercell has an adjustable geometric structure, denoted x in the main text. In forward modeling we build some mathematical model or algorithm, denoted $\hat{f}$, for computing the behavior of the system, denoted y, given some setting of x. One widely used method for forward modeling is computational simulation, however, in some cases we can dramatically accelerate forward modeling using a neural network. Using this acceleration, one can perform design by rapidly evaluating $\hat{y} = \hat{f}(x)$ for different candidate settings of x, and then comparing $\hat{y}$ to a desired system behavior, denoted y^*. In inverse modeling we build a model, termed $\hat{g}$, that can predict a setting of x that would yield a desired set of properties, denoted y^*. Deep Inverse Models are a class of DNNs that have been shown capable of directly making accurate inverse predictions $\hat{x}$ for complex metasurfaces.

determination of a surrogate model from data (often CEMS data), denoted $\hat{f}(x)$ which approximates the true function $f(x)$. In Fig. 40(c) the open black symbols represent the same x points used in (b) for simulation, but now they are used in the deep learning workflow to determine the surrogate function $\hat{f}$, represented by the dashed blue curve. The surrogate function $\hat{f}(x)$ is significantly faster to evaluate than performing CEMS. Past results have demonstrated that one evaluation of $\hat{f}(x)$ compared to one numerical simulation is nearly 10^6 times faster.

Next we discuss in greater detail where DL has been successful in EM materials, and the roadmap for realizing the greater potential for DL to automate human reasoning.

1. State of the art

Where is deep learning currently most successful? Although DL has been applied for a variety of purposes in EM materials, its *primary* success has been as an instrument to dramatically accelerate forward and inverse modeling. The goal of forward modeling is to uncover some, yet unknown, mathematical relationship of the form $y = f(x)$, that relates the parameters of an experiment, denoted x, to the corresponding measurements obtained from that experiment, denoted y. In the context of metasurfaces, x might quantify parameters such as a metasurface geometry (e.g., radii and height of cylinders), its bulk construction material, or the illumination of the material; similarly, the observations encoded in y might include electric/magnetic field measurements, or absorption,[1063] reflection,[1064] transmission[1065] spectra, measured at a specific frequencies. On the other hand, the goal of inverse modeling is to construct some model of the form $x = \hat{g}(y)$, wherein we can provide some desired experimental observation, and then have the model efficiently produce the experimental parameters that would give rise to those observations. These two basic objectives are illustrated in Fig. 41. We next explain how forward and inverse modeling have been utilized EM metasurfaces, to important effect.

Forward modeling. DL accelerates forward modeling by *automating* the process of uncovering f from observational data. In practice DL is usually implemented with some type of DNN which is essentially a parameterized function, denoted $\hat{f}_\theta$. The parameters of the DNN are denoted θ and they influence the relationship between the input to the DNN and its output, so that $\hat{f}_\theta$ can be made to accurately approximate a wide variety of complex functions depending upon the settings of θ. To approximate a forward function, DNNs assume the availability of N empirical observations of the form $D = (x_i, y_i)_{i=1}^N$, which is typically procured by CEMS in EM applications, and where N may vary substantially across applications. The DNN is then "trained" to approximate the relationship between x and y by iteratively adjusting the parameters θ in a way that tends to shrink the error between predictions made by the DNN, denoted $\hat{y} = \hat{f}(x)$ and the true setting of y associated with the input setting provided to the DNN, x. In other words, $\hat{f}(x_i) \approx y_i$ for most of the $x_i \in D$. Given a large enough DNN (i.e., enough adjustable parameters), it has been shown that a DNN can approximate any underlying function to an arbitrary degree of accuracy.[1066,1067] In practice however, the accuracy of the model obtained may vary depending upon many factors (e.g., the available training data, N, or the complexity of the true underlying function that we wish to approximate).

Once the model $\hat{f}$ is constructed, it can be used to make accurate predictions for settings of x that were not present in D. This process is essentially regression analysis, for which there are many techniques. However, in contrast to previous approaches, DL has been demonstrated to often produce much more accurate approximations for challenging high-dimensional systems that exhibit complex (e.g., highly non-linear) relationships between x and y. Furthermore, and crucially, DL models have been shown in some cases to make predictions for novel settings of x at a speed that is several orders of magnitude faster than CEMS, e.g., by a factor of nearly 10^6. Therefore, using $\hat{f}(x)$, it is possible to rapidly explore the behavior of the system under study, which can aid scientists with theoretical investigations.

In addition to scientific investigation, forward modeling can also be used to accelerate design. In contrast to modeling, the process of *design* involves the manipulation of experimental parameters to achieve a certain system behavior. In other words, we wish to find some setting of x that will result in a particular desired setting of y. A common design strategy involves using a forward model to evaluate different candidate settings of x until one is found that produces the desired behavior. For advanced materials CEMS is often the only available means of evaluating the properties of arbitrary settings of x. CEMS is often computationally expensive however, creating a major bottleneck to design. In such cases DL can be utilized to build a fast

TABLE I. A list of three major components for construction of a deep neural network: Data, Architecture, and Loss. The NN architectures shown are some of the most commonly employed in photonic metasurfaces and include: residual neural network (RNN), convolutional neural network (CNN), multi-layer perceptron (MLP), graph neural network (GNN). Here the Transformer is a broad class of neural networks with similar applicability as MLPs, and Generative Models are NNs that can be trained to create novel instances of data that resemble those from some collection of data.

Data	Architecture	Loss function
Experiments	RNNs	Error metric, e.g. MSE
Simulations	CNNs	Differential equation
	FCNs	Algebraic equation
	GNNs	Complexity penalties
	Transformers	

16 July 2024 09:29:41

© Author(s) 2024

TABLE II. Examples of specialized DNN approaches to perform inverse modeling, often for the purpose of design.

Model	Type	Applications to AEM problems
Tandem (TD)	Deterministic	Liu *et al.*,[522] Ma *et al.*,[1068] Gao *et al.*,[1069] and Hou *et al.*[1070] So *et al.*,[1071] Long *et al.*,[1072] He *et al.*,[1073] and Xu *et al.*[1074] Ashalley *et al.*,[1075] Mall *et al.*,[1076] and Pilozzi *et al.*[1077] Phan *et al.*,[1078] Singh *et al.*,[1079] and Malkiel *et al.*[1080]
Mixture Manifold Networks (MMN)	Deterministic	Spell *et al.*[1081]
Genetic Algorithm (GA)	Optimization	Zhang *et al.*,[312] Johnson and Rahmat-Samii,[1082] and Deng *et al.*[1061] Forestiere *et al.*[1083] and Li *et al.*[1084]
Neural Adjoint (NA)	Optimization	Deng *et al.*[1085] and Peurifoy *et al.*[1086] Asano *et al.*[678] and Miyatake *et al.*[1087]
Variational Auto-encoder (VAE)	Probabilistic	Ma *et al.*,[1088,1089] Qiu *et al.*,[1090] and Kudyshev *et al.*[1091,1092] Shi *et al.*,[1093] Liu *et al.*,[1094] and Kiarashinejad *et al.*[1095]
Mixture Density Network (MDN)	Probabilistic	Unni *et al.*[1096,1097]
Invertible Neural Networks (INN)	Probabilistic	Ren *et al.*[1098]
Generative Adversarial Networks (GAN)	Probabilistic	Wen *et al.*[1099]

approximation to f, permitting a more efficient and effective design. Consequently, DL represents a powerful tool to accelerate this type of forward design procedure.[1100]

State-of-the-art DL most often takes the form of DNNs, which have a large number of free design choices, sometimes called hyperparameters, that must be chosen to suit the particular system under study. Some of the most important choices are the data utilized for training, the model architecture (i.e., what functional form does $\hat{f}$ or $\hat{g}$ take), and the loss function(i.e., what criteria is used to identify the "best" model during training). Fortunately, there are a number of highly effective choices for these hyperparameters depending upon properties of the problem, of which some are listed in Table I. The number of neural network hyperparameters is vast and we do not attempt to include an exhaustive list here. For the reader interested in learning more we refer to reviews on these topics.[1101–1104]

Inverse modeling. Despite the acceleration provided by DL, the forward design procedure can quickly become intractable for advanced photonic metasurfaces with many free design parameters (e.g., x is high-dimensional), or the number of candidate settings for each design parameter is large. Another powerful capability of DNNs is so-called inverse modeling, whereby a DNN utilizes data to build a model of the form $x = \hat{g}(y)$ with the property that $f(\hat{g}(y)) = y$; in other words, the DNN approximates the inverse of f. In principle then, a scientist can specify a precise set of desired EM properties, denoted y^*, and the DNN will produce the design that will yield those desired properties—a transformative capability depicted in the top path of Fig. 41. This approach essentially uses DL for regression, similar to modeling and forward design, except with the roles of x and y reversed. However, this reversal of roles introduces some significant technical difficulties for regression, such as the so-called non-uniqueness problem, where several different settings of x can produce the same desired setting of y^*. Non-uniqueness causes conventional DL methods to fail, however, substantial recent work has focused upon specialized DL models—termed deep inverse models (DIMs)—that can overcome these challenges. Recent studies have demonstrated that DIMs can be trained successfully to rapidly identify designs that achieve customized settings of y^*, and do so for highly complex EM material systems.[1098,1105]

There are various DIMs which have been applied to photonic metasurfaces and in Table II we list some of these models, their type, and references to associated studies. DIMs fall into three basic categories—namely *Deterministic*, *Optimization*, and *Probabilistic*. Broadly, each class of model represents a trade-off between computational cost (e.g., speed) and design accuracy. Optimization approaches initialize a large population of randomly chosen candidate solutions and then sequentially improve all of them in parallel—a computationally intensive process, but one that often achieves the highest design accuracies. Like Optimization methods, Probabilistic DIMs typically initialize a large set of candidate solutions, but rather than incrementally optimizing them, they try to make the quality of these initial estimates higher by learning a probability distribution of where good solutions are likely to exist, given some target y^*. These approaches are relatively fast because they avoid sequential processing, but they typically yield less-accurate solutions because their solutions are still randomly drawn. Deterministic methods attempt to learn a direct mapping from y^* to the appropriate design that will yield y^*. Consequently these approaches require just one evaluation of a DNN (e.g., for Tandem), or just a few evaluations in parallel (e.g., MMN), making them computationally fast. There are also hybrid methods that combine different types of DIMs, or combine DIMs with traditional optimization approaches (see review in Deng *et al.*[1061]) Further information about DIMs for photonic metasurfaces can be found in recent reviews of the topic.[177,1098,1106]

2. Future directions and outlook

Although DL has become a powerful tool to accelerate EM modeling and design, the long-term potential of DL is far greater. The future promise of DL, and AI more broadly, is to enhance and automate the role of human reasoning within the scientific process, as shown in Fig. 39. Currently however the reasoning capabilities of the most successful DL approaches—namely DNNs—are relatively limited

16 July 2024 09:29:41

© Author(s) 2024

compared to humans. Although there are several limitations of DNNs compared to humans, we highlight two specific limitations that are especially influential: (i) world modeling, and (ii) deductive reasoning.

World modeling refers here to the ability of an intelligent agent (e.g., a DNN) to represent and utilize knowledge of objects in the world, and their known relationships (e.g., physical laws), when reasoning. For example, if we wish to build a model relating the position of a vehicle on a road, y, as a function of time, x, it is helpful to know that the vehicle is powered by a combustion engine, thereby limiting its maximum speed and rates of acceleration. This knowledge immediately and dramatically reduces the number of potential explanatory models, yet building a DNN that can represent and utilize such information when training (i.e., building a model) still requires substantial time of a human expert, and often still doesn't fully leverage this information. Consequently DNNs often lack world models altogether, or they are simplistic and limited in scope.

Deductive reasoning refers here to the ability of an intelligent agent to use existing knowledge to draw valid conclusions about the world via logic. In the context of physics, deductive reasoning might include, for example, the use of mathematics to deduce closed-form solutions to Maxwell's equations under specific conditions. Another example may be that field measurements from a EM material must obey Maxwell's equations, and therefore any exact model of the system [e.g., of the form $y = f(x)$] must also obey Maxwell's equations. Although DNNs sometimes incorporate the results of human deductive reasoning (e.g., so-called physics-informed neural networks, or Lorentzian Neural Networks) they do not explicitly perform deductive reasoning. Like world modeling, deductive reasoning can be used to dramatically reduce the number of valid models of observed data, and also ensure certain levels of generality.

Near-term research directions. The most acute consequence of DNN's limited reasoning capabilities is that it limits their *generalization* capabilities; that is, their ability to make inferences (e.g., predictions) for scenarios (e.g., inputs) that were not present in their training data. Consequently, DNNs typically require substantial quantities of training data to build accurate models, which is problematic because these data are typically generated by expensive and/or time-consuming CEMS, and it must be generated independently for each unique problem (i.e., physical system) under consideration. Furthermore, the quantity of data required to achieve a particular level of modeling accuracy grows rapidly with respect to the complexity of the problem under consideration (e.g., the dimensionality of x and y, and the nonlinearity of f).[1107] At the same time, CEMS is also often more computationally intensive for such problems, limiting the quantity of data that can be obtained. Therefore, data inefficiency represents a major limitation of DL, undermining its value even in applications where it has been highly successful. Importantly it also makes DL completely impracticable for many important open problems in EM, such as those involving multi-physics or multi-scale problems.[1108] A variety of research is under way to improve the data efficiency of DNNs. These approaches are relatively superficial, in the sense that they do not significantly improve fundamental reasoning capabilities of DNNs, but they are also often more tractable, and have demonstrated some effectiveness:

- *Physics-guided learning:* These approaches try to utilize known physical laws or principles to guide the interpretation of empirical data, ultimately reducing the amount of data needed. For example, so-called physics-informed neural networks (PINNs) encourage any DL model to be consistent with Maxwell's equations.[1109]
- *Transfer and incremental learning:* These approaches attempt to build upon knowledge gained from one problem—perhaps a problem with substantial quantities of data—and leverage it to aid the construction of a model for a new problem. Transfer learning is widely used in the broader DL community, and it has also recently been shown to dramatically reduce the quantity of data needed to solve novel metasurface problems as well.[1110,1111]
- *Active learning:* These approaches attempt to identify data points that are most "informative," in the sense that the model can improve its accuracy faster, and thereby use less total training data.[1112]
- *Modeling ill-posed problems:* This research area is unique to inverse modeling, where non-uniqueness is a major obstacle to building inverse models. This is an active and important area of research for ultimately building effective deep inverse models.[1098]

Long-term research directions. Long-term DL research should aim to endow DL methods with more sophisticated reasoning capabilities, such as general World Modeling and Deduction. Achieving these goals represents a tremendous challenge; however, some progress is being made within the AI research community. Here we list three promising areas of current research that may endow DL with these two more sophisticated reasoning capabilities.

- *Large language models (LLMs):*[1113,1114] LLMs have recently demonstrated the capability of representing human language, and using it to perform some basic reasoning. If successful, LLMs represent one way to provide DNNs with knowledge about physical systems, and potentially perform deductive reasoning.
- *Neuro-symbolic models:*[1115–1117] These approaches attempt to combine the existing capabilities of DNNs (e.g., data-driven models) with powerful existing symbolic reasoning engines, thereby providing DNNs with the capability to apply deductive reasoning.
- *Causal models*[1118,1119] These approaches attempt to use deductive reasoning to help DNNs to distinguish between spurious correlations and causal relationships present in data.

Although we highlight these areas of DL research, it is noteworthy that there are many important active areas of DL research (e.g., interpretability)

Outlook. Since its emergence roughly a decade ago, DL has had a significant impact on many fields, including EM metasurfaces. Among their successes, DNNs have been especially useful for utilizing empirical data (in particular from CEMS) to build computationally efficient approximate models that can dramatically accelerate the modeling and design of complex photonic metasurfaces. The capabilities of DNNs are quite robust for these tasks, and they have quickly become pervasive within the EM research community. Consequently, we expect DL, serving in this capacity, to become an important tool for modeling and design of EM materials, alongside other tools such as theory and CEMS. Despite their impact however, DL represents a relatively rudimentary form of reasoning about empirical data. The long-term potential of DL, insofar as it is an AI technique, is tremendous. The long-term objective of AI is endow machines with human-level intelligence. Currently, DL fundamentally lacks important reasoning capabilities of

16 July 2024 09:29:41

© Author(s) 2024

humans, for example, explicit world modeling and deductive reasoning. If DL or other AI techniques can be endowed with these more sophisticated forms of reasoning, it may result in much greater advances than has yet been provided by DL. Furthermore, DL possesses some advantages over humans; specifically, DL possesses substantially greater computation speed and memory capacity. Consequently, upon possession of human-like reasoning capabilities, it may also dramatically accelerate the rate at which such reasoning is done, considerably accelerating science. Although it is unclear how quickly DL and AI will progress, important inroads have been made toward tackling some of the aforementioned reasoning limitations it possesses (e.g., with LLMs, and neuro-symbolic models). Given the tremendous potential impact of advances in AI, and the commensurate investment in its development, we anticipate that it will be an increasingly important area of research within EM metasurfaces.

ACKNOWLEDGMENTS

W.J.P. and J.M.M. acknowledge support from the Department of Energy under U.S. Department of Energy (DOE) (No. DESC0014372).

XIX. COMPLEX-VALUED SINGULARITIES FOR METASURFACE DESIGNS

Aloke Jana, Zijin Yang, Rémi Colom, Qinghua Song, and Patrice Genevet

patrice.genevet@mines.edu

Optical singularities are points at which a physical quantity, such as the phase, polarization, polarization ellipticity, etc., is not defined, but around which this same physical quantity can take almost any value. This latter property is very beneficial for designing photonic devices with desired optical response. Moreover, singularities are ubiquitous in nanophotonics as they generically occur when varying at least two optical or geometrical parameters of the system. Here, we present approaches to design nanophotonic building blocks with desired optical responses via singularity position engineering. In particular, we show that the control of the positions of zeros and poles of optical response functions (e.g., reflection, transmission coefficient or scattering, and Jones matrices), the so-called singularities, can be used to design optical metasurfaces with desired amplitude and phase behaviors. Additionally, breaking the in-plane symmetries of the metasurface is shown to achieve a phase singularity for only one circular polarization state, while its orthogonal counterpart remains unmodulated, thereby opening new avenues for the information multiplexing with nanophotonic designs. Sharing similarities and inspiration from established works in signal processing and control theory, it is expected that the control of the position of complex-valued singularities in the "pole-zero complex-plane," for example relying on symmetries, would provide new design methodologies in photonics.

A. Introduction

Optical singularities refer to points or regions, either in the physical or parameter space, where certain optical or electromagnetic properties become undefined within the vicinity of steep gradients, as illustrated in Fig. 42. In ray optics, singularities manifest as points or

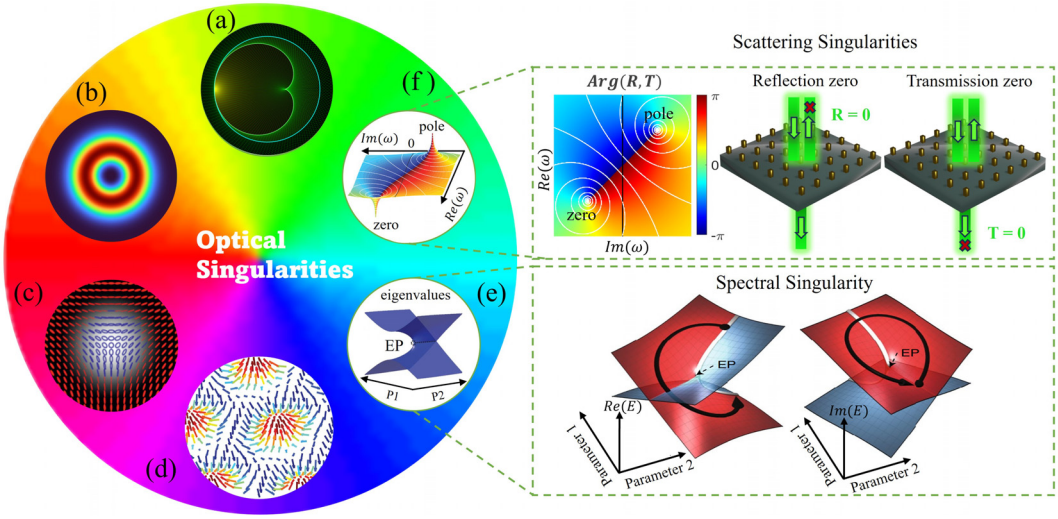

FIG. 42. Optical singularities and their topological features. (a) Depiction of a catacaustic formed by a circle with the source positioned on the circle. (b) Vortex beam associated with the phase singularity of the complex scalar wave, (c) polarization singularity of the vector beam, (d) optical skyrmion lattice, (e) exceptional points: depiction of the topological features of non-Hermitian systems linked with the degeneracy of the eigenvalue spectrum. Inset illustrates the real and imaginary parts of the eigenvalue spectrum in the parametric space. (f) Scattering singularities featuring a zero-pole pair of the complex reflection/transmission coefficients. Inset displays the phase profile of reflection/transmission coefficients, along with a simple illustration of the reflection/transmission zero condition of the scattering processes. Figure (a) reproduced with permission from "Catacaustics, Resultants and Kissing Conics — Greg Egan," https://www.gregegan.net/SCIENCE/Catacaustics/Catacaustics.html (2012). Copyright Author(s);[1153] (c) reproduced with permission from Copyright Hindawi Publishing Corporation;[1129] (d) reproduced with permission from Tsesses *et al.*, Science **361**, 993 (2018). Copyright 2018 AAAS;[1130] (e) reproduced with permission from Miri and Alu, Science **363**, eaar7709 (2019). Copyright 2019 AAAS;[39] (e) reproduced with permission from Ozdemir *et al.*, Nat. Mater. **18**, 783 (2019). Copyright 2019 Nature Publishing Group;[1136] and (f) reproduced with permission from Colom *et al.*, Laser and Photonics Rev. **17**(6), 2200976 (2023). Copyright 2023 Wiley-VCH.[1154] Copyright remains with the respective publishers.

16 July 2024 09:29:41

© Author(s) 2024

lines of extreme light intensity (caustics) known as optical catastrophes. Meanwhile, phase singularities can be found in complex scalar wave fields as a form of vortices, wavefront dislocation, or nodal lines.[1120–1124] This ensemble of phenomena belongs to the realm of Singular optics. One very familiar example of a singular optics phenomenon is the existence of Laguerre Gaussian beams having zero intensity lines along the optical axis and a helical phase front associated with an intrinsic orbital angular momentum.[1125–1127] Incorporating the vector nature of EM waves gives rise to additional polarization singularities.[1128] These polarization singularities can manifest as singularities in one or more parameters of the polarization ellipse, such as the azimuthal angle and ellipticity angle, resulting in features like C points and L lines.[1129] Skyrmions are the stable topological defects of the three-dimensional vector field that exhibit promising applications in the domain of magnetic storage and spintronics. Similar possibilities, i.e., optical information, transfer, and storage arise in the realm of the photonic system by utilizing the topological properties of three-dimensional EM waves.[1130] Over the decades, singularities in optical systems have been studied extensively in different scenarios starting from the seminal work "Dislocation in wave trains" by Berry and Ney to "Observation of the optical mobius strips."[1123,1131–1135] In addition, recent advancements of spectral singularities associated with non-Hermitian systems have led down to fertile ground, revolutionizing various fundamental and technological aspects.[39,1136–1139] It's well known that a closed and conservative system governed by Hermitian Hamiltonian exhibits real eigenvalues with orthogonal eigenvectors due to its unitary evolution nature. Instead, open and non-conservative systems, described by non-Hermitian Hamiltonians, exhibit complex eigenvalues and non-orthogonal eigenvectors. Non-Hermitian systems possess many features with no counterpart in Hermitian systems. For example, exceptional points, a new type of degeneracies, may occur in non-Hermitian systems. They correspond to the degeneracy of two or more eigenvalues along with the coalescence of their associated eigenvectors. These EPs are linked with sharp transitions in the eigenvalue spectrum, capable of dramatically altering the response of the system. Exceptional points are very important in parity-time symmetric systems as they are associated with spontaneous symmetry breaking. They thus separate regions of the parameter space where the Hamiltonian spectrum is real from regions where the eigenfrequencies occur in complex conjugated pairs.[112] Interestingly, parity-time (PT) symmetric systems can display entirely real eigenvalue spectra despite being governed by non-Hermitian Hamiltonian. While EPs are initially discovered in the context of quantum mechanical Hamiltonians, realizing EPs experimentally in quantum systems poses significant challenges. However, optical and photonic systems have emerged as promising platforms for exploring non-Hermitian physics. This is primarily due to the controllable introduction of optical gain and loss—non-conservative elements in these systems. Given their design versatility, metasurfaces (MSs) represent a convenient approach to study and validate non-Hermitian concepts in photonics. MSs are two-dimensional artificial structures consisting of subwavelength unit cells which exhibit peculiar electromagnetic responses, not achievable in natural materials. Most importantly, the response of MSs building blocks, i.e., nanostructures, are characterized by the scattering matrices, which are inherently non-Hermitian. The non-Hermitian nature of metasurfaces greatly influences their scattering properties. This requires to look at the properties of coefficients of the scattering, reflection or transmission coefficients in the complex-frequency plane. Phase singularities of these coefficients such as zeros and poles play a fundamental role. In addition to the position of single zeros, two or more of these quantities can merge in the complex plane, potentially exhibiting EP behavior. This characteristic also holds true for the conventional Jones matrix, which describes changes in the polarization state between input and output channels. Therefore, the non-hermicity of the scattering/Jones matrices provides a ubiquitous tool to control and manipulate the properties of EM waves. By tuning the geometry and changing the composition of the individual unit cells, anomalous light propagation or scattering effect, including unidirectional propagation, polarization and diffraction control, maximum helical dichroism, ultrasensitive sensing and biosensors, imaging, and surface waves, can be studied.[5,880,1140–1151] Interestingly, even the most basic zeros of the system response functions, such as the complex reflection/transmission function, also exhibit phase singularities associated with non-trivial topological charge of $C = \frac{1}{2\pi}\oint_{\gamma} \nabla(\phi) d\omega$, where ϕ is the response phase function and the integration is carried out along a path γ enclosing the singular zero response point in two-dimensional parameter space. It turns out that the latter reflection and transmission zeros play a leading, and often neglected, role in the design of photonic systems, including MSs.[1152]

This roadmap article focuses on these recent developments, drawing some of the perspectives and implications offered by the complex-valued zeros and EPs singularities of transfer functions for the design of innovative photonic systems. This manuscript is organized into three sections. In Sec. XIX C, we begin by introducing the basic notion of zeros in electromagnetic quantities and elucidate the impact of the position of singularities in the complex frequency plane, such as zeros and poles, emphasizing the influence of symmetries on altering system responses. We discuss two examples of MSs designs relying on the complex-valued singularity approach in reflection and transmission. In Sec. XIX D, we address a new wavefront engineering mechanism—topology-protected 2π phase accumulation for a specific polarization channel by encircling EPs in the parameter space. Furthermore, the construction of EP pairs is harnessed to achieve unidirectional full-color vectorial holography employing a wavelength-multiplexing scheme. Finally, in Sec. XIX E, we delve into the potential future prospects of complex-valued singularities particularly higher-order ones. We address a novel phase excursion mechanism associated with the zero mode conversion in parametric space and the designing of ingenious toolboxes that would exploit the control theory methodology for nanophotonics design.

B. Designing metasurfaces according to the position of complex-plane zero singularities

MSs may be considered as linear systems which transform inputs into outputs. These transformations are mediated by transfer functions or matrices which generally depend on the frequencies and directions of the input signals. Depending on the situation and the type of MS to be designed, the transfer function can be the reflection or transmission coefficient or even the $S-$ or the Jones $J-$ matrix. Designing a MS often amounts to looking for the right set of geometrical and optical parameters allowing one to obtain the desired amplitude and phase of the transfer function for a given frequency or an interval of frequencies. One can therefore take inspiration from other fields concerned with the design of linear systems such as electronics or control

16 July 2024 09:29:41

© Author(s) 2024

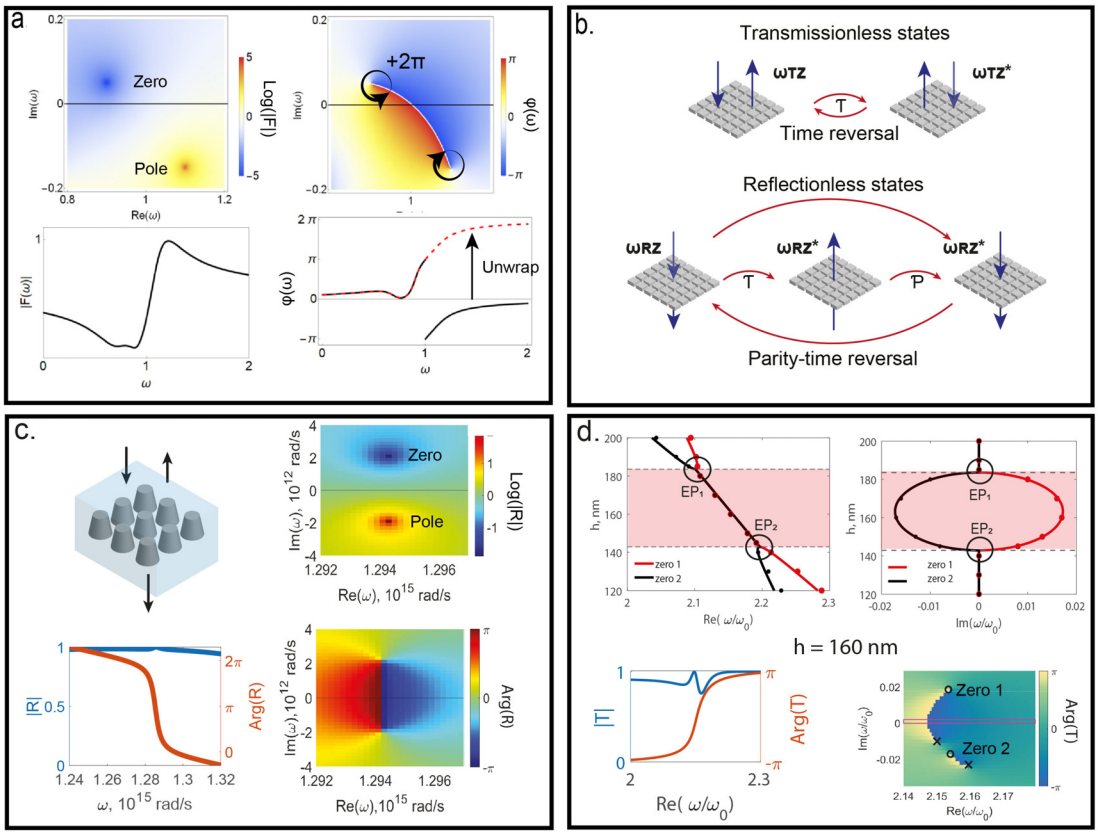

FIG. 43. (a). Behaviors of the amplitude and phase of a function possessing a zero and a pole in the complex frequency plane (top) and on the real axis (bottom). (b). Symmetries of transmissionless (top) and reflectionless states (bottom). (c). Silicon nanocone MS possessing a reflection zero and pole complex conjugated and whose amplitude remains large and constant while the phase varies from 0 to 2π. (d). (Top) trajectories of a couple of transmission zeros of a Sb_2S_3 nanocube MS as the height of the nanocubes h is varied. At two degeneracies of the two zeros, there is a transition between a situation where zeros are real and one where they are complex conjugated. (bottom) At $h = 160$ nm, one zero is in the upper part of the complex plane and almost complex-conjugated of a pole leading to a high amplitude and a variation of the phase between 0 and 2π for the transmission coefficient. Figure (b) reproduced with permission from Colom *et al.*, Laser and Photonics Rev. **17**(6), 2200976 (2023). Copyright 2023 Wiley-VCH;[1154] (c) reproduced with permission from Mikheeva *et al.*, Optica **10**, 1287 (2023).Copyright 2023 OSA;[40] (d) reproduced with permission from Colom *et al.*, Laser and Photonics Rev. **17**(6), 2200976 (2023). Copyright 2023 Wiley-VCH.[1154] Copyright remains with the respective publishers.

engineering to describe and design MSs.[1155] In these fields, it is common to look at the analytic continuation of response functions $F(\omega)$ of the systems in the complex-frequency plane. As discussed above, the necessity of analyzing the response at complex frequencies is rooted in the non-Hermitian nature of scattering processes used for the design of metasurfaces, particularly the resonant ones that suffer from scattering losses, and also sometime, of additional absorption losses.

Of particular importance are the zeros and poles of the response functions which generally occur in the complex-frequency plane. As displayed in Fig. 43(a), simple zeros and poles are a given type of topological defects at which the phase is singular and around which the phase behaves like a vortex with a 2π winding counterclockwise around zeros and clockwise around poles (more generally it winds $2n\pi$ times for nth order phase singularities). Their topological charge C, as defined earlier, is, respectively, $+1$ and -1 when choosing a contour γ encircling the singularity in the complex frequency plane. In this study, the phase winding direction adheres to the right-hand rule, where 2π increase in the phase is defined as counterclockwise. The well-defined sense of rotation of the phase comes from the fact that we consider analytic functions.[1126,1156] These phase singularities bring fundamental deeper topological aspects to the study and design of MSs. In this section, we will discuss approaches to shape the optical response based on the control of the relative positions of these phase singularities in the complex-frequency plane. We will also discuss the relationship between zeros of transmission, reflection, and $S-$ matrix coefficients and the symmetries of MSs. Finally, we will provide two examples of MS designs that rely on this approach, one in reflection and another in transmission.

The analytic continuation in the complex-frequency plane of response functions $F(\omega)$ can be expanded according to the Weierstrass expansion[1157,1158] depending on both zeros $\omega_{z,n}$ and poles $\omega_{p,n}$ of the response functions,

$$F(\omega) = A\exp(iB\omega)\prod_n \frac{\omega-\omega_{z,n}}{\omega-\omega_{p,n}}. \quad (9)$$

16 July 2024 09:29:41

© Author(s) 2024

It is well known that $\omega_{p,n}$ generally occur in the lower part of the complex plane [for a $\exp(-i\omega t)$ time convention] in passive photonic systems because of causality. However, a special occurs for the bound state in the continuum (BIC), poles can occur at real frequencies. To preserve energy conservation, this can only occur when they merge with a zero.[141]

Zeros may on the contrary occur at any position in the whole complex plane. Depending on the positions of zeros, the variations of the response functions display different behaviors as a function of the input frequency. To illustrate this, let us first consider the case of a single zero-pole pair in the expansion (9) with $A=1$ and $B=0$, $i.e. F(\omega) = \frac{\omega-\omega_{RZ}}{\omega-\omega_P}$. It has been shown in Ref. 1156, that when the zero is in the lower part of the complex plane, there is generally a dip in the amplitude of the response function and the phase varies only on a small phase interval (usually smaller than π). When the zero is on the real axis, the response function cancels out for a certain frequency and as a result, there is a π phase jump. Eventually, as illustrated in Fig. 43(a), when there is a zero in the upper part of the complex plane, the phase spans the full $[0, 2\pi]$ interval as the frequency is varied passing across the line separating the zero-pole pair. This property is better evidenced when the phase is unwrapped. Moreover, if the zero becomes complex-conjugate of the pole, one obtains a similar response as a Gires–Tournois etalon,[40,1159] i.e., a constant and unitary amplitude alongside with a 2π phase variation. This shows that one can use the position of zeros and poles of response functions as a design methodology to address MS with the desired response in both amplitude and phase.

To this end, it is necessary to have a good understanding of the rules constraining the positions of zeros in the complex-frequency plane. These constraints are related to the symmetries of the MS. It is for example well known that time-reversal symmetry imposes that zeros of the $S-$ matrix coefficients are complex-conjugated of poles for lossless passive systems. Let us consider the symmetries governing the positions of transmission and reflection zeros. These symmetries are illustrated in Fig. 43(b) for normal incidence for transmission zeros (top) and reflection zeros (bottom). Delving into the scenario of a passive, lossless MS with a transmission zero at the frequency ω_{TZ}, the time-reversal transformation leaves the MS invariant while causing a reversal of momenta in the incident and reflected waves. Consequently, the time-reversed counterpart of a transmissionless state is also a transmissionless state. As time-reversal implies complex conjugation of frequency, one can conclude that a lossless MS possessing a transmission zero ω_{TZ} also possesses a transmission zero at the frequency ω^*_{TZ}. As a consequence, illuminating this device at normal incidence should display transmission zeros at real frequencies or pairs of complex-conjugated transmission zeros. This is reminiscent of eigenvalues of $PT-$ symmetric Hamiltonian in the unbroken and broken phases.[1160]

Regarding reflection zeros, their positions depend not only on the time-reversal symmetry but also on the mirror symmetry with respect to the median plane of the MS which will be called Parity $(P-)$symmetry in the following discussion. Let us consider a lossless MS possessing a reflection zero ω_{RZ}. Time-reversal transformation amounts to reversing the momenta of the incident and transmitted waves, and as a result, this MS also possesses a reflection zero for the light impinging from the other side at the frequency ω^*_{RZ}. If the MS also preserves $P-$ symmetry, it possesses two reflection zeros for light impinging from the same side at the frequencies ω_{RZ} and ω^*_{RZ}. Just like transmission zeros, reflection zeros are consequently either real or occur in complex-conjugated pairs. On the other hand, when $P-$ symmetry is broken, symmetry constrained are lifted and ω_{RZ} can be complex-valued. In fact, by breaking the MS $P-$ symmetry, one can control the coupling coefficients of its modes to the top γ_{Top} and the bottom γ_{Bottom}. From the temporal coupled mode theory, one finds that a zero and pole of the reflection coefficient of a lossless MS illuminated from the top with a resonance frequency whose real part is ω_0 take the following expressions:[40]

$$\begin{aligned} \omega_{\mathbf{RZ}} &= \omega_0 + i\gamma_{\mathrm{Top}} - i\gamma_{\mathrm{Bottom}}, \\ \omega_{\mathbf{P}} &= \omega_0 - i\gamma_{\mathrm{Top}} - i\gamma_{\mathrm{Bottom}}. \end{aligned} \tag{10}$$

It is thus clear that $P-$ symmetry breaking allows control of the imaginary part of reflection zeros and their relative positions to the poles.

Let us illustrate the usefulness of this insight for designing MSs with a desired optical response. To create optical components such as meta-deflectors or metalenses, it is necessary to use MSs whose response function amplitude is large to ensure a good efficiency of the component. It is also important that the phase of the response functions spans the full $[0, 2\pi]$ to be able to generate arbitrary phase gradients. As explained before, this condition on the phase requires to design structures to possess a zero in the upper part of the complex plane while the condition on the amplitude requires that this zero is complex conjugated of the pole. Let us show how to fulfill these conditions for a MS working in reflection and another working in transmission.

For the reflection case, it appears from the expression of reflection zeros and poles (10) that it is necessary to cancel out the coupling of the mode to the bottom channel to obtain complex conjugated zeros and poles. This condition is quite intuitive as the energy transmitted can be considered as loss altering the reflection-based MS efficiency. To achieve this condition, we considered in Ref. 40 a MS consisting of an array of silicon 600 nm high nanopillar with a period of 800 nm embedded in a medium with a homogeneous refractive index equal to 1.5. The symmetry was broken by reducing the diameter at the top D_{Top} of the pillar compared to the diameter D_{Bottom} at the bottom which is equal to 500 nm leading to a truncated cone geometry as shown in the top left of Fig. 43(c). For a ratio $D_{Top}/D_{Bottom} = 0.84$, γ_{Bottom} is almost zero for the resonance we consider and the zero and pole are consequently almost complex conjugated as can be seen in the right panels of Fig. 43(c). As a result, the amplitude of the reflection coefficient is almost unitary and the phase spans the full 2π interval as shown in the bottom left figure of Fig. 43(c).

The design of MS in transmission for normal incidence fulfilling the condition of zero-pole pairs which are complex conjugated is more challenging since the position of zeros does not depend on the spatial symmetries of the structure (as long as there is no polarization conversion). Yet, a solution exists for MSs working in the regime where zeros are complex-conjugated. This is in fact the underlying mechanism describing the physics of dielectric Huygens MSs.[362,1154] To illustrate this, we consider a MS consisting of an array of nanocubes of Sb_2S_3. The top figures in Fig. 43(d) show the trajectories of the real and imaginary parts of a couple of transmission zeros as the height of the nanodisks is varied. It appears that there are two distinct heights (≈140 and

16 July 2024 09:29:41

© Author(s) 2024

≈180 nm) at which transmission zeros are degenerated, this represents a specific type of exceptional points, previously dubbed scattering EPs.[1154,1161] In the height interval between these two degeneracies, the two zeros are complex conjugated while they are real outside this interval. As a result, one zero gets almost complex conjugated of a pole. The amplitude thus remains large while the phase varies from 0 to 2π as seen in the bottom plots in Fig. 43(d). Interestingly and unexpectedly, the nature of the 2π-phase modulation as a function of the real frequency is due to the crossing of the branch-cut connecting only one zero-pole pair, and it is not due to the sum of two resonances, as previously stated. The full phase modulation occurring here results from a spontaneous symmetry-breaking behavior, as previously discussed in the framework of topological photonics.[1162,1163] As shown herein, avoided crossing in non-Hermitian systems involves pairs of complex singularities. This behavior contrasts drastically with the more conventional avoided crossing of resonances in Hermitian systems.

C. Asymmetric full 2π phase engineering based on exceptional points in metasurfaces

EPs may manifest in more complex-valued linear operators that represent input-output conversion relationships, with the scattering matrix and Jones matrix being the most typical among them. Taking the second-order Jones matrix as an example, particularly under the circular polarization basis, EPs correspond to conditions for which only one of the off diagonal terms cancel out while the other remains

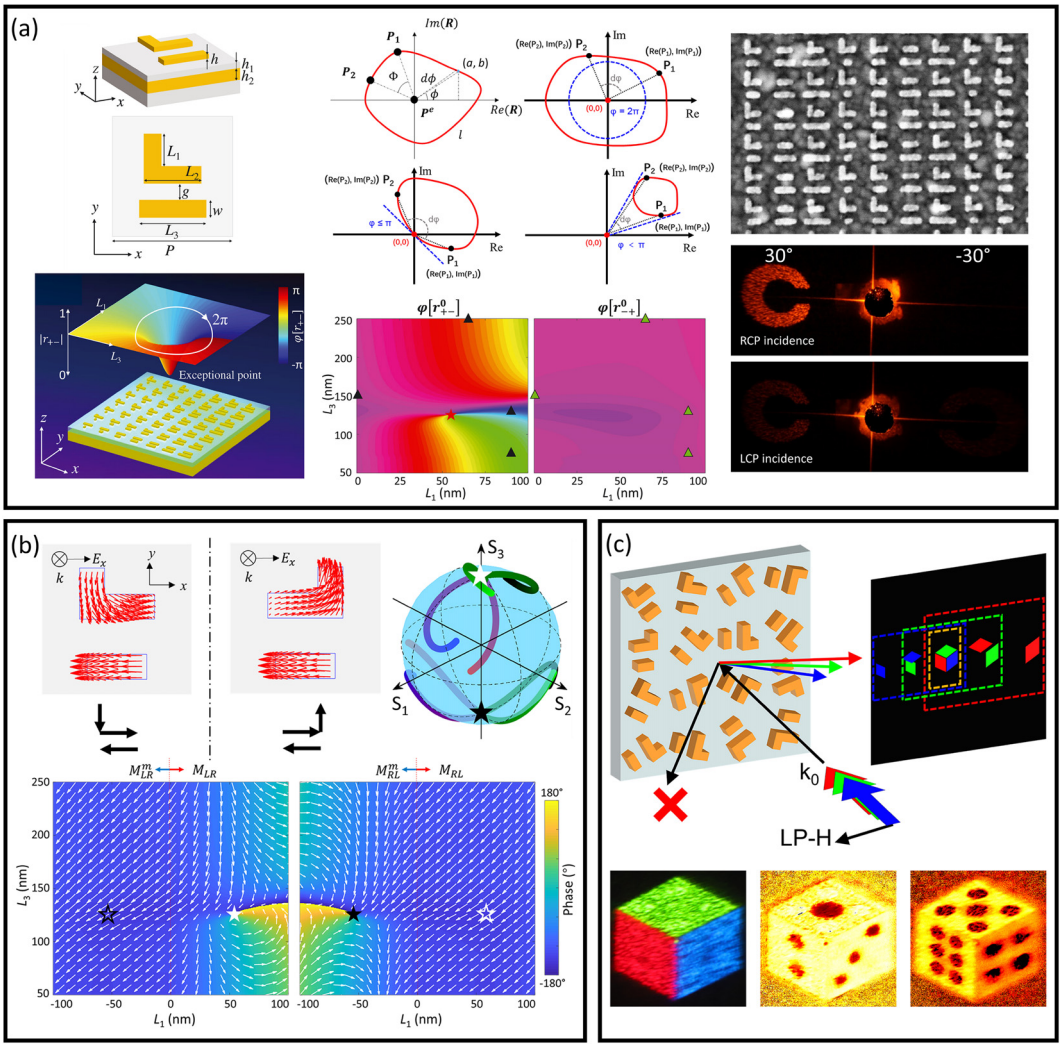

FIG. 44. Exceptional points manifested in Jones matrix systems for asymmetric phase engineering. (a) Schematic diagram and results of achieving topologically protected 2π phase by encircling exceptional points. (b) Construction of a pair of exceptional points with orthogonal polarization state using mirror-symmetry strategy. (c) Illustration of asymmetric full-color vectorial holography using exceptional point pairs. (a) Reproduced with permission from Song *et al.*, Science **373**, 1133 (2021). Copyright 2021 AAAS;[37] (b) reproduced with permission from Yang *et al.*, Nat. Commun. **15**, 232 (2024). Copyright 2024 Nature Publishing Group;[1165] and (c) reproduced with permission from Yang *et al.*, Nano Lett., **24**, 844–851 (2024). Copyright 2024 ACS.[1166] Copyright remains with the respective publishers.

16 July 2024 09:29:41

© Author(s) 2024

not null, i.e., $T_{+-} = 0$ and T_{-+} different from 0. This happens when the two eigen-polarizations of the Jones matrix coalesce and both correspond to the right or left handed circular polarization, where + and − represent left circular polarization (LCP) to right circular polarization (RCP), respectively. This signifies the suppression of the conversion channel from LCP to RCP, resulting in a zero or singularity point in the T_{+-} channel. There is consequently a reflection or transmission zero for one conversion channel but not the other which will be useful for information multiplexing. The construction and observation of such EPs have been presented in previous papers.[1131,1164] Building upon these works, some of the authors of the present paper have implemented a new type of functional device by harnessing the robust topological phase, namely, the exceptional topological (ET) phase, by encircling the EPs. Using a meta-structure as shown in Fig. 44(a), by manipulating the dimensions of the structure in two orthogonal directions, we can attain desired x- and y-polarized resonances, facilitating the construction of an EP of the Jones matrix associated with the cancelation of T_{+-} channel. Importantly, upon achieving a closed loop encircling the EPs in the parameter space, a phase accumulation of $\varphi = 2\pi$ will occur, which is attributed to the phase vortex existing around the singularity in the complex plane. Considering any point $\mathbf{R}$ on the complex plane, there is

$$P(\mathbf{R}) = Re(\mathbf{R}) + i\,Im(\mathbf{R}), \tag{11}$$

where $P(\mathbf{R})$ represents the position function and $Re(\mathbf{R})$ and $Im(\mathbf{R})$ represent the real and imaginary parts of $\mathbf{R}$, respectively. Therefore, the phase of $P(\mathbf{R})$ can be described as

$$\varphi[P(\mathbf{R})] = \arctan\frac{Im(\mathbf{R})}{Re(\mathbf{R})}. \tag{12}$$

When $\mathbf{R}$ moves continuously in parameter space from P_1 to P_2, the resulting accumulated phase can be given by the integral form:

$$\phi = \int_{P_1}^{P_2} \varphi[P(\mathbf{R})]\, d\varphi. \tag{13}$$

According to Fig. 44(a) and Eq. (13), it is evident that a phase accumulation of 2π solely occurs when the loop encircles the zero point (or singularity) while failing to achieve full-phase modulation when the singular point moves away from the loop. The above analysis underscores the distinctive nature of channel T_{+-}, differing from its cross-polarization channel T_{-+}, as the latter's nearly constant amplitude distribution lacks the topological protection of the singular points. Leveraging this unique property, we successfully achieved the decoupling of two circularly polarized lights. Specifically, upon incidence of the RCP beam, a holographic image of the letter "C" appears at the designed 30° angle, while under LCP incidence, no corresponding image appears. Furthermore, by combining the Pancharatnam–Berry (PB) phase and ET phase, more sophisticated information multiplexing can be realized. This new phase modulation mechanism, together with resonant scattering, guided mode propagation phase, and orientation-related phase retardation, enriches the optical control methods, while its ease of implementation and compatibility with other phase-control mechanisms also open the avenue for the application of topological phenomena in the optical wavefront modulation. However, due to the inherent asymmetric behavior caused by the handedness of EP, current EP systems are confined to operation within a specific circular polarization state and lack the versatility to engineer arbitrary states. A PB phase, equal but opposite in phase for both circular polarization states, is generally picked up by rotating polarization-converting optics. Operating specifically at an EP is shown to suppress one of the polarization-conversion channels, thus ensuring that PB-phase is encoded on only one of the polarization-conversion channels asymmetrically. To expand this specific asymmetric response of the EP photonic systems, researchers obtained the enantiomer S^m of the $\underline{L}$-shaped meta-structure (S) through a general mirror-symmetry strategy.[1165] As shown in Fig. 44(b), upon E_x incidence, the current distribution of the vertical arm in the meta-structure S^m switches the flow direction relative to its counterpart in S, resulting in the degeneracy point of the eigenstates flipping from RCP to LCP, corresponding to the north and south poles of the Poincaré sphere, respectively. Therefore, in the parameter space defined by the two arms of the meta-structure (L_1, L_3), a pair of singularity points induced by EPs are obtained, manifesting as zero conversion coefficients for the two channels of M_{LR} and M_{RL}^m at $(L_1, L_3) = (52\,\text{nm}, 119\,\text{nm})$. Interestingly, these two singularities give rise to phase vortices characterized by opposite topological charges in the parameter space. By judicious arrangements of structures S and S^m on the same MS, the resultant output polarization can be expressed as[37]

$$\langle S|S\rangle = A_+ e^{i\varphi_+}|+\rangle + A_- e^{i\varphi_-}|-\rangle, \tag{14}$$

where A represents amplitude and φ represents the corresponding phase. According to Eq. (14), coupling a pair of EPs breaks the limitation of the circular output polarization state. By adjusting the amplitude ratio and phase difference of the two rows of meta-structures, a full-polarization state covering the Poincaré sphere can be constructed while maintaining the unidirectional asymmetric imaging properties of the EP system. In brief, this work extends the application of EP to any arbitrary polarization state, surpassing the inherent limitations of the asymmetric response brought by EP to the system, and enhancing the potential for topological wavefront shaping applications. Furthermore, based on the construction of the aforementioned EP pairs, they have achieved a unique unidirectional full-color vectorial hologram by introducing a wavelength-multiplexing strategy,[1166] as shown in Fig. 44(c). Since the EPs can maintain the asymmetry of conversion in a wide wavelength range, the designed full-color vectorial hologram can still achieve optimized energy distribution. This asymmetric full-color holographic strategy based on EP pairs is expected to be widely used in more complex application systems such as information security and virtual reality.

D. Concluding remarks and future perspective

In conclusion, we have presented methods to design MSs to achieve various functionalities by engineering the positions of zeros of R, T, S, and J via parameter tuning. Wavefront engineering relies on strategically placing complex-valued singularities in the parameter space while exploiting exceptional points (EPs) of the Jones matrix enabling asymmetric full 2π phase modulation and full-color vectorial holography. However, it is crucial to clarify a common misconception about the EPs of the Jones matrix as discussed in Sec. XIX D. Although they exhibit singular behavior in the parametric space, they are not the actual singular points of the linear system itself. Recent studies highlight that the degeneracy of 2 zeros of the S-matrix is associated with EPs, particularly those linked to coherent perfect absorption (CPA), with phase-sensitive single-mode absorption.[1167] The attainment of resonant, absorbing, and CPA EPs in linear systems provides a versatile platform for controlling scattering responses. Additionally, the

16 July 2024 09:29:41

© Author(s) 2024

potential for full 2π phase modulation with nearly 100% transmittance has been demonstrated using a glide-symmetric bilayer MS.[1168] Recognizing the sensitivity of higher-order singularities to the perturbations, consideration of these in photonic systems can enhance sensitivity and robustness to their locations in the complex frequency plane. Notably, the geometric phase associated with spatial mode transformation would allow innovative implementation of the zeros in the mode conversion process. Akin to the exceptional ET phase in polarization channels, a novel phase-addressing mechanism can be realized by encircling the singular points of the conversion polarization coefficients in the parametric space. Drawing inspiration from the principles of control theory, wherein the placement of poles and zeros is crucial for shaping a system's behavior, including its stability, frequency response, and transient dynamic. This principle is similarly critical in nanophotonic device design, where the location of poles and zeros in the complex frequency plane profoundly influences properties such as transmission, reflection, and phase modulation, making it feasible to define the real-axis response and tailor nano-geometry based on the strategic placement of these topological singularities. Adopting control theory methodologies in photonics could thus pave the way to a new paradigm for designing nanophotonics devices.

XX. MULTIPOLAR DESIGN METHODS FOR METASURFACES

Carsten Rockstuhl, Karim Achouri, Andrey B. Evlyukhin, Ulrich Lemmer, and Ivan Fernandez-Corbaton

carsten.rockstuhl@kit.edu

An efficient, fast, and reliable framework for the theoretical description and the numerical analysis of the optical properties of metasurfaces is vital to their exploration from a fundamental science perspective and for their integration into applications. Here, we review one such framework that resides on the broader framework of a semi-analytical scattering theory. In that description, the incident and scattered fields are expanded into a multipolar series, and their relation is expressed by a matrix-vector product where the matrix is called the transition or T-matrix. Besides summarizing the state-of-the-art of the method, we elaborate on current research questions and oversee future developments.

A. Introduction

Computational means are nowadays indispensable for exploring the optical properties of metasurfaces.[94,1169] On the one hand, we can design them *in silico* according to predefined needs, achieving an optical response on-demand before any fabrication. In addition to being essential for the design, computational means are useful for obtaining insights into aspects notoriously challenging to measure. An example of the latter would be the vectorial details of the near-field distribution, an important quantity for nonlinear metasurfaces or those used for light management in solar cells. On the other hand, we can simulate the optical response of fabricated devices to explain measured quantities. Particularly for complicated metasurfaces, e.g., stacked ones, the measured response often does not correspond to what had been predicted before because of imperfections in the fabrication process. Here, simulations might help disclose the deviations and suggest what to improve in a further fabrication round.

The numerical analysis of optical metasurfaces is particularly successful because multiple numerical tools that solve the governing equations, i.e., the Maxwell equations, have been developed and equipped with suitable constitutive relations. These tools are mainly derived from the general field of numerical mathematics and rely on discretizing the Maxwell equations by finite differences or finite elements in the time or frequency domain.[1170,1171] Also, for strictly periodic metasurfaces, various grating algorithms to describe diffractive optical elements and photonic crystals[1172] were developed. However, while indisputably helpful, the direct numerical solution of Maxwell equations often complicates obtaining insights into the governing physics of metasurfaces. Especially for metasurfaces, assembled from what is frequently called the meta-atoms and analyzed in terms of the multipolar response induced in such meta-atoms, a discussion that is closer to scattering theory is suggested to be often superior.

This Perspective article aims to give an overview of the recent developments of such a framework for the multipolar description of metasurfaces. The framework tremendously relies on the notion of scattering theory.[1173] Initially, it puts the description of the optical response of the individual meta-atom into focus. It derives from that a set of insights into the optical functionality of entire metasurfaces. We emphasize that the optical response of the individual meta-atom is typically expressed by a T-matrix or generalized polarizabilities.[1174] While both expressions can be made interchangeable, they are different. For example, the T-matrix relies on a problem formulation in spherical coordinates, while the polarizabilities use Cartesian coordinates. Here, we start from the multipolar description using the T-matrix and establish the link to polarizabilities at a later stage.

B. State of the art

1. Theoretical framework of a multipolar description

The multipolar description of a metasurface has to start with the multipolar description of its meta-atom. In the framework of scattering theory in the frequency domain, we initially seek elementary solutions to Maxwell equations that arise from their separability in spherical coordinates.[1175] These vector spherical harmonics expand the incident and the scattered field from the meta-atom as

$$\begin{aligned}\mathbf{E}^{\mathrm{inc}}(\mathbf{r},\omega) &= \sum_{j=1}^{\infty}\sum_{m=-j}^{j} q^{e}_{jm}(\omega)\mathbf{N}^{(1)}_{jm}(\mathbf{r},\omega) + q^{m}_{jm}(\omega)\mathbf{M}^{(1)}_{jm}(\mathbf{r},\omega),\\ \mathbf{E}^{\mathrm{sca}}(\mathbf{r},\omega) &= \sum_{j=1}^{\infty}\sum_{m=-j}^{j} b^{e}_{jm}(\omega)\mathbf{N}^{(3)}_{jm}(\mathbf{r},\omega) + b^{m}_{jm}(\omega)\mathbf{M}^{(3)}_{jm}(\mathbf{r},\omega),\end{aligned} \tag{15}$$

where $\mathbf{N}^{(n)}_{jm}(\mathbf{r},\omega)$ and $\mathbf{M}^{(n)}_{jm}(\mathbf{r},\omega)$ are the vector spherical harmonics. These modes have well-defined frequency ω, angular momentum squared j, and angular momentum along a specific axis m. Physically, the fields with $j=1$ are dipolar fields, with $j=2$ quadrupolar fields, etc. We distinguish modes with electric parity $\mathbf{N}$ and magnetic parity $\mathbf{M}$. Finally, we distinguish between those vector spherical harmonics expanding the incident and the scattered field using the index $n=1$ and $n=3$, respectively. Instead of parity, a helicity base can also be chosen, especially if chiral light–matter interactions are at stake. The

16 July 2024 09:29:41

© Author(s) 2024

relation between the concatenated amplitudes expanding the incident field $\mathbf{q}$ and scattered field $\mathbf{b}$ from a meta-atom in a linear response is written as

$$\mathbf{b}(\omega) = \mathbf{T}(\omega)\mathbf{q}(\omega), \tag{16}$$

where the T-matrix $\mathbf{T}(\omega)$ had been introduced, which entirely characterizes the optical response of the meta-atom.[1176] For a sphere, the T-matrix can be built analytically as a diagonal matrix containing the Mie-coefficients. For an arbitrary shaped object, the T-matrix can be obtained numerically by multiple means.[1177] They all rely on exciting the meta-atom with different illuminations, computing and expanding the scattered fields into vector spherical harmonics, and reconstructing the T-matrix that links all the different incident and scattered field amplitudes determined numerically.

In the following, we discuss metasurfaces made from a periodic arrangement of identical meta-atoms.[1178] Disordered metasurfaces or spatially inhomogeneous metasurfaces can also be considered. However, they are covered in other perspective articles in this APL Roadmap. While considering an arbitrary chosen meta-atom to be the central one, we can write the field illuminating the particle as a superposition of the external illumination and the scattered field from all the other particles. By dropping the frequency argument, this can be written as

$$\mathbf{b} = \mathbf{T}\left(\mathbf{q} + \sum_{\mathbf{R}}{}'\mathbf{C}^{(3)}(-\mathbf{R})\mathbf{b}_{\mathbf{R}}\right), \tag{17}$$

where $\mathbf{C}^{(3)}(-\mathbf{R})$ are the lattice coupling matrices that convert the scattered field from meta-atom i into an incident field on the central meta-atom. The prime in the sum indicates that the central particle is

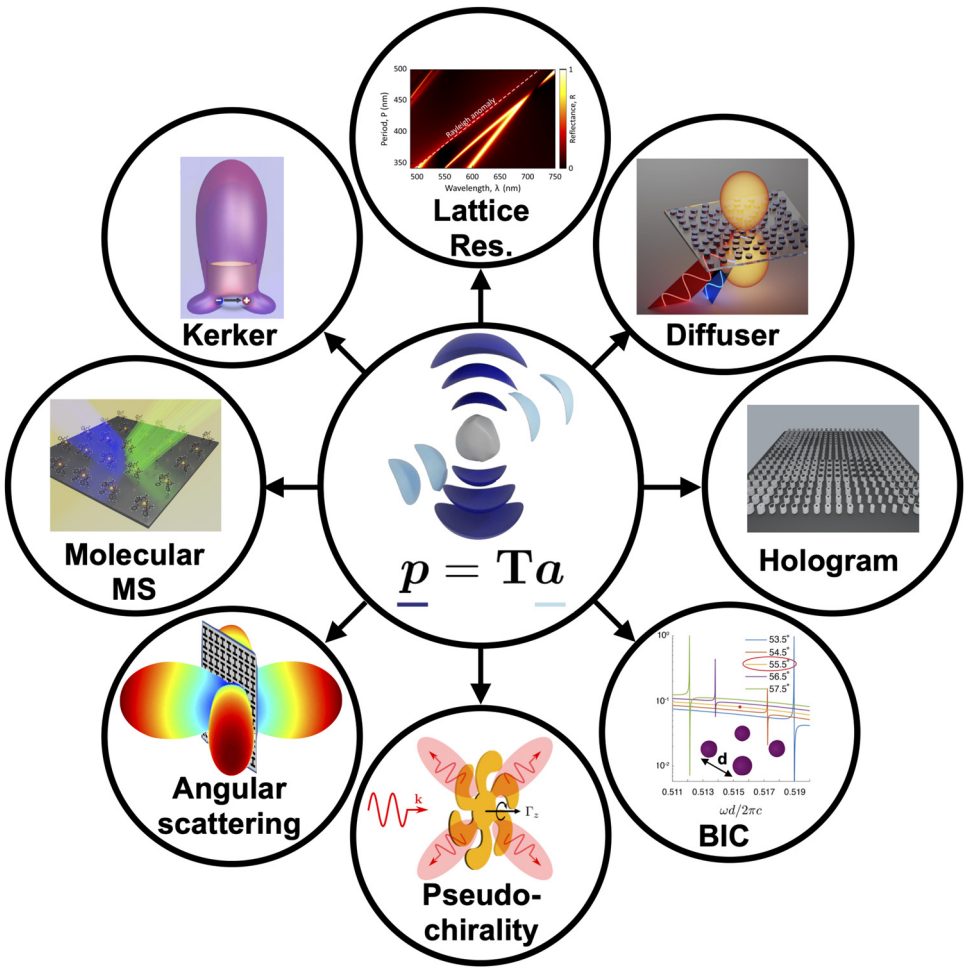

FIG. 45. Illustration of some phenomena and applications explored in the context of metasurfaces and which can be discussed extremely convenient using the multipolar description. Starting at midnight and going clockwise, the phenomena are lattice resonances (figure adapted from Ref. 1179). Then we have diffusers as discussed in this roadmap also in the context of disordered metasurfaces (figure adapted from Ref. 1180). Next, we have holograms. Then, we have bound-states-in-the-continuum (BIC) that require a multipolar analysis in their design (figure adapted from Ref. 1181). As the following phenomena, we have mentioned here pseudochirality and then angular scattering. Finally, we also mention as a possible domain of exploration molecular metasurfaces. At last, we have as an example the wide field of Kerker effects (figure adapted from Ref. 1182). All figures reproduced (adapted) with permission from the respective Journals and copyright remains with the original publishers.

16 July 2024 09:29:41

© Author(s) 2024

excluded. Considering plane wave illumination characterized by a transverse wave vector that expresses the phase variation of the incident field across the metasurface and exploiting the Bloch theorem, we can write the scattered field amplitude from each meta-atom forming the metasurface as

$$\mathbf{b}_{\mathbf{R}} = e^{i\mathbf{k}_{\parallel}\cdot\mathbf{R}}\mathbf{b}. \tag{18}$$

Substituting this expression into Eq. (17) and solving it for the scattered field amplitude vector, we obtain

$$\mathbf{b} = \left(\mathbb{I} - \mathbf{T}\sum_{\mathbf{R}}{}'\mathbf{C}^{(3)}(-\mathbf{R})e^{i\mathbf{k}_{\parallel}\cdot\mathbf{R}}\right)^{-1}\mathbf{T}\mathbf{q}. \tag{19}$$

This equation is intuitive and says that the external illumination induces multipole moments that expand the scattered field. The response is mediated by the T-matrix of the meta-atom renormalized by the interaction with all the other meta-atoms forming the lattice. Their amplitudes can be expressed by summing up the scattered field from all the particles forming the lattice and projecting it onto the plane wave constituting the discrete diffraction orders. These amplitudes of the diffraction orders are the primary quantity of the solution to the problem, and many further properties of interest can be extracted from them. Examples are reflectance and transmittance spectra or their phases, polarization-dependent quantities, or near- and far-fields, to mention only a few selected ones. This is at that heart of many optical phenomena that can be explored. We mention some of these phenomena and applications thereof in Fig. 45 and elaborate on some of them further below.

Also, scattering matrices can be defined that express reflection and transmission upon illuminating the metasurface from both directions. These scattering matrices constitute the primary object of obtaining the response from stacked metasurfaces. Layer-doubling techniques are very efficient for getting the response from stacked metasurfaces.[1183]

2. Numerical implementation

The aforementioned theoretical framework is highly susceptible to numerical implementation. The algebraic formulation reduces the computational complexity to solving matrix-vector products. With the analytical availability of T-matrices for spheres, it is no surprise that the first numerical implementations of the above-sketched framework were done nearly 30 years ago.[1184] At that time, the algorithms were mainly used to explore photonic crystals made from spheres and gratings from high-index dielectric or metallic spheres, which we call metasurfaces today.

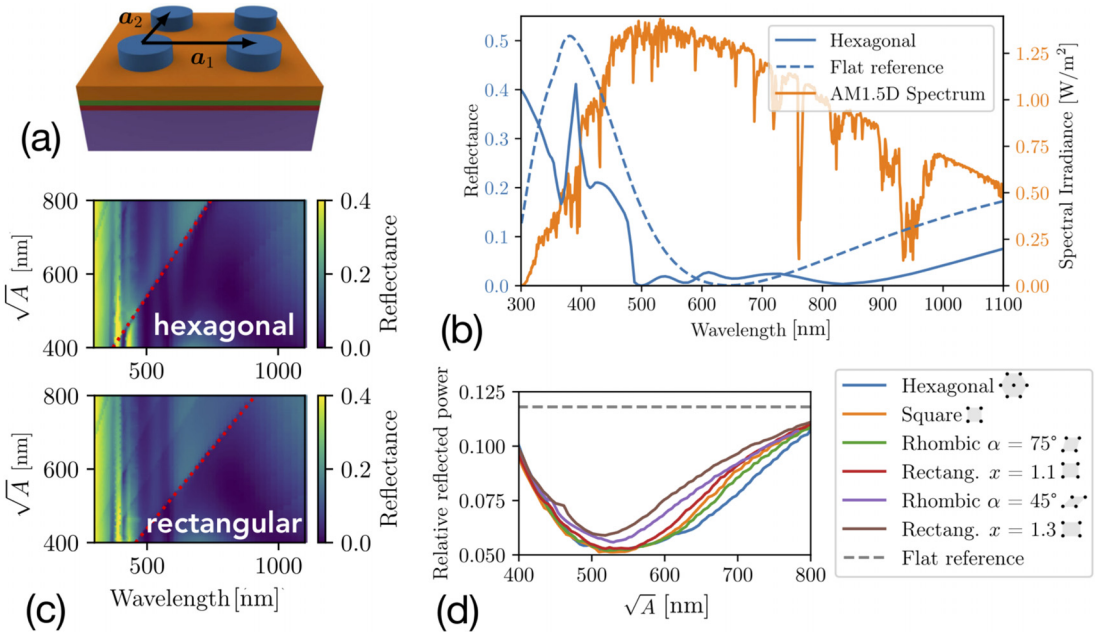

FIG. 46. A computational example to highlight the strength of the multipolar description of metasurfaces. (a) Geometry of the considered example: The layer sequence corresponds to ITO (orange), amorphous silicon p-doped (green) and intrinsic (red), and crystalline silicon (purple). A metasurface made from titanium dioxide disks with a height of 100 nm and a radius of 150 nm lies on top of that layer stack. The lattice and the period would be subject to variations. (b) Example of a hexagonal lattice with a square root of the unit cell area equal to $\sqrt{A} = 520$ nm, we show the simulated reflectance at normal incidence and the reference reflectance from a sample without the metasurface. The figure also shows an AM1.5D spectrum. (c) Reflectance of the sample as a function of the wavelength and the lattice size for two different types of lattices, i.e., once for a hexagonal lattice and once for a rectangular lattice with an aspect ratio of 1.3. (d) When weighting the reflectance with the AM1.5D spectrum and integrating between 300 and 1100 nm, we obtain a measure for the current loss due to reflectance. That quantity is shown for different lattices and different lattice sizes. An optimum can be identified from that FIG. Thanks to the effective multipolar description, the computation is extremely fast. The T-matrix of the disk needs to be calculated only once for each frequency. And the reflectance analysis from the lattice are eventually matrix-vector-products of a small size, which can be done very efficiently. FIG adapted from Ref. 1178. All figures reproduced (adapted) with permission from the respective Journals and copyright remains with the original publishers.

16 July 2024 09:29:41

© Author(s) 2024

With the renewed interest in expressing the response of meta-atoms as building blocks of metamaterials on a multipolar basis, various groups developed numerical tools to study the optical response from metasurfaces. The key aspect of all implementations is the evaluation of the lattice couplings in Eq. (19). Here, Ewald summation techniques are exploited that split the badly converging sums into a part evaluated in real space and a part evaluated in reciprocal space.[1185] Current development revolves around the computations of lattice sums along different dimensions and considering multiple meta-atoms per unit cell.[1186] That latter would be needed when studying bound states in the continuum or topological metasurfaces. The proper consideration of particles closely space above substrates or the consideration of particles that penetrate their respective circumscribing spheres is also explored.[1187] Finally, it remains to be mentioned that various codes have been made publicly available.[1188–1190] A representative analysis of the optical response of a metasurface for an application as a light management structure is discussed in Fig. 46. All the simulations shown in that figure were computed within 4.6 h on an ordinary desktop PC. That includes the computation of the T-matrix of the considered disk. Performing the same simulations using a finite-element code would have taken 2.6 years. The analysis highlights the strength of the multipolar description of the metasurface.[1178]

However, it needs to be clearly said that the approach is less preferred in specific situations. For example, when only the specific response to a specific excitation of a fixed metasurface is needed, the additional overhead of computing the T-matrix first that allows us to express the response to any given illumination is not justified. This should be the largest weakness of the method. Moreover, other methods, including both full-wave Maxwell solvers and semi-analytical techniques, are equally applicable to model metasurfaces. Common full-wave solvers utilize finite element or finite difference methods in either time or frequency domain. Alternatively, semi-analytical approaches such as the rigorous coupled wave analysis (RCWA) can be effectively used. Initially developed for dielectric gratings, the RCWA has been adapted for photonic crystals, metamaterials, and metasurfaces with a strictly periodic arrangement of identical unit cells.

In the RCWA method, one first solves for Bloch-periodic eigenmodes of Maxwell's equations within a metasurface assumed to be invariant in the principal propagation direction. These eigenmodes are represented in a plane wave basis, with interface conditions subsequently applied to determine the amplitudes of modes excited within the metasurface and the adjacent spaces. This method is particularly suited for metasurfaces with discrete heights, treating the metasurface as a single layer. However, for metasurfaces with continuously varying surface profiles, the profile must be segmented into different layers. While RCWA rapidly predicts the optical response of a metasurface, it does not provide extensive physical insights. Here, the multipolar scattering framework is preferable, as it highlights the influence of individual unit cells on the optical response.

Moreover, although RCWA is efficient for metasurfaces with discrete heights, the analysis becomes more complex and time-consuming for continuously varying profiles or metasurfaces composed of free-form particles. Each layer requires solving a dedicated eigenvalue problem, and if the unit cell varies within a supercell, the expansion must include many plane waves, slowing the computation significantly. The complexity of these computations typically scales cubically with the number of plane waves, imposing practical limits on the size of the unit cell that can be effectively analyzed. So, if a simulation of the response from a reasonably sized, uniformly heighted unit cell of a metasurface is required, a method like RCWA is a viable option. For all other configurations, the T-matrix-based scattering approach is more appropriate, provided that the additional computational effort to determine the T-matrix of the scatterer is worth it.

3. Analytical investigations

While the multipolar description constitutes a powerful tool to explore the functionality of metasurfaces numerically, it unfolds its forte when considered from an analytical perspective.[1191] Two aspects are important.

First, explicit analytical expressions for many quantities of interest can be derived under some restricted settings. When isotropic scatterers are considered, i.e., spheres, the T-matrices reduce to a diagonal one, and only a few coefficients are non-zero. Moreover, while theoretically, the T-matrix is infinite in size and numerically truncated to a sufficiently large size to ensure convergence behavior, it is analytically feasible to consider only a few lowest-order multipolar orders. Furthermore, high-symmetry lattices, e.g., square and subwavelength lattices, can be assumed to lower the complexity of the setting. Then, eventually, the system gets reduced in complexity, and explicit analytical equations can be expressed for most quantities of interest. For example, the reflection and transmission amplitude at normal or oblique incidence can be easily expressed. This dramatically simplifies the analysis and allows for parametric investigations of effects such as bound states in the continuum, lattice resonances, polarization filters, or diffraction gratings. We wish to make clear that the formulated assumptions are only made for convenience to reach manageable expressions. It ultimately is up to the convenience and efforts of the person who uses the method to decide up to which degree of complexity they would like to work analytically. One can easily derive analytical expressions for any observable quantity by lifting the assumption on isotropic scatterer and a square and subwavelength lattice, and one can also consider arbitrary higher multipolar orders, it is just that the expressions get longer and are not that handy anymore. In cases with too many unknowns, the problem can always be treated numerically. It is just that closed-form analytical expressions are no longer reasonable. We leave it up to the researcher to decide up to which order they wish to consider on analytical grounds.

Second, the entries of the T-matrix themselves do not attain arbitrary values. For example, for spheres, they can be parametrically expressed using a single angle θ_j bound between $-\pi/2$ and $\pi/2$ for lossless particles. For absorbing particles, a second angle θ_j' bound between 0 and $\pi/2$ parametrizes the dissipation.[1192] The possible value of a Mie coefficient reads then

$$b_j = \frac{1}{1 - i\tan\theta_j + \tan\theta_j'}. \tag{20}$$

This constitutes a significant simplification, as a desired response can be adjusted by identifying the Mie angles of all involved entries of the T-matrix. Combined with the analytical expressions, the necessary properties of the meta-atom in terms of Mie angles can be identified that provide a metasurface with a response on demand can be identified. Identifying suitable particles with the specified properties is a secondary problem that inverse-design techniques can solve.

16 July 2024 09:29:41

© Author(s) 2024

C. Future directions and outlook

1. A description using polarizabilities

So far, the description has focused on an analysis using T-matrices that express the scattering response using basis functions in a spherical coordinate system. Sometimes, that is inconvenient, and a discussion in multipole moments linked to specific directions in a Cartesian coordinate system may be more intuitive. Then, one speaks of multipolar polarizabilities that are induced instead of the amplitudes of the vector spherical harmonics.[1193] Instead of speaking of a T-matrix, we speak of the Cartesian multipole moments and polarizabilities. When care is taken to eliminate the trace and the redundant components of the Cartesian tensors, the change between Cartesian and spherical multipoles is merely a change of basis. It has no implication on the physics as long as no additional approximations are made.

Expressions exist to convert between these amplitudes of the spherical harmonics and the Cartesian multipole moments. For example, the two lowest-order electric coefficients can be converted as[1174]

$$\begin{aligned} \varepsilon_d^{-1}\mathbf{p} &= \frac{\zeta_1}{ik_d^3}\mathbf{M}_{\text{Dipole}}\mathbf{b}_1^e, \\ k_d\varepsilon_d^{-1}\mathbf{Q} &= \frac{\zeta_2}{ik_d^3}\mathbf{M}_{\text{Quadrupole}}\mathbf{b}_2^e, \end{aligned} \tag{21}$$

where the matrices that connect the electric multipole moments in a spherical basis ($\mathbf{b}_1^e$ and $\mathbf{b}_w^e$) to a Cartesian basis ($\mathbf{p}$ and $\mathbf{Q}$) are

$$\begin{aligned} \mathbf{M}_{\text{Dipole}} &= \frac{1}{\sqrt{2}}\begin{bmatrix} 1 & 0 & -1 \\ -i & 0 & -i \\ 0 & \sqrt{2} & 0 \end{bmatrix}, \\ \mathbf{M}_{\text{Quadrupole}} &= \frac{1}{\sqrt{2}}\begin{bmatrix} -i & 0 & 0 & 0 & i \\ 0 & -i & 0 & -i & 0 \\ 0 & 0 & \sqrt{2} & 0 & 0 \\ 0 & 1 & 0 & -1 & 0 \\ 1 & 0 & 0 & 0 & 1 \end{bmatrix}. \end{aligned} \tag{22}$$

Similar matrices also exist for higher-order terms.[1191] In these expressions, k_d is the wavenumber in the background medium with a permittivity ε_d, and $\zeta_j = \sqrt{(2j+1)!\pi}$. Using that framework, T-matrices can be converted into polarizabilities with the same simplicity. For example, the electric dipolar part of the T-matrix $\mathbf{T}_{\text{ee}}$ can be converted into the electric dipolar polarizability matrix $\boldsymbol{\alpha}_{\text{ee}}$ as

$$\mathbf{T}_{\text{ee}} = -\frac{Z_d k_d^3 c}{6\pi i}\mathbf{M}_{\text{Dipole}}\boldsymbol{\alpha}_{\text{ee}}\mathbf{M}_{\text{Dipole}}^{-1}, \tag{23}$$

with Z_d the impedance of the background medium. Then, all the details described above can be expressed in polarizabilities and Cartesian multipole moments. Besides the numerical analysis, semi-analytical expressions for observables that provide valuable insights can also be obtained.

In the framework of the analytical treatment discussed above, for example, for metasurfaces composed of identical isotropic meta-atoms, the electric field coefficients of reflection r and transmission t at the condition of the normal incidence of an external linear x-polarized plane wave can be represented as[1194]

$$\begin{aligned} t &= 1 + \frac{ik_d}{E_0 2S_L\varepsilon_0\varepsilon_d}\left(p_x + \frac{m_y}{c_d} - \frac{ik_d Q_{xz}}{6} - \frac{ik_d M_{yz}}{2c_d} + \cdots\right), \\ r &= \frac{ik_d}{E_0 2S_L\varepsilon_0\varepsilon_d}\left(p_x - \frac{m_y}{c_d} + \frac{ik_d Q_{xz}}{6} - \frac{ik_d M_{yz}}{2c_d} + \cdots\right), \end{aligned} \tag{24}$$

where E_0 is the incident electric field at the center of meta-atoms, S_L is the surface area of the metasurface elementary cell, and c_d is the light speed in the surrounding medium. For the above equations, we assume that the metasurface plane coincides with the xy-plane of the Cartesian coordinate system, and the incident wave of the frequency ω is $(E_0, 0, 0)e^{i(k_d z - \omega t)}$. The considered Cartesian multipole moments of the meta-atoms ($\mathbf{p}$ and $\mathbf{m}$ are the electric and magnetic dipole moments, and $\mathbf{Q}$ and $\mathbf{M}$ are the electric and magnetic quadrupole moments, respectively) enter through the components that provide radiation in a direction perpendicular to the metasurface. Therefore, there is a useful opportunity to combine multipole moments with the same parity symmetry (with respect to inversion)[1195] into one group and introduce the corresponding effective multipole $M^{(p)}$ and its effective polarizability $\alpha^{(p)}$, for the even (odd) multipole moments $p \to e$ ($p \to o$).[1179] So that for the case (24) one can write

$$t = 1 + \frac{ik_d}{2S_L}(\alpha^{(o)} + \alpha^{(e)}), \tag{25}$$

$$r = \frac{ik_d}{2S_L}(\alpha^{(o)} - \alpha^{(e)}), \tag{26}$$

where $\alpha^{(o)} = M^{(o)}/(E_0\varepsilon_0\varepsilon_d) = (p_x - ik_d M_{yz}/2c_d + \cdots)/(E_0\varepsilon_0\varepsilon_d)$ and $\alpha^{(e)} = M^{(e)}/(E_0\varepsilon_0\varepsilon_d) = (m_y/c_d - ik_d Q_{xz}/6 + \cdots)/(E_0\varepsilon_0\varepsilon_d)$. From the representation (25) and (26) one can see that the lattice anapole effect, when the light wave transmits through the metasurface without changes in amplitude and phase, is realized if $\alpha^{(o)} = 0$ and $\alpha^{(e)} = 0$ independently, that is due to destructive superposition between contributions of the multipole moments of the same inverse parity symmetry. In contrast, the lattice Kerker effect (only the suppression of reflection) is realized for $\alpha^{(o)} = \alpha^{(e)}$ due to the destructive superposition between the multipole moments with different inverse parity symmetry. The case of a bianisotropic response (when multipole coupling exists between the multipole moments of different inverse parity) can also be involved in this approach.[1196,1197]

Note that we have been talking about the effective polarizability of meta-atoms inside a metasurface so far. However, significant advantages can be obtained if the polarizability of single meta-atoms and the so-called lattice sums are considered.[70,1198,1199] Recently, a strategy has been proposed to tune a symmetry-protected bound state in the continuum in the desired spectral range by directly determining the period of a metasurface consisting of building blocks with known electric or magnetic dipole polarizabilities. This can be explicitly obtained from the point of intersection (coincidence) between the real part of the corresponding inverse dipole polarizability of an individual building block (meta-atom) and the real part of the corresponding lattice sum, taking into account inter-particle interaction in the metasurface. In particular, it is shown that to obtain a bound state in the continuum at the resonant wavelength λ_R of an individual meta-atoms, the period of a metasurface with a square cell must be equal to $\approx 0.71\lambda_R$.[1200] In the case of including the resonant contribution of multipoles of various orders into the metasurface model, the approximation of effective polarizabilities and lattice sums makes it possible to study the lattice-induced

16 July 2024 09:29:41

© Author(s) 2024

interaction between these multipoles in a semi-analytical form.[1199] In some cases, such coupling can lead to the suppression of contributions from certain groups of multipoles and the implementation of anapole states or quasi-bound states in the continuum.

2. Multipolar interface conditions

In parallel to the elaboration of the T-matrix mentioned above method, an alternative metasurface modeling technique has been developed based on generalized sheet transition conditions (GSTC).[1201–1205] This modeling technique relies on the premise that a metasurface acts as a discontinuity that may be modeled as a homogenous polarizable sheet whose response is described in terms of effective material parameters. For this purpose, the concept of polarizabilities is generally replaced by that of susceptibilities, as the latter is more commonly used to describe the response of a material from the perspective of a Cartesian lattice. The main difference between these two modeling techniques is that the T-matrix approach focuses on the scattering response of individual meta-atoms to build up to the response of the overall metasurface by including the coupling between the meta-atoms. In contrast, the GSTC method ignores the granular response of the meta-atoms and rather directly relates the fields interacting with the metasurface to its susceptibilities, which intrinsically includes the coupling between the meta-atoms.[1202–1205]

Fundamentally, the GSTC models how the fields and their spatial derivatives interact with a metasurface. This model is derived by expanding these fields, along with the metasurface polarization densities, in terms of a series of derivatives of the Dirac delta distribution. This rigorous foundation makes the GSTC ideal for modeling conventional dipolar metasurfaces and opens the door for including more complex interactions. As such, they now include second-order nonlinear polarizations,[1206] time-varying modulations,[1205] multipolar contributions, and nonlocal responses.[1207,1208] Another strength of the GSTC is that they can be used for both synthesis, i.e., finding the metasurface susceptibilities in terms of specified fields, and for analysis, i.e., computing the fields scattered by a metasurface with known susceptibilities. For instance, it has been demonstrated using the GSTC that nonlocal responses are required to synthesize perfectly refractive metasurfaces.[1169] Several numerical schemes have been developed for the analysis, such as finite-difference frequency- and time-domain techniques, a finite element method, and a spectral-domain integral-equation technique, that can compute the fields scattered by a metasurface under arbitrary illumination conditions.[1209]

Finally, connecting the susceptibilities to the geometry of actual meta-atoms is typically achieved using equations that relate these susceptibilities to the metasurface full-wave simulated scattering parameters.[1205] While effective, this approach remains slow and cumbersome. For this reason, a methodology to connect the susceptibilities directly to the T-matrix of meta-atoms, which should significantly simplify the metasurface practical implementation procedure, is being actively developed. Note that it is currently already possible to map the dipolar polarizabilities of a metasurface with its corresponding dipolar susceptibilities.[1205]

3. Further developments

Finally, we wish to reflect on selected advanced topics currently under development in the context of the multipolar description of metasurfaces. Generally, the multipolar decomposition of the optical response of meta-atoms allows one to understand and engineer notable and beneficial effects, such as directional radiation. As understood by Kerker *et al.*,[1210] the interference of the fields radiated by an electric dipole and a magnetic dipole can result in highly directional far-fields. The effect has been engineered and demonstrated in different frequency bands for samples under far-field illumination[962,1211] and for dipolar emitters near the nanostructures.[1212] Understanding these effects is a major challenge and many open questions remain, partially mentioned in this contribution to the roadmap but partially also in other contributions.

Moreover, the formalism introduced here cannot just be applied to artificially structured macroscopic materials but also to other (nano-) photonic systems. A major stream of efforts goes into developing metasurfaces with molecular building blocks.[1213] From a gigantically large chemical space, the individual molecules can be chosen that are periodically arranged using different techniques, and materials can be provided that inherit their linear, bianisotropic, or nonlinear properties from the individual molecules. In a multi-scale effort, the framework described here can be used to express the properties of these materials from first principles and to study their interaction with light. To reach such a description, quantum-chemical tools, mostly time-dependent density functional theory, compute the T-matrix of an individual molecule or an aggregate. Afterward, periodically arranged molecules accessible, e.g., with surface-anchored metallic organic frameworks can be studied in detail. The detailed and accurate description of the molecules that surpasses a phenomenologically motivated description of a molecule as a polarizable two-level system provides unprecedented insights. Furthermore, hybrid systems can be explored where molecular and traditional scatterers are seamlessly blended.

Moreover, the metasurfaces can be homogenized in some cases, and effective properties can be assigned to a film so that the optical response from the metasurface and the effectively homogenous medium agree.[1214] This unlocks novel possibilities when integrating metasurfaces into the design of more traditional optical elements. While the theory is well-established in dipole approximation, nonlocal metasurfaces are within reach and are currently being discussed. In these metasurfaces, higher-order multipolar components have a significant contribution. The complexity in their description advances, and more sophisticated properties are in reach. The nonlocal character, generally, leads to an angle dependent response, that can be used for image processing purposes. In addition, it unlocks the opportunity to multiplex the response depending on, e.g., the angle of incidence. Such a multiplexing can add enhanced functionality to the devices. Additionally, deriving generalized impedance, admittance, or even susceptibility tensors from the T-matrices or polarizabilities renormalized by the two-dimensional lattice interactions can be of practical benefit. It allows us to study and exploit the renormalization of the properties of the scatterer due to the lattice interaction and enables shaping the optical response actually not just by choosing a specific meta-atom, but rather by combining the meta-atom and the lattice. Exploiting the renormalization can lead to effects such as a giant magnetic dipolar moments, which may in turn find applications when perceiving impedance-matched optical devices with vanishing reflection losses.

Finally, significant efforts are currently in place to solve the inverse problem, i.e., instead of quantifying the optical response of a

16 July 2024 09:29:41

© Author(s) 2024

given metasurface, we aim to identify the metasurface that provides an optical response on demand.[1106] We have touched on that issue already in Sec. XX C 3. Yet/However it can also be done with established methods from inverse design, such as topology optimization or Bayesian optimization, tools that effectively exploit gradient information, genetic algorithms, or particle swarm optimization. Moreover, techniques from the field of machine learning are explored. However, for individual design problems, the efforts in generating data used for training artificial neural networks (ANNs) usually exceed by far the efforts to solve the inverse problem directly. Yet/However independent of that, the community actively explores scenarios where using ANNs is appealing.

D. Conclusions

This mini-review gave an overview of a highly flexible approach to theoretically and computationally explore the optical response of metasurfaces. It resides on the language of scattering theory, where initially, the interaction of light with a localized object, i.e., the meta-atom, is studied on semi-analytical grounds. That can be done with the T-matrix or the polarizability matrix, depending on whether a spherical or Cartesian coordinate system is considered. Thanks to the efficient evaluation of lattice sums, the interaction among the meta-atoms forming the metasurface is assessed, and the optical response in terms of reflection and transmission from metasurfaces can be evaluated. It needs to be emphasized that the computational approach is highly efficient, and the design and analysis of metasurfaces is tremendously accelerated. Yet/however it is also a framework that can be reduced to obtain handy analytical expressions to discuss numerical observables on analytical grounds. Multiple current developments were sketched.

What remains is to elaborate shortly on open issues. One aspect concerns densely packed metasurfaces made from asymmetric objects. The scattering formalism assumes that the circumscribing spheres of adjacent objects do not penetrate, as otherwise, the Rayleigh hypothesis breaks down. That restriction limits the types of metasurfaces that can be considered. The problem can be circumvented with concepts such as distributed T-matrices, where multiple origins are considered to expand the field into vector spherical harmonics, but the approach is yet premature. Moreover, combining the considered framework with methods from inverse design is ongoing, and we can expect much progress in this field. One aspect needs to be highlighted here, and it concerns the simulation of metasurfaces made from a spatially inhomogeneous arrangement of meta-atoms, which can be handled by considering rather large supercells. Spatially inhomogeneous metasurfaces are needed for many applications, e.g., meta-lenses, meta-holograms, and other optical meta-devices. The design of these devices usually follows a three-step procedure. First, the complex transmission function at each spatial location is identified by suitable means. Second, the optical response from a periodically arranged unit cell with varying geometrical parameters is simulated and stored in some lookup table. Last, the particles are fetched from the lookup and placed to the position of the unit cell where they shall provide the desired complex response. However, this approach does not consider the fact that the response of the meta-atom in an inhomogenous environment is not the same as that of the same meta-atom in a periodic arrangement. In consequence, the metasurface shows a degraded efficiency. Optimizing the spatial details of the unit cell by methods from the field of inverse design is potentially the key to reach devices of very high efficiency, as these coupling effects need to be considered. The general framework described here can handle these effects, but efforts are needed to formulate everything in a differentiable form and to use it in an inverse design framework.

Furthermore, the combination of the optical properties of the metasurface with other physical phenomena would tremendously widen the range of use cases. One example would be photothermal behavior, where the dissipation of energy changes the temperature of the medium, which in turn changes the material properties, which changes the optical response. In general, many other effects could be considered to work toward switchable and tunable metasurfaces.

Finally, the extension of the formalism to treat nonlinear effects can safely be foreseen as a direction for future developments. Many of the other contributions in this roadmap will also serve as a guide for open issues that can be tackled with dedicated improvements to the framework sketched in this contribution.

ACKNOWLEDGMENTS

C.R. and U.L. acknowledge support through the Deutsche Forschungsgemeinschaft (DFG, German Research Foundation) under Germany's Excellence Strategy via the Excellence Cluster 3D Matter Made to Order (EXC-2082/1, Grant No. 390761711). A.B.E. acknowledges support through the Cluster of Excellence PhoenixD (EXC 2122, Project ID No. 390833453). I.F.-C. and C.R. acknowledge support through the CRC Waves: Analysis and Numerics (SFB 1173, Grant No. 258734477. K.A. acknowledges funding from the Swiss National Science Foundation (Project No. PZ00P2_193221). We all wish to acknowledge contributions to this work from our past and current group members, for which we are deeply grateful.

AUTHOR DECLARATIONS

Conflict of Interest

The authors have no conflicts to disclose.

Author Contributions

S.A.S., R.F.O., and M.K. conceived and organized this roadmap, including selecting the section topics and lead authors. These three authors contributed equally and may claim first authorship. The following authors led individual sections (in order of the sections): Andrea Alu, Isabelle Staude, Rupert F. Oulton, Alasdair W. Clark, Maria Kafesaki, Anatoly V. Zayats, Stefan Maier, Xianzhong Chen, Andrea Di Falco, Maria V. Chekhova, Ren-Min Ma, Rachel Grange, Mohsen Rahmani, Andrei Faraon, R. Sapienza, Philippe Lalanne, Sebastian A. Schulz, Willie J. Padilla, Patrice Genevet and Carsten Rockstuhl. These authors supervised the writing of their relevant sections, selected their coauthors and determined the overall direction of their perspectives. All other authors contributed to the perspective articles under which they are listed. The author list is in order of appearance in the document.

Sebastian A. Schulz, Rupert. F. Oulton, Mitchell Kenney conceived and coordinated the roadmap together. All three act as joint corresponding and joint first authors for the full document.

Sebastian A. Schulz: Conceptualization (equal); Writing – original draft (equal); Writing – review & editing (equal). **Rupert F. Oulton:**

16 July 2024 09:29:41

© Author(s) 2024

Conceptualization (equal); Writing – original draft (equal); Writing – review & editing (equal). **Mitchell Kenney:** Conceptualization (equal); Writing – original draft (equal); Writing – review & editing (equal). **Andrea Alù:** Conceptualization (supporting); Writing – original draft (equal); Writing – review & editing (equal). **Isabelle Staude:** Conceptualization (supporting); Writing – original draft (equal); Writing – review & editing (equal). **Ayesheh Bashiri:** Writing – original draft (equal); Writing – review & editing (equal). **Zlata Fedorova:** Writing – original draft (equal); Writing – review & editing (equal). **Radoslaw Kolkowski:** Writing – original draft (equal); Writing – review & editing (equal). **A. Femius Koenderink:** Writing – original draft (equal); Writing – review & editing (equal). **Xiaofei Xiao:** Writing – original draft (equal); Writing – review & editing (equal). **John Yang:** Writing – original draft (equal); Writing – review & editing (equal). **William J. Peveler:** Writing – original draft (equal); Writing – review & editing (equal). **Alasdair W. Clark:** Conceptualization (supporting); Writing – original draft (equal); Writing – review & editing (equal). **George Perrakis:** Writing – original draft (equal); Writing – review & editing (equal). **Anna C. Tasolamprou:** Writing – original draft (equal); Writing – review & editing (equal). **Maria Kafesaki:** Conceptualization (supporting); Writing – original draft (equal); Writing – review & editing (equal). **Anastasiia Zaleska:** Writing – original draft (equal); Writing – review & editing (equal). **Wayne Dickson:** Writing – original draft (equal); Writing – review & editing (equal). **David Richards:** Writing – original draft (equal); Writing – review & editing (equal). **Anatoly Zayats:** Conceptualization (supporting); Writing – original draft (equal); Writing – review & editing (equal). **Haoran Ren:** Writing – original draft (equal); Writing – review & editing (equal). **Yuri Kivshar:** Writing – original draft (equal); Writing – review & editing (equal). **Stefan Maier:** Conceptualization (supporting); Writing – original draft (equal); Writing – review & editing (equal). **Xianzhong Chen:** Conceptualization (supporting); Writing – original draft (equal); Writing – review & editing (equal). **Muhammad Afnan-Ansari:** Writing – original draft (equal); Writing – review & editing (equal). **Yuhui Gan:** Writing – original draft (equal); Writing – review & editing (equal). **Arseny Alexeev:** Writing – original draft (equal); Writing – review & editing (equal). **Thomas F. Krauss:** Writing – original draft (equal); Writing – review & editing (equal). **Andrea di Falco:** Conceptualization (supporting); Writing – original draft (equal); Writing – review & editing (equal). **Sylvain D. Gennaro:** Writing – original draft (equal); Writing – review & editing (equal). **Tomás Santiago-Cruz:** Writing – original draft (equal); Writing – review & editing (equal). **Igal Brener:** Writing – original draft (equal); Writing – review & editing (equal). **Maria V. Chekhova:** Conceptualization (supporting); Writing – original draft (equal); Writing – review & editing (equal). **Ren-Min Ma:** Conceptualization (supporting); Writing – original draft (equal); Writing – review & editing (equal). **Viola V. Vogler-Neuling:** Writing – original draft (equal); Writing – review & editing (equal). **Helena C. Weigand:** Writing – original draft (equal); Writing – review & editing (equal). **Ülle-Linda Talts:** Writing – original draft (equal); Writing – review & editing (equal). **Irene Occhiodori:** Writing – original draft (equal); Writing – review & editing (equal). **Rachel Grange:** Conceptualization (supporting); Writing – original draft (equal); Writing – review & editing (equal). **Mohsen Rahmani:** Conceptualization (supporting); Writing – original draft (equal); Writing – review & editing (equal). **Lei Xu:** Writing – original draft (equal); Writing – review & editing (equal). **S. M. Kamali:** Writing – original draft (equal); Writing – review & editing (equal). **E. Arbabi:** Writing – original draft (equal); Writing – review & editing (equal). **Andrei Faraon:** Conceptualization (supporting); Writing – original draft (equal); Writing – review & editing (equal). **A. C. Harwood:** Writing – original draft (equal); Writing – review & editing (equal). **S. Vezzoli:** Writing – original draft (equal); Writing – review & editing (equal). **Riccardo Sapienza:** Conceptualization (supporting); Writing – original draft (equal); Writing – review & editing (equal). **Philippe Lalanne:** Conceptualization (supporting); Writing – original draft (equal); Writing – review & editing (equal). **Alexandre Dmitriev:** Writing – original draft (equal); Writing – review & editing (equal). **Carsten Rockstuhl:** Conceptualization (supporting); Writing – original draft (equal); Writing – review & editing (equal). **Alexander Sprafke:** Writing – original draft (equal); Writing – review & editing (equal). **Kevin Vynck:** Writing – original draft (equal); Writing – review & editing (equal). **Jeremy Upham:** Conceptualization (supporting); Writing – original draft (equal); Writing – review & editing (equal). **M. Zahirul Alam:** Writing – original draft (equal); Writing – review & editing (equal). **Israel De Leon:** Writing – original draft (equal); Writing – review & editing (equal). **Robert W. Boyd:** Writing – original draft (equal); Writing – review & editing (equal). **Willie J. Padilla:** Conceptualization (supporting); Writing – original draft (equal); Writing – review & editing (equal). **Jordan M. Malof:** Writing – original draft (equal); Writing – review & editing (equal). **Aloke Jana:** Writing – original draft (equal); Writing – review & editing (equal). **Zijin Yang:** Writing – original draft (equal); Writing – review & editing (equal). **Rémi Colom:** Writing – original draft (equal); Writing – review & editing (equal). **Patrice Genevet:** Conceptualization (supporting); Writing – original draft (equal); Writing – review & editing (equal). **Karim Achouri:** Writing – original draft (equal); Writing – review & editing (equal). **Andrey B. Evlyukhin:** Writing – original draft (equal); Writing – review & editing (equal). **Ulrich Lemmer:** Writing – original draft (equal); Writing – review & editing (equal). **Ivan Fernandez-Corbaton:** Writing – original draft (equal); Writing – review & editing (equal).

DATA AVAILABILITY

Data sharing is not applicable to this article as no new data were created or analyzed in this study.

REFERENCES

[1]N. Meinzer, W. Barnes, and I. Hooper, Nat. Photonics **8**, 889 (2014).
[2]N. Yu and F. Capasso, Nat. Mater. **13**, 139 (2014).
[3]S. M. Choudhury, D. Wang, K. Chaudhuri, C. DeVault, A. V. Kildishev, A. Boltasseva, and V. M. Shalaev, Nanophotonics **7**, 959 (2018).
[4]A. I. Kuznetsov, M. L. Brongersma, J. Yao, M. K. Chen, U. Levy, D. P. Tsai, N. I. Zheludev, A. Faraon, A. Arbabi, N. Yu, D. Chanda, K. B. Crozier, A. V. Kildishev, H. Wang, J. K. W. Yang, J. G. Valentine, P. Genevet, J. A. Fan, O. D. Miller, A. Majumdar, J. E. Fröch, D. Brady, F. Heide, A. Veeraraghavan, N. Engheta, A. Alù, A. Polman, H. A. Atwater, P. Thureja, R. Paniagua-Dominguez, S. T. Ha, A. I. Barreda, J. A. Schuller, I. Staude, G. Grinblat, Y. Kivshar, S. Peana, S. F. Yelin, A. Senichev, V. M. Shalaev, S. Saha, A. Boltasseva, J. Rho, D. K. Oh, J. Kim, J. Park, R. Devlin, and R. A. Pala, ACS Photonics **11**, 816 (2024).
[5]N. Yu, P. Genevet, M. Kats, F. Aieta, J. Tetienne, F. Capasso, and Z. Gaburro, Science **334**, 333 (2011).

16 July 2024 09:29:41

© Author(s) 2024

[6]X. Ni, N. K. Emani, A. V. Kildishev, A. Boltasseva, and V. M. Shalaev, Science **335**, 427 (2012).
[7]B. A. Munk, *Frequency Selective Surfaces: Theory and Design* (Wiley, New York, 2000).
[8]D. Pozar, S. Targonski, and H. Syrigos, IEEE Trans. Antennas Propagat. **45**, 287 (1997).
[9]E. Hasman, V. Kleiner, G. Biener, and A. Niv, Appl. Phys. Lett. **82**, 328 (2003).
[10]P. Lalanne, S. Astilean, P. Chavel, E. Cambril, and H. Launois, Opt. Lett. **23**, 1081 (1998).
[11]F. Monticone, N. M. Estakhri, and A. Alù, Phys. Rev. Lett. **110**, 203903 (2013).
[12]C. Pfeiffer and A. Grbic, Phys. Rev. Lett. **110**, 197401 (2013).
[13]H.-T. Chen, A. Taylor, and N. Yu, Rep. Prog. Phys. **79**, 076401 (2016).
[14]N. Mohammadi Estakhri and A. Alù, Phys. Rev. X **6**, 041008 (2016).
[15]D. N. Neshev and A. E. Miroshnichenko, Nat. Photonics **17**, 26 (2023).
[16]A. Arbabi, Y. Horie, M. Bagheri, and A. Faraon, Nat. Nanotechnol. **10**, 937 (2015).
[17]Metalenz, see https://metalenz.com/
[18]Meta materials, Inc., see https://metamaterial.com/
[19]Y. Liu, X. Liu, X. Mu, T. Hou, J. Xu, M. D. Renzo, and N. Al-Dhahir, IEEE Commun. Surv. Tutorials **23**, 1546 (2021).
[20]G. Zheng, H. Mühlenbernd, M. Kenney, G. Li, T. Zentgraf, and S. Zhang, Nat. Nanotechnol. **10**, 308 (2015).
[21]E. Arbabi, A. Arbabi, S. M. Kamali, Y. Horie, and A. Faraon, Optica **3**, 628 (2016).
[22]Y. Wang, Q. Chen, W. Yang, Z. Ji, L. Jin, X. Ma, Q. Song, A. Boltasseva, J. Han, V. M. Shalaev, and S. Xiao, Nat. Commun **15**, 5560 (2021).
[23]A. Epstein and G. V. Eleftheriades, J. Opt. Soc. Am. B **33**, A31 (2016).
[24]C. P. Jisha, S. Nolte, and A. Alberucci, Laser Photonics Rev. **15**, 2100003 (2021).
[25]F. Presutti and F. Monticone, Optica **7**, 624 (2020).
[26]D. A. B. Miller, Science **379**, 41 (2023).
[27]Y. Ra'di, D. L. Sounas, and A. Alù, Phys. Rev. Lett. **119**, 067404 (2017).
[28]Y. Raadi and A. Alu, IEEE Photonics J. **14**, 1–13 (2022).
[29]A. Overvig and A. Alù, Laser Photonics Rev. **16**, 2100633 (2022).
[30]A. Overvig and A. Alù, Adv. Photonics **3**, 026002 (2021).
[31]S. C. Malek, A. C. Overvig, A. Alù, and N. Yu, Light: Sci. Appl. **11**, 246 (2022).
[32]H. Ren, G. Briere, X. Fang, P. Ni, R. Sawant, S. Héron, S. Chenot, S. Vézian, B. Damilano, V. Brändli, S. Maier, and P. Genevet, Nat. Commun. **10**, 2986 (2019).
[33]J.-H. Song, J. van de Groep, S. J. Kim, and M. L. Brongersma, Nat. Nanotechnol. **16**, 1224 (2021).
[34]E. Cortés, F. Wendisch, L. Sortino, A. Mancini, S. Ezendam, S. Saris, L. De, S. Menezes, A. Tittl, H. Ren, and S. Maier, Chem. Rev. **122**, 15082 (2022).
[35]G.-Y. Lee, J.-Y. Hong, S. Hwang, S. Moon, H. Kang, S. Jeon, H. Kim, J.-H. Jeong, and B. Lee, Nat. Commun. **9**, 4562 (2018).
[36]K. Wang, M. Chekhova, and Y. Kivshar, Phys. Today **75**(8), 38 (2022).
[37]Q. Song, M. Odeh, J. Zúñiga-Pérez, B. Kanté, and P. Genevet, Science **373**, 1133 (2021).
[38]A. Krasnok, D. Baranov, H. Li, M.-A. Miri, F. Monticone, and A. Alú, Adv. Opt. Photonics **11**, 892 (2019).
[39]M.-A. Miri and A. Alu, Science **363**, eaar7709 (2019).
[40]E. Mikheeva, R. Colom, K. Achouri, A. Overvig, F. Binkowski, J.-Y. Duboz, S. Cueff, S. Fan, S. Burger, A. Alù *et al.*, Optica **10**, 1287 (2023).
[41]H. Kwon, D. Sounas, A. Cordaro, A. Polman, and A. Alù, Phys. Rev. Lett. **121**, 173004 (2018).
[42]Y. Zhou, H. Zheng, I. I. Kravchenko, and J. Valentine, Nat. Photonics **14**, 316 (2020).
[43]M. Cotrufo, A. Arora, S. Singh, and A. Alù, Nat. Commun. **14**, 7078 (2023).
[44]A. Silva, F. Monticone, G. Castaldi, V. Galdi, A. Alù, and N. Engheta, Science **343**, 160 (2014).
[45]H. Zheng, Q. Liu, I. I. Kravchenko, X. Zhang, Y. Huo, and J. G. Valentine, "Multichannel meta-imagers for accelerating machine vision," Nat. Nanotechnol. (unpublished) (2024).
[46]A. Cordaro, B. Edwards, V. Nikkhah, A. Alù, N. Engheta, and A. Polman, Nat. Nanotechnol. **18**, 365 (2023).
[47]A. C. Overvig, S. A. Mann, and A. Alù, Phys. Rev. X **11**, 021050 (2021).
[48]P. Iyer, R. Decrescent, Y. Mohtashami, G. Lheureux, N. Butakov, A. Alhassan, C. Weisbuch, S. Nakamura, S. Denbaars, and J. Schuller, Nat. Photonics **14**, 543 (2020).
[49]N. Muhammad, Y. Chen, C.-W. Qiu, and G. P. Wang, Nano Lett. **21**, 967 (2021).
[50]A. M. Shaltout, V. M. Shalaev, and M. L. Brongersma, Science **364**, eaat3100 (2019).
[51]Y. Li, M. R. Krisshnamurthi, W. Luo, A. K. Swan, X. Ling, and R. Paiella, Opt. Mater. Express **12**, 4528 (2022).
[52]J. Lee, M. Tymchenko, C. Argyropoulos, P.-Y. Chen, F. Lu, F. Demmerle, G. Boehm, M.-C. Amann, A. Alu, and M. A. Belkin, Nature **511**, 65 (2014).
[53]G. Li, S. Zhang, and T. Zentgraf, Nat. Rev. Mater. **2**, 17010 (2017).
[54]R. Kolkowski, S. Kovaios, and A. F. Koenderink, Phys. Rev. Res. **3**, 023185 (2021).
[55]S.-Q. Li, X. Xu, R. Maruthiyodan Veetil, V. Valuckas, R. Paniagua-Domínguez, and A. I. Kuznetsov, Science **364**, 1087 (2019).
[56]D. L. Sounas and A. Alù, Nat. Photonics **11**, 774 (2017).
[57]A. Vaskin, R. Kolkowski, A. F. Koenderink, and I. Staude, Nanophotonics **8**, 1151 (2019).
[58]S. Yuan, X. Qiu, C. Cui, L. Zhu, Y. Wang, Y. Li, J. Song, Q. Huang, and J. Xia, ACS Nano **11**, 10704 (2017).
[59]S. Liu, A. Vaskin, S. Addamane, B. Leung, M. Tsai, Y. Yang, P. Vabishchevich, G. Keeler, G. Wang, X. He, Y. Kim, N. Hartmann, H. Htoon, S. Doorn, M. Zilk, T. Pertsch, G. Balakrishnan, M. Sinclair, I. Staude, and I. Brener, Nano Lett. **18**, 6906 (2018).
[60]Y. Mohtashami, R. A. DeCrescent, L. K. Heki, P. P. Iyer, N. A. Butakov, M. S. Wong, A. Alhassan, W. J. Mitchell, S. Nakamura, S. P. DenBaars, and J. A. Schuller, Nat. Commun. **12**, 3591 (2021).
[61]Y.-J. Lu, R. Sokhoyan, W.-H. Cheng, G. Kafaie Shirmanesh, A. R. Davoyan, R. A. Pala, K. Thyagarajan, and H. A. Atwater, Nat. Commun. **8**, 1631 (2017).
[62]C.-Y. Chang, C.-L. Yu, C.-A. Lin, H.-T. Lin, A. B. Lee, Z.-Z. Chen, L.-S. Lu, W.-H. Chang, H.-C. Kuo, and M.-H. Shih, ACS Appl. Nano Mater. **3**, 6855 (2020).
[63]L. Liu, W. Liu, F. Wang, H. Cheng, D.-Y. Choi, J. Tian, Y. Cai, and S. Chen, Nano Lett. **22**, 6342 (2022).
[64]W.-J. Joo, J. Kyoung, M. Esfandyarpour, S.-H. Lee, H. Koo, S. Song, Y.-N. Kwon, S. H. Song, J. C. Bae, A. Jo, M.-J. Kwon, S. H. Han, S.-H. Kim, S. Hwang, and M. L. Brongersma, Science **370**, 459 (2020).
[65]S. Cao, Y. Jin, H. Dong, T. Guo, J. He, and S. He, J. Phys.: Mater. **4**, 035001 (2021).
[66]G. Lozano, D. J. Louwers, S. R. Rodríguez, S. Murai, O. T. Jansen, M. A. Verschuuren, and J. Gómez Rivas, Light: Sci. Appl. **2**, e66 (2013).
[67]I. Staude, T. Pertsch, and Y. S. Kivshar, ACS Photonics **6**, 802 (2019).
[68]R. Mupparapu, T. Bucher, and I. Staude, Adv. Phys.: X **5**, 1734083 (2020).
[69]Y. Liu, S. C. Lau, W.-H. Cheng, A. Johnson, Q. Li, E. Simmerman, O. Karni, J. Hu, F. Liu, M. L. Brongersma, T. F. Heinz, and J. A. Dionne, Nano Lett. **23**, 6124 (2023).
[70]V. G. Kravets, A. V. Kabashin, W. L. Barnes, and A. N. Grigorenko, Chem. Rev. **118**, 5912 (2018).
[71]S. I. Azzam and A. V. Kildishev, Adv. Opt. Mater. **9**, 2001469 (2021).
[72]A. Bashiri, A. Vaskin, K. Tanaka, M. Steinert, T. Pertsch, and I. Staude, ACS Nano **18**, 506 (2023).
[73]K. Koshelev, S. Lepeshov, M. Liu, A. Bogdanov, and Y. Kivshar, Phys. Rev. Lett. **121**, 193903 (2018).
[74]A. H. Schokker and A. F. Koenderink, Optica **3**, 686 (2016).
[75]P. Törmä and W. L. Barnes, Rep. Prog. Phys. **78**, 013901 (2014).
[76]D. Wang, W. Wang, M. P. Knudson, G. C. Schatz, and T. W. Odom, Chem. Rev. **118**, 2865 (2017).
[77]T. Gu, H. J. Kim, C. Rivero-Baleine, and J. Hu, Nat. Photonics **17**, 48 (2023).
[78]A. F. Koenderink, ACS Photonics **4**, 710 (2017).
[79]A. Krasnok, S. Glybovski, M. Petrov, S. Makarov, R. Savelev, P. Belov, C. Simovski, and Y. S. Kivshar, Appl. Phys. Lett. **108**, 211105 (2016).

16 July 2024 09:29:41

© Author(s) 2024

[80]K. Tanaka, E. Plum, J. Y. Ou, T. Uchino, and N. I. Zheludev, Phys. Rev. Lett. **105**, 227403 (2010).
[81]L. Zhu, S. Yuan, C. Zeng, and J. Xia, Adv. Opt. Mater. **8**, 1901830 (2020).
[82]M. Ramezani, A. Halpin, A. I. Fernández-Domínguez, J. Feist, S. R.-K. Rodriguez, F. J. Garcia-Vidal, and J. Gómez Rivas, Optica **4**, 31 (2017).
[83]A. Vaskin, J. Bohn, K. E. Chong, T. Bucher, M. Zilk, D.-Y. Choi, D. N. Neshev, Y. S. Kivshar, T. Pertsch, and I. Staude, ACS Photonics **5**, 1359 (2018).
[84]J. Lin, Q. Sun, W. Feng, S. Guo, Z. Liu, H. Liang, and J. Li, Adv. Photonics Res. **2**, 2000145 (2021).
[85]Y.-Y. Xie, P.-N. Ni, Q.-H. Wang, Q. Kan, G. Briere, P.-P. Chen, Z.-Z. Zhao, A. Delga, H.-R. Ren, H.-D. Chen, C. Xu, and P. Genevet, Nat. Nanotechnol. **15**, 125 (2020).
[86]C. Huang, C. Zhang, S. Xiao, Y. Wang, Y. Fan, Y. Liu, N. Zhang, G. Qu, H. Ji, J. Han, L. Ge, Y. S. Kivshar, and Q. Song, Science **367**, 1018 (2020).
[87]X. Zhang, Y. Liu, J. Han, Y. S. Kivshar, and Q. Song, Science **377**, 1215 (2022).
[88]P. P. Iyer, N. Karl, S. Addamane, S. D. Gennaro, M. B. Sinclair, and I. Brener, Nat. Photonics **17**, 588 (2023).
[89]J. Bohn, T. Bucher, K. E. Chong, A. Komar, D.-Y. Choi, D. N. Neshev, Y. S. Kivshar, T. Pertsch, and I. Staude, Nano Lett. **18**, 3461 (2018).
[90]Y. Chang, J. Wei, and C. Lee, Nanophotonics **9**, 3049 (2020).
[91]Y. Chen, J. Feng, Y. Huang, W. Chen, R. Su, S. Ghosh, Y. Hou, Q. Xiong, and C.-W. Qiu, Nat. Mater. **22**, 1065 (2023).
[92]T. Bucher, A. Vaskin, R. Mupparapu, F. J. Löchner, A. George, K. E. Chong, S. Fasold, C. Neumann, D.-Y. Choi, F. Eilenberger, F. Setzpfandt, Y. S. Kivshar, T. Pertsch, A. Turchanin, and I. Staude, ACS Photonics **6**, 1002 (2019).
[93]S. Vadia, J. Scherzer, K. Watanabe, T. Taniguchi, and A. Högele, Nano Lett. **23**, 614 (2023).
[94]B. Gallinet, J. Butet, and O. J. Martin, Laser Photonics Rev. **9**, 577 (2015).
[95]G. Yoon and J. Rho, Comput. Phys. Commun. **264**, 107846 (2021).
[96]Y. Chen, Y. Zhang, and A. Femius Koenderink, Opt. Express **25**, 21358 (2017).
[97]F. Capolino, D. R. Jackson, D. R. Wilton, and L. B. Felsen, IEEE Trans. Antennas Propagat. **55**, 1644 (2007).
[98]S. Zhang, E. R. Martins, A. G. Diyaf, J. I. Wilson, G. A. Turnbull, and I. D. Samuel, Synth. Met. **205**, 127 (2015).
[99]V. Su, C. Chu, G. Sun, and D. Tsai, Opt. Express **26**, 13148 (2018).
[100]A. Vaskin, S. Liu, S. Addamane, P. P. Vabishchevich, Y. Yang, G. Balarishnan, M. B. Sinclair, T. Pertsch, I. Brener, and I. Staude, Opt. Express **29**, 5567 (2021).
[101]I. Staude, V. V. Khardikov, N. T. Fofang, S. Liu, M. Decker, D. N. Neshev, T. S. Luk, I. Brener, and Y. S. Kivshar, ACS Photonics **2**, 172 (2015).
[102]Z. F. Sadrieva, I. S. Sinev, K. L. Koshelev, A. Samusev, I. V. Iorsh, O. Takayama, R. Malureanu, A. A. Bogdanov, and A. V. Lavrinenko, ACS Photonics **4**, 723 (2017).
[103]N. Li, Z. Xu, Y. Dong, T. Hu, Q. Zhong, Y. H. Fu, S. Zhu, and N. Singh, Nanophotonics **9**, 3071 (2020).
[104]G. Brière, P. Ni, S. Héron, S. Chenot, S. Vézian, V. Brändli, B. Damilano, J.-Y. Duboz, M. Iwanaga, and P. Genevet, Adv. Opt. Mater. **7**, 1801271 (2019).
[105]A. I. Kuznetsov, A. B. Evlyukhin, M. R. Goncalves, C. Reinhardt, A. Koroleva, M. L. Arnedillo, R. Kiyan, O. Marti, and B. N. Chichkov, ACS Nano **5**, 4843 (2011).
[106]M. Vellaichamy, M. Škarabot, and I. Muševič, Liq. Cryst. **50**, 935 (2023).
[107]S. Karaveli, S. Wang, G. Xiao, and R. Zia, ACS Nano **7**, 7165 (2013).
[108]R. A. DeCrescent, N. R. Venkatesan, C. J. Dahlman, R. M. Kennard, X. Zhang, W. Li, X. Du, M. L. Chabinyc, R. Zia, and J. A. Schuller, Sci. Adv. **6**, eaay4900 (2020).
[109]R. Kolkowski and A. Shevchenko, Nanophotonics **12**, 3443 (2023).
[110]M. Yoshida, S. Katsuno, T. Inoue, J. Gelleta, K. Izumi, M. De Zoysa, K. Ishizaki, and S. Noda, Nature **618**, 727 (2023).
[111]J. W. You, Z. Lan, Q. Ma, Z. Gao, Y. Yang, F. Gao, M. Xiao, and T. J. Cui, Photonics Res. **11**, B65 (2023).
[112]R. El-Ganainy, K. G. Makris, M. Khajavikhan, Z. H. Musslimani, S. Rotter, and D. N. Christodoulides, Nat. Phys. **14**, 11–19 (2018).
[113]Y. Zeng, U. Chattopadhyay, B. Zhu, B. Qiang, J. Li, Y. Jin, L. Li, A. G. Davies, E. H. Linfield, B. Zhang, Y. Chong, and Q. J. Wang, Nature **578**, 246 (2020).
[114]M. Lyubarov, Y. Lumer, A. Dikopoltsev, E. Lustig, Y. Sharabi, and M. Segev, Science **377**, 425 (2022).
[115]R. W. Boyd, A. L. Gaeta, and E. Giese, *Springer Handbook of Atomic, Molecular, and Optical Physics* (Springer, 2008), pp. 1097–1110.
[116]T. Santiago-Cruz, V. Sultanov, H. Zhang, L. Krivitsky, and M. Chekhova, Opt. Lett. **46**, 653 (2021).
[117]G. B. Lemos, V. Borish, G. D. Cole, S. Ramelow, R. Lapkiewicz, and A. Zeilinger, Nature **512**, 409 (2014).
[118]G. Brida, M. Genovese, and I. R. Berchera, Nat. Photonics **4**, 227 (2010).
[119]G. Triginer Garces, H. M. Chrzanowski, S. Daryanoosh, V. Thiel, A. L. Marchant, R. B. Patel, P. C. Humphreys, A. Datta, and I. A. Walmsley, Appl. Phys. Lett. **117**, 024002 (2020).
[120]C. A. Casacio, L. S. Madsen, A. Terrasson, M. Waleed, K. Barnscheidt, B. Hage, M. A. Taylor, and W. P. Bowen, Nature **594**, 201 (2021).
[121]E. Pearce, N. R. Gemmell, J. Flórez, J. Ding, R. F. Oulton, A. S. Clark, and C. C. Phillips, Opt. Continuum **2**, 2386 (2023).
[122]S. R. Marder, D. N. Beratan, and L.-T. Cheng, Science **252**, 103 (1991).
[123]S. R. Marder, L.-T. Cheng, B. G. Tiemann, A. C. Friedli, M. Blanchard-Desce, J. W. Perry, and J. Skindhøj, Science **263**, 511 (1994).
[124]M. P. Nielsen, X. Shi, P. Dichtl, S. A. Maier, and R. F. Oulton, Science **358**, 1179 (2017).
[125]A. Autere, H. Jussila, Y. Dai, Y. Wang, H. Lipsanen, and Z. Sun, Adv. Mater. **30**, 1705963 (2018).
[126]H.-W. Guo, Z. Hu, Z.-B. Liu, and J.-G. Tian, Adv. Funct. Mater. **31**, 2007810 (2021).
[127]Z. Sun, A. Martinez, and F. Wang, Nat. Photonics **10**, 227 (2016).
[128]B. Guo, Q.-l. Xiao, S.-h. Wang, and H. Zhang, Laser Photonics Rev. **13**, 1800327 (2019).
[129]K. O'Brien, H. Suchowski, J. Rho, A. Salandrino, B. Kante, X. Yin, and X. Zhang, Nat. Mater. **14**, 379 (2015).
[130]T. Pertsch and Y. Kivshar, MRS Bull. **45**, 210 (2020).
[131]V. Giannini, A. I. Fernández-Domínguez, S. C. Heck, and S. A. Maier, Chem. Rev. **111**, 3888 (2011).
[132]D. Smirnova and Y. S. Kivshar, Optica **3**, 1241 (2016).
[133]P. Genevet, F. Capasso, F. Aieta, M. Khorasaninejad, and R. Devlin, Optica **4**, 139 (2017).
[134]M. F. Limonov, M. V. Rybin, A. N. Poddubny, and Y. S. Kivshar, Nat. Photonics **11**, 543 (2017).
[135]B. Sain, C. Meier, and T. Zentgraf, Adv. Photonics **1**, 024002 (2019).
[136]G. Quaranta, G. Basset, O. J. Martin, and B. Gallinet, Laser Photonics Rev. **12**, 1800017 (2018).
[137]J. Zhang, J. Ma, M. Parry, M. Cai, R. Camacho-Morales, L. Xu, D. Neshev, and A. Sukhorukov, Sci. Adv. **8**, 4240 (2022).
[138]L. Michaeli, S. Keren-Zur, O. Avayu, H. Suchowski, and T. Ellenbogen, Phys. Rev. Lett. **118**, 243904 (2017).
[139]R. Czaplicki, A. Kiviniemi, J. Laukkanen, J. Lehtolahti, M. Kuittinen, and M. Kauranen, Opt. Lett. **41**, 2684 (2016).
[140]K. Koshelev, A. Bogdanov, and Y. Kivshar, Sci. Bull. **64**, 836 (2019).
[141]C. W. Hsu, B. Zhen, A. D. Stone, J. D. Joannopoulos, and M. Soljačić, Nat. Rev. Mater. **1**, 16048 (2016).
[142]Y. Zhao, Y. Yang, and H.-B. Sun, PhotoniX **2**, 3 (2021).
[143]B. Metzger, L. Gui, J. Fuchs, D. Floess, M. Hentschel, and H. Giessen, Nano Lett. **15**, 3917 (2015).
[144]G. Li, S. Chen, N. Pholchai, B. Reineke, P. W. H. Wong, E. Y. B. Pun, K. W. Cheah, T. Zentgraf, and S. Zhang, Nat. Mater. **14**, 607 (2015).
[145]M. R. Shcherbakov, D. N. Neshev, B. Hopkins, A. S. Shorokhov, I. Staude, E. V. Melik-Gaykazyan, M. Decker, A. A. Ezhov, A. E. Miroshnichenko, I. Brener, A. A. Fedyanin, and Y. S. Kivshar, Nano Lett. **14**, 6488 (2014).
[146]G. Grinblat, Y. Li, M. P. Nielsen, R. F. Oulton, and S. A. Maier, Nano Lett. **16**, 4635 (2016).
[147]M. R. Shcherbakov, A. S. Shorokhov, D. N. Neshev, B. Hopkins, I. Staude, E. V. Melik-Gaykazyan, A. A. Ezhov, A. E. Miroshnichenko, I. Brener, A. A. Fedyanin, and Y. S. Kivshar, ACS Photonics **2**, 578 (2015).
[148]T. Shibanuma, G. Grinblat, P. Albella, and S. A. Maier, Nano Lett. **17**, 2647 (2017).
[149]H. Liu, C. Guo, G. Vampa, J. L. Zhang, T. Sarmiento, M. Xiao, P. H. Bucksbaum, J. Vučković, S. Fan, and D. A. Reis, Nat. Phys. **14**, 1006 (2018).

16 July 2024 09:29:41

© Author(s) 2024

[150]B. Hopkins, D. S. Filonov, A. E. Miroshnichenko, F. Monticone, A. Alù, and Y. S. Kivshar, ACS Photonics **2**, 724 (2015).
[151]A. P. Anthur, H. Zhang, R. Paniagua-Dominguez, D. A. Kalashnikov, S. T. Ha, T. W. Maß, A. I. Kuznetsov, and L. Krivitsky, Nano Lett. **20**, 8745 (2020).
[152]K. Koshelev, S. Kruk, E. Melik-Gaykazyan, J.-H. Choi, A. Bogdanov, H.-G. Park, and Y. Kivshar, Science **367**, 288 (2020).
[153]Y. Yang, J. Lu, A. Manjavacas, T. S. Luk, H. Liu, K. Kelley, J.-P. Maria, E. L. Runnerstrom, M. B. Sinclair, S. Ghimire *et al.*, Nat. Phys. **15**, 1022 (2019).
[154]M. Z. Alam, S. A. Schulz, J. Upham, I. D. Leon, and R. W. Boyd, Nat. Photonics **12**, 79 (2018).
[155]A. Xomalis, X. Zheng, R. Chikkaraddy, Z. Koczor-Benda, E. Miele, E. Rosta, G. A. Vandenbosch, A. Martínez, and J. J. Baumberg, Science **374**, 1268 (2021).
[156]L. Kühner, L. Sortino, R. Berté, J. Wang, H. Ren, S. A. Maier, Y. Kivshar, and A. Tittl, Nat. Commun. **13**, 4992 (2022).
[157]C. Gigli and G. Leo, Opto-Electron. Adv. **5**, 210093 (2022).
[158]S. Gennaro, M. Rahmani, V. Giannini, H. Aouani, T. Sidiropoulos, M. Navarro-Cía, S. Maier, and R. Oulton, Nano Lett. **16**, 5278 (2016).
[159]E. Rahimi and R. Gordon, Adv. Opt. Mater. **6**, 1800274 (2018).
[160]P.-Y. Chen, C. Argyropoulos, and A. Alù, Nanophotonics **1**, 221 (2012).
[161]L. Wang, S. Kruk, K. Koshelev, I. Kravchenko, B. Luther-Davies, and Y. Kivshar, Nano Lett. **18**, 3978 (2018).
[162]M. Celebrano, X. Wu, M. Baselli, S. Großmann, P. Biagioni, A. Locatelli, C. De Angelis, G. Cerullo, R. Osellame, B. Hecht *et al.*, Nat. Nanotechnol. **10**, 412 (2015).
[163]S. Kruk and Y. Kivshar, ACS Photonics **4**, 2638 (2017).
[164]M. W. Klein, C. Enkrich, M. Wegener, and S. Linden, Science **313**, 502 (2006).
[165]Y. Yang and S. I. Bozhevolnyi, Nanotechnology **30**, 204001 (2019).
[166]G. Grinblat, Y. Li, M. P. Nielsen, R. F. Oulton, and S. A. Maier, ACS Photonics **4**, 2144 (2017).
[167]Y. Yang, V. A. Zenin, and S. I. Bozhevolnyi, ACS Photonics **5**, 1960 (2018).
[168]G. F. Walsh and L. Dal Negro, Nano Lett. **13**, 3111 (2013).
[169]K. Thyagarajan, J. Butet, and O. J. Martin, Nano Lett. **13**, 1847 (2013).
[170]L. Wang, S. Kruk, L. Xu, M. Rahmani, D. Smirnova, A. Solntsev, I. Kravchenko, D. Neshev, and Y. Kivshar, Nanoscale **9**, 2201 (2017).
[171]T. Liu, S. Xiao, B. Li, M. Gu, H. Luan, and X. Fang, Front. Nanotechnol. **4**, 891892 (2022).
[172]S. Kruk, M. Weismann, A. Y. Bykov, E. A. Mamonov, I. A. Kolmychek, T. Murzina, N. C. Panoiu, D. N. Neshev, and Y. S. Kivshar, ACS Photonics **2**, 1007 (2015).
[173]L. Wang, A. S. Shorokhov, P. N. Melentiev, S. Kruk, M. Decker, C. Helgert, F. Setzpfandt, A. A. Fedyanin, Y. S. Kivshar, and D. N. Neshev, ACS Photonics **3**, 1494 (2016).
[174]S.-D. Liu, E. S. P. Leong, G.-C. Li, Y. Hou, J. Deng, J. H. Teng, H. C. Ong, and D. Y. Lei, ACS Nano **10**, 1442 (2016).
[175]F. H. Stillinger and D. R. Herrick, Phys. Rev. A **11**, 446 (1975).
[176]D. Marinica, A. Borisov, and S. Shabanov, Phys. Rev. Lett. **100**, 183902 (2008).
[177]Z. Liu, J. Wang, B. Chen, Y. Wei, W. Liu, and J. Liu, Nano Lett. **21**, 7405 (2021).
[178]N. Bernhardt, K. Koshelev, S. J. White, K. W. C. Meng, J. E. Froch, S. Kim, T. T. Tran, D.-Y. Choi, Y. Kivshar, and A. S. Solntsev, Nano Lett. **20**, 5309 (2020).
[179]M. J. Huttunen, P. Rasekh, R. W. Boyd, and K. Dolgaleva, Phys. Rev. A **97**, 053817 (2018).
[180]S. Keren-Zur, M. Tal, S. Fleischer, D. M. Mittleman, and T. Ellenbogen, Nat. Commun. **10**, 1778 (2019).
[181]E. Minerbi, S. Keren-Zur, and T. Ellenbogen, Nano Lett. **19**, 6072 (2019).
[182]D. Polyushkin, E. Hendry, E. Stone, and W. Barnes, Nano Lett. **11**, 4718 (2011).
[183]L. Luo, I. Chatzakis, J. Wang, F. B. Niesler, M. Wegener, T. Koschny, and C. M. Soukoulis, Nat. Commun. **5**, 3055 (2014).
[184]M. Z. Alam, I. De Leon, and R. W. Boyd, Science **352**, 795 (2016).
[185]L. Caspani, R. Kaipurath, M. Clerici, M. Ferrera, T. Roger, J. Kim, N. Kinsey, M. Pietrzyk, A. Di Falco, V. Shalaev, A. Boltasseva, and D. Faccio, Phys. Rev. Lett. **116**, 233901 (2016).
[186]N. Engheta, Science **340**, 286 (2013).
[187]T. S. Luk, D. De Ceglia, S. Liu, G. A. Keeler, R. P. Prasankumar, M. A. Vincenti, M. Scalora, M. B. Sinclair, and S. Campione, Appl. Phys. Lett. **106**, 151103 (2015).
[188]X. Niu, X. Hu, S. Chu, and Q. Gong, Adv. Opt. Mater. **6**, 1701292 (2018).
[189]S. Campione, I. Brener, and F. Marquier, Phys. Rev. B **91**, 121408 (2015).
[190]L. Li, Z. Liu, X. Ren, S. Wang, V.-C. Su, M.-K. Chen, C. Chu, H. Kuo, B. Liu, W. Zang, G. Guo, L. Zhang, Z. Wang, S. Zhu, and D. Tsai, Science **368**, 1487 (2020).
[191]H. Aouani, M. Rahmani, M. Navarro-Cía, and S. A. Maier, Nat. Nanotechnol. **9**, 290 (2014).
[192]A. Melikyan, L. Alloatti, A. Muslija, D. Hillerkuss, P. C. Schindler, J. Li, R. Palmer, D. Korn, S. Muehlbrandt, D. Van Thourhout *et al.*, Nat. Photonics **8**, 229 (2014).
[193]T. J. Duffin, M. P. Nielsen, F. Diaz, S. Palomba, S. A. Maier, and R. F. Oulton, Opt. Lett. **41**, 155 (2016).
[194]W. Chen, P. Roelli, H. Hu, S. Verlekar, S. P. Amirtharaj, A. I. Barreda, T. J. Kippenberg, M. Kovylina, E. Verhagen, A. Martínez *et al.*, Science **374**, 1264 (2021).
[195]C. Gigli, T. Wu, G. Marino, A. Borne, G. Leo, and P. Lalanne, ACS Photonics **7**, 1197 (2020).
[196]K. Frizyuk, I. Volkovskaya, D. Smirnova, A. Poddubny, and M. Petrov, Phys. Rev. B **99**, 075425 (2019).
[197]R. Camacho-Morales, M. Rahmani, S. Kruk, L. Wang, L. Xu, D. A. Smirnova, A. S. Solntsev, A. Miroshnichenko, H. H. Tan, F. Karouta *et al.*, Nano Lett. **16**, 7191 (2016).
[198]V. F. Gili, L. Carletti, F. Chouchane, G. Wang, C. Ricolleau, D. Rocco, A. Lemaître, I. Favero, L. Ghirardini, M. Finazzi, M. Celebrano, C. De Angelis, and G. Leo, Nanophotonics **7**, 517 (2017).
[199]A. V. Kildishev, A. Boltasseva, and V. M. Shalaev, Science **339**, 1232009 (2013).
[200]S. Keren-Zur, O. Avayu, L. Michaeli, and T. Ellenbogen, ACS Photonics **3**, 117 (2016).
[201]S. Chen, G. Li, F. Zeuner, W. H. Wong, E. Y. B. Pun, T. Zentgraf, K. W. Cheah, and S. Zhang, Phys. Rev. Lett. **113**, 033901 (2014).
[202]W. Ye, F. Zeuner, X. Li, B. Reineke, S. He, C.-W. Qiu, J. Liu, Y. Wang, S. Zhang, and T. Zentgraf, Nat. Commun. **7**, 11930 (2016).
[203]B. Liu, B. Sain, B. Reineke, R. Zhao, C. Meier, L. Huang, Y. Jiang, and T. Zentgraf, Adv. Opt. Mater. **8**, 1902050 (2020).
[204]M. Jin, Z. Hu, X. Liu, and G. Li, Laser Photonics Rev. **17**, 2300174 (2023).
[205]N. Segal, S. Keren-Zur, N. Hendler, and T. Ellenbogen, Nat. Photonics **9**, 180 (2015).
[206]O. Wolf, S. Campione, A. Benz, A. P. Ravikumar, S. Liu, T. S. Luk, E. A. Kadlec, E. A. Shaner, J. F. Klem, M. B. Sinclair *et al.*, Nat. Commun. **6**, 7667 (2015).
[207]E. Almeida, O. Bitton, and Y. Prior, Nat. Commun. **7**, 12533 (2016).
[208]H. Ren, X. Fang, J. Jang, J. Bürger, J. Rho, and S. A. Maier, Nat. Nanotechnol. **15**, 948 (2020).
[209]T. Cui, B. Bai, H.-B. Sun, T. Cui, B. Bai, and H. Sun, Adv. Funct. Mater. **29**, 1806692 (2019).
[210]W. Cai, A. P. Vasudev, and M. L. Brongersma, Science **333**, 1720 (2011).
[211]W. Ding, L. Zhou, and S. Y. Chou, Nano Lett. **14**, 2822 (2014).
[212]L. Kang, Y. Cui, S. Lan, S. P. Rodrigues, M. L. Brongersma, and W. Cai, Nat. Commun. **5**, 4680 (2014).
[213]K.-T. Lee, M. Taghinejad, J. Yan, A. S. Kim, L. Raju, D. K. Brown, and W. Cai, ACS Photonics **6**, 2663 (2019).
[214]J. Yu, S. Park, I. Hwang, D. Kim, F. Demmerle, G. Boehm, M.-C. Amann, M. A. Belkin, and J. Lee, Nat. Photonics **16**, 72 (2022).
[215]S. Kim, J. Jin, Y.-J. Kim, I.-Y. Park, Y. Kim, and S.-W. Kim, Nature **453**, 757 (2008).
[216]I.-Y. Park, S. Kim, J. Choi, D.-H. Lee, Y.-J. Kim, M. F. Kling, M. I. Stockman, and S.-W. Kim, Nat. Photonics **5**, 677 (2011).
[217]M. Krüger, M. Schenk, and P. Hommelhoff, Nature **475**, 78 (2011).
[218]G. Herink, D. R. Solli, M. Gulde, and C. Ropers, Nature **483**, 190 (2012).
[219]S. Sederberg, F. Kong, F. Hufnagel, C. Zhang, E. Karimi, and P. B. Corkum, Nat. Photonics **14**, 680 (2020).
[220]S. Han, H. Kim, Y. W. Kim, Y.-J. Kim, S. Kim, I.-Y. Park, and S.-W. Kim, Nat. Commun. **7**, 13105 (2016).

16 July 2024 09:29:41

© Author(s) 2024

[221]M. Sivis, M. Taucer, G. Vampa, K. Johnston, A. Staudte, A. Y. Naumov, D. Villeneuve, C. Ropers, and P. Corkum, Science **357**, 303 (2017).
[222]G. Vampa, B. Ghamsari, S. Siadat Mousavi, T. Hammond, A. Olivieri, E. Lisicka-Skrek, A. Y. Naumov, D. Villeneuve, A. Staudte, P. Berini *et al.*, Nat. Phys. **13**, 659 (2017).
[223]K. Imasaka, T. Kaji, T. Shimura, and S. Ashihara, Opt. Express **26**, 21364 (2018).
[224]H. Im, K. C. Bantz, N. C. Lindquist, C. L. Haynes, and S.-H. Oh, Nano Lett. **10**, 2231 (2010).
[225]J. Lee, N. Nookala, J. S. Gomez-Diaz, M. Tymchenko, F. Demmerle, G. Boehm, M.-C. Amann, A. Alù, and M. A. Belkin, Adv. Opt. Mater. **4**, 664 (2016).
[226]H.-H. Hsiao, C. H. Chu, and D. P. Tsai, "Metasurfaces: Fundamentals and applications of metasurfaces (Small Methods 4/2017)," Small Methods **1** (2017).
[227]H. Altug, S.-H. Oh, S. Maier, and J. Homola, Nat. Nanotechnol. **17**, 5 (2022).
[228]F. Mazzotta, T. Johnson, A. Dahlin, J. Shaver, S.-H. Oh, and F. Höök, ACS Photonics **2**, 256 (2015).
[229]S. S. Kruk, R. Camacho-Morales, L. Xu, M. Rahmani, D. A. Smirnova, L. Wang, H. H. Tan, C. Jagadish, D. N. Neshev, and Y. S. Kivshar, Nano Lett. **17**, 3914 (2017).
[230]D. Nguyen, S. Lee, and I. Kim, Biosensors **13**, 631 (2023).
[231]S. Unser, I. Bruzas, J. He, and L. Sagle, Sensors **15**, 15684 (2015).
[232]J. He, M. Boegli, I. Bruzas, W. Lum, and L. Sagle, Anal. Chem. **87**, 11407 (2015).
[233]A. Rapisarda, N. Giamblanco, and G. Marletta, J. Colloid Interface Sci. **487**, 141 (2017).
[234]J. Guerreiro, V. Bochenkov, K. Runager, H. Aslan, M. Dong, J. Enghild, V. De Freitas, M. Ferreira Sales, and D. Sutherland, ACS Sens. **1**, 258 (2016).
[235]X. Cheng, G. Wallace, F. Lagugné-Labarthet, and K. Kerman, ACS Appl. Mater. Interfaces **7**, 4081 (2015).
[236]J. Zhou, F. Tao, J. Zhu, S. Lin, Z. Wang, X. Wang, J.-Y. Ou, Y. Li, and Q. Liu, Nanophotonics **8**, 307 (2019).
[237]J. Sperling, G. Macias, S. Neale, and A. Clark, ACS Appl. Mater. Interfaces **10**, 34774 (2018).
[238]A. Clark and J. Cooper, Angew. Chem. **124**, 3622 (2012).
[239]A. Clark, D. Thompson, D. Graham, and J. Cooper, Adv. Mater. **26**, 4286 (2014).
[240]S. Aćimović, M. Ortega, V. Sanz, J. Berthelot, J. Garcia-Cordero, J. Renger, S. Maerkl, M. Kreuzer, and R. Quidant, Nano Lett. **14**, 2636 (2014).
[241]Y. Shen, J. Zhou, T. Liu, Y. Tao, R. Jiang, M. Liu, G. Xiao, J. Zhu, Z.-K. Zhou, X. Wang, C. Jin, and J. Wang, Nat. Commun. **4**, 2381 (2013).
[242]Z. Li, Y. Zhu, Y. Hao, M. Gao, M. Lu, A. Stein, A.-H. A. Park, J. Hone, Q. Lin, and N. Yu, ACS Photonics **6**, 501 (2019).
[243]D. Rodrigo, A. Tittl, N. Ait-Bouziad, A. John-Herpin, O. Limaj, C. Kelly, D. Yoo, N. Wittenberg, S.-H. Oh, H. Lashuel, and H. Altug, Nat. Commun. **9**, 2160 (2018).
[244]N. Bontempi, K. Chong, H. Orton, I. Staude, D.-Y. Choi, I. Alessandri, Y. Kivshar, and D. Neshev, Nanoscale **9**, 4972 (2017).
[245]Y. Wang, M. Ali, E. Chow, L. Dong, and M. Lu, Biosens. Bioelectron. **107**, 224 (2018).
[246]O. Yavas, M. Svedendahl, P. Dobosz, V. Sanz, and R. Quidant, Nano Lett. **17**, 4421 (2017).
[247]O. Yavas, M. Svedendahl, and R. Quidant, ACS Nano **13**, 4582 (2019).
[248]G. Triggs, Y. Wang, C. Reardon, M. Fischer, G. Evans, and T. Krauss, Optica **4**, 229 (2017).
[249]J. Wang, J. Kühne, T. Karamanos, C. Rockstuhl, S. Maier, and A. Tittl, Adv. Funct. Mater. **31**, 2104652 (2021).
[250]A. Leitis, A. Tittl, M. Liu, B. Lee, M. Gu, Y. Kivshar, and H. Altug, "Angle-multiplexed all-dielectric metasurfaces for broadband molecular fingerprint retrieval," Sci. Adv. **5**, eaaw2871 (2019).
[251]F. Yesilkoy, E. Arvelo, Y. Jahani, M. Liu, A. Tittl, V. Cevher, Y. Kivshar, and H. Altug, Nat. Photonics **13**, 390 (2019).
[252]C. Jack, A. Karimullah, R. Leyman, R. Tullius, V. Rotello, G. Cooke, N. Gadegaard, L. Barron, and M. Kadodwala, Nano Lett. **16**, 5806 (2016).
[253]S. Yoo and Q. Park, Nanophotonics **8**, 249 (2019).
[254]S. Wallace, M. Kartau, T. Kakkar, C. Davis, A. Szemiel, I. Samardzhieva, S. Vijayakrishnan, S. Cole, G. De Lorenzo, E. Maillart, K. Gautier, A. Lapthorn, A. Patel, N. Gadegaard, M. Kadodwala, E. Hutchinson, and A. Karimullah, ACS Sens. **8**, 3338 (2023).
[255]M. Rodier, C. Keijzer, J. Milner, A. Karimullah, A. Roszak, L. Barron, N. Gadegaard, A. Lapthorn, and M. Kadodwala, Nanoscale Horiz. **5**, 336 (2020).
[256]M. Manoccio, M. Esposito, E. Primiceri, A. Leo, V. Tasco, M. Cuscunà, D. Zuev, Y. Sun, G. Maruccio, A. Romano, A. Quattrini, G. Gigli, and A. Passaseo, Nano Lett. **21**, 6179 (2021).
[257]F. Neubrech, C. Huck, K. Weber, A. Pucci, and H. Giessen, Chem. Rev. **117**, 5110 (2017).
[258]M. Seo and H. Park, Adv. Opt. Mater. **8**, 2070010 (2020).
[259]O. Guselnikova, H. Lim, H. Kim, S. Kim, A. Gorbunova, M. Eguchi, P. Postnikov, T. Nakanishi, T. Asahi, J. Na, and Y. Yamauchi, Small **18**, 2107182 (2022).
[260]X. Wang, S.-C. Huang, S. Hu, S. Yan, and B. Ren, Nat. Rev. Phys. **2**, 253 (2020).
[261]H. Aouani, M. Rahmani, H. Šípová, V. Torres, K. Hegnerová, M. Beruete, J. Homola, M. Hong, M. Navarro-Cía, and S. Maier, J. Phys. Chem. C **117**, 18620 (2013).
[262]A. Clark and J. Cooper, Small **7**, 119 (2011).
[263]O. Guselnikova, R. Elashnikov, V. Svorcik, M. Kartau, C. Gilroy, N. Gadegaard, M. Kadodwala, A. Karimullah, and O. Lyutakov, Nanoscale Horiz. **8**, 499 (2023).
[264]I. Alessandri and J. Lombardi, *Quantum Sensing and Nano Electronics and Photonics XV* (SPIE, 2016).
[265]J. Cambiasso, M. König, E. Cortés, S. Schlücker, and S. Maier, ACS Photonics **5**, 1546 (2018).
[266]A. Prasad, J. Choi, Z. Jia, S. Park, and M. Gartia, Biosens. Bioelectron. **130**, 185 (2019).
[267]A. Cetin, D. Etezadi, B. Galarreta, M. Busson, Y. Eksioglu, and H. Altug, ACS Photonics **2**, 1167 (2015).
[268]M. Couture, K. Ray, H.-P. Poirier-Richard, A. Crofton, and J.-F. Masson, ACS Sens. **1**, 287 (2016).
[269]J. Park, H. Im, S. Hong, C. Castro, R. Weissleder, and H. Lee, ACS Photonics **5**, 487 (2018).
[270]H. Im, H. Shao, Y. Park, V. Peterson, C. Castro, R. Weissleder, and H. Lee, Nat. Biotechnol. **32**, 490 (2014).
[271]K. S. Yang, H. Im, S. Hong, I. Pergolini, A. F. del Castillo, R. Wang, S. Clardy, C.-H. Huang, C. Pille, S. Ferrone, R. Yang, C. M. Castro, H. Lee, C. F. del Castillo, and R. Weissleder, Sci. Transl. Med. **9**, eaal3226 (2017).
[272]J. Jackman, E. Linardy, D. Yoo, J. Seo, W. Ng, D. Klemme, N. Wittenberg, S. Oh, and N. Cho, Small **12**, 1159 (2016).
[273]X. Shi, D. Verschueren, and C. Dekker, Nano Lett. **18**, 8003 (2018).
[274]J.-A. Huang, M. Mousavi, Y. Zhao, A. Hubarevich, F. Omeis, G. Giovannini, M. Schütte, D. Garoli, and F. De Angelis, Nat. Commun. **10**, 5321 (2019).
[275]D. Verschueren, S. Pud, X. Shi, L. De Angelis, L. Kuipers, and C. Dekker, ACS Nano **13**, 61 (2019).
[276]D. Verschueren, X. Shi, and C. Dekker, Small Methods **3**, 1800465 (2019).
[277]J. Sperling, B. Poursat, L. Savage, I. Christie, C. Cuthill, B. Aekbote, K. Mcguire, A. Karimullah, J. Robbie, W. Sloan, C. Gauchotte-Lindsay, W. Peveler, and A. Clark, Environ. Sci.: Nano **10**, 3500 (2023).
[278]B. Li, X. Li, Y. Dong, B. Wang, D. Li, Y. Shi, and Y. Wu, Anal. Chem. **89**, 10639 (2017).
[279]N. Kim, M. Thomas, M. Bergholt, I. Pence, H. Seong, P. Charchar, N. Todorova, A. Nagelkerke, A. Belessiotis-Richards, D. Payne, A. Gelmi, I. Yarovsky, and M. Stevens, Nat. Commun. **11**, 207 (2020).
[280]W. Peveler, M. Yazdani, and V. Rotello, ACS Sens. **1**, 1282 (2016).
[281]Y. Geng, W. Peveler, and V. Rotello, Angew. Chem., Int. Ed. **58**, 5190 (2019).
[282]J.-F. Masson, J. Biggins, and E. Ringe, Nat. Nanotechnol. **18**, 111 (2023).
[283]X. Lu, K. Suslick, and Z. Li, Anal. Sens. **3**, e202200050 (2023).
[284]N. Fahimi-Kashani and M. Hormozi-Nezhad, Anal. Chem. **88**, 8099 (2016).
[285]F. Shahdost-Fard, A. Bigdeli, and M. Hormozi-Nezhad, ACS Chem. Neurosci. **12**, 3157 (2021).
[286]F. Ghasemi, M. Hormozi-Nezhad, and M. Mahmoudi, Nanoscale **10**, 6361 (2018).
[287]S. Abbasi-Moayed, A. Orouji, and M. Hormozi-Nezhad, Biosensors **13**, 803 (2023).

16 July 2024 09:29:41

© Author(s) 2024

[288]G. Macias, J. Sperling, W. Peveler, G. Burley, S. Neale, and A. Clark, Nanoscale **11**, 15216 (2019).
[289]W. Li and S. Fan, Opt. Express **26**(12), 15995 (2018).
[290]E. A. Goldstein, A. P. Raman, and S. Fan, Nat. Energy **2**, 17143 (2017).
[291]G. Perrakis, A. C. Tasolamprou, G. Kenanakis, E. N. Economou, S. Tzortzakis, and M. Kafesaki, Opt. Express **28**, 18548 (2020).
[292]W. Li, S. Buddhiraju, and S. Fan, Light: Sci. Appl. **9**, 68 (2020).
[293]G. Ulpiani, G. Ranzi, J. Feng, and M. Santamouris, Energy Build. **243**, 110990 (2021).
[294]R. Y. M. Wong, C. Y. Tso, C. Y. H. Chao, B. Huang, and M. P. Wan, Sol. Energy Mater. Sol. Cells **186**, 330–339 (2018).
[295]M. Wei, W. Wu, D. Li, H. Xu, Y. Lu, and W. Song, Sol. Energy **207**, 471–478 (2020).
[296]A. P. Raman, M. A. Anoma, L. Zhu, E. Rephaeli, and S. Fan, Nature **515**, 540 (2014).
[297]K. Tang, K. Dong, J. Li, M. P. Gordon, F. G. Reichertz, H. Kim, Y. Rho, Q. Wang, C. Y. Lin, C. P. Grigoropoulos, A. Javey, J. J. Urban, J. Yao, R. Levinson, and J. Wu, Science **374**, 1504 (2021).
[298]J. Fan, C. Fu, and T. Fu, Appl. Therm. Eng. **165**, 114585 (2020).
[299]S. Y. Heo, G. J. Lee, D. H. Kim, Y. J. Kim, S. Ishii, M. S. Kim, T. J. Seok, B. J. Lee, H. Lee, and Y. M. Song, Sci. Adv. **6**, eabb1906 (2020).
[300]J. W. Cho, Y. J. Lee, J. H. Kim, R. Hu, E. Lee, and S. K. Kim, ACS Nano **17**, 10442 (2023).
[301]M. Hossain, B. Jia, M. Gu, M. Hossain, B. Jia, and M. Gu, Adv. Opt. Mater **3**, 1047 (2015).
[302]Y. Zhai, Y. Ma, S. N. David, D. Zhao, R. Lou, G. Tan, R. Yang, and X. Yin, Science **355**(80), 1062 (2017).
[303]S. R. Wu, K. L. Lai, and C. M. Wang, Sci. Rep. **8**, 7684 (2018).
[304]S. Wang, T. Jiang, Y. Meng, R. Yang, G. Tan, and Y. Long, Science **374**, 1501 (2021).
[305]G. Perrakis, A. C. Tasolamprou, G. Kenanakis, E. N. Economou, S. Tzortzakis, and M. Kafesaki, ACS Photonics **9**, 1327 (2022).
[306]G. Perrakis, A. C. Tasolamprou, G. Kenanakis, E. N. Economou, S. Tzortzakis, and M. Kafesaki, Sci. Rep. **11**, 11552 (2021).
[307]J. Jaramillo–Fernandez, G. L. Whitworth, J. A. Pariente, A. Blanco, P. D. Garcia, C. Lopez, and C. M. Sotomayor–Torres, Small **15**, 1905290 (2019).
[308]Y. Tsurimaki, X. Qian, S. Pajovic, F. Han, M. Li, and G. Chen, Phys. Rev. B **101**, 165426 (2020).
[309]T. Liu, L. Huang, W. Hong, Y. Sun, Y. Ling, J. Luan, and G. Yuan, Opt. Express **25**(12), 13648 (2017).
[310]A. Serebryannikov, E. Ozbay, Z. Wang, J. D. Chong, J. D. Joannopoulos, and M. Soljacic, Opt. Express **17**(16), 13335 (2009).
[311]M. Ono, K. Chen, W. Li, and S. Fan, "Self-adaptive radiative cooling based on phase change materials," Opt. Express **26**, A777–A787 (2018).
[312]S. Zhang, L. Liu, S. Ren, Z. Li, Y. Zhao, Z. Yang, R. Hu, J. Qu *et al.*, Opto-Electron. Adv. **3**, 200003 (2020).
[313]W. Wang, Z. Zhao, Q. Zou, B. Hong, W. Zhang, and G. P. Wang, J. Mater. Chem. C **8**, 3192 (2020).
[314]X. Wu and C. Wang, Sol. Energy Mater. Sol. Cells **215**, 110662 (2020).
[315]Q. Wang, T. Liu, L. Li, C. Huang, J. Wang, M. Xiao, Y. Li, and W. Li, Nanophotonics **13**, 793 (2024).
[316]M. Liu, S. Xia, W. Wan, J. Qin, H. Li, C. Zhao, L. Bi, and C. W. Qiu, Nat. Mater. **22**, 1196 (2023).
[317]K. J. Shayegan, S. Biswas, B. Zhao, S. Fan, and H. A. Atwater, Nat. Photonics **17**, 891–896 (2023).
[318]J. Mandal, Y. Yang, N. Yu, and A. P. Raman, Joule **4**, 1350 (2020).
[319]J. Mandal, Y. Fu, A. C. Overvig, M. Jia, K. Sun, N. N. Shi, H. Zhou, X. Xiao, N. Yu, and Y. Yang, Science **362**(80), 315 (2018).
[320]M. Cagnoni, A. Tibaldi, J. S. Dolado, and F. Cappelluti, iScience **25**, 105320 (2022).
[321]G. Kenanakis, A. Xomalis, A. Selimis, M. Vamvakaki, M. Farsari, M. Kafesaki, C. M. Soukoulis, and E. N. Economou, ACS Photonics **2**, 287 (2015).
[322]M. Piccardo, V. Ginis, A. Forbes, S. Mahler, A. A. Friesem, N. Davidson, H. Ren, A. H. Dorrah, F. Capasso, F. T. Dullo, B. S. Ahluwalia, A. Ambrosio, S. Gigan, N. Treps, M. Hiekkamaki, R. Fickler, M. Kues, D. Moss, R. Morandotti, J. Riemensberger, T. J. Kippenberg, J. Faist, G. Scalari, N. Picqué, T. W. Hansch, G. Cerullo, C. Manzoni, L. A. Lugiato, M. Brambilla, L. Columbo, A. Gatti, F. Prati, A. Shiri, A. F. Abouraddy, A. Alu, E. Galiffi, J. B. Pendry, and P. A. Huidobro, J. Opt. **24**(1), 013001 (2021).
[323]P. Wang, A. V. Krasavin, L. Liu, Y. Jiang, Z. Li, X. Guo, L. Tong, and A. V. Zayats, Chem. Rev. **122**, 15031 (2022).
[324]P. Wang, M. E. Nasir, A. V. Krasavin, W. Dickson, Y. Jiang, and A. V. Zayats, Acc. Chem. Res. **52**, 3018 (2019).
[325]P. Wang, A. V. Krasavin, F. N. Viscomi, A. M. Adawi, J. G. Bouillard, L. Zhang, D. J. Roth, L. Tong, and A. V. Zayats, Laser Photonics Rev. **12**, 1800179 (2018).
[326]L. Mascaretti, Y. Chen, O. Henrotte, O. Yesilyurt, V. M. Shalaev, A. Naldoni, and A. Boltasseva, ACS Photonics **10**, 4079 (2023).
[327]Y. Pei, Y. Cheng, J. Chen, W. Smith, P. Dong, P. M. Ajayan, M. Ye, and J. Shen, J. Mater. Chem. A **6**, 23220 (2018).
[328]Y. Wu, W. Yang, Y. Fan, Q. Song, and S. Xiao, Sci. Adv. **5**, eaax0939 (2019).
[329]S. Sun, Z. Zhou, C. Zhang, Y. Gao, Z. Duan, S. Xiao, and Q. Song, ACS Nano **11**, 4445 (2017).
[330]L. Hüttenhofer, F. Eckmann, A. Lauri, J. Cambiasso, E. Pensa, Y. Li, E. Cortés, I. D. Sharp, and S. A. Maier, ACS Nano **14**, 2456 (2020).
[331]L. Hüttenhofer, M. Golibrzuch, O. Bienek, F. J. Wendisch, R. Lin, M. Becherer, I. D. Sharp, S. A. Maier, and E. Cortés, Adv. Energy Mater. **11**, 2102877 (2021).
[332]J. Capitolis, M. Hamandi, M. Hochedel, S. El–Jallal, E. Drouard, C. Chevalier, J. Leclercq, J. Penuelas, T. Dursap, S. Brottet, B. Devif, H. S. Nguyen, G. Berhault, J. Chovelon, C. Ferronato, C. Guillard, E. Puzenat, N. Crespo–Monteiro, S. Reynaud, Y. Jourlin, M. Bugnet, and C. Seassal, Nano Select **3**, 108 (2022).
[333]A. Zaleska, A. Zayats, and W. Dickson, Proc. SPIE **12746**, PC127460B (2023); available at https://www.spiedigitallibrary.org/conference-proceedings-of-spie/PC12746/PC127460B/Enhancing-photochemical-reduction-via-copper-based-metamaterial-catalysts/10.1117/12.2687802.full.
[334]L. Yuan, Y. Zhao, A. Toma, V. Aglieri, B. Gerislioglu, Y. Yuan, M. Lou, A. Ogundare, A. Alabastri, P. Nordlander, and N. J. Halas, Nano Lett. **24**, 172 (2024).
[335]S. Deng, B. Zhang, P. Choo, P. J. M. Smeets, and T. W. Odom, Nano Lett. **21**, 1523 (2021).
[336]M.-J. Yu, C.-L. Chang, H.-Y. Lan, Z.-Y. Chiao, Y.-C. Chen, H. W. Howard Lee, Y.-C. Chang, S.-W. Chang, T. Tanaka, V. Tung, H.-H. Chou, and Y.-J. Lu, ACS Photonics **8**, 3125 (2021).
[337]J. Khurgin, A. Y. Bykov, and A. V. Zayats, "Hot-electron dynamics in plasmonic nanostructures," arXiv:2302.10247 (2023).
[338]J. U. Salmón-Gamboa, M. Romero-Gómez, D. J. Roth, A. V. Krasavin, P. Wang, W. Dickson, and A. V. Zayats, Nanoscale Adv. **3**, 767 (2021).
[339]J. U. Salmón-Gamboa, M. Romero-Gómez, D. J. Roth, M. J. Barber, P. Wang, S. M. Fairclough, M. E. Nasir, A. V. Krasavin, W. Dickson, and A. V. Zayats, Faraday Discuss. **214**, 387 (2019).
[340]A. Y. Bykov, D. J. Roth, G. Sartorello, J. U. Salmón-Gamboa, and A. V. Zayats, Nanophotonics **10**, 2929 (2021).
[341]Y. Zhang, W. Guo, Y. Zhang, and W. D. Wei, Adv. Mater. **33**, 2006654 (2021).
[342]A. Naldoni, Z. A. Kudyshev, L. Mascaretti, S. P. Sarmah, S. Rej, J. P. Froning, O. Tomanec, J. E. Yoo, D. Wang, Š. Kment, T. Montini, P. Fornasiero, V. M. Shalaev, P. Schmuki, A. Boltasseva, and R. Zbořil, Nano Lett. **20**, 3663 (2020).
[343]N. T. Nguyen, M. Xia, P. N. Duchesne, L. Wang, C. Mao, F. M. Ali, T. Yan, P. Li, Z.-H. Lu, and G. A. Ozin, Nano Lett. **21**, 1311 (2021).
[344]P. Wang, A. V. Krasavin, M. E. Nasir, W. Dickson, and A. V. Zayats, Nat. Nanotechnol. **13**, 159 (2018).
[345]C. O. Karaman, A. Y. Bykov, F. Kiani, G. Tagliabue, and A. V. Zayats, Nat. Commun. **15**, 703 (2024).
[346]M. K. Chen, X. Liu, Y. Sun, and D. P. Tsai, Chem. Rev. **122**, 15356 (2022).
[347]A. Thomas, J. George, A. Shalabney, M. Dryzhakov, S. J. Varma, J. Moran, T. Chervy, X. Zhong, E. Devaux, C. Genet, J. A. Hutchison, and T. W. Ebbesen, Angew. Chem., Int. Ed. **55**, 11462 (2016).
[348]A. Y. Bykov, Y. Xie, A. V. Krasavin, and A. V. Zayats, Nano Lett. **23**, 2786 (2023).
[349]A. Brodsky, N. Kaplan, and K. Goldberg, Micros. Today **29**, 60 (2021).
[350]H. He, M. E. J. Friese, N. R. Heckenberg, and H. Rubinsztein-Dunlop, Phys. Rev. Lett. **75**, 826 (1995).
[351]A. Mosk, A. Lagendijk, G. Lerosey, and M. Fink, Nat. Photonics **6**, 283 (2012).
[352]J. Huisken, J. Swoger, F. Del Bene, J. Wittbrodt, and E. Stelzer, Science **305**, 1007 (2004).

16 July 2024 09:29:41

© Author(s) 2024

[353]X. Fang, H. Ren, and M. Gu, Nat. Photonics **14**, 102 (2020).
[354]J. Wang, J.-Y. Yang, I. Fazal, N. Ahmed, Y. Yan, H. Huang, Y. Ren, Y. Yue, S. Dolinar, M. Tur, and A. Willner, Nat. Photonics **6**, 488 (2012).
[355]N. Bozinovic, Y. Yue, Y. Ren, M. Tur, P. Kristensen, H. Huang, A. Willner, and S. Ramachandran, Science **340**, 1545 (2013).
[356]Y. Tang, K. Li, X. Zhang, J. Deng, G. Li, and E. Brasselet, Nat. Photonics **14**, 658 (2020).
[357]W. Brullot, M. Vanbel, T. Swusten, and T. Verbiest, Sci. Adv. **2**, 1501349 (2016).
[358]S.-Y. Huang, J. Zhang, C. Karras, R. Förster, R. Heintzmann, and J.-S. Huang, ACS Photonics **8**, 130 (2020).
[359]C. Li, J. Jang, T. Badloe, T. Yang, J. Kim, J. Kim, M. Nguyen, S. Maier, J. Rho, H. Ren, and I. Aharonovich, eLight **3**, 19 (2023).
[360]P. Ornelas, I. Nape, R. De Mello Koch, and A. Forbes, Nat. Photonics **18**, 258–266 (2024).
[361]T. Stav, A. Faerman, E. Maguid, D. Oren, V. Kleiner, E. Hasman, and M. Segev, Science **361**, 1101 (2018).
[362]M. Decker, I. Staude, M. Falkner, J. Dominguez, D. N. Neshev, I. Brener, T. Pertsch, and Y. S. Kivshar, Adv. Opt. Mater. **3**, 813 (2015).
[363]K. Chong, I. Staude, A. James, J. Dominguez, S. Liu, S. Campione, G. Subramania, T. Luk, M. Decker, D. Neshev, I. Brener, and Y. Kivshar, Nano Lett. **15**, 5369 (2015).
[364]D. Lin, P. Fan, E. Hasman, and M. Brongersma, Science **345**, 298 (2014).
[365]J. Mueller, N. Rubin, R. Devlin, B. Groever, and F. Capasso, Phys. Rev. Lett. **118**, 113901 (2017).
[366]R. Devlin, A. Ambrosio, N. Rubin, J. Mueller, and F. Capasso, Science **358**, 896 (2017).
[367]A. Forbes, M. Oliveira, and M. Dennis, Light: Sci. App. **11**, 253 (2021).
[368]A. Zannotti, C. Denz, M. Alonso, and M. Dennis, Nat. Commun. **11**, 3597 (2020).
[369]A. Dorrah, N. Rubin, M. Tamagnone, A. Zaidi, and F. Capasso, Nat. Commun. **12**, 6249 (2021).
[370]A. Dorrah, N. Rubin, A. Zaidi, M. Tamagnone, and F. Capasso, Nat. Photonics **15**, 287 (2021).
[371]S. Divitt, W. Zhu, C. Zhang, H. Lezec, and A. Agarwal, Science **364**, 890 (2019).
[372]A. Chong, C. Wan, J. Chen, and Q. Zhan, Nat. Photonics **14**, 350 (2020).
[373]L. Chen, W. Zhu, P. Huo, J. Song, H. Lezec, T. Xu, and A. Agrawal, Sci. Adv. **8**, 8314 (2022).
[374]H. Sroor, Y.-W. Huang, B. Sephton, D. Naidoo, A. Vallés, V. Ginis, C.-W. Qiu, A. Ambrosio, F. Capasso, and A. Forbes, Nat. Photonics **14**, 498 (2020).
[375]M. Piccardo, M. D. Oliveira, A. Toma, V. Aglieri, A. Forbes, and A. Ambrosio, "Vortex laser arrays with topological charge control and self-healing of defects," in *Conference on Lasers and Electro-Optics* (Optica Publishing Group, 2022), pp. 1–7.
[376]H. Ren, J. Jang, C. Li, A. Aigner, M. Plidschun, J. Kim, J. Rho, M. Schmidt, and S. Maier, Nat. Commun. **13**, 4183 (2022).
[377]C. Li, T. Wieduwilt, F. Wendisch, A. Márquez, L. Menezes, S. Maier, M. Schmidt, and H. Ren, Nat. Commun. **14**, 7222 (2023).
[378]H. Ren, W. Shao, Y. Li, F. Salim, and M. Gu, Sci. Adv. **6**, 4261 (2019).
[379]C. Liu, S. Zhang, S. Maier, and H. Ren, Phys. Rev. Lett. **129**, 267401 (2022).
[380]P. Huo, C. Zhang, W. Zhu, M. Liu, S. Zhang, S. Zhang, L. Chen, H. Lezec, A. Agrawal, Y. Lu, and T. Xu, Nano Lett. **20**, 2791 (2020).
[381]S. Wang, L. Li, S. Wen, R. Liang, Y. Liu, F. Zhao, and Y. Yang, Nano Lett. **24**, 356 (2023).
[382]T. Dinter, L. Kühner, C. Li, T. Weber, A. Tittl, S. A. Maier, J. M. Dawes, and H. Ren, in *Proceedings of the 2022 Conference on Lasers and Electro-Optics Pacific Rim (CLEOPR)* (Optica Publishing Group, 2022).
[383]A. Solntsev, G. Agarwal, and Y. Kivshar, Nat. Photonics **15**, 327 (2021).
[384]T. Santiago-Cruz, S. Gennaro, O. Mitrofanov, S. Addamane, J. Reno, I. Brener, and M. Chekhova, Science **377**, 991 (2022).
[385]A. Aigner, A. Tittl, J. Wang, T. Weber, Y. Kivshar, S. Maier, and H. Ren, Sci. Adv. **8**, 4816 (2022).
[386]C.-F. Pan, H. Wang, and J. K. Yang, in *Optica Imaging Congress (3D, COSI, DH, FLatOptics, is, pcAOP)* (Optica Publishing Group, 2023).
[387]F. Mei, G. Qu, X. Sha, J. Han, M. Yu, H. Li, Q. Chen, Z. Ji, J. Ni, C.-W. Qiu, Q. Song, Y. Kivshar, and S. Xiao, Nat. Commun. **14**, 6410 (2023).
[388]C. Richards, C. Ocier, D. Xie, H. Gao, T. Robertson, L. Goddard, R. Christiansen, D. Cahill, and P. Braun, Nat. Commun. **14**, 3119 (2023).
[389]J. Bütow, J. Eismann, V. Sharma, D. Brandmüller, and P. Banzer, Nat. Photonics **18**, 243–249 (2024).
[390]S. Chen, K. Li, J. Deng, G. Li, and S. Zhang, Nano Lett. **20**, 8549 (2020).
[391]S. S. Kruk, L. Wang, B. Sain, Z. Dong, J. Yang, T. Zentgraf, and Y. Kivshar, Nat. Photonics **16**, 561 (2022).
[392]L. Huang, X. Chen, H. Mühlenbernd, H. Zhang, S. Chen, B. Bai, Q. Tan, G. Jin, K. Cheah, C. Qiu, J. Li, T. Zentgraf, and S. Zhang, Nat. Commun. **15**, 2808 (2013).
[393]G. Tricoles, Appl. Opt. **26**, 4351 (1987).
[394]T. Todorov, L. Nikolova, K. Stoyanova, and N. Tomova, "Polarization holography. 3: Some applications of polarization holographic recording," Appl. Opt. **24**, 785–788 (1985).
[395]L. Liu, R. Wang, Y. Sun, Y. Jin, and A. Wu, Nanophotonics **12**, 3159 (2023).
[396]L. Nikolova and P. Ramanujam, *Polarization Holography* (Cambridge University Press, 2009).
[397]A. V. Krishnamoorthy, F. Xu, J. E. Ford, and Y. Fainman, "Polarization-controlled multistage switch based on polarization-selective computer-generated holograms," Appl. Opt. **36**, 997–1010 (1997).
[398]F. Xu, J. E. Ford, and Y. Fainman, "Polarization-selective computer-generated holograms: Design, fabrication, and applications," Appl. Opt. **34**, 256–266 (1995).
[399]J. Ford, Y. Fainman, F. Xu, and K. Urquhart, Opt. Lett. **18**, 456 (1993).
[400]R. K. Kostuk, M. Kato, and Y.-T. Huang, "Polarization properties of substrate-mode holographic interconnects," Appl. Opt. **29**, 3848–3854 (1990).
[401]M. Ansari, I. Kim, D. Lee, M. Waseem, M. Zubair, N. Mahmood, T. Badloe, S. Yerci, T. Tauqeer, M. Mehmood, and J. Rho, Laser Photonics Rev **13**, 1900065 (2019).
[402]M. Ansari, I. Kim, I. Rukhlenko, M. Zubair, S. Yerci, T. Tauqeer, M. Mehmood, and J. Rho, Nanoscale Horiz. **5**, 57 (2020).
[403]M. Naveed, J. Kim, M. Ansari, I. Kim, Y. Massoud, J. Kim, D. Oh, T. Badloe, J. Lee, and Y. Kim, ACS Appl. Mater. Interfaces **14**, 31194 (2022).
[404]M. Ansari, M. Qasim Mehmood, M. Waseem, I. Kim, N. Mahmood, T. Tauqeer, S. Yerci, and J. Rho, in *Conference on Lasers and Electro-Optics CLEO, FF2B* (IEEE, 2019), Vol. 7.
[405]H. Khaliq, K. Riaz, M. Zubair, M. Ansari, T. Naeem, and M. Mehmood, in *SPIE Nanoscience + Engineering* (SPIE, 2020), pp. 88–93.
[406]X. Chen, L. Huang, H. Mühlenbernd, G. Li, B. Bai, Q. Tan, G. Jin, C. Qiu, S. Zhang, and T. Zentgraf, Nat. Commun. **3**, 1198 (2012).
[407]D. Wen, F. Yue, G. Li, G. Zheng, K. Chan, S. Chen, M. Chen, K. Li, P. Wong, K. Cheah, E. Yue Bun Pun, S. Zhang, and X. Chen, Nat. Commun. **6**, 8241 (2015).
[408]I. Kim, W. Kim, K. Kim, M. Ansari, M. Mehmood, T. Badloe, Y. Kim, J. Gwak, H. Lee, Y. Kim, and J. Rho, Sci. Adv. **7**, 9943 (2021).
[409]I. Kim, M. Ansari, M. Mehmood, W. Kim, J. Jang, M. Zubair, Y. Kim, and J. Rho, Adv. Mater. **32**, 2004664 (2020).
[410]M. Naveed, J. Kim, I. Javed, M. Ansari, J. Seong, Y. Massoud, T. Badloe, I. Kim, K. Riaz, and M. Zubair, Adv. Opt. Mater. **10**, 2200196 (2022).
[411]M. Naveed, M. Ansari, I. Kim, T. Badloe, J. Kim, D. Oh, K. Riaz, T. Tauqeer, U. Younis, and M. Saleem, Microsyst. Nanoeng. **7**, 5 (2021).
[412]M. Ansari, T. Tauqeer, M. Zubair, and M. Mehmood, Nanophotonics **9**, 963 (2020).
[413]F. Zhang, M. Pu, X. Li, P. Gao, X. Ma, J. Luo, H. Yu, and X. Luo, Adv. Funct. Mater. **27**, 1704295 (2017).
[414]Z. Deng, J. Deng, X. Zhuang, S. Wang, K. Li, Y. Wang, Y. Chi, X. Ye, J. Xu, G. Wang, R. Zhao, X. Wang, Y. Cao, X. Cheng, G. Li, and X. Li, Nano Lett. **18**, 2885 (2018).
[415]X. Guo, J. Zhong, B. Li, S. Qi, Y. Li, P. Li, D. Wen, S. Liu, B. Wei, and J. Zhao, Adv. Mater. **34**, 2103192 (2022).
[416]I. Dolev, I. Epstein, and A. Arie, Phys. Rev. Lett. **109**, 203903 (2012).
[417]M. Ozaki, J. Kato, and S. Kawata, Science **332**, 218 (2011).
[418]N. C. Pégard and J. W. Fleischer, "Optimizing holographic data storage using a fractional Fourier transform," Opt. Lett. **36**, 2551–2553 (2011).
[419]D. Grier, Nature **424**, 810 (2003).
[420]P. Midgley and R. Dunin-Borkowski, Nat. Mater. **8**, 271 (2009).
[421]C. Barsi, W. Wan, and J. Fleischer, Nat. Photonics **3**, 211 (2009).
[422]H. Zhang, Q. Tan, and G. Jin, Opt. Eng. **51**, 075801 (2012).

16 July 2024 09:29:41

© Author(s) 2024

[423]F. Yue, C. Zhang, X. Zang, D. Wen, B. Gerardot, S. Zhang, and X. Chen, Light **7**, 17129 (2017).
[424]X. Zang, F. Dong, F. Yue, C. Zhang, L. Xu, Z. Song, M. Chen, P. Chen, G. Buller, Y. Zhu, S. Zhuang, W. Chu, S. Zhang, and X. Chen, Adv. Mater. **30**, 1707499 (2018).
[425]Y. Intaravanne, J. Han, R. Wang, A. Ma, S. Li, S. Chen, and X. Chen, Adv. Photonics Res **2**, 2000046 (2021).
[426]L. Huang, Y. Yu, and L. Cao, Nano Lett. **13**, 3559 (2013).
[427]D. Wen, J. Cadusch, J. Meng, and K. Crozier, Nano Lett. **21**, 1735 (2021).
[428]Y. Intaravanne, M. Ansari, H. Ahmed, N. Bileckaja, H. Yin, and X. Chen, ACS Photonics **10**, 544 (2023).
[429]B. Xiong, Y. Liu, Y. Xu, L. Deng, C. Chen, J. Wang, R. Peng, Y. Lai, Y. Liu, and M. Wang, Science **379**, 294 (2023).
[430]W. Wan, J. Gao, and X. Yang, ACS Nano **10**, 10671 (2016).
[431]X. Zang, H. Ding, Y. Intaravanne, L. Chen, Y. Peng, J. Xie, Q. Ke, A. Balakin, A. Shkurinov, X. Chen, Y. Zhu, and S. Zhuang, Laser Photonics Rev. **13**, 1900182 (2019).
[432]B. Wang and C. Zhao, Annu. Rev. Heat Transfer **23**, 231 (2020).
[433]R. Wang, Y. Intaravanne, S. Li, J. Han, S. Chen, J. Liu, S. Zhang, L. Li, and X. Chen, Nano Lett. **21**, 2081 (2021).
[434]Y. Intaravanne, R. Wang, H. Ahmed, Y. Ming, Y. Zheng, Z. Zhou, Z. Li, S. Chen, S. Zhang, and X. Chen, Light: Sci. App. **11**, e302 (2022).
[435]Y. Intaravanne, M. Ansari, H. Ahmed, and X. Chen, Adv. Opt. Mater. **12**, 2203097 (2024).
[436]R. Wang, M. Ansari, H. Ahmed, Y. Li, W. Cai, Y. Liu, S. Li, J. Liu, L. Li, and X. Chen, Light: Sci. Appl. **12**, 103 (2023).
[437]Z. Wang, G. Yuan, M. Yang, J. Chai, Q. Wu, T. Wang, M. Sebek, D. Wang, L. Wang, S. Wang, D. Chi, G. Adamo, C. Soci, H. Sun, K. Huang, and J. Teng, Nano Lett. **20**, 7964 (2020).
[438]P. Wu, R. Sokhoyan, G. Kafaie, W.-H. Shirmanesh, H. Cheng, P. Atwater, R. Wu, G. Sokhoyan, W. Shirmanesh, H. Cheng, H. Atwater Thomas, J. Watson, and Atwater, Adv. Opt. Mater. **9**, 2100230 (2021).
[439]T. Badloe, I. Kim, Y. Kim, J. Kim, and J. Rho, Adv. Sci. **8**, 2102646 (2021).
[440]B. C. Kress, *Optical Architectures for Augmented-, Virtual-, and Mixed-Reality Headsets*, SPIE Press Monograph Vol. PM316 (Society of Photo-Optical Instrumentation Engineers, Bellingham, Washington DC, 2020).
[441]J. Xiong, K. Yin, K. Li, and S.-T. Wu, Adv. Photonics Res. **2**, 2000049 (2021).
[442]C.-H. Chang, R. K. Heilmann, R. C. Fleming, J. Carter, E. Murphy, M. L. Schattenburg, T. C. Bailey, J. G. Ekerdt, R. D. Frankel, and R. Voisin, J. Vac. Sci. Technol. B **21**, 2755 (2003).
[443]M. Khorasaninejad and F. Capasso, Science **358**, eaam8100 (2017).
[444]J. Xiong, E.-L. Hsiang, Z. He, T. Zhan, and S.-T. Wu, Light **10**, 216 (2021).
[445]T. Levola and P. Laakkonen, Opt. Express. **15**, 2067 (2007).
[446]A. Alexeev, see https://waveoptics.ar/events/digital-aachen-polymer-optics/ for "Mass production of high performance optics: WaveOptics [EB/OL] (2021-11-15)," 2023.
[447]E. Khaidarov, H. Hao, R. Paniagua-Domínguez, Y. F. Yu, Y. H. Fu, V. Valuckas, S. L. K. Yap, Y. T. Toh, J. S. K. Ng, and A. I. Kuznetsov, Nano Lett. **17**, 6267 (2017).
[448]Y. Li, S. Chen, H. Liang, X. Ren, L. Luo, Y. Ling, S. Liu, Y. Su, and S.-T. Wu, PhotoniX **3**, 29 (2022).
[449]F. Aieta, P. Genevet, M. A. Kats, N. Yu, R. Blanchard, Z. Gaburro, and F. Capasso, Nano Lett. **12**, 4932 (2012).
[450]W. T. Chen, A. Y. Zhu, V. Sanjeev, M. Khorasaninejad, Z. Shi, E. Lee, and F. Capasso, Nat. Nanotechnol. **13**(3), 220 (2018).
[451]Y. Sun, Y. Liu, T. Wu, J. Li, H. Fan, and X. Wang, Results Phys. **46**, 106286 (2023).
[452]R. Zheng, R. Pan, G. Geng, Q. Jiang, S. Du, L. Huang, C. Gu, and J. Li, Nat. Commun. **13**, 4292 (2022).
[453]W. Song, X. Liang, S. Li, D. Li, R. Paniagua-Domínguez, K. H. Lai, Q. Lin, Y. Zheng, and A. I. Kuznetsov, Laser Photonics Rev. **15**, 2000538 (2021).
[454]I. Kim, G. Yoon, J. Jang, P. Genevet, K. T. Nam, and J. Rho, ACS Photonics **5**, 3876 (2018).
[455]M. Haghtalab, M. Tamagnone, A. Y. Zhu, S. Safavi-Naeini, and F. Capasso, ACS Photonics **7**, 991 (2020).
[456]T. Lin, T. Zhan, J. Zou, F. Fan, and S.-T. Wu, Opt. Express **28**, 38616 (2020).
[457]H. Liang, A. Martins, B.-H. V. Borges, J. Zhou, E. R. Martins, J. Li, and T. F. Krauss, Optica **6**, 1461 (2019).
[458]S. Wang, P. C. Wu, V.-C. Su, Y.-C. Lai, M.-K. Chen, H. Y. Kuo, B. H. Chen, Y. H. Chen, T.-T. Huang, J.-H. Wang, R.-M. Lin, C.-H. Kuan, T. Li, Z. Wang, S. Zhu, and D. P. Tsai, Nat. Nanotechnol. **13**, 227 (2018).
[459]A. Martins, K. Li, J. Li, H. Liang, D. Conteduca, B.-H. V. Borges, T. F. Krauss, and E. R. Martins, ACS Photonics **7**, 2073 (2020).
[460]S. Lan, X. Zhang, M. Taghinejad, S. Rodrigues, K.-T. Lee, Z. Liu, and W. Cai, ACS Photonics **6**, 864 (2019).
[461]S.-S. Kim, C. Chun, J.-C. Hong, and D.-Y. Kim, J. Mater. Chem. **16**, 370 (2006).
[462]J. Kim, W. Kim, D. K. Oh, H. Kang, H. Kim, T. Badloe, S. Kim, C. Park, H. Choi, H. Lee, and J. Rho, Light **12**(1), 68 (2023).
[463]I. R. Howell, V. J. Einck, D. Nees, B. Stadlober, and J. J. Watkins, Opt. Laser Technol. **141**, 107101 (2021).
[464]S. Zhang, H. Zhou, B. Liu, Z. Su, and L. Huang, ACS Photonics **10**, 2045 (2023).
[465]D. K. Oh, T. Lee, B. Ko, T. Badloe, J. G. Ok, and J. Rho, Front. Optoelectron. **14**, 229 (2021).
[466]Y. Hu, L. Li, R. Wang, J. Song, H. Wang, H. Duan, J. Ji, and Y. Meng, Engineering **7**, 1623 (2021).
[467]D. K. Nikolov, A. Bauer, F. Cheng, H. Kato, A. N. Vamivakas, and J. P. Rolland, Sci. Adv. **7**, eabe5112 (2021).
[468]S. M. Kamali, A. Arbabi, E. Arbabi, Y. Horie, and A. Faraon, Nat. Commun. **7**(1), 11618 (2016).
[469]J. Burch, D. Wen, X. Chen, and A. Di Falco, Sci. Rep. **7**, 4520 (2017).
[470]J. Burch and A. Di Falco, ACS Photonics **5**, 1762 (2018).
[471]H. Chen, W.-B. Lu, M.-Y. Geng, B.-Y. Yu, C. Zhang, X.-Z. Bo, M.-Z. Li, Z.-H. Kou, J.-L. Zhan, and Z.-G. Liu, Adv. Mater. Technol. **8**, 2301111 (2023).
[472]T. Badloe, J. Kim, I. Kim, W.-S. Kim, W. S. Kim, Y.-K. Kim, and J. Rho, Light **11**, 118 (2022).
[473]Y. V. Izdebskaya, Z. Yang, V. G. Shvedov, D. N. Neshev, and I. V. Shadrivov, Nano Lett. **23**, 9825 (2023).
[474]S. Lepeshov and A. Krasnok, Nat. Nanotechnol. **16**, 615 (2021).
[475]J. Shields, C. R. De Galarreta, H. Penketh, Y.-Y. Au, J. Bertolotti, and C. D. Wright, Adv. Opt. Mater. **11**, 2300765 (2023).
[476]S. Vatani, B. Barahimi, and M. K. Moravvej-Farshi, Sci. Rep. **12**(1), 21490 (2022).
[477]O. Hemmatyar, S. Abdollahramezani, H. Taghinejad, and A. Adibi, in *Conference on Lasers and Electro-Optics (CLEO)* (2021), pp. 1–2.
[478]D. Lee, J. Gwak, T. Badloe, S. Palomba, and J. Rho, Nanoscale Adv. **2**, 605 (2020).
[479]D. Klyshko, *Photons and Nonlinear Optics* (Routledge, 2018).
[480]G. Lewis, Nature **118**, 874 (1926).
[481]F. Dell'anno, S. Siena, and F. Illuminati, Phys. Rep. **428**, 53 (2006).
[482]B. Lounis and M. Orrit, Rep. Prog. Phys. **68**, 1129 (2005).
[483]H. Kimble, M. Dagenais, and L. Mandel, Phys. Rev. Lett. **39**, 691 (1977).
[484]H. Kimble, Nature **453**, 1023 (2008).
[485]F. Diedrich and H. Walther, Phys. Rev. Lett. **58**, 203 (1987).
[486]B. Lounis and W. Moerner, Nature **407**, 491 (2000).
[487]P. Michler, A. Imamoğlu, M. Mason, P. Carson, G. Strouse, and S. Buratto, Nature **406**, 968 (2000).
[488]X. Brokmann, G. Messin, P. Desbiolles, E. Giacobino, M. Dahan, and J. Hermier, New J. Phys. **6**, 99 (2004).
[489]X. Ma, A. James, N. Hartmann, J. Baldwin, J. Dominguez, M. Sinclair, T. Luk, O. Wolf, S. Liu, S. Doorn, H. Htoon, and I. Brener, ACS Nano **11**, 6431 (2017).
[490]C. Kurtsiefer, S. Mayer, P. Zarda, and H. Weinfurter, Phys. Rev. Lett. **85**, 290 (2000).
[491]I. Aharonovich, D. Englund, and M. Toth, Nat Photonics **10**, 631 (2016).
[492]S. Harris, M. Oshman, and R. Byer, Phys. Rev. Lett. **18**, 732 (1967).
[493]B. Mollow and R. Glauber, Phys. Rev. **160**, 1076 (1967).
[494]S. Akhmanov, V. Fadeev, R. Khohlov, and O. Chunaev, JETP Lett. **6**, 575–578 (1967).
[495]D. Magde and H. Mahr, Phys. Rev. Lett. **18**, 905 (1967).
[496]D. Kleinman, Phys. Rev. **174**, 1027 (1968).
[497]D. Burnham and D. Weinberg, Phys. Rev. Lett. **25**, 84 (1970).

16 July 2024 09:29:41

© Author(s) 2024

[498]X. Li, J. Chen, P. Voss, J. Sharping, and P. Kumar, Opt. Express. **12**, 3737 (2004).
[499]H. Takesue and K. Inoue, Phys. Rev. A **70**, 31802 (2004).
[500]I. Staude and J. Schilling, Nat. Photonics **11**, 274 (2017).
[501]F. Ding, A. Pors, and S. Bozhevolnyi, Rep. Prog. Phys. **81**, 026401 (2018).
[502]S. Chang, X. Guo, and X. Ni, Annu. Rev. Mater. Res. **48**, 279 (2018).
[503]L. Carletti, A. Locatelli, O. Stepanenko, G. Leo, and C. Angelis, Opt. Express **23**, 26544 (2015).
[504]V. F. Gili, L. Carletti, A. Locatelli, D. Rocco, M. Finazzi, L. Ghirardini, I. Favero, C. Gomez, A. Lemaître, M. Celebrano, C. De Angelis, and G. Leo, Opt. Express **24**, 15965 (2016).
[505]F. Timpu, A. Sergeyev, N. Hendricks, and R. Grange, ACS Photonics **4**, 76 (2017).
[506]A. Krasnok, M. Tymchenko, and A. Alù, Mater. Today **21**, 8–21 (2018).
[507]P. Vabishchevich, S. Liu, M. Sinclair, G. Keeler, G. Peake, and I. Brener, ACS Photonics **5**, 1685 (2018).
[508]S. Liu, P. P. Vabishchevich, A. Vaskin, J. L. Reno, G. A. Keeler, M. B. Sinclair, I. Staude, and I. Brener, Nat. Commun. **9**, 2507 (2018).
[509]F. Löchner, A. Fedotova, S. Liu, G. Keeler, G. Peake, S. Saravi, M. Shcherbakov, S. Burger, A. Fedyanin, I. Brener, T. Pertsch, F. Setzpfandt, and I. Staude, ACS Photonics **5**, 1786 (2018).
[510]M. Rahmani, G. Leo, I. Brener, A. Zayats, S. Maier, C. De Angelis, H. Tan, V. Gili, F. Karouta, R. Oulton, K. Vora, M. Lysevych, I. Staude, L. Xu, A. Miroshnichenko, C. Jagadish, and D. Neshev, Opto-Electron. Adv. **1**, 18002101 (2018).
[511]S. Gennaro, Y. Li, S. Maier, and R. Oulton, ACS Photonics **5**, 3166 (2018).
[512]M. Timofeeva, L. Lang, F. Timpu, C. Renaut, A. Bouravleuv, I. Shtrom, G. Cirlin, and R. Grange, Nano Lett. **18**, 3695 (2018).
[513]L. Carletti, S. Kruk, A. Bogdanov, C. Angelis, and Y. Kivshar, Phys. Rev. Res. **1**, 023016 (2019).
[514]M. Shcherbakov, F. Eilenberger, and I. Staude, J. Appl. Phys. **126**, 857051 (2019).
[515]S. Gennaro, Y. Li, S. Maier, and R. Oulton, ACS Photonics **6**, 2335 (2019).
[516]L. Bonacina, P.-F. Brevet, M. Finazzi, and M. Celebrano, J. Appl. Phys. **127**(23), 230901 (2020).
[517]A. Fedotova, L. Carletti, A. Zilli, F. Setzpfandt, I. Staude, A. Toma, M. Finazzi, C. De Angelis, T. Pertsch, D. Neshev, and M. Celebrano, ACS Photonics **9**, 3745 (2022).
[518]S. Gennaro, R. Sarma, and I. Brener, Nanotechnology **33**, 402001 (2022).
[519]P. Vabishchevich and Y. Kivshar, Photon. Res. **11**, B50–B64 (2023).
[520]J. Smalley, F. Vallini, S. Montoya, L. Ferrari, S. Shahin, C. Riley, B. Kanté, E. Fullerton, Z. Liu, and Y. Fainman, Nat. Commun. **8**, 13793 (2017).
[521]T. Tran, D. Wang, Z.-Q. Xu, A. Yang, M. Toth, T. Odom, and I. Aharonovich, Nano Lett. **17**, 2634 (2017).
[522]D. Liu, Y. Tan, E. Khoram, and Z. Yu, ACS Photonics **5**, 1365 (2018).
[523]M. Iwanaga, T. Mano, and N. Ikeda, ACS Photonics **5**, 897 (2018).
[524]S. Yu, C.-W. Qiu, Y. Chong, S. Torquato, and N. Park, Nat. Rev. **6**, 226 (2021).
[525]Y. Kan and S. Bozhevolnyi, Adv. Opt. Mater. **11**, 2202759 (2023).
[526]T. Santiago-Cruz, A. Fedotova, V. Sultanov, M. A. Weissflog, D. Arslan, M. Younesi, T. Pertsch, I. Staude, F. Setzpfandt, and M. Chekhova, Nano Lett. **21**, 4423 (2021).
[527]M. Parry, A. Mazzanti, A. Poddubny, G. Valle, D. Neshev, and A. Sukhorukov, Adv. Photonics **3**, 055001 (2021).
[528]A. Mazzanti, M. Parry, A. Poddubny, G. Valle, D. Neshev, and A. Sukhorukov, New J. Phys. **24**, 035006 (2022).
[529]C. Son, V. Sultanov, T. Santiago-Cruz, A. Anthur, H. Zhang, R. Paniagua-Dominguez, L. Krivitsky, A. Kuznetsov, and M. Chekhova, Nanoscale **15**, 2567 (2023).
[530]K. Wang, J. Titchener, S. Kruk, L. Xu, H.-P. Chung, M. Parry, I. Kravchenko, Y.-H. Chen, A. Solntsev, Y. Kivshar, D. Neshev, and A. Sukhorukov, Science **361**, 1104 (2018).
[531]A. Vega, T. Pertsch, F. Setzpfandt, and A. Sukhorukov, Phys. Rev. Appl. **16**, 64032 (2021).
[532]S. Lung, K. Wang, K. Kamali, J. Zhang, M. Rahmani, D. Neshev, and A. Sukhorukov, ACS Photonics **7**, 3015 (2020).
[533]Q. Li, W. Bao, Z. Nie, Y. Xia, Y. Xue, Y. Wang, S. Yang, and X. Zhang, Nat Photonics **15**, 267 (2021).
[534]P. Georgi, M. Massaro, K.-H. Luo, B. Sain, N. Montaut, H. Herrmann, T. Weiss, G. Li, C. Silberhorn, and T. Zentgraf, Light **8**, 70 (2019).
[535]P. Jha, N. Shitrit, J. Kim, X. Ren, Y. Wang, and X. Zhang, ACS Photonics **5**, 971 (2018).
[536]W. J. Kort-Kamp, A. K. Azad, and D. A. Dalvit, Phys. Rev. Lett. **127**, 043603 (2021).
[537]Y. Park, H. Kim, J.-Y. Lee, W. Ko, K. Bae, and K.-S. Cho, Nanophotonics **9**, 1023 (2020).
[538]H. Huang, S. Zheng, and W. Sun, Opt. Express. **30**, 28345 (2022).
[539]Y. Kan, S. Andersen, F. Ding, S. Kumar, C. Zhao, and S. Bozhevolnyi, Adv. Mater. **32**, 1907832 (2020).
[540]E. Purcell, "Proceedings of the American Physical Society," Phys. Rev. **69**, 674 (1946).
[541]X. Liu, Y. Kan, S. Kumar, L. Kulikova, V. Davydov, V. Agafonov, C. Zhao, and S. Bozhevolnyi, Adv. Mater. **36**, 2304495 (2023).
[542]Y. Bao, Q. Lin, R. Su, Z.-K. Zhou, J. Song, J. Li, and X.-H. Wang, Sci. Adv. **6**, 8761 (2020).
[543]C. Okoth, A. Cavanna, T. Santiago-Cruz, and M. Chekhova, Phys. Rev. Lett. **123**, 263602 (2019).
[544]V. Sultanov, T. Santiago-Cruz, and M. Chekhova, Opt. Lett. **47**, 3872 (2022).
[545]M. Liscidini and J. Sipe, Phys. Rev. Lett. **111**, 193602 (2013).
[546]J. Yang, P. Dichtl, J. Gutierrez, C. Phillips, A. Clark, and R. Oulton, "Stimulated emission tomography analysis of plasmonic nanoantennas," in *Active Photonic Platforms 2022*, edited by G. S. Subramania and S. Foteinopoulou (SPIE, 2022), p. 86.
[547]B. Jin, D. Mishra, and C. Argyropoulos, Nanoscale **13**, 19903 (2021).
[548]J. Mertens, M. Kleemann, R. Chikkaraddy, P. Narang, and J. Baumberg, Nano Lett. **17**, 2568 (2017).
[549]S. Liu, G. Keeler, J. Reno, M. Sinclair, and I. Brener, Adv. Opt. Mater. **4**, 1457 (2016).
[550]G. Marino, C. Gigli, D. Rocco, A. Lemaître, I. Favero, C. De Angelis, and G. Leo, ACS Photonics **6**, 1226 (2019).
[551]F. Timpu, J. Sendra, C. Renaut, L. Lang, M. Timofeeva, M. Buscaglia, V. Buscaglia, and R. Grange, ACS Photonics **6**, 545 (2019).
[552]R. Savo, A. Morandi, J. S. Müller, F. Kaufmann, F. Timpu, M. Reig Escalé, M. Zanini, L. Isa, and R. Grange, Nat. Photonics **14**(12), 740 (2020).
[553]G. Marino, A. Solntsev, L. Xu, V. Gili, L. Carletti, A. Poddubny, M. Rahmani, D. Smirnova, H. Chen, A. Lemaître, G. Zhang, A. Zayats, C. De Angelis, G. Leo, A. Sukhorukov, and D. Neshev, Optica **6**, 1416 (2019).
[554]R. Loudon, *The Quantum Theory of Light*, 3rd ed. (Oxford University Press, 2000).
[555]A. Zilli, V. Sultanov, M. Poloczek, M. Ferrera, Y. Luan, E. Kokkinakis, T. Santiago-Cruz, L. Carletti, M. Finazzi, A. Toma, M. Chekhova, and M. Celebrano, "Spontaneous parametric down-conversion beaming from a lithium niobate nanostructured resonator," in *CLEO 2023* (Optica Publishing Group, 2023), Paper No. FTu4C-8.
[556]T. Santiago-Cruz, A. Fedotova, V. Sultanov, M. Weissflog, M. Younesi, I. Staude, T. Pertsch, F. Setzpfandt, and M. Chekhova, in *Conference on Lasers and Electro-Optics* (Optica Publishing Group, 2021).
[557]N. Hanh Duong, G. Saerens, F. Timpu, M. Buscaglia, V. Buscaglia, A. Morandi, J. Müller, A. Maeder, F. Kaufmann, A. Solntsev, and R. Grange, Opt. Mater. Express **12**, 3696 (2022).
[558]G. Saerens, T. Dursap, I. Hesner, N. Duong, A. Solntsev, A. Morandi, A. Maeder, A. Karvounis, P. Regreny, R. Chapman, A. Danescu, N. Chauvin, J. Penuelas, and R. Grange, Nano Lett. **23**, 3245 (2023).
[559]Q. Guo, X.-Z. Qi, L. Zhang, M. Gao, S. Hu, W. Zhou, W. Zang, X. Zhao, J. Wang, B. Yan, M. Xu, Y.-K. Wu, G. Eda, Z. Xiao, S. Yang, H. Gou, Y. Feng, G.-C. Guo, W. Zhou, X.-F. Ren, C.-W. Qiu, S. Pennycook, and A. Wee, Nature **613**, 53 (2023).
[560]R. Sarma, J. Xu, D. De Ceglia, L. Carletti, S. Campione, J. Klem, M. Sinclair, M. Belkin, and I. Brener, Nano Lett. **22**, 896 (2022).
[561]R. Sarma, D. De Ceglia, N. Nookala, M. Vincenti, S. Campione, O. Wolf, M. Scalora, M. Sinclair, M. Belkin, and I. Brener, ACS Photonics **6**, 1458 (2019).
[562]J. Ma, J. Zhang, Y. Jiang, T. Fan, M. Parry, D. Neshev, and A. Sukhorukov, Nano Lett. **23**, 8091 (2023).
[563]V. Sultanov and M. Chekhova, ACS Photonics **11**, 2–6 (2023).

16 July 2024 09:29:41

© Author(s) 2024

[564]C. Okoth, A. Cavanna, N. Joly, and M. Chekhova, Phys. Rev. A **99**, 43809 (2019).
[565]H. Yokoyama and S. Brorson, J. Appl. Phys. **66**, 4801 (1989).
[566]G. Bjork and Y. Yamamoto, IEEE J. Quantum Electron. **27**, 2386 (1991).
[567]Y. Yamamoto, S. Machida, and G. Björk, Phys. Rev. A **44**, 657 (1991).
[568]H. Yokoyama, K. Nishi, T. Anan, Y. Nambu, S. Brorson, E. Ippen, and M. Suzuki, Opt. Quant. Electron. **24**, S245 (1992).
[569]S. Mccall, A. Levi, R. Slusher, S. Pearton, and R. Logan, Appl. Phys. Lett. **60**, 289 (1992).
[570]O. Painter, R. Lee, A. Scherer, A. Yariv, J. O'brien, P. Dapkus, and I. Kim, Science **284**, 1819 (1999).
[571]M. Huang, S. Mao, H. Feick, H. Yan, Y. Wu, H. Kind, E. Weber, R. Russo, and P. Yang, Science **292**, 1897 (2001).
[572]D. Bergman and M. Stockman, Phys. Rev. Lett. **90**, 027402 (2003).
[573]R. Oulton, V. Sorger, T. Zentgraf, R.-M. Ma, C. Gladden, L. Dai, G. Bartal, and X. Zhang, Nature **461**, 629 (2009).
[574]M. T. Hill, M. Marell, E. S. P. Leong, B. Smalbrugge, Y. Zhu, M. Sun, P. J. van Veldhoven, E. J. Geluk, F. Karouta, Y.-S. Oei, R. Nötzel, C.-Z. Ning, and M. K. Smit, Opt. Express **17**, 11107 (2009).
[575]M. Noginov, G. Zhu, A. Belgrave, R. Bakker, V. Shalaev, E. Narimanov, S. Stout, E. Herz, T. Suteewong, and U. Wiesner, Nature **460**, 1110 (2009).
[576]W. Zhou, M. Dridi, J. Suh, C. Kim, D. Co, M. Wasielewski, G. Schatz, and T. Odom, Nat. Nanotechnol. **8**, 506 (2013).
[577]A. Yang, T. Hoang, M. Dridi, C. Deeb, M. Mikkelsen, G. Schatz, and T. Odom, Nat. Commun. **6**, 6939 (2015).
[578]D. Wang, A. Yang, W. Wang, Y. Hua, R. Schaller, G. Schatz, and T. Odom, Nat. Nanotechnol. **12**, 889 (2017).
[579]D. Wang, M. Bourgeois, W.-K. Lee, R. Li, D. Trivedi, M. Knudson, W. Wang, G. Schatz, and T. Odom, Nano Lett. **18**, 4549 (2018).
[580]P. St-Jean, V. Goblot, E. Galopin, A. Lemaître, T. Ozawa, L. Le Gratiet, I. Sagnes, J. Bloch, and A. Amo, Nat. Photonics **11**, 651 (2017).
[581]B. Bahari, A. Ndao, F. Vallini, A. E. Amili, Y. Fainman, and B. Kanté, Science **358**, 636 (2017).
[582]M. Parto, S. Wittek, H. Hodaei, G. Harari, M. Bandres, J. Ren, M. Rechtsman, M. Segev, D. Christodoulides, and M. Khajavikhan, Phys. Rev. Lett. **120**, 113901 (2018).
[583]H. Zhao, P. Miao, M. H. Teimourpour, S. Malzard, R. El-Ganainy, H. Schomerus, and L. Feng, Nat. Commun. **9**, 981 (2018).
[584]Y. Ota, R. Katsumi, K. Watanabe, S. Iwamoto, and Y. Arakawa, Commun. Phys. **1**, 86 (2018).
[585]M. Bandres, S. Wittek, G. Harari, M. Parto, J. Ren, M. Segev, D. Christodoulides, and M. Khajavikhan, Science **359**, eaar4005 (2018).
[586]G. Harari, M. Bandres, Y. Lumer, M. Rechtsman, Y. Chong, M. Khajavikhan, D. Christodoulides, and M. Segev, Science **359**, eaar4003 (2018).
[587]S. Klembt, T. Harder, O. Egorov, K. Winkler, R. Ge, M. Bandres, M. Emmerling, L. Worschech, T. Liew, M. Segev, C. Schneider, and S. Höfling, Nature **562**, 552 (2018).
[588]C. Han, M. Lee, S. Callard, C. Seassal, and H. Jeon, Light **8**, 40 (2019).
[589]H. Zhao, X. Qiao, T. Wu, B. Midya, S. Longhi, and L. Feng, Science **365**, 1163 (2019).
[590]Z.-K. Shao, H.-Z. Chen, S. Wang, X.-R. Mao, Z.-Q. Yang, S.-L. Wang, X.-X. Wang, X. Hu, and R.-M. Ma, Nat. Nanotechnol. **15**, 67 (2020).
[591]Z.-Q. Yang, Z.-K. Shao, H.-Z. Chen, X.-R. Mao, and R.-M. Ma, Phys. Rev. Lett. **125**, 13903 (2020).
[592]D. Smirnova, A. Tripathi, S. Kruk, M.-S. Hwang, H.-R. Kim, H.-G. Park, and Y. Kivshar, Light **9**, 127 (2020).
[593]W. Noh, H. Nasari, H.-M. Kim, Q. Le-Van, Z. Jia, C.-H. Huang, and B. Kanté, Opt. Lett. **45**, 4108 (2020).
[594]W. Zhang, X. Xie, H. Hao, J. Dang, S. Xiao, S. Shi, H. Ni, Z. Niu, C. Wang, K. Jin, X. Zhang, and X. Xu, Light **9**, 109 (2020).
[595]C. Han, M. Kang, and H. Jeon, ACS Photonics **7**, 2027 (2020).
[596]H.-R. Kim, M.-S. Hwang, D. Smirnova, K.-Y. Jeong, Y. Kivshar, and H.-G. Park, Nat. Commun. **11**, 5758 (2020).
[597]B. Bahari, L. Hsu, S. Pan, D. Preece, A. Ndao, A. El Amili, Y. Fainman, and B. Kanté, Nat. Phys. **17**, 700 (2021).
[598]J.-H. Choi, W. Hayenga, Y. Liu, M. Parto, B. Bahari, D. Christodoulides, and M. Khajavikhan, Nat. Commun. **12**, 3434 (2021).
[599]A. Dikopoltsev, T. Harder, E. Lustig, O. Egorov, J. Beierlein, A. Wolf, Y. Lumer, M. Emmerling, C. Schneider, S. Höfling, M. Segev, and S. Klembt, Science **373**, 1514 (2021).
[600]T. Harder, M. Sun, O. Egorov, I. Vakulchyk, J. Beierlein, P. Gagel, M. Emmerling, C. Schneider, U. Peschel, I. Savenko, S. Klembt, and S. Höfling, ACS Photonics **8**, 1377 (2021).
[601]T. Harder, O. Egorov, C. Krause, J. Beierlein, P. Gagel, M. Emmerling, C. Schneider, U. Peschel, S. Höfling, and S. Klembt, ACS Photonics **8**, 3193 (2021).
[602]M. Dusel, S. Betzold, T. Harder, M. Emmerling, J. Beierlein, J. Ohmer, U. Fischer, R. Thomale, C. Schneider, S. Höfling, and S. Klembt, Nano Lett. **21**, 6398 (2021).
[603]X. Liu, L. Zhao, D. Zhang, and S. Gao, Opt. Express **30**, 4965 (2022).
[604]R. Contractor, W. Noh, W. Redjem, W. Qarony, E. Martin, S. Dhuey, A. Schwartzberg, and B. Kanté, Nature **608**, 692 (2022).
[605]P. Gagel, T. Harder, S. Betzold, O. Egorov, J. Beierlein, H. Suchomel, M. Emmerling, A. Wolf, U. Peschel, S. Höfling, C. Schneider, and S. Klembt, ACS Photonics **9**, 405 (2022).
[606]L. Yang, G. Li, X. Gao, and L. Lu, Nat. Photonics **16**, 279 (2022).
[607]Y.-G. Sang, J.-Y. Lu, Y.-H. Ouyang, H.-Y. Luan, J.-H. Wu, J.-Y. Li, and R.-M. Ma, Nat. Commun. **13**, 6485 (2022).
[608]J. Tian, Q. Tan, Y. Wang, Y. Yang, G. Yuan, G. Adamo, and C. Soci, Nat. Commun. **14**, 1433 (2023).
[609]S. Han, J. Cui, Y. Chua, Y. Zeng, L. Hu, M. Dai, F. Wang, F. Sun, S. Zhu, L. Li, A. Davies, E. Linfield, C. Tan, Y. Kivshar, and Q. Wang, Light: Sci. Appl. **12**, 145 (2023).
[610]Z. Gao, X. Qiao, M. Pan, S. Wu, J. Yim, K. Chen, B. Midya, L. Ge, and L. Feng, Phys. Rev. Lett. **130**, 263801 (2023).
[611]J. Ma, T. Zhou, M. Tang, H. Li, Z. Zhang, X. Xi, M. Martin, T. Baron, H. Liu, Z. Zhang, S. Chen, and X. Sun, Light. Sci. Appl. **12**, 255 (2023).
[612]M.-S. Hwang, H.-R. Kim, J. Kim, B.-J. Yang, Y. Kivshar, and H.-G. Park, Nat. Photonics **18**, 286 (2023).
[613]K. Rong, X. Duan, B. Wang, D. Reichenberg, A. Cohen, C.-L. Liu, P. Mohapatra, A. Patsha, V. Gorovoy, S. Mukherjee, V. Kleiner, A. Ismach, E. Koren, and E. Hasman, Nat. Mater. **22**, 1085 (2023).
[614]X. Duan, B. Wang, K. Rong, C.-L. Liu, V. Gorovoy, S. Mukherjee, V. Kleiner, E. Koren, and E. Hasman, Science **381**, 1429 (2023).
[615]J. Wu, S. Ghosh, Y. Gan, Y. Shi, S. Mandal, H. Sun, B. Zhang, T. Liew, R. Su, and Q. Xiong, Sci. Adv. **9**, eadg4322 (2023).
[616]Z. Li, X.-W. Luo, D. Lin, A. Gharajeh, J. Moon, J. Hou, C. Zhang, and Q. Gu, Phys. Rev. Lett. **131**, 023202 (2023).
[617]A. Kodigala, T. Lepetit, Q. Gu, B. Bahari, Y. Fainman, and B. Kanté, Nature **541**, 196 (2017).
[618]S. T. Ha, Y. H. Fu, N. K. Emani, Z. Pan, R. M. Bakker, R. Paniagua-Domínguez, and A. I. Kuznetsov, Nat. Nanotech. **13**, 1042 (2018).
[619]V. Mylnikov, S. T. Ha, Z. Pan, V. Valuckas, R. Paniagua-Domínguez, H. V. Demir, and A. I. Kuznetsov, ACS Nano **14**, 7338 (2020).
[620]M.-S. Hwang, H.-C. Lee, K.-H. Kim, K.-Y. Jeong, S.-H. Kwon, K. Koshelev, Y. Kivshar, and H.-G. Park, Nat. Commun. **12**, 4135 (2021).
[621]Y. Yu, A. Sakanas, A. Zali, E. Semenova, K. Yvind, and J. Mørk, Nat. Photonics **15**, 758 (2021).
[622]J. Dixon, M. Lawrence, D. Barton, and J. Dionne, Phys. Rev. Lett. **126**, 123201 (2021).
[623]Y. Ren, P. Li, Z. Liu, Z. Chen, Y.-L. Chen, C. Peng, and J. Liu, Sci. Adv. **8**, eade8817 (2022).
[624]H. Hodaei, M.-A. Miri, M. Heinrich, D. N. Christodoulides, and M. Khajavikhan, Science **346**, 975 (2014).
[625]L. Feng, Z. Wong, R.-M. Ma, Y. Wang, and X. Zhang, Science **346**, 972 (2014).
[626]M. Brandstetter, M. Liertzer, C. Deutsch, P. Klang, J. Schöberl, H. Türeci, G. Strasser, K. Unterrainer, and S. Rotter, Nat. Commun. **5**, 4034 (2014).
[627]B. Peng, Özdemir, S. Rotter, H. Yilmaz, M. Liertzer, F. Monifi, C. Bender, F. Nori, and L. Yang, Science **346**, 328 (2014).
[628]H. Hodaei, M. Miri, A. Hassan, W. Hayenga, M. Heinrich, D. Christodoulides, and M. Khajavikhan, Opt. Lett. **40**, 4955 (2015).

16 July 2024 09:29:41

© Author(s) 2024

[629]K.-H. Kim, M.-S. Hwang, H.-R. Kim, J.-H. Choi, Y.-S. No, and H.-G. Park, Nat. Commun. **7**, 13893 (2016).
[630]H. Hodaei, M. Miri, A. Hassan, W. Hayenga, M. Heinrich, D. Christodoulides, and M. Khajavikhan, Laser Photonics Rev. **10**, 494 (2016).
[631]P. Miao, Z. Zhang, J. Sun, W. Walasik, S. Longhi, N. Litchinitser, and L. Feng, Science **353**, 464 (2016).
[632]X.-Y. Wang, H.-Z. Chen, Y. Li, B. Li, and R.-M. Ma, Chin. Phys. B **25**, 124211 (2016).
[633]N. Zhang, Z. Gu, K. Wang, M. Li, L. Ge, S. Xiao, and Q. Song, Laser Photonics Rev. **11**, 1700052 (2017).
[634]Z. Gao, S. Fryslie, B. Thompson, M. Johnson, and K. Choquette, Optica **4**, 323 (2017).
[635]W. Liu, M. Li, R. Guzzon, E. Norberg, J. Parker, M. Lu, L. Coldren, and J. Yao, Nat. Commun. **8**, 15389 (2017).
[636]J. Ren, M. Parto, S. Wittek, M. Hokmabadi, D. Christodoulides, and M. Khajavikhan, Opt. Express **26**, 27153 (2018).
[637]R. Yao, C. Lee, V. Podolskiy, and W. Guo, Laser Photonics Rev. **13**, 1800154 (2019).
[638]M. Hokmabadi, N. Nye, R. El-Ganainy, D. Christodoulides, and M. Khajavikhan, Science **363**, 623 (2019).
[639]B. Midya, H. Zhao, X. Qiao, P. Miao, W. Walasik, Z. Zhang, N. Litchinitser, and L. Feng, Photonics Res. **7**, 363 (2019).
[640]X. Qiao, B. Midya, Z. Gao, Z. Zhang, H. Zhao, T. Wu, J. Yim, R. Agarwal, N. Litchinitser, and L. Feng, Science **372**, 403 (2021).
[641]X.-R. Mao, Z.-K. Shao, H.-Y. Luan, S.-L. Wang, and R.-M. Ma, Nat. Nanotechnol. **16**, 1099 (2021).
[642]H.-Y. Luan, Y.-H. Ouyang, Z.-W. Zhao, W.-Z. Mao, and R.-M. Ma, Nature **624**, 282 (2023).
[643]A. Raun, H. Tang, X. Ni, E. Mazur, and E. Hu, ACS Photonics **10**, 3001 (2023).
[644]J. Guan, J. Hu, Y. Wang, M. Tan, G. Schatz, and T. Odom, Nat. Nanotechnol. **18**, 514 (2023).
[645]R. M. Ma and R. F. Oulton, Nat. Nanotech. **14**, 12 (2019).
[646]S. Wang, X.-Y. Wang, B. Li, H.-Z. Chen, Y.-L. Wang, L. Dai, R. F. Oulton, and R.-M. Ma, Nat. Commun. **8**, 1889 (2017).
[647]R.-M. Ma and S.-Y. Wang, Nanophotonics **10**, 3623 (2021).
[648]S.-L. Wang, S. Wang, X.-K. Man, and R.-M. Ma, Nanophotonics **9**, 3403 (2020).
[649]S. Wang, H.-Z. Chen, and R.-M. Ma, Nano Lett. **18**, 7942 (2018).
[650]J. Joannopoulos, P. Villeneuve, and S. Fan, Nature **386**, 143 (1997).
[651]K. Vahala, Nature **424**, 839 (2003).
[652]M. Soljačić and J. Joannopoulos, Nat. Mater. **3**, 211 (2004).
[653]S. Noda, M. Fujita, and T. Asano, Nat. Photonics **1**, 449 (2007).
[654]T. Baba, Nat. Photonics **2**, 465 (2008).
[655]T. Kippenberg, S. Spillane, and K. Vahala, Appl. Phys. Lett. **85**, 6113 (2004).
[656]J. Schuller, E. Barnard, W. Cai, Y. Jun, J. White, and M. Brongersma, Nat. Mater. **9**, 193 (2010).
[657]D. Gramotnev and S. Bozhevolnyi, Nat. Photonics **4**, 83 (2010).
[658]Y. Liu and X. Zhang, Chem. Soc. Rev. **40**, 2494 (2011).
[659]O. Hess, J. B. Pendry, S. A. Maier, R. F. Oulton, J. M. Hamm, and K. L. Tsakmakidis, Nat. Mater. **11**, 573 (2012).
[660]M. Kauranen and A. V. Zayats, Nat. Photonics **6**, 737 (2012).
[661]P. Berini and I. De Leon, Nat. Photonics **6**, 16 (2012).
[662]M. S. Tame, K. R. McEnery, K. Özdemir, J. Lee, S. A. Maier, and M. S. Kim, Nat. Phys. **9**, 329 (2013).
[663]D. Vernooy, V. Ilchenko, H. Mabuchi, E. Streed, and H. Kimble, Opt. Lett. **23**, 247 (1998).
[664]S. Spillane, T. Kippenberg, K. Vahala, K. Goh, E. Wilcut, and H. Kimble, Phys. Rev. A **71**, 013817 (2005).
[665]P. Del'haye, A. Schliesser, O. Arcizet, T. Wilken, R. Holzwarth, and T. Kippenberg, Nature **450**, 1214 (2007).
[666]A. Savchenkov, A. Matsko, V. Ilchenko, and L. Maleki, Opt. Express **15**, 6768 (2007).
[667]M. Pöllinger, D. O'shea, F. Warken, and A. Rauschenbeutel, Phys. Rev. Lett. **103**, 53901 (2009).
[668]J. Zhu, S. Ozdemir, Y.-F. Xiao, L. Li, L. He, D.-R. Chen, and L. Yang, Nat. Photonics **4**, 46 (2010).
[669]X. Jiang, L. Shao, S.-X. Zhang, X. Yi, J. Wiersig, L. Wang, Q. Gong, M. Lončar, L. Yang, and Y.-F. Xiao, Science **358**, 344 (2017).
[670]A. Shitikov, I. Bilenko, N. Kondratiev, V. Lobanov, A. Markosyan, and M. Gorodetsky, Optica **5**, 1525 (2018).
[671]B.-S. Song, S. Noda, T. Asano, and Y. Akahane, Nat. Mater. **4**, 207 (2005).
[672]Q. Quan and M. Loncar, Opt. Express **19**, 18529 (2011).
[673]Y. Lai, S. Pirotta, G. Urbinati, D. Gerace, M. Minkov, V. Savona, A. Badolato, and M. Galli, Appl. Phys. Lett. **104**, 241101 (2014).
[674]F. Alpeggiani, L. Andreani, and D. Gerace, Appl. Phys. Lett. **107**, 261110 (2015).
[675]M. Minkov, V. Savona, and D. Gerace, Appl. Phys. Lett. **111**, 131104 (2017).
[676]T. Asano, Y. Ochi, Y. Takahashi, K. Kishimoto, and S. Noda, Opt. Express **25**, 1769 (2017).
[677]H. Choi, M. Heuck, and D. Englund, Phys. Rev. Lett. **118**, 223605 (2017).
[678]T. Asano and S. Noda, Opt. Express **26**, 32704 (2018).
[679]M. Li, H. Liang, R. Luo, Y. He, J. Ling, and Q. Lin, Optica **6**, 860 (2019).
[680]B.-S. Song, T. Asano, S. Jeon, H. Kim, C. Chen, D. Kang, and S. Noda, Optica **6**, 991 (2019).
[681]J. Kern, S. Großmann, N. Tarakina, T. Häckel, M. Emmerling, M. Kamp, J.-S. Huang, P. Biagioni, J. Prangsma, and B. Hecht, Nano Lett. **12**, 5504 (2012).
[682]C. Ciracì, R. Hill, J. Mock, Y. Urzhumov, A. Fernández-Domínguez, S. Maier, J. Pendry, A. Chilkoti, and D. Smith, Science **337**, 1072 (2012).
[683]R. Chikkaraddy, B. De Nijs, F. Benz, S. Barrow, O. Scherman, E. Rosta, A. Demetriadou, P. Fox, O. Hess, and J. Baumberg, Nature **535**, 127 (2016).
[684]J. Baumberg, J. Aizpurua, M. Mikkelsen, and D. Smith, Nat. Mater. **18**, 668 (2019).
[685]I. Epstein, D. Alcaraz, Z. Huang, V.-V. Pusapati, J.-P. Hugonin, A. Kumar, X. Deputy, T. Khodkov, T. Rappoport, J.-Y. Hong, N. Peres, J. Kong, D. Smith, and F. Koppens, Science **368**, 1219 (2020).
[686]W. Li, Q. Zhou, P. Zhang, and X.-W. Chen, Phys. Rev. Lett. **126**, 257401 (2021).
[687]Z. Liu, Y. Xu, Y. Lin, J. Xiang, T. Feng, Q. Cao, J. Li, S. Lan, and J. Liu, Phys. Rev. Lett. **123**, 253901 (2019).
[688]Z. Chen, X. Yin, J. Jin, Z. Zheng, Z. Zhang, F. Wang, L. He, B. Zhen, and C. Peng, Sci. Bull. **67**, 359 (2022).
[689]R.-M. Ma, H.-Y. Luan, Z.-W. Zhao, W.-Z. Mao, S.-L. Wang, Y.-H. Ouyang, and Z.-K. Shao, Fundam. Res. **3**, 537 (2023).
[690]C. He, Y. Shen, and A. Forbes, Light: Sci. Appl. **11**, 205 (2022).
[691]Z. Zhang, H. Zhao, S. Wu, T. Wu, X. Qiao, Z. Gao, R. Agarwal, S. Longhi, N. Litchinitser, L. Ge, and L. Feng, Nature **612**, 246 (2022).
[692]M. Knudson, R. Li, D. Wang, W. Wang, R. Schaller, and T. Odom, ACS Nano **13**, 7435 (2019).
[693]L. Allen, M. W. Beijersbergen, R. J. C. Spreeuw, and J. P. Woerdman, Phys. Rev. A **45**, 8185 (1992).
[694]X. Wang, Z. Nie, Y. Liang, J. Wang, T. Li, and B. Jia, Nanophotonics **7**, 1533 (2018).
[695]R.-M. Ma, Nat. Phys. **17**, 673 (2021).
[696]B. Qi, H. Chen, L. Ge, P. Berini, and R. Ma, Adv. Opt. Mater. **7**, 1900694 (2019).
[697]H.-Z. Chen, T. Liu, H.-Y. Luan, R.-J. Liu, X.-Y. Wang, X.-F. Zhu, Y.-B. Li, Z.-M. Gu, S.-J. Liang, H. Gao, L. Lu, L. Ge, S. Zhang, J. Zhu, and R.-M. Ma, Nat. Phys. **16**, 571 (2020).
[698]X.-Y. Wang, H.-Z. Chen, S. Wang, L. Ge, S. Zhang, and R.-M. Ma, Nanophotonics **11**, 1905 (2022).
[699]D. N. Nikogosyan, *Nonlinear Optical Crystals: A Complete Survey* (Springer, 2005).
[700]G. Poberaj, H. Hu, W. Sohler, and P. Günter, Laser Photonics Rev. **6**, 488 (2012).
[701]M. Zhang, C. Wang, P. Kharel, D. Zhu, and M. Lončar, "Integrated lithium niobate electro-optic modulators: When performance meets scalability," Optica **8**, 652–667 (2021).
[702]W. Sohler, H. Hu, R. Ricken, V. Quiring, C. Vannahme, H. Herrmann, D. Büchter, S. Reza, W. Grundkötter, S. Orlov, H. Suche, R. Nouroozi, and Y. Min, Opt. Photonics News **19**, 24 (2008).
[703]G. Jacucci, B. W. Longbottom, C. C. Parkins, S. A. F. Bon, and S. Vignolini, J. Mater. Chem. C **9**, 2695 (2021).

16 July 2024 09:29:41

© Author(s) 2024

[704]D. Serrano, J. Karlsson, A. Fossati, A. Ferrier, and P. Goldner, Nat. Commun. **9**, 2127 (2018).
[705]A. Karvounis, F. Timpu, V. V. Vogler-Neuling, R. Savo, and R. Grange, Adv. Opt. Mater. **8**, 2001249 (2020).
[706]B. Gao, M. Ren, W. Wu, H. Hu, W. Cai, and J. Xu, Laser Photonics Rev. **13**, 1800312 (2019).
[707]J. Ma, F. Xie, W. Chen, J. Chen, W. Wu, W. Liu, Y. Chen, W. Cai, M. Ren, and J. Xu, Laser Photonics Rev. **15**, 2000521 (2021).
[708]J. Gao, M. A. Vincenti, J. Frantz, A. Clabeau, X. Qiao, L. Feng, M. Scalora, and N. M. Litchinitser, Nat. Commun. **12**, 5833 (2021).
[709]H. Weigand, V. V. Vogler-Neuling, M. R. Escalé, D. Pohl, F. U. Richter, A. Karvounis, F. Timpu, and R. Grange, ACS Photonics **8**, 3004 (2021).
[710]A. Weiss, C. Frydendahl, J. Bar-David, R. Zektzer, E. Edrei, J. Engelberg, N. Mazurski, B. Desiatov, and U. Levy, ACS Photonics **9**, 605 (2022).
[711]C. Damgaard-Carstensen, M. Thomaschewski, and S. I. Bozhevolnyi, Nanoscale **14**, 11407 (2022).
[712]M. Modaresialam, Z. Chehadi, T. Bottein, M. Abbarchi, and D. Grosso, Chem. Mater. **33**, 5464 (2021).
[713]M. A. Verschuuren, M. Megens, Y. Ni, H. Van Sprang, and A. Polman, Adv. Opt. Technol. **6**, 243 (2017).
[714]C. J. Barbé, B. Barbé, M. A. Harmer, and G. W. Scherer, "Sol-gel synthesis of potassium titanyl phosphate: Solution chemistry and gelation," J. Sol-Gel Sci. Technol. **9**, 183–199 (1997).
[715]B. I. Edmondson, S. Kwon, J. E. Ortmann, A. A. Demkov, M. J. Kim, and J. G. Ekerdt, J. Am. Ceram. Soc. **103**, 5700 (2020).
[716]Ü. Linda Talts, H. C. Weigand, G. Saerens, P. Benedek, J. Winiger, V. Wood, J. Leuthold, V. Vogler-Neuling, and R. Grange, Small **19**, 2304355 (2023).
[717]R. F. Ali, J. A. Busche, S. Kamal, D. J. Masiello, and B. D. Gates, Light. Sci. Appl. **12**, 99 (2023).
[718]F. Alarslan, L. Vittadello, J. Klein, Q. A. Khan, C. Kijatkin, M. Haase, H. Schäfer, M. Imlau, and M. Steinhart, Adv. Eng. Mater. **24**, 2101159 (2021).
[719]S. Park, C.-H. Kim, W.-J. Lee, S. Sung, and M.-H. Yoon, Mater. Sci. Eng.: R: Rep. **114**, 1–22 (2017).
[720]V. J. Einck, M. Torfeh, A. McClung, D. E. Jung, M. Mansouree, A. Arbabi, and J. J. Watkins, ACS Photonics **8**, 2400 (2021).
[721]V. V. Vogler-Neuling, R. Savo, D. Pohl, N. R. Hendricks, L. Lang, M. Timofeeva, B. Schneider, F. U. Richter, F. Timpu, S. Monneret, F. Starsich, and R. Grange, Phys. Status Solidi (b) **257**, 1900755 (2020).
[722]H. Weigand, V. V. Vogler-Neuling, O. Pitz, Ü. L. Talts, F. Timpu, A. Karvounis, J. Winiger, P. Benedek, V. Wood, J. Leuthold, and R. Grange, in Conference on Lasers and Electro-Optics (2022).
[723]V. V. Vinogradov, Y. M. Komova, A. V. Vinogradov, and V. V. Vinogradov, Nanotechnol. Russ. **9**, 87 (2014).
[724]V. V. Vogler-Neuling, A. Karvounis, A. Morandi, H. Weigand, E. Dénervaud, and R. Grange, "Photonic assemblies of randomly oriented nanocrystals for engineered nonlinear and electro-optic effects," ACS Photonics **9**(7), 2193–2203 (2022).
[725]G. Brusatin, P. Innocenzi, M. Guglielmi, A. Abbotto, L. Beverina, G. A. Pagani, M. Casalboni, and F. Sarcinelli, J. Non-Cryst. Solids **345–346**, 575 (2004).
[726]H. Nasu, *Handbook of Sol-Gel Science and Technology*, 2005th ed. (Kluwer Academic Publishers, Springer, 2017), Vol. **1**.
[727]B. I. Edmondson, S. Kwon, C. H. Lam, J. E. Ortmann, A. A. Demkov, M. J. Kim, and J. G. Ekerdt, J. Am. Ceram. Soc. **103**, 1209 (2020).
[728]V. V. Vogler-Neuling, Ü.-L. Talts, R. Ferraro, H. Weigand, G. Finco, J. Winiger, P. Benedek, J. Kusch, A. Karvounis, V. Wood, J. Leuthold, and R. Grange, arXiv:2310.03386 (2023).
[729]D. Bokov, A. Turki Jalil, S. Chupradit, W. Suksatan, M. Javed Ansari, I. H. Shewael, G. H. Valiev, and E. Kianfar, Adv. Mater. Sci. Eng. **2021**, 1.
[730]C. Gigli, G. Marino, A. Artioli, D. Rocco, C. De Angelis, J. Claudon, J.-M. Gérard, and G. Leo, Optica **8**, 269 (2021).
[731]H. Choi, J. Kim, W. Kim, J. Seong, C. Park, M. Choi, N. Kim, J. Ha, C. W. Qiu, J. Rho, and H. Lee, PhotoniX **4**, 18 (2023).
[732]Z. Peng, Y. Zhang, C. L. R. Choi, P. Zhang, T. Wu, and Y. K. Chan, Nanoscale **15**, 11403 (2023).
[733]B. Schumm and S. Kaskel, "Nanoimprint lithography for photovoltaic applications," in *Solar Cell Nanotechnology*, edited by A. Tiwari, R. Boukherroub, and M. Sharon (Wiley, 2013).
[734]J. Gutierrez, A. Tercjak, I. Garcia, L. Peponi, and I. Mondragon, Nanotechnology **19**, 155607 (2008).
[735]M. Karayianni and S. Pispas, J. Polym. Sci. **59**, 1874 (2021).
[736]T. Das Gupta, L. Martin-Monier, W. Yan, A. Le Bris, T. Nguyen-Dang, A. G. Page, K.-T. Ho, F. Yesilköy, H. Altug, Y. Qu *et al.*, Nat. Nanotechnol. **14**, 320 (2019).
[737]M.-H. Chen, W.-N. Chou, V.-C. Su, C.-H. Kuan, and H. Y. Lin, Sci. Rep. **11**, 6500 (2021).
[738]S. H. Ahn and L. J. Guo, ACS Nano **3**, 2304 (2009).
[739]L. Zhang, S. Chang, X. Chen, Y. Ding, M. T. Rahman, Y. Duan, M. Stephen, and X. Ni, Nano Lett. **23**, 51 (2023).
[740]J.-S. Park, S. W. D. Lim, A. Amirzhan, H. Kang, K. Karrfalt, D. Kim, J. Leger, A. Urbas, M. Ossiander, Z. Li, and F. Capasso, ACS Nano **18**, 3187 (2024).
[741]R. Patra, S. Agarwal, S. Kondaraju, and S. S. Bahga, Opt. Commun. **389**, 74 (2017).
[742]D. Bouwmeester, J.-W. Pan, K. Mattle, M. Eibl, H. Weinfurter, and A. Zeilinger, Nature **390**, 575 (1997).
[743]A. Arbabi and A. Faraon, Sci. Rep. **7**, 43722 (2017).
[744]S. A. Maier *et al.*, *Plasmonics: Fundamentals and Applications* (Springer, 2007), Vol. 1.
[745]V. Klimov, *Nanoplasmonics* (CRC Press, 2014).
[746]A. F. Koenderink, A. Alu, and A. Polman, Science **348**, 516 (2015).
[747]A. I. Kuznetsov, A. E. Miroshnichenko, M. L. Brongersma, Y. S. Kivshar, and B. Luk'yanchuk, Science **354**, aag2472 (2016).
[748]Z. Zheng, D. Rocco, H. Ren, O. Sergaeva, Y. Zhang, K. B. Whaley, C. Ying, D. de Ceglia, C. De-Angelis, M. Rahmani, and L. Xu, Nanophotonics **12**, 4255–4281 (2023).
[749]K. Koshelev and Y. Kivshar, Acs Photonics **8**, 102 (2020).
[750]S. Colella, M. Mazzeo, A. Rizzo, G. Gigli, and A. Listosrti, J. Phys. Chem. Lett. **7**, 4322 (2016).
[751]A. S. Shorokhov, E. V. Melik-Gaykazyan, D. A. Smirnova, B. Hopkins, K. E. Chong, D.-Y. Choi, M. R. Shcherbakov, A. E. Miroshnichenko, D. N. Neshev, A. A. Fedyanin, and Y. S. Kivshar, Nano Lett. **16**, 4857 (2016).
[752]M. P. Nielsen, L. Lafone, A. Rakovich, T. P. Sidiropoulos, M. Rahmani, S. A. Maier, and R. F. Oulton, Nano Lett. **16**, 1410 (2016).
[753]M. Caldarola, P. Albella, E. Cortés, M. Rahmani, T. Roschuk, G. Grinblat, R. F. Oulton, A. V. Bragas, and S. A. Maier, Nat. Commun. **6**, 7915 (2015).
[754]K. Ikeda, Y. Shen, and Y. Fainman, Opt. Express **15**, 17761 (2007).
[755]A. I. Kuznetsov, A. E. Miroshnichenko, Y. H. Fu, J. Zhang, and B. Luk'yanchuk, Sci. Rep. **2**, 492 (2012).
[756]Z. Wang, T. Li, A. Soman, D. Mao, T. Kananen, and T. Gu, Nat. Commun. **10**, 3547 (2019).
[757]N. I. Zheludev and Y. S. Kivshar, Nat. Mater. **11**, 917 (2012).
[758]M. R. Shcherbakov, P. P. Vabishchevich, A. S. Shorokhov, K. E. Chong, D.-Y. Choi, I. Staude, A. E. Miroshnichenko, D. N. Neshev, A. A. Fedyanin, and Y. S. Kivshar, Nano Lett. **15**, 6985 (2015).
[759]D. Rocco, A. Tognazzi, M. Gandolfi, C. Gigli, A. Zilli, L. Carletti, A. Locatelli, G. Leo, G. Della Valle, M. Finazzi *et al.*, *Fundamentals and Applications of Nonlinear Nanophotonics* (Elsevier, 2024), pp. 131–165.
[760]M. Sheik-Bahae, A. A. Said, T.-H. Wei, D. J. Hagan, and E. W. Van Stryland, IEEE J. Quantum Electron. **26**, 760 (1990).
[761]C. Kuo, S. Vong, R. Cohen, and G. Stringfellow, J. Appl. Phys. **57**, 5428 (1985).
[762]J. Cambiasso, G. Grinblat, Y. Li, A. Rakovich, E. Cortés, and S. A. Maier, Nano Lett. **17**, 1219 (2017).
[763]S. Person, M. Jain, Z. Lapin, J. J. Sáenz, G. Wicks, and L. Novotny, Nano Lett. **13**, 1806 (2013).
[764]S. Liu, M. B. Sinclair, S. Saravi, G. A. Keeler, Y. Yang, J. Reno, G. M. Peake, F. Setzpfandt, I. Staude, T. Pertsch, and I. Brener, Nano Lett. **16**, 5426 (2016).
[765]R. Camacho-Morales, L. Xu, H. Zhang, S. T. Ha, L. Krivitsky, A. I. Kuznetsov, M. Rahmani, and D. Neshev, Nano Lett. **22**, 6141 (2022).
[766]A. Rogacheva, V. Fedotov, A. Schwanecke, and N. Zheludev, Phys. Rev. Lett. **97**, 177401 (2006).
[767]N. Liu, H. Liu, S. Zhu, and H. Giessen, Nat. Photonics **3**, 157 (2009).
[768]H. Zhao, X. Wang, S. Liu, and Y. Zhang, Opto-Electron. Adv. **6**, 220012 (2023).

16 July 2024 09:29:41

© Author(s) 2024

[769]J. C. Zhang, M. K. Chen, Y. Fan, Q. Chen, S. Chen, J. Yao, X. Liu, S. Xiao, and D. P. Tsai, Opto-Electron. Adv. **7**, 230171 (2024).
[770]R. Zhao, L. Huang, and Y. Wang, PhotoniX **1**, 20 (2020).
[771]Y. Zhou, I. I. Kravchenko, H. Wang, J. R. Nolen, G. Gu, and J. Valentine, Nano Lett. **18**, 7529 (2018).
[772]Y. Zhou, I. I. Kravchenko, H. Wang, H. Zheng, G. Gu, and J. Valentine, Light. Sci. Appl. **8**, 80 (2019).
[773]K. Tanaka, D. Arslan, S. Fasold, M. Steinert, J. Sautter, M. Falkner, T. Pertsch, M. Decker, and I. Staude, ACS Nano **14**, 15926 (2020).
[774]E. Bermúdez-Ureña and U. Steiner, ACS Photonics **6**, 2198 (2019).
[775]G. Marino, D. Rocco, C. Gigli, G. Beaudoin, K. Pantzas, S. Suffit, P. Filloux, I. Sagnes, G. Leo, and C. De Angelis, Nanophotonics **10**, 1837 (2021).
[776]F. Vennberg, A. P. Ravishankar, and S. Anand, Nanophotonics **11**, 4755 (2022).
[777]A. Y. Zhu, A. I. Kuznetsov, B. Luk'yanchuk, N. Engheta, and P. Genevet, Nanophotonics **6**, 452 (2017).
[778]C.-W. Qiu, T. Zhang, G. Hu, and Y. Kivshar, Nano Lett. **21**, 5461 (2021).
[779]P. Tonkaev, I. S. Sinev, M. V. Rybin, S. V. Makarov, and Y. Kivshar, Chem. Rev. **122**, 15414 (2022).
[780]W. Fan, S. Zhang, N.-C. Panoiu, A. Abdenour, S. Krishna, R. Osgood, K. Malloy, and S. Brueck, Nano Lett. **6**, 1027 (2006).
[781]Y. Pu, R. Grange, C.-L. Hsieh, and D. Psaltis, Phys. Rev. Lett. **104**, 207402 (2010).
[782]D. Lehr, J. Reinhold, I. Thiele, H. Hartung, K. Dietrich, C. Menzel, T. Pertsch, E.-B. Kley, and A. Tünnermann, Nano Lett. **15**, 1025 (2015).
[783]V. F. Gili, L. Ghirardini, D. Rocco, G. Marino, I. Favero, I. Roland, G. Pellegrini, L. Duò, M. Finazzi, L. Carletti, A. Locatelli, A. Lemaître, D. Neshev, C. De Angelis, G. Leo, and M. Celebrano, Beilstein J. Nanotechnol. **9**, 2306 (2018).
[784]N. Mendelson, D. Chugh, J. R. Reimers, T. S. Cheng, A. Gottscholl, H. Long, C. J. Mellor, A. Zettl, V. Dyakonov, P. H. Beton *et al.*, Nat. Mater. **20**, 321 (2021).
[785]A. G. S. Vilasam, S. Adhikari, B. Gupta, S. Balendhran, N. Higashitarumizu, J. Tournet, L. Li, A. Javey, K. B. Crozier, S. Karuturi *et al.*, Nanotechnology **34**, 495601 (2023).
[786]A. Gupta, T. Sakthivel, and S. Seal, Prog. Mater. Sci. **73**, 44 (2015).
[787]M. Yakushev, V. Vasil'ev, S. Dvoretskiĭ, A. Kozlov, A. Novoselov, Y. G. Sidorov, B. Fomin, A. Aseev, and E. Degtyarev, J. Opt. Technol. **76**, 777 (2009).
[788]L. Ohnoutek, J.-Y. Kim, J. Lu, B. J. Olohan, D. M. Răsădean, G. D. Pantoș, N. A. Kotov, and V. K. Valev, Nat. Photonics **16**, 126 (2022).
[789]J. Xiong, Z.-H. Zhang, Z. Li, P. Zheng, J. Li, X. Zhang, Z. Gao, Z. Wei, G. Zheng, S.-P. Wang *et al.*, Light. Sci. Appl. **12**, 286 (2023).
[790]Z. Li, J. S. Smalley, R. Haroldson, D. Lin, R. Hawkins, A. Gharajeh, J. Moon, J. Hou, C. Zhang, W. Hu *et al.*, ACS Photonics **7**, 1754 (2020).
[791]C. Zhang, S. Xiao, Y. Wang, Y. Gao, Y. Fan, C. Huang, N. Zhang, W. Yang, and Q. Song, Laser Photonics Rev. **13**, 1900079 (2019).
[792]G. Long, G. Adamo, J. Tian, M. Klein, H. N. Krishnamoorthy, E. Feltri, H. Wang, and C. Soci, Nat. Commun. **13**, 1551 (2022).
[793]Y. Fan, Y. Wang, N. Zhang, W. Sun, Y. Gao, C.-W. Qiu, Q. Song, and S. Xiao, Nat. Commun. **10**, 2085 (2019).
[794]G. Cai, Y. Li, Y. Zhang, X. Jiang, Y. Chen, G. Qu, X. Zhang, S. Xiao, J. Han, S. Yu *et al.*, Nat. Mater. **23**, 71 (2023).
[795]S. Wang, X. Liu, and P. Zhou, Adv. Mater. **34**, 2106886 (2022).
[796]S. M. Reimann and M. Manninen, Rev. Mod. Phys. **74**, 1283 (2002).
[797]H. Huang, A. C. Overvig, Y. Xu, S. C. Malek, C.-C. Tsai, A. Alù, and N. Yu, Nat. Nanotechnol. **18**, 580 (2023).
[798]A. Nemati, Q. Wang, M. Hong, J. Teng *et al.*, Opto-Electron. Adv. **1**, 18000901 (2018).
[799]A. Nemati, Q. Wang, N. S. S. Ang, W. Wang, M. Hong, J. Teng *et al.*, Opto-Electron. Adv. **4**, 200088 (2021).
[800]Y.-C. Ling and S. J. B. Yoo, Nanophotonics **12**, 3851 (2023).
[801]K. Zangeneh Kamali, L. Xu, N. Gagrani, H. H. Tan, C. Jagadish, A. Miroshnichenko, D. Neshev, and M. Rahmani, Light. Sci. Appl. **12**, 40 (2023).
[802]X. Ni, Z. J. Wong, M. Mrejen, Y. Wang, and X. Zhang, Science **349**, 1310 (2015).
[803]S. Karepov and T. Ellenbogen, Opt. Lett. **45**, 1379 (2020).
[804]C. Zhang, J. Jing, Y. Wu, Y. Fan, W. Yang, S. Wang, Q. Song, and S. Xiao, ACS Nano **14**, 1418 (2019).
[805]J. Yu, Z. Liu, M. Wang, C. Wang, G. Chen, Z. Cui, T. Wang, H. Yang, X. Wang, and X. Chen, Adv. Mater. **34**, 2102560 (2022).
[806]H.-S. Ee and R. Agarwal, Nano Lett. **16**, 2818 (2016).
[807]H. A. Rowland, Am. J. Sci. **s3–26**, 87 (1883).
[808]F. Wadsworth, Astrophys. J. **3**, 47 (1896).
[809]D. W. Wilson, P. D. Maker, R. E. Muller, P. Z. Mouroulis, and J. Backlund, "Recent advances in blazed grating fabrication by electron-beam lithography," Proc. SPIE **5173**, 51730E (2003).
[810]H. Li, X. Peng, C. Guan, and H. Hu, Micromachines **13**, 1689 (2022).
[811]T. Stone and N. George, Appl. Opt. **27**, 2960 (1988).
[812]R. Skidanov, S. Ganchevskaya, V. Vasil'ev, and V. Podlipnov, Opt. Spectrosc. **129**, 581–585 (2021).
[813]A. Wood, Appl. Opt. **31**, 2253 (1992).
[814]L. Josefsson and P. Persson, *Conformal Array Antenna Theory and Design* (John Wiley & Sons, 2006).
[815]H. Schippers, J. Verpoorte, P. Jorna, A. Hulzinga, A. Meijerink, C. Roeloffzen, R. G. Heideman, A. Leinse, and M. Wintels, in *2008 International ITG Workshop on Smart Antennas* (IEEE, 2008), pp. 343–350.
[816]D. Germain, D. Seetharamdoo, S. Nawaz Burokur, and A. de Lustrac, Appl. Phys. Lett. **103**, 124102 (2013).
[817]Y. Shang and Z. Shen, IEEE Trans. Antennas Propag. **65**, 2386 (2017).
[818]Z. H. Jiang, L. Kang, and D. H. Werner, Nat. Commun. **8**, 356 (2017).
[819]K. Wu, P. Coquet, Q. J. Wang, and P. Genevet, Nat. Commun. **9**, 3494 (2018).
[820]J. Cheng, S. Jafar-Zanjani, and H. Mosallaei, Sci. Rep. **6**, 38440 (2016).
[821]D. Zhang, W. Yu, T. Wang, Z. Lu, and Q. Sun, Opt. Express **18**, 15009 (2010).
[822]S. M. Kamali, E. Arbabi, A. Arbabi, Y. Horie, and A. Faraon, Laser Photonics Rev. **10**, 1002 (2016).
[823]A. She, S. Zhang, S. Shian, D. R. Clarke, and F. Capasso, Sci. Adv. **4**, eaap9957 (2018).
[824]R. Fang, A. Ghasemi, D. A. Zeze, and M. Keshavarz Hedayati, J. Appl. Phys. **132**, 133102 (2022).
[825]J. Li, H. Fan, H. Ye, T. Wu, Y. Sun, X. Wang, and Y. Liu, Nanomaterials **12**, 2387 (2022).
[826]L. Zhu, J. Kapraun, J. Ferrara, and C. J. Chang-Hasnain, Optica **2**, 255 (2015).
[827]M. L. Tseng, J. Yang, M. Semmlinger, C. Zhang, P. Nordlander, and N. J. Halas, Nano Lett. **17**, 6034 (2017).
[828]A. Arbabi, E. Arbabi, M. Mansouree, S. Han, S. M. Kamali, Y. Horie, and A. Faraon, Sci. Rep. **10**, 7124 (2020).
[829]M. Faraji-Dana, E. Arbabi, A. Arbabi, S. M. Kamali, H. Kwon, and A. Faraon, Nat. Commun. **9**, 4196 (2018).
[830]T. Phan, D. Sell, E. W. Wang, S. Doshay, K. Edee, J. Yang, and J. A. Fan, Light. Sci. Appl. **8**, 48 (2019).
[831]S. Aksu, M. Huang, A. Artar, A. A. Yanik, S. Selvarasah, M. R. Dokmeci, and H. Altug, Adv. Mater. **23**, 4422 (2011).
[832]B. Ko, T. Badloe, Y. Yang, J. Park, J. Kim, H. Jeong, C. Jung, and J. Rho, Nat. Commun. **13**, 6256 (2022).
[833]J. Zhu, Z. Wang, S. Lin, S. Jiang, X. Liu, and S. Guo, Biosens. Bioelectron. **150**, 111905 (2020).
[834]K. Xiong, D. Tordera, G. Emilsson, O. Olsson, U. Linderhed, M. P. Jonsson, and A. B. Dahlin, Nano Lett. **17**, 7033 (2017).
[835]M. Atighilorestani, H. Jiang, and B. Kaminska, Adv. Opt. Mater. **6**, 1801179 (2018).
[836]E. Galiffi, R. Tirole, S. Yin, H. Li, S. Vezzoli, P. A. Huidobro, M. G. Silveirinha, R. Sapienza, A. Alù, and J. B. Pendry, Adv. Photonics **4**, 014002 (2022).
[837]T. Liu, J.-Y. Ou, K. F. MacDonald, and N. I. Zheludev, Nat. Phys. **19**, 986 (2023).
[838]J. Mendonca, *Theory of Photon Acceleration* (CRC Press, 2000), Vol. 1.
[839]A. Przadka, S. Feat, P. Petitjeans, V. Pagneux, A. Maurel, and M. Fink, Phys. Rev. Lett. **109**, 064501 (2012).
[840]G. Lerosey, J. de Rosny, A. Tourin, A. Derode, G. Montaldo, and M. Fink, Phys. Rev. Lett. **92**, 193904 (2004).
[841]L. Zhang, X. Q. Chen, S. Liu, Q. Zhang, J. Zhao, J. Y. Dai, G. D. Bai, X. Wan, Q. Cheng, G. Castaldi, V. Galdi, and T. J. Cui, Nat. Commun. **9**, 4334 (2018).

16 July 2024 09:29:41

© Author(s) 2024

[842]E. A. A. Pogna, M. Marsili, D. De Fazio, S. Dal Conte, C. Manzoni, D. Sangalli, D. Yoon, A. Lombardo, A. C. Ferrari, A. Marini, G. Cerullo, and D. Prezzi, ACS Nano **10**, 1182 (2016).
[843]Z. Dong, H. Li, T. Wan, Q. Liang, Z. Yang, and B. Yan, "Quantum time reflection and refraction of ultracold atoms," Nat. Photon. **18**, 68–73 (2024).
[844]S. A. Mann, N. Nookala, S. C. Johnson, M. Cotrufo, A. Mekawy, J. F. Klem, I. Brener, M. B. Raschke, A. Alù, and M. A. Belkin, Optica **8**, 606 (2021).
[845]Z. Hayran, J. B. Khurgin, and F. Monticone, Opt. Mater. Express **12**, 3904 (2022).
[846]N. Engheta, Science **379**, 1190 (2023).
[847]R. W. Boyd, *Nonlinear Optics* (Academic Press, New York, 2003).
[848]Y. Tamashevich, T. Shubitidze, L. Dal Negro, and M. Ornigotti, APL Photonics **9**, 016105 (2024).
[849]M. Clerici, N. Kinsey, C. DeVault, J. Kim, E. G. Carnemolla, L. Caspani, A. Shaltout, D. Faccio, V. Shalaev, A. Boltasseva, and M. Ferrera, Nat. Commun. **8**, 15829 (2017).
[850]J. B. Khurgin, M. Clerici, and N. Kinsey, Laser Photonics Rev. **15**, 2000291 (2021).
[851]V. Bruno, C. DeVault, S. Vezzoli, Z. Kudyshev, T. Huq, S. Mignuzzi, A. Jacassi, S. Saha, Y. Shah, S. Maier, D. Cumming, A. Boltasseva, M. Ferrera, M. Clerici, D. Faccio, R. Sapienza, and V. Shalaev, Phys. Rev. Lett. **124**, 043902 (2020).
[852]S. Vezzoli, V. Bruno, C. DeVault, T. Roger, V. M. Shalaev, A. Boltasseva, M. Ferrera, M. Clerici, A. Dubietis, and D. Faccio, Phys. Rev. Lett. **120**, 043902 (2018).
[853]J. B. Pendry, Science **322**, 71 (2008).
[854]E. Lustig, O. Segal, S. Saha, E. Bordo, S. N. Chowdhury, Y. Sharabi, A. Fleischer, A. Boltasseva, O. Cohen, V. M. Shalaev, and M. Segev, Nanophotonics **12**, 2221 (2023).
[855]J. Bohn, T. S. Luk, C. Tollerton, S. W. Hutchings, I. Brener, S. Horsley, W. L. Barnes, and E. Hendry, Nat. Commun. **12**, 1017 (2021).
[856]S. Horsley, E. Galiffi, and Y.-T. Wang, Phys. Rev. Lett. **130**, 203803 (2023).
[857]M. Ren, W. Cai, and J. Xu, Adv. Mater. **32**, 1806317 (2020).
[858]V. Pacheco-Peña and N. Engheta, Optica **7**, 323 (2020).
[859]V. Pacheco-Peña and N. Engheta, Phys. Rev. B **104**, 214308 (2021).
[860]A. Akbarzadeh, N. Chamanara, and C. Caloz, Opt. Lett. **43**, 3297 (2018).
[861]R. Tirole, E. Galiffi, J. Dranczewski, T. Attavar, B. Tilmann, Y.-T. Wang, P. A. Huidobro, A. Alú, J. B. Pendry, S. A. Maier, S. Vezzoli, and R. Sapienza, "Saturable time-varying mirror based on an epsilon-near-zero material," Phys. Rev. Appl. **18**, 054067 (2022).
[862]D. Faccio and E. M. Wright, Science **377**, 368 (2022).
[863]E. Galiffi, Y.-T. Wang, Z. Lim, J. B. Pendry, A. Alù, and P. A. Huidobro, Phys. Rev. Lett. **125**, 127403 (2020).
[864]S. F. Koufidis, T. T. Koutserimpas, and M. W. McCall, Opt. Lett. **48**, 4500 (2023).
[865]I.-W. Un, S. Sarkar, and Y. Sivan, Phys. Rev. Appl. **19**, 044043 (2023).
[866]E. E. Narimanov, "Ultrafast optical modulation by virtual interband transitions," arXiv:2310.15908 (2023).
[867]M. R. Shcherbakov, K. Werner, Z. Fan, N. Talisa, E. Chowdhury, and G. Shvets, Nat. Commun. **10**, 1345 (2019).
[868]K. Lee, J. Park, S. Lee, S. Baek, J. Park, F. Rotermund, and B. Min, Nanophotonics **11**, 2045 (2022).
[869]P. A. Shafirin, V. V. Zubyuk, A. A. Fedyanin, and M. R. Shcherbakov, Nanophotonics **11**, 4053 (2022).
[870]M. R. Shcherbakov, R. Lemasters, Z. Fan, J. Song, T. Lian, H. Harutyunyan, and G. Shvets, Optica **6**, 1441 (2019).
[871]G. Grinblat, H. Zhang, M. P. Nielsen, L. Krivitsky, R. Berté, Y. Li, B. Tilmann, E. Cortés, R. F. Oulton, A. I. Kuznetsov *et al.*, Sci. Adv. **6**, eabb3123 (2020).
[872]N. Karl, P. P. Vabishchevich, M. R. Shcherbakov, S. Liu, M. B. Sinclair, G. Shvets, and I. Brener, Nano Lett. **20**, 7052 (2020).
[873]P. P. Vabishchevich, A. Vaskin, N. Karl, J. L. Reno, M. B. Sinclair, I. Staude, and I. Brener, Appl. Phys. Lett. **118**, 211105 (2021).
[874]R. Tirole, B. Tilmann, L. d S. Menezes, S. Vezzoli, R. Sapienza, and S. A. Maier, "Nonlinear dielectric epsilon near-zero hybrid nanogap antennas," arXiv:2308.07109 (2023).
[875]K. Pang, M. Z. Alam, Y. Zhou, C. Liu, O. Reshef, K. Manukyan, M. Voegtle, A. Pennathur, C. Tseng, X. Su, H. Song, Z. Zhao, R. Zhang, H. Song, N. Hu, A. Almaiman, J. M. Dawlaty, R. W. Boyd, M. Tur, and A. E. Willner, Nano Lett. **21**, 5907 (2021).
[876]L. Yuan, Q. Lin, M. Xiao, and S. Fan, Optica **5**, 1396 (2018).
[877]P. Lalanne, J. Opt. Soc. Am. A **16**, 2517 (1999).
[878]Z. Bomzon, V. Kleiner, and E. Hasman, Opt. Lett. **26**, 1424 (2001).
[879]M. Karimi, M. Z. Alam, J. Upham, O. Reshef, and R. W. Boyd, Nanophotonics **12**, 1733 (2023).
[880]M. Khorasaninejad, W. T. Chen, R. C. Devlin, J. Oh, A. Y. Zhu, and F. Capasso, Science **352**, 1190 (2016).
[881]S. Tsesses, R. Dahan, K. Wang, T. Bucher, K. Cohen, O. Reinhardt, G. Bartal, and I. Kaminer, Nat. Mater. **22**, 345 (2023).
[882]Q. Wang, E. T. F. Rogers, B. Gholipour, C.-M. Wang, G. Yuan, J. Teng, and N. I. Zheludev, Nat. Photonics **10**, 60 (2015).
[883]T. Wu, M. Menarini, Z. Gao, and L. Feng, Nat. Photonics **17**, 710 (2023).
[884]J. Y. Ou, E. Plum, L. Jiang, and N. I. Zheludev, Nano Lett. **11**, 2142 (2011).
[885]Q. Fan, A. M. Shaltout, J. van de Groep, M. L. Brongersma, and A. M. Lindenberg, ACS Photonics **10**, 2467 (2023).
[886]O. Hernandez, E. Papagiakoumou, D. Tanese, K. Fidelin, C. Wyart, and V. Emiliani, Nat. Commun. **7**, 11928 (2016).
[887]X. Lin, Y. Rivenson, N. T. Yardimci, M. Veli, Y. Luo, M. Jarrahi, and A. Ozcan, Science **361**, 1004 (2018).
[888]J. B. Pendry, E. Galiffi, and P. A. Huidobro, J. Opt. Soc. Am. B **38**, 3360 (2021).
[889]X. Guo, Y. Ding, Y. Duan, and X. Ni, Light. Sci. Appl. **8**, 123 (2019).
[890]D. Ramaccia, D. L. Sounas, A. Alù, A. Toscano, and F. Bilotti, IEEE Trans. Antennas Propag. **68**, 1607 (2020).
[891]D. Ramaccia, D. L. Sounas, A. Alù, A. Toscano, and F. Bilotti, Phys. Rev. B **95**, 075113 (2017).
[892]S. Taravati and A. A. Kishk, Phys. Rev. B **99**, 075101 (2019).
[893]X. Wang, V. S. Asadchy, S. Fan, and S. A. Tretyakov, ACS Photonics **8**, 3034 (2021).
[894]P. A. Huidobro, E. Galiffi, S. Guenneau, R. V. Craster, and J. B. Pendry, Proc. Natl. Acad. Sci. U. S. A. **116**, 24943 (2019).
[895]D. Oue, K. Ding, and J. B. Pendry, Phys. Rev. Res. **4**, 013064 (2022).
[896]S. A. R. Horsley and J. B. Pendry, Proc. Natl. Acad. Sci. U. S. A. **120**, e2302652120 (2023).
[897]Y. Mazor and A. Alù, Phys. Rev. B **99**, 045407 (2019).
[898]E. Galiffi, P. A. Huidobro, and J. B. Pendry, Phys. Rev. Lett. **123**, 206101 (2019).
[899]Z. Hu, C. Liu, and G. Li, Adv. Phys. X. **8**, 2234136 (2023).
[900]M. Minot, J. Opt. Soc. Am. **66**, 515 (1976).
[901]H. Deckman, C. Wronski, H. Witzke, and E. Yablonovitch, Appl. Phys. Lett **42**, 968 (1983).
[902]M. Moskovits, Rev. Mod. Phys. **57**, 783 (1985).
[903]C. Bohren and D. Huffman, *Absorption and Scattering of Light by Small Particles* (Wiley, 1983).
[904]T. Yamaguchi, S. Yoshida, and A. Kinbara, Thin Solid Films **21**, 173 (1974).
[905]P. Beckmann and A. Spizzichino, *The Scattering of Electromagnetic Waves from Rough Surfaces* (Artech House, 1987).
[906]D. Bedeaux and J. Vlieger, *Optical Properties of Surfaces* (Imperial College Press, 2004).
[907]A. G. Voronovich, *Wave Scattering from Rough Surfaces* (Springer Science & Business Media, 2013).
[908]J. Goodman, *Speckle Phenomena in Optics: Theory and Applications* (Roberts & Compagy, 2004).
[909]L. Tsang and J. Kong, *Scattering of Electromagnetic Waves: Advanced Topics* (John Wiley & Sons, 2004), Vol. 26.
[910]R. Wang, R. Wang, J. Han, J. Han, J. Liu, J. Liu, H. Tian, W. Sun, L. Li, L. Li, X. Chen, and X. Chen, Opt. Lett. **45**, 3506 (2020).
[911]M. Mishchenko, L. Travis, and A. Lacis, *Scattering, Absorption, and Emission of Light by Small Particles* (Cambridge University Press, 2002).
[912]See 15s://scattport.org/index.php/light-scattering-software/t-matrixcodes for "The SCATTPORT Website" (2024).
[913]J. Taboada, J. Rivero, F. Obelleiro, M. Araújo, and L. Landesa, J. Opt. Soc. Am. A **28**, 1341 (2011).
[914]D. Solis, J. Taboada, F. Obelleiro, L. Liz-Marzán, and F. Garcia De Abajo, ACS Nano **8**, 7559 (2014).
[915]M. Bertrand, A. Devilez, J. Hugonin, P. Lalanne, and K. Vynck, J. Opt. Soc. Am. A **37**, 70 (2020).

16 July 2024 09:29:41

© Author(s) 2024

[916]K. Vynck, C. Rockstuhl, A. Sprafke, A. Dmitriev, and P. Lalanne, "Disordered optical metasurfaces: From basics to applications" (unpublished).
[917]N. Tucher, H. T. Gebrewold, and B. Bläsi, Opt. Express **26**, A937 (2018).
[918]K. Vynck, R. Pacanowski, A. Agreda, A. Dufay, X. Granier, and P. Lalanne, Nat. Mater. **21**, 1035 (2022).
[919]D. Theobald, D. Beutel, L. Borgmann, H. Mescher, G. Gomard, C. Rockstuhl, and U. Lemmer, J. Quant. Spectrosc. Radiat. Transfer **272**, 107802 (2021).
[920]K. Vynck, A. Pitelet, L. Bellando, and P. Lalanne, *Adventures in Contemporary Electromagnetic Theory*, edited by T. G. Mackay and A. Lakhtakia (Springer, 2023).
[921]M. Peña-Gomar, F. Castillo, A. García-Valenzuela, R. Barrera, and E. Pérez, Appl. Opt. **45**, 626 (2006).
[922]A. García-Valenzuela, E. Gutiérrez-Reyes, and R. Barrera, J. Opt. Soc. Am. A **29**, 1161 (2012).
[923]A. Agreda, T. Wu, A. Hereu, M. Treguer-Delapierre, G. Drisko, K. Vynck, and P. Lalanne, ACS Nano **17**, 6362 (2023).
[924]H. Schift, J. Vac. Sci. Technol. **26**, 458 (2008).
[925]D. Qin, Y. Xia, and G. M. Whitesides, Nat. Protoc. **5**, 491 (2010).
[926]T. Andersson, Thin Solid Films **29**, L21 (1975).
[927]R. Aroca and F. Martin, J. Raman Spectrosc. **16**, 156 (1985).
[928]A. A. Kulkarni and G. S. Doer, Nanotechnology **33**, 292001 (2022).
[929]A. Alvarez–Fernandez, C. Cummins, M. Saba, U. Steiner, G. Fleury, V. Ponsinet, and S. Guldin, Adv. Opt. Mater. **9**, 2100175 (2021).
[930]L. Shi, J. Harris, R. Fenollosa, I. Rodriguez, X. Lu, B. Korgel, and F. Meseguer, Nat. Commun. **4**, 1904 (2013).
[931]C. Trompoukis, I. Massiot, V. Depauw, O. Daif, K. Lee, A. Dmitriev, I. Gordon, R. Mertens, and J. Poortmans, Opt. Express **24**, A191 (2016).
[932]G. M. Akselrod, J. Huang, T. B. Hoang, P. T. Bowen, L. Su, D. R. Smith, and M. H. Mikkelsen, Adv. Mater. **27**, 8028 (2015).
[933]J. M. Romo-Herrera, R. A. Alvarez-Puebla, and L. M. Liz-Marzán, Nanoscale **3**, 1304 (2011).
[934]V. Lotito and T. Zambelli, Adv. Colloid Interface Sci. **246**, 217 (2017).
[935]Y. Wang, M. Zhang, Y. Lai, and L. Chi, Nano Today **22**, 36 (2018).
[936]V. Lotito and T. Zambelli, Adv. Colloid Interface Sci. **284**, 102252 (2020).
[937]K. Vynck, M. Burresi, F. Riboli, and D. S. Wiersma, Nat. Mater. **11**, 1017 (2012).
[938]P. Mao, C. Liu, F. Song, M. Han, S. Maier, and S. Zhang, Nat. Commun. **11**, 1538 (2020).
[939]N. Dalloz, Van Doan Le, M. Hebert, B. Eles, M. A. Flores Figueroa, C. Hubert, H. Ma, N. Sharma, F. Vocanson, S. Ayala, and N. Destouches, Adv. Mater. **34**, 2104054 (2022).
[940]H. Yasuda, R. Matsuno, N. Koito, H. Hosoda, T. Tani, and M. Naya, Appl. Phys. Lett. **111**, 231105 (2017).
[941]D. Veksler, E. Maguid, N. Shitrit, D. Ozeri, V. Kleiner, and E. Hasman, ACS Photonics **2**, 661 (2015).
[942]M. Jang, Y. Horie, A. Shibukawa, J. Brake, Y. Liu, S. Kamali, A. Arbabi, H. Ruan, A. Faraon, and C. Yang, Nat. Photonics **12**, 84 (2018).
[943]C. Hsu, B. Zhen, W. Qiu, O. Shapira, B. Delacy, J. D. Joannopoulos, and M. Soljačić, Nat. Commun. **5**, 3152 (2014).
[944]H. Chu, X. Xiong, N. Fang, F. Wu, R. Jia, R. Peng, M. Wang, and Y. Lai, "Transparent matte surfaces enabled by asymmetric diffusion of white light," arXiv:2303.12333 (2023).
[945]S. Fasold, S. Linß, T. Kawde, M. Falkner, M. Decker, T. Pertsch, and I. Staude, ACS Photonics **5**, 1773 (2018).
[946]R. Siddique, J. Mertens, H. Hölscher, and S. Vignolini, Light: Sci. Appl. **6**, e17015 (2017).
[947]P. Mao, C. Liu, Y. Niu, Y. Qin, F. Song, M. Han, R. Palmer, S. Maier, and S. Zhang, Adv. Mater. **33**, 2007623 (2021).
[948]H. Galinski, G. Favraud, H. Dong, J. S. Totero Gongora, G. Favaro, M. Döbeli, R. Spolenak, A. Fratalocchi, and F. Capasso, Light: Sci. Appl. **6**, e16233 (2017).
[949]N. Destouches, N. Sharma, and M. Vangheluwe, Adv. Funct. Mater. **31**, 2010430 (2021).
[950]P. Cencillo-Abad, D. Franklin, P. Mastranzo-Ortega, J. Sanchez-Mondragon, and D. Chanda, Sci. Adv. **9**, 7207 (2023).
[951]K. Xiong, O. Olsson, J. Svirelis, C. Palasingh, J. Baumberg, and A. Dahlin, Adv. Mater. **33**, e2403476 (2021).
[952]H. J. Gläser, Appl. Opt. **47**, C193 (2008).
[953]G. Jönsson, D. Tordera, T. Pakizeh, M. Jaysankar, V. Miljkovic, L. Tong, M. Jonsson, and A. Dmitriev, Nano Lett. **17**, 6766 (2017).
[954]I. Haechler, N. Ferru, G. Schnoering, E. Mitridis, T.,M. Schutzius, and D. Poulikakos, Nat. Nanotechnol. **18**, 137 (2023).
[955]V. Maiorov, Opt. Spectrosc. **124**, 594 (2018).
[956]Z. Ding, H. Li, X. Li, X. Fan, J. Jaramillo–Fernandez, L. Pattelli, J. Zhao, S. Niu, Y. Li, and H. Xu, Adv. Mater. Interfaces **11**, 2300603 (2023).
[957]C. Liu, T. Wu, P. Lalanne, and S. A. Maier, Nano Lett. **24**, 4641 (2024).
[958]A. Jouanin, J. Hugonin, and P. Lalanne, Adv. Funct. Mater. **26**, 6215 (2016).
[959]Y. Donie, D. Theobald, S. Moghadamzadeh, A. Mertens, I. Hossain, U. Paetzold, U. Lemmer, and G. Gomard, Adv. Opt. Mater. **9**, 2001610 (2021).
[960]P. Mao, C. Liu, X. Li, M. Liu, Q. Chen, M. Han, S. Maier, E. Sargent, and S. Zhang, Light Sci. Appl. **10**, 2047 (2021).
[961]M. Fusella, R. Saramak, R. Bushati *et al.*, Nature **585**, 379 (2020).
[962]Y. Fu, A. Kuznetsov, A. Miroshnichenko, Y. Yu, and B. Luk'yanchuk, Nat. Commun. **4**, 1527 (2013).
[963]M. F. Picardi, A. V. Zayats, and F. J. Rodríguez-Fortuño, Phys. Rev. Lett. **120**, 117402 (2018).
[964]K. Vynck, R. Pierrat, R. Carminati, L. Froufe-Pérez, F. Scheffold, R. Sapienza, S. Vignolini, and J. S. Saenz, Rev. Mod. Phys. **95**, 45003 (2023).
[965]P. Piechulla, B. Fuhrmann, E. Slivina, C. Rockstuhl, R. Wehrspohn, and A. Sprafke, Adv. Opt. Mater. **9**, 2100186 (2021).
[966]J. Buencuerpo, J. M. Llorens, J. M. Ripalda, M. A. Steiner, and A. C. Tamboli, Opt. Laser Technol. **142**, 107224 (2021).
[967]E. C. Abad, H. J. Joyce, and L. C. Hirst, ACS Photonics **9**, 2724 (2022).
[968]N. Tavakoli, R. Spalding, P. Koppejan, G. Gkantzounis, C. Wang, R. Röhrich, E. Kontoleta, A. Koenderink, R. Sapienza, M. Florescu, and E. Alarcon-Llado, ACS Photonics **9**, 1206 (2022).
[969]M. R. Jones, N. C. Seeman, and C. A. Mirkin, Science **347**, 1260901 (2015).
[970]H. Feng, X. Lu, W. Wang, N. Kang, and J. Mays, Polymers **9**, 494 (2017).
[971]K.-H. Jeong, J. Kim, and L. Lee, Science **312**, 557 (2006).
[972]H. Ko, M. Stoykovich, J. Song, V. Malyarchuk, W. Choi, C.-J. Yu, J. Geddes III, J. Xiao, S. Wang, Y. Huang, and J. A. Rogers, Nature **454**, 748 (2008).
[973]K. Lodewijks, V. Miljkovic, I. Massiot, A. Mekonnen, R. Verre, E. Olsson, and A. Dmitriev, Sci. Rep. **6**, 28490 (2016).
[974]H. Li, J. Wu, X. Huang, Z. Yin, J. Liu, and H. Zhang, ACS Nano **8**, 6563 (2014).
[975]M. Aghajamali, I. T. Cheong, and J. G. C. Veinot, Langmuir **34**, 9418 (2018).
[976]I. Massiot, C. Trompoukis, K. Lodewijks, V. Depauw, and A. Dmitriev, Nanoscale **8**, 11461 (2016).
[977]I. Liberal and N. Engheta, Nat. Photonics **11**, 149 (2017).
[978]O. Reshef, I. De Leon, M. Z. Alam, and R. W. Boyd, Nat. Rev. Mater. **4**, 535 (2019).
[979]M. A. Vincenti, D. de Ceglia, A. Ciattoni, and M. Scalora, Phys. Rev. A **84**, 063826 (2011).
[980]V. G. Veselago, Sov. Phys. Usp. **10**, 509 (1968).
[981]J. B. Pendry, Phys. Rev. Lett. **85**, 3966 (2000).
[982]Y. Li, S. Kita, P. Muñoz, O. Reshef, D. I. Vulis, M. Yin, M. Lončar, and E. Mazur, Nat. Photonics **9**, 738 (2015).
[983]N. Kinsey, C. DeVault, A. Boltasseva, and V. M. Shalaev, Nat. Rev. Mater. **4**, 742 (2019).
[984]R. Liu, Q. Cheng, T. Hand, J. J. Mock, T. J. Cui, S. A. Cummer, and D. R. Smith, Phys. Rev. Lett. **100**, 023903 (2008).
[985]J. Zhou, J. Zhao, Q. Wu, C.-F. Chen, M. Lei, G. Chen, F. Tian, and Z. Liu, Adv. Funct. Mater. **32**, 2204734 (2022).
[986]B. Edwards, A. Alù, M. E. Young, M. Silveirinha, and N. Engheta, Phys. Rev. Lett. **100**, 033903 (2008).
[987]T. G. Folland, G. Lu, A. Bruncz, J. R. Nolen, M. Tadjer, and J. D. Caldwell, ACS Photonics **7**, 614 (2020).
[988]S. W. Jun, J. H. Yim, J. Park, S. Lee, and Y. H. Ahn, Laser Photonics Rev. **18**, 2300726 (2023).
[989]P. B. Johnson and R. W. Christy, Phys. Rev. B **6**, 4370 (1972).
[990]C. Rizza, A. Di Falco, and A. Ciattoni, Appl. Phys. Lett. **99**, 221107 (2011).
[991]R. Maas, J. Parsons, N. Engheta, and A. Polman, Nat. Photonics **7**, 907 (2013).
[992]X. Li, C. Rizza, S. A. Schulz, A. Ciattoni, and A. D. Falco, APL Photonics **4**, 056107 (2019).

16 July 2024 09:29:41

© Author(s) 2024

[993]S. Suresh, O. Reshef, M. Z. Alam, J. Upham, M. Karimi, and R. W. Boyd, ACS Photonics **8**, 125 (2020).
[994]W. Jaffray, S. Saha, V. M. Shalaev, A. Boltasseva, and M. Ferrera, Adv. Opt. Photonics **14**, 148 (2022).
[995]I. Liberal, Y. Li, and N. Engheta, Nanophotonics **7**, 1117 (2018).
[996]G. V. Naik, J. Kim, and A. Boltasseva, Opt. Mater. Express **1**, 1090 (2011).
[997]Y. Gui, M. Miscuglio, Z. Ma, M. H. Tahersima, S. Sun, R. Amin, H. Dalir, and V. J. Sorger, Sci. Rep. **9**, 11279 (2019).
[998]T. Taliercio and P. Biagioni, Nanophotonics **8**, 949 (2019).
[999]E. Sachet, C. T. Shelton, J. S. Harris, B. E. Gaddy, D. L. Irving, S. Curtarolo, B. F. Donovan, P. E. Hopkins, P. A. Sharma, A. L. Sharma, J. Ihlefeld, S. Franzen, and J.-P. Maria, Nat. Mater. **14**, 414 (2015).
[1000]B. G. Lewis and D. C. Paine, MRS Bull. **25**, 22 (2000).
[1001]D. S. Ginley and C. Bright, MRS Bull. **25**, 15 (2000).
[1002]E. Fortunato, D. Ginley, H. Hosono, and D. C. Paine, MRS Bull. **32**, 242 (2007).
[1003]M. Silveirinha and N. Engheta, Phys. Rev. Lett. **97**, 157403 (2006).
[1004]A. Alù, M. G. Silveirinha, A. Salandrino, and N. Engheta, Phys. Rev. B **75**, 155410 (2007).
[1005]R. W. Boyd, *Nonlinear Optics* (Elsevier, 2020).
[1006]A. Ciattoni and E. Spinozzi, Phys. Rev. A **85**, 043806 (2012).
[1007]A. Capretti, Y. Wang, N. Engheta, and L. Dal Negro, Opt. Lett. **40**, 1500 (2015).
[1008]O. Reshef, E. Giese, M. Zahirul Alam, I. De Leon, J. Upham, and R. W. Boyd, Opt. Lett. **42**, 3225 (2017).
[1009]A. S. Barker, H. W. Verleur, and H. J. Guggenheim, Phys. Rev. Lett. **17**, 1286 (1966).
[1010]N. Kinsey, C. DeVault, J. Kim, M. Ferrera, V. M. Shalaev, and A. Boltasseva, Optica **2**, 616 (2015).
[1011]Y. Zhou, M. Z. Alam, M. Karimi, J. Upham, O. Reshef, C. Liu, A. E. Willner, and R. W. Boyd, Nat. Commun. **11**, 2180 (2020).
[1012]R. Tirole, E. Galiffi, J. Dranczewski, T. Attavar, B. Tilmann, Y.-T. Wang, P. A. Huidobro, A. Alú, J. B. Pendry, S. A. Maier, S. Vezzoli, and R. Sapienza, arXiv:2202.05937 (2022).
[1013]J. Baxter, A. Pérez-Casanova, L. Cortes-Herrera, A. Calà Lesina, I. De Leon, and L. Ramunno, Adv. Photonics Res. **4**, 2200280 (2023).
[1014]M. Abb, P. Albella, J. Aizpurua, and O. L. Muskens, Nano Lett. **11**, 2457 (2011).
[1015]S. A. Schulz, A. A. Tahir, M. Z. Alam, J. Upham, I. D. Leon, and R. W. Boyd, Phys. Rev. A **93**, 063846 (2016).
[1016]M. H. Ebrahim, A. Marini, V. Bruno, N. Kinsey, J. B. Khurgin, D. Faccio, and M. Clerici, Appl. Phys. Lett. **119**, 221101 (2021).
[1017]B. J. Eggleton, B. Luther-Davies, and K. Richardson, Nat. Photonics **5**, 141 (2011).
[1018]M. Abb, Y. Wang, C. H. de Groot, and O. L. Muskens, Nat. Commun. **5**, 4869 (2014).
[1019]J. Deng, Y. Tang, S. Chen, K. Li, A. V. Zayats, and G. Li, Nano Lett. **20**, 5421 (2020).
[1020]Y. Lu, X. Feng, Q. Wang, X. Zhang, M. Fang, W. E. Sha, Z. Huang, Q. Xu, L. Niu, X. Chen, C. Ouyang, Y. Yang, X. Zhang, E. Plum, S. Zhang, J. Han, and W. Zhang, Nano Lett. **21**, 7699 (2021).
[1021]M. Karimi, K. M. Awan, Y. Vaddi, R. Alaee, J. Upham, M. Z. Alam, and R. W. Boyd, Nano Lett. **23**, 11555 (2023).
[1022]C. K. Dass, H. Kwon, S. Vangala, E. M. Smith, J. W. Cleary, J. Guo, A. Alù, and J. R. Hendrickson, ACS Photonics **7**, 174 (2019).
[1023]E. Minerbi, S. Sideris, J. B. Khurgin, and T. Ellenbogen, Nano Lett. **22**, 6194 (2022).
[1024]S. Sideris, E. Minerbi, C. McDonnell, and T. Ellenbogen, ACS Photonics **9**, 3981 (2022).
[1025]W. Shi, H. Liu, and Z. Wang, Nanomaterials **11**, 3424 (2021).
[1026]K. Wang, M. Li, H.-H. Hsiao, F. Zhang, M. Seidel, A.-Y. Liu, J. Chen, E. Devaux, C. Genet, and T. Ebbesen, ACS Photonics **8**, 2791 (2021).
[1027]H. Ghobadi, H. L. Offerhaus, J. A. Alvarez-Chavez, M. Morales-Masis, and I. De Leon, Opt. Express **31**, 8775 (2023).
[1028]H. Ma, P. M. Bendix, and L. B. Oddershede, Nano Lett. **12**, 3954 (2012).
[1029]P. Berini, ACS Photonics **9**, 2204 (2022).
[1030]G. K. Shirmanesh, R. Sokhoyan, P. C. Wu, and H. A. Atwater, ACS Nano **14**, 6912 (2020).
[1031]L. C. Wynne, H. T. Ballantyne, X. Li, A. D. Falco, and S. A. Schulz, Photonics Nanostruct. **42**, 100844 (2020).
[1032]L. Cheng, R. Alaee, A. Safari, M. Karimi, L. Zhang, and R. W. Boyd, ACS Photonics **8**, 585 (2021).
[1033]F. Capolino and F. Capolino, *Applications of Metamaterials* (CRC Press, 2017).
[1034]R. Marques, F. Martin, and M. Sorolla, *Metamaterials with Negative Parameters*, Wiley Series in Microwave and Optical Engineering (Wiley-Blackwell, Chichester, England, 2007).
[1035]N. Engheta and R. W. Ziolkowski, *Metamaterials* (John Wiley & Sons, Nashville, TN, 2006).
[1036]C. Simovski and S. Tretyakov, *An Introduction to Metamaterials and Nanophotonics an Introduction to Metamaterials and Nanophotonics* (Cambridge University Press, Cambridge, England, 2020).
[1037]C. Caloz, D. R. Jackson, and T. Itoh, *Leaky-Wave Antennas*, 1st ed., edited by F. B. Gross, Frontiers in Antennas: Next Generation Design & Engineering (McGraw-Hill Education, New York, 2011).
[1038]X. Liu, T. Starr, A. F. Starr, and W. J. Padilla, Phys. Rev. Lett. **104**, 207403 (2010).
[1039]W. J. Padilla, A. J. Taylor, C. Highstrete, M. Lee, and R. D. Averitt, Phys. Rev. Lett. **96**, 107401 (2006).
[1040]H.-T. Chen, J. F. O'Hara, A. K. Azad, A. J. Taylor, R. D. Averitt, D. B. Shrekenhamer, and W. J. Padilla, Nat. Photonics **2**, 295–298 (2008).
[1041]W. C. Chew *et al.*, *Fast and Efficient Algorithms in Computational Electromagnetics*, Antennas & Propagation Library (Artech House, Norwood, MA, 2001).
[1042]J. C. Maxwell, *A Dynamical Theory of the Electromagnetic Field* (Scottish Academic Press, Edinburgh, 1982).
[1043]J. Maxwell, *A Treatise on Electricity and Magnetism Volumes 1 and 2*, Cambridge Library Collection—Physical Sciences (Cambridge University Press, Cambridge, England, 2010).
[1044]A. Sommerfeld, Math. Ann. **47**, 317 (1896).
[1045]A. Sommerfeld, "Über die Ausbreitung der Wellen in der drahtlosen Telegraphie," Ann. Phys. **333**, 665–736 (1909).
[1046]L. Rayleigh, Philos. Mag. **43**, 125 (1897).
[1047]G. Mie, "Beiträge zur Optik trüber Medien, speziell kolloidaler Metallösungen," Ann. Phys. **330**, 377–445 (1908).
[1048]D. Hondros, Ann. Phys. **335**, 905 (1909).
[1049]J. Nicholson, Proc. London Math. Soc. **9**, 67 (1911).
[1050]P. Debye, Annalen der Physik **335**, 57 (1909).
[1051]D. Hondros and P. Debye, Ann. Phys. **337**, 465 (1910).
[1052]G. Pelosi, A. Savini, and S. Selleri, in *7th IEEE History of Electrotechnology Conference (HISTELCON)* (IEEE, 2021).
[1053]K. Yee, IEEE Trans. Antennas Propag. **14**, 302 (1966).
[1054]R. F. Harrington, *Field Computation by Moment Methods*, IEEE Press Series on Electromagnetic Wave Theory (IEEE Publications, Piscataway, NJ, 1993).
[1055]J. Jin, *The Finite Element Method in Electromagnetics*, 3rd ed., Wiley—IEEE (John Wiley & Sons, Nashville, TN, 2014).
[1056]S. Russell and P. Norvig, *Artificial Intelligence*, 4th ed. (Pearson, Upper Saddle River, NJ, 2020).
[1057]I. Goodfellow, Y. Bengio, and A. Courville, *Deep Learning* (MIT Press, 2016).
[1058]T. Hastie, R. Tibshirani, and J. Friedman, in *The Elements of Statistical Learning*, Springer Series in Statistics (Springer New York, New York, NY, 2009).
[1059]P. R. Wiecha, A. Lecestre, N. Mallet, and G. Larrieu, Nat. Nanotechnol. **14**, 237 (2019).
[1060]B. Xiong, Y. Xu, W. Li, W. Ma, T. Chu, and Y. Liu, Adv. Opt. Mat. **12**, 2302200 (2024).
[1061]L. Deng, Y. Xu, and Y. Liu, Photonics Nanostruct. **52**, 101073 (2022).
[1062]A. Ueno, H.-I. Lin, F. Yang, S. An, L. Martin-Monier, M. Y. Shalaginov, T. Gu, and J. Hu, Nanophotonics **12**, 3491 (2023).
[1063]W. J. Padilla and K. Fan, in *Metamaterial Electromagnetic Wave Absorbers* (Springer International Publishing, Cham, 2022), pp. 125–155.
[1064]P. Moitra, B. A. Slovick, W. Li, I. I. Kravchencko, D. P. Briggs, S. Krishnamurthy, and J. Valentine, ACS Photonics **2**, 692 (2015).
[1065]H.-T. Chen, J. Zhou, J. F. O'Hara, F. Chen, A. K. Azad, and A. J. Taylor, Phys. Rev. Lett. **105**, 073901 (2010).
[1066]G. Cybenko, Math. Control, Signals Syst. **2**, 303 (1989).
[1067]K. Hornik, M. Stinchcombe, and H. White, Neural Networks **2**, 359 (1989).

16 July 2024 09:29:41

© Author(s) 2024

[1068]W. Ma, F. Cheng, and Y. Liu, ACS Nano **12**, 6326 (2018).
[1069]L. Gao, X. Li, D. Liu, L. Wang, and Z. Yu, Adv. Mater. **31**, 1905467 (2019).
[1070]Z. Hou, T. Tang, J. Shen, C. Li, and F. Li, Nanoscale Res. Lett. **15**, 83 (2020).
[1071]S. So, J. Mun, and J. Rho, ACS Appl. Mater. Interfaces **11**, 24264 (2019).
[1072]Y. Long, J. Ren, Y. Li, and H. Chen, Appl. Phys. Lett. **114**, 181105 (2019).
[1073]J. He, C. He, C. Zheng, Q. Wang, and J. Ye, Nanoscale **11**, 17444 (2019).
[1074]L. Xu, M. Rahmani, Y. Ma, D. A. Smirnova, K. Z. Kamali, F. Deng, Y. K. Chiang, L. Huang, H. Zhang, S. Gould, D. N. Neshev, and A. E. Miroshnichenko, Adv. Photonics **2**, 026003 (2020).
[1075]E. Ashalley, K. Acheampong, L. Vázquez, P. Yu, A. Neogi, A. O. Govorov, and Z. Wang, Photonics Res. **8**, 1213 (2020).
[1076]A. Mall, A. Patil, D. Tamboli, A. Sethi, and A. Kumar, J. Phys. D **53**, 49LT01 (2020).
[1077]L. Pilozzi, F. A. Farrelly, G. Marcucci, and C. Conti, Commun. Phys. **1**, 57 (2018).
[1078]A. D. Phan, C. V. Nguyen, P. T. Linh, T. V. Huynh, V. D. Lam, A.-T. Le, and K. Wakabayashi, Crystals **10**, 125 (2020).
[1079]R. Singh, A. Agarwal, and B. W. Anthony, Opt. Express **28**, 27893 (2020).
[1080]I. Malkiel, M. Mrejen, A. Nagler, U. Arieli, L. Wolf, and H. Suchowski, Light **7**, 60 (2018).
[1081]G. P. Spell, S. Ren, L. M. Collins, and J. M. Malof, in *Proceedings of the AAAI Conference on Artificial Intelligence* (AAAI-23 Technical Tracks 8. 2023), Vol. 37, pp. 9874–9881.
[1082]J. Johnson and V. Rahmat-Samii, IEEE Antennas Propag. Mag. **39**, 7 (1997).
[1083]C. Forestiere, A. J. Pasquale, A. Capretti, G. Miano, A. Tamburrino, S. Y. Lee, B. M. Reinhard, and L. D. Negro, Nano Lett. **12**, 2037 (2012).
[1084]C.-J. Li, Y.-C. Fang, and M.-C. Cheng, Opt. Express **17**, 10177 (2009).
[1085]Y. Deng, J. Dong, S. Ren, O. Khatib, M. Soltani, V. Tarokh, W. Padilla, and J. Malof, in Thirty-Fifth Conference on Neural Information Processing Systems Datasets and Benchmarks Track (Round 2), 2021.
[1086]J. Peurifoy, Y. Shen, L. Jing, Y. Yang, F. Cano-Renteria, B. G. DeLacy, J. D. Joannopoulos, M. Tegmark, and M. Soljačić, Sci. Adv. **4**, eaar4206 (2018).
[1087]Y. Miyatake, N. Sekine, K. Toprasertpong, S. Takagi, and M. Takenaka, Jpn. J. Appl. Phys. **59**, SGGE09 (2020).
[1088]W. Ma, F. Cheng, Y. Xu, Q. Wen, and Y. Liu, Adv. Mater. **31**, 1901111 (2019).
[1089]W. Ma and Y. Liu, Sci. China Phys., Mech. Astron. **63**, 284212 (2020).
[1090]T. Qiu, X. Shi, J. Wang, Y. Li, S. Qu, Q. Cheng, T. Cui, and S. Sui, Adv. Sci. **6**, 1900128 (2019).
[1091]Z. A. Kudyshev, A. V. Kildishev, V. M. Shalaev, and A. Boltasseva, Appl. Phys. Rev. **7**, 021407 (2020).
[1092]Z. A. Kudyshev, A. V. Kildishev, V. M. Shalaev, and A. Boltasseva, Nanophotonics **10**, 371 (2020).
[1093]X. Shi, T. Qiu, J. Wang, X. Zhao, and S. Qu, J. Phys. D **53**, 275105 (2020).
[1094]Z. Liu, L. Raju, D. Zhu, and W. Cai, IEEE J. Emerging Sel. Top. Circuits Syst. **10**, 126 (2020).
[1095]Y. Kiarashinejad, S. Abdollahramezani, and A. Adibi, npj Comput. Mater. **6**, 12 (2020).
[1096]R. Unni, K. Yao, X. Han, M. Zhou, and Y. Zheng, Nanophotonics **10**, 4057 (2021).
[1097]R. Unni, K. Yao, and Y. Zheng, ACS Photonics **7**, 2703 (2020).
[1098]S. Ren, A. Mahendra, O. Khatib, Y. Deng, W. J. Padilla, and J. M. Malof, Nanoscale **14**, 3958 (2022).
[1099]F. Wen, J. Jiang, and J. A. Fan, ACS Photonics **7**, 2098 (2020).
[1100]C. C. Nadell, B. Huang, J. M. Malof, and W. J. Padilla, Opt. Express **27**, 27523 (2019).
[1101]W. Ma, Z. Liu, Z. A. Kudyshev, A. Boltasseva, W. Cai, and Y. Liu, Nat. Photonics **15**, 77 (2021).
[1102]L. Huang, L. Xu, and A. E. Miroshnichenko, in *Advances and Applications in Deep Learning* (IntechOpen, 2020).
[1103]J. Jiang, M. Chen, and J. A. Fan, Nat. Rev. Mater. **6**, 679 (2020).
[1104]P. R. Wiecha, A. Arbouet, C. Girard, and O. L. Muskens, Photonics Res. **9**, B182 (2021).
[1105]O. Khatib, S. Ren, J. Malof, and W. J. Padilla, Adv. Funct. Mater. **31**, 2101748 (2021).
[1106]S. So, T. Badloe, J. Noh, J. Rho, J. Rho, and J. Bravo-Abad, Nanophotonics **9**, 1041 (2020).
[1107]C. M. Bishop, *Pattern Recognition and Machine Learning*, Information Science and Statistics, 1st ed. (Springer, New York, NY, 2006).
[1108]S. Yan and Y. Liu, Int. J. Numer. Modell. **34**, e2969 (2021).
[1109]S. Cuomo, V. S. Di Cola, F. Giampaolo, G. Rozza, M. Raissi, and F. Piccialli, J. Sci. Comput. **92**, 88 (2022).
[1110]Y. Bengio, in *Proceedings of ICML Workshop on Unsupervised and Transfer Learning* (JMLR Workshop and Conference Proceedings, 2012), pp. 17–36.
[1111]A. R. Zamir, A. Sax, W. Shen, L. J. Guibas, J. Malik, and S. Savarese, in *Proceedings of the IEEE Conference on Computer Vision and Pattern Recognition (CVPR)* (IEEE, 2018), pp. 3712–3722.
[1112]R. Pestourie, Y. Mroueh, T. V. Nguyen, P. Das, and S. G. Johnson, npj Comput. Mater. **6**, 164 (2020).
[1113]K. M. Jablonka, Q. Ai, A. Al-Feghali, S. Badhwar, J. D. Bocarsly, A. M. Bran, S. Bringuier, L. C. Brinson, K. Choudhary, D. Circi *et al.*, Digital Discovery **2**, 1233 (2023).
[1114]Y. Li, Z. Lin, S. Zhang, Q. Fu, B. Chen, J.-G. Lou, and W. Chen, arXiv:2206.02336 (2022).
[1115]T. H. Trinh, Y. Wu, Q. V. Le, H. He, and T. Luong, Nature **625**, 476 (2024).
[1116]S. Amizadeh, H. Palangi, A. Polozov, Y. Huang, and K. Koishida, in *International Conference on Machine Learning* (PMLR, 2020), pp. 279–290.
[1117]J. Mao, C. Gan, P. Kohli, J. B. Tenenbaum, and J. Wu, in *International Conference on Learning Representations* (International Conference on Learning Representations, ICLR, 2019).
[1118]B. Schölkopf, F. Locatello, S. Bauer, N. R. Ke, N. Kalchbrenner, A. Goyal, and Y. Bengio, Proc. IEEE **109**, 612 (2021).
[1119]S. Wang, S. Sankaran, and P. Perdikaris, arXiv:2203.07404 (2022).
[1120]J. F. Nye and M. V. Berry, "Dislocations in wave trains," Proc. R. Soc. Lond. **336**, A336165–190 (1974).
[1121]J. Hajnal, Proc. R. Soc. London A **414**, 433 (1987).
[1122]P. Coullet, L. Gil, and F. Rocca, Opt. Commun. **73**, 403 (1989).
[1123]J. Nye and F. J. Wright, "Natural focusing and fine structure of light: Caustics and wave dislocations," Am. J. Phys. **68**, 776 (2000).
[1124]M. V. Berry and M. R. Dennis, Proc. R. Soc. A **459**, 1261 (2003).
[1125]Y. Shen, X. Wang, Z. Xie, C. Min, X. Fu, Q. Liu, M. Gong, and X. Yuan, Light **8**, 90 (2019).
[1126]G. J. Gbur, *Singular Optics* (CRC Press, 2016).
[1127]J. Leach, M. R. Dennis, J. Courtial, and M. J. Padgett, New J. Phys. **7**, 55 (2005).
[1128]M. R. Dennis, K. O'holleran, and M. J. Padgett, in *Progress in Optics* (Elsevier, 2009), Vol. 53, pp. 293–363.
[1129]Ruchi, P. Senthilkumaran, and S. K. Pal, Int. J. Opt. **2020**, 2812803.
[1130]S. Tsesses, E. Ostrovsky, K. Cohen, B. Gjonaj, N. H. Lindner, and G. Bartal, Science **361**, 993 (2018).
[1131]S. H. Park, S.-G. Lee, S. Baek, T. Ha, S. Lee, B. Min, S. Zhang, M. Lawrence, and T.-T. Kim, Nanophotonics **9**, 1031 (2020).
[1132]S. W. D. Lim, J.-S. Park, M. L. Meretska, A. H. Dorrah, and F. Capasso, Nat. Commun. **12**, 4190 (2021).
[1133]D. Sugic, R. Droop, E. Otte, D. Ehrmanntraut, F. Nori, J. Ruostekoski, C. Denz, and M. R. Dennis, Nat. Commun. **12**, 6785 (2021).
[1134]A. J. Vernon, M. R. Dennis, and F. J. Rodríguez-Fortuño, arXiv:2301.03540 (2023).
[1135]M. V. Berry, Light **12**, 238 (2023).
[1136]Ş. K. Özdemir, S. Rotter, F. Nori, and L. Yang, Nat. Mater. **18**, 783 (2019).
[1137]K. Ding, C. Fang, and G. Ma, Nat. Rev. Phys. **4**, 745 (2022).
[1138]Y. Fan, H. Liang, J. Li, D. P. Tsai, and S. Zhang, ACS Photonics **9**, 2872 (2022).
[1139]A. Li, H. Wei, M. Cotrufo, W. Chen, S. Mann, X. Ni, B. Xu, J. Chen, J. Wang, S. Fan *et al.*, Nat. Nanotechnol. **18**, 706 (2023).
[1140]M. Mehmood, S. Mei, S. Hussain, K. Huang, S. Siew, L. Zhang, T. Zhang, X. Ling, H. Liu, J. Teng *et al.*, Adv. Mater. **28**, 2533 (2016).
[1141]P.-Y. Chen and J. Jung, Phys. Rev. Appl. **5**, 064018 (2016).
[1142]W. Chen, Ş. Kaya Özdemir, G. Zhao, J. Wiersig, and L. Yang, Nature **548**, 192 (2017).
[1143]S. Dong, G. Hu, Q. Wang, Y. Jia, Q. Zhang, G. Cao, J. Wang, S. Chen, D. Fan, W. Jiang *et al.*, ACS Photonics **7**, 3321 (2020).
[1144]N. Nye, A. Halawany, C. Markos, M. Khajavikhan, and D. Christodoulides, Phys. Rev. Appl. **13**, 064005 (2020).
[1145]M. Farhat, M. Yang, Z. Ye, and P.-Y. Chen, ACS Photonics **7**, 2080 (2020).

16 July 2024 09:29:41

© Author(s) 2024

[1146]Z. Li, G. Cao, C. Li, S. Dong, Y. Deng, X. Liu, J. S. Ho, and C.-W. Qiu, PIER. **171**, 1–20 (2021).
[1147]X. Li, C. Hu, Y. Tian, Y. Liu, H. Chen, Y. Xu, M.-H. Lu, and Y. Fu, Sci. Bull. **68**, 2555 (2023).
[1148]M. Coppolaro, M. Moccia, G. Castaldi, A. Alù, and V. Galdi, IEEE Trans. Microwave Theory Tech. **69**, 2060 (2021).
[1149]J.-H. Park, A. Ndao, W. Cai, L. Hsu, A. Kodigala, T. Lepetit, Y.-H. Lo, and B. Kanté, Nat. Phys. **16**, 462 (2020).
[1150]Y. Xu, L. Li, H. Jeong, S. Kim, I. Kim, J. Rho, and Y. Liu, Sci. Adv. **9**, eadf3510 (2023).
[1151]H. Alaeian and J. A. Dionne, Phys. Rev. B **89**, 075136 (2014).
[1152]F. Binkowski, F. Betz, R. Colom, P. Genevet, and S. Burger, arXiv:2307.04654 (2023).
[1153]G. Egan, see https://www.gregegan.net/SCIENCE/Catacaustics/Catacaustics.html for more information about catacaustics, resultants and kissing conics.
[1154]R. Colom, E. Mikheeva, K. Achouri, J. Zuniga-Perez, N. Bonod, O. J. Martin, S. Burger, and P. Genevet, Laser Photonics Rev. **17**, 2200976 (2023).
[1155]A. B. Williams and F. J. Taylor, *Electronic Filter Design Handbook* (McGraw-Hill Education, 2006).
[1156]S. A. R. Horsley and M. Woolley, Nat. Phys. **17**, 348 (2021).
[1157]V. Grigoriev, S. Varault, G. Boudarham, B. Stout, J. Wenger, and N. Bonod, Phys. Rev. A **88**, 063805 (2013).
[1158]V. Grigoriev, A. Tahri, S. Varault, B. Rolly, B. Stout, J. Wenger, and N. Bonod, Phys. Rev. A **88**, 011803 (2013).
[1159]M. Elsawy, C. Kyrou, E. Mikheeva, R. Colom, J.-Y. Duboz, K. Z. Kamali, S. Lanteri, D. Neshev, and P. Genevet, Laser Photonics Rev. **17**, 2200880 (2023).
[1160]C. M. Bender, in *Time and Science: Volume 3: Physical Sciences and Cosmology* (World Scientific, 2023), pp. 285–310.
[1161]Y. Kang and A. Z. Genack, Phys. Rev. B **103**, L100201 (2021).
[1162]A. Guo, G. Salamo, D. Duchesne, R. Morandotti, M. Volatier-Ravat, V. Aimez, G. Siviloglou, and D. Christodoulides, Phys. Rev. Lett. **103**, 093902 (2009).
[1163]C. E. Rüter, K. G. Makris, R. El-Ganainy, D. N. Christodoulides, M. Segev, and D. Kip, Nat. Phys. **6**, 192 (2010).
[1164]M. Lawrence, N. Xu, X. Zhang, L. Cong, J. Han, W. Zhang, and S. Zhang, Phys. Rev. Lett. **113**, 093901 (2014).
[1165]Y. Yang, P. S. Huang, Y. T. Lin *et al.* "Creating pairs of exceptional points for arbitrary polarization control: Asymmetric vectorial wavefront modulation," Nat Commun 15, 232 (2024).
[1166]Z. Yang *et al.*, Nano Lett. **24**, 844–851 (2024).
[1167]C. Wang, W. R. Sweeney, A. D. Stone, and L. Yang, Science **373**, 1261 (2021).
[1168]K. Y. Lee, K. W. Yoo, F. Monticone, and J. W. Yoon, arXiv:2311.08766 (2023).
[1169]G. Lavigne, K. Achouri, V. S. Asadchy, S. A. Tretyakov, and C. Caloz, IEEE Trans. Antennas Propag. **66**, 1321 (2018).
[1170]A. Taflove, S. C. Hagness, and M. Piket-May, *Electrical Engineering Handbook* (Academic Press, 2005), Vol. **3**, 629–670.
[1171]J. Pomplun, S. Burger, L. Zschiedrich, and F. Schmidt, Phys. Status Solidi B **244**, 3419 (2007).
[1172]M. G. Moharam, E. B. Grann, D. A. Pommet, and T. K. Gaylord, J. Opt. Soc. Am. A **12**, 1068 (1995).
[1173]C. F. Bohren and D. R. Huffman, *Absorption and Scattering of Light by Small Particles* (John Wiley & Sons, 2008).
[1174]R. Alaee, C. Rockstuhl, and I. Fernandez-Corbaton, Adv. Opt. Mater. **7**, 1800783 (2019).
[1175]P. Morse and H. Feshbach, *Methods of Theoretical Physics* (McGraw-Hill, New York, 1953).
[1176]P. Waterman, Proc. IEEE **53**, 805 (1965).
[1177]G. Demésy, J.-C. Auger, and B. Stout, J. Opt. Soc. Am. A **35**, 1401 (2018).
[1178]D. Beutel, A. Groner, C. Rockstuhl, and I. Fernandez-Corbaton, J. Opt. Soc. Am. B **38**, 1782 (2021).
[1179]I. Allayarov, A. B. Evlyukhin, and A. C. Lesina, Opt. Express **32**, 5641 (2024).
[1180]D. Arslan, A. Rahimzadegan, S. Fasold, M. Falkner, W. Zhou, M. Kroychuk, C. Rockstuhl, T. Pertsch, and I. Staude, Adv. Mater. **34**, 2105868 (2022).
[1181]S. Gladyshev, T. D. Karamanos, L. Kuhn, D. Beutel, T. Weiss, C. Rockstuhl, and A. Bogdanov, Nanophotonics **12**, 3767 (2023).
[1182]R. Alaee, R. Filter, D. Lehr, F. Lederer, and C. Rockstuhl, Opt. Lett. **40**, 2645 (2015).
[1183]N. Stefanou, V. Yannopapas, and A. Modinos, Comput. Phys. Commun. **113**, 49 (1998).
[1184]N. Stefanou, V. Yannopapas, and A. Modinos, Comput. Phys. Commun. **132**, 189 (2000).
[1185]A. Y. Toukmaji and J. A. Board, Jr., Comput. Phys. Commun. **95**, 73 (1996).
[1186]D. Beutel, I. Fernandez-Corbaton, and C. Rockstuhl, Phys. Rev. A **107**, 013508 (2023).
[1187]A. Egel, Y. Eremin, T. Wriedt, D. Theobald, U. Lemmer, and G. Gomard, J. Quant. Spectrosc. Radiat. Transfer **202**, 279 (2017).
[1188]A. Egel, L. Pattelli, G. Mazzamuto, D. S. Wiersma, and U. Lemmer, J. Quant. Spectrosc. Radiat. Transfer **199**, 103 (2017).
[1189]D. Schebarchov, A. Fazel-Najafabadi, E. Le Ru, and B. Auguié, J. Quant. Spectrosc. Radiat. Transfer **284**, 108131 (2022).
[1190]D. Beutel, I. Fernandez-Corbaton, and C. Rockstuhl, arXiv:2309.03182 (2023).
[1191]A. Rahimzadegan, T. D. Karamanos, R. Alaee, A. G. Lamprianidis, D. Beutel, R. W. Boyd, and C. Rockstuhl, Adv. Opt. Mater. **10**, 2102059 (2022).
[1192]A. Rahimzadegan, R. Alaee, C. Rockstuhl, and R. W. Boyd, Opt. Express **28**, 16511 (2020).
[1193]J. Mun, S. So, J. Jang, and J. Rho, ACS Photonics **7**, 1153 (2020).
[1194]P. D. Terekhov, V. E. Babicheva, K. V. Baryshnikova, A. S. Shalin, A. Karabchevsky, and A. B. Evlyukhin, Phys. Rev. B **99**, 045424 (2019).
[1195]M. Poleva, K. Frizyuk, K. Baryshnikova, A. Evlyukhin, M. Petrov, and A. Bogdanov, Phys. Rev. B **107**, L041304 (2023).
[1196]V. S. Asadchy, A. Díaz-Rubio, and S. A. Tretyakov, Nanophotonics **7**, 1069 (2018).
[1197]H. Ma, A. B. Evlyukhin, A. E. Miroshnichenko, F. Zhu, S. Duan, J. Wu, C. Zhang, J. Chen, B. Jin, W. J. Padilla *et al.*, Adv. Opt. Mater. **12**, 2301968 (2023).
[1198]A. B. Evlyukhin, V. R. Tuz, V. S. Volkov, and B. N. Chichkov, Phys. Rev. B **101**, 205415 (2020).
[1199]V. E. Babicheva and A. B. Evlyukhin, J. Appl. Phys. **129**(4), 040902 (2021).
[1200]A. B. Evlyukhin, M. A. Poleva, A. V. Prokhorov, K. V. Baryshnikova, A. E. Miroshnichenko, and B. N. Chichkov, Laser Photonics Rev. **15**, 2100206 (2021).
[1201]M. Idemen, *Discontinuities in the Electromagnetic Field* (IEEE Press Wiley, Piscataway, NJ; Hoboken, NJ, 2011).
[1202]E. Kuester, M. Mohamed, M. Piket-May, and C. Holloway, IEEE Trans. Antennas Propag. **51**, 2641 (2003).
[1203]C. Holloway, M. Mohamed, E. Kuester, and A. Dienstfrey, IEEE Trans. Electromagn. Compat. **47**, 853 (2005).
[1204]M. Albooyeh, S. Tretyakov, and C. Simovski, Ann. Phys. **528**, 721 (2016).
[1205]K. Achouri and C. Caloz, *Electromagnetic Metasurfaces: Theory and Applications* (Wiley-IEEE Press, Hoboken, NJ, 2021).
[1206]K. Achouri, G. D. Bernasconi, J. Butet, and O. J. F. Martin, IEEE Trans. Antennas Propag. **66**, 6061 (2018).
[1207]K. Achouri, V. Tiukuvaara, and O. J. F. Martin, IEEE Trans. Antennas Propag. **70**, 11946 (2022).
[1208]V. Tiukuvaara, O. J. F. Martin, and K. Achouri, Opt. Express **31**, 22982 (2023).
[1209]Y. Vahabzadeh, N. Chamanara, K. Achouri, and C. Caloz, IEEE J. Multiscale Multiphys. Comput. Tech. **3**, 37 (2018).
[1210]M. Kerker, D. S. Wang, and C. L. Giles, J. Opt. Soc. Am. **73**, 765 (1983).
[1211]Y. Yang, A. E. Miroshnichenko, S. V. Kostinski, M. Odit, P. Kapitanova, M. Qiu, and Y. S. Kivshar, Phys. Rev. B **95**, 165426 (2017).
[1212]A. T. M. Yeşilyurt, M. Sanz-Paz, F. Zhu, X. Wu, K. S. Sunil, G. P. Acuna, and J.-S. Huang, ACS Nano **17**, 19189 (2023).
[1213]B. Zerulla, M. Krstić, D. Beutel, C. Holzer, C. Wöll, C. Rockstuhl, and I. Fernandez-Corbaton, Adv. Mater. **34**, 2200350 (2022).
[1214]A. K. Iyer, A. Alu, and A. Epstein, IEEE Trans. Antennas Propag. **68**, 1223 (2020).

16 July 2024 09:29:41

© Author(s) 2024

AFFILIATIONS

[1]SUPA, School of Physics and Astronomy, University of St Andrews, St. Andrews, United Kingdom
[2]Blackett Laboratory, Imperial College London, London SW7 2AZ, United Kingdom
[3]Nottingham University, Nottingham, United Kingdom
[4]Photonics Initiative, Advanced Science Research Center, City University of New York, New York, New York 10031, USA
[5]Physics Program, Graduate Center, City University of New York, New York, New York 10016, USA
[6]Institute of Solid State Physics, Abbe Center of Photonics, Friedrich Schiller University Jena, 07743 Jena, Germany
[7]Department of Applied Physics, Aalto University, Espoo, Finland
[8]Department of Information in Matter and Center for Nanophotonics, NWO-I Institute AMOLF, Amsterdam, The Netherlands
[9]School of Chemistry, University of Glasgow, Glasgow, United Kingdom
[10]James Watt School of Engineering, University of Glasgow, Glasgow, United Kingdom
[11]Institute of Electronic Structure and Laser (IESL), Foundation for Research and Technology—Hellas (FORTH), 70013 Heraklion, Crete, Greece
[12]Department of Physics, National and Kapodistrian University of Athens, 15784 Athens, Greece
[13]Department of Materials Science and Technology, University of Crete, 70013 Heraklion, Crete, Greece
[14]Department of Physics and London Centre for Nanotechnology, King's College London, London, United Kingdom
[15]School of Physics and Astronomy, Faculty of Science, Monash University, Melbourne, Victoria 3800, Australia
[16]Nonlinear Physics Center, Research School of Physics, Australian National University, Canberra, ACT 2601, Australia
[17]Department of Physics, Imperial College London, London SW7 2AZ, United Kingdom
[18]School of Engineering and Physical Sciences, Heriot-Watt University, Edinburgh EH14 4AS, United Kingdom
[19]School of Physics and Astronomy, University of St Andrews, North Haugh, St Andrews KY16 9SS, United Kingdom
[20]Snap Inc., 141 Park Drive, Milton, Abingdon OX14 4SE, United Kingdom
[21]School of Physics, Engineering and Technology, University of York, York YO10 5DD, United Kingdom
[22]Meta Reality Labs, Redmond, Washington 98052, USA
[23]Sandia National Laboratory, Albuquerque, New Mexico 87185, USA
[24]Max-Planck Institute for the Science of Light, Erlangen, Germany
[25]State Key Laboratory for Mesoscopic Physics and Frontiers Science Center for Nano-optoelectronics, School of Physics, Peking University, Beijing, China
[26]University of Fribourg, Adolphe Merkle Institute, Soft Matter Physics Group, Chemin des Verdiers 4, 1700 Fribourg, Switzerland
[27]ETH Zurich, Department of Physics, Institute for Quantum Electronics, Optical Nanomaterial Group, Auguste-Piccard-Hof 1, 8093 Zurich, Switzerland
[28]Advanced Optics and Photonics Laboratory, Nottingham Trent University, Nottingham, United Kingdom
[29]Apple Inc, 2200 Martin Ave, Santa Clara, California 95050, USA
[30]Meta Platforms, Inc, 10301 Willows Road NE, Redmond, Washington 98052, USA
[31]Engineering and Applied Science, California Institute of Technology, Pasadena, California 91125, USA
[32]Laboratoire Photonique Numérique et Nanosciences (LP2N), Université de Bordeaux, Institut d'Optique Graduate School, CNRS, 33400 Talence, France
[33]Department of Physics, University of Gothenburg, 41296 Gothenburg, Sweden
[34]Institute of Theoretical Solid State Physics, Karlsruhe Institute of Technology (KIT), Kaiserstraße 12, Karlsruhe 76131, Germany
[35]Institute of Nanotechnology, Karlsruhe Institute of Technology (KIT), Kaiserstraße 12, Karlsruhe 76131, Germany
[36]Institute of Physics, Martin Luther University Halle-Wittenberg, 06120 Halle, Germany
[37]Institut Lumière Matière (iLM), Université Claude Bernard Lyon 1, CNRS, 69100 Villeurbanne, France
[38]Department of Physics, University of Ottawa, Ottawa, Ontario K1N 6N5, Canada
[39]Nexus for Quantum Technologies, University of Ottawa, Ottawa, Ontario K1N 6N5, Canada
[40]ASML Netherlands B. V., De Run 6501, 5504 DR Veldhoven, The Netherlands
[41]School of Electrical Engineering and Computer Science, University of Ottawa, Ottawa, Ontario K1N 6N5, Canada
[42]Department of Electrical and Computer Engineering, Duke University, Durham, North Carolina 27705, USA
[43]Department of Computer Science, University of Montana, Missoula, Montana 59812, USA
[44]Physics Department, Colorado School of Mines, 1523 Illinois St., Golden, Colorado 80401, USA
[45]Tsinghua Shenzhen International Graduate School, Tsinghua University, Shenzhen 518055, China
[46]Université Côte d'Azur, CNRS, CRHEA, 06560 Valbonne, France
[47]Nanophotonics and Metrology Laboratory, Institute of Electrical and Microengineering, École Polytechnique Fédérale de Lausanne, Route Cantonale, 1015 Lausanne, Switzerland
[48]Institute of Quantum Optics, Leibniz University Hannover, Welfengarten 1, Hannover 30167, Germany
[49]Cluster of Excellence PhoenixD, Leibniz University Hannover, Welfengarten 1A, Hannover 30167, Germany
[50]Light Technology Institute, Karlsruhe Institute of Technology (KIT), Kaiserstraße 12, 76131 Karlsruhe, Germany
[51]Institute of Microstructure Technology, Karlsruhe Institute of Technology (KIT), Kaiserstraße 12, 76131 Karlsruhe, Germany

16 July 2024 09:29:41

© Author(s) 2024